Nanotechnology based therapeutic approaches to iron-induced oxidative stress in an *in vitro* model of Parkinson's disease

Leah Rose Mursaleen

A thesis submitted in partial fulfilment of the requirements of the University of Westminster for the degree of Doctor of Philosophy.

This research programme was carried out in collaboration with the School of Pharmacy, University College London.

July 2021

Abstract

In Parkinson's disease (PD), excess free iron drives the accumulation of toxic hydroxyl radicals within mitochondria of dopaminergic neurons, resulting in sustained oxidative stress and cellular damage. The blood-brain barrier (BBB) prevents most pharmaceuticals from entering the brain, therefore, to enable the advancement of potential antioxidant and iron chelator therapies for PD, limiting factors such as brain penetrance and bioavailability need to be overcome. This study aimed to develop novel nanocarrier delivery systems of the antioxidants curcumin, n-acetylcysteine (NAC) and hydroxytyrosol (HT), alone or combined with the iron chelator deferoxamine (DFO), to protect against rotenone-induced parkinsonism in SH-SY5Y cells, and in a co-cultured hCMEC/D3 - SH-SY5Y cellular BBB model.

Nanocarriers were prepared using Pluronic® F68 (P68) or Solutol® HS 15 (Sol), with or without the mitochondrial targetter dequalinium (DQA), by modified thin-film hydration. For all experiments, the mean of six replicates was calculated for each treatment. All formulations demonstrated high encapsulation efficiency (65 – 98%) and suitable nanocarrier size for brain penetrance (< 200 nm). All nanocarriers significantly protected against rotenone-reduced cell viability ($p < 0.01$), except Sol and Sol+DQA curcumin+DFO where some cytotoxicity was observed. The addition of DQA to the P68 nanocarriers increased cellular antioxidant activity by up to 65%. All P68+DQA nanoformulations significantly protected against rotenone-induced increased iron ($p < 0.01$) and lipid peroxidation ($p < 0.0001$). The addition of DFO to curcumin and HT P68+DQA nanocarriers resulted in increased antioxidant activity and protection against rotenone across all parameters, whereas the highest concentration of P68+DQA NAC was as protective as the combination with DFO. P68+DQA nanoformulation enhanced the mean BBB passage of curcumin, NAC, HT and DFO by 49%, 28%, 50% and 49%, respectively ($p < 0.01$). Mitochondrial localisation assessments showed consistent co-location of the P68+DQA nanocarriers within mitochondria. In each case, the P68+DQA nanocarriers increased the ability of curcumin, NAC, HT and/or DFO, to protect against rotenone induced cytotoxicity and oxidative stress by up to 19% and 14% (respectively) following BBB passage ($p < 0.05$).

These results indicate that the P68+DQA nanocarriers were successful at enhancing the protective effects of curcumin, NAC, HT and/or DFO by increasing the brain penetrance and targeted delivery of the associated drugs. Overall, this study demonstrates for the first time the formulation and delivery of these curcumin, NAC, HT and/or DFO nanocarriers to protect against oxidative stress induced by rotenone in SH-SY5Y cells alone and following passage across a hCMEC/D3 BBB model. This study highlights the effectiveness of the P68+DQA nanocarriers in fully utilising the therapeutic benefit of these antioxidants for PD and provides strong evidence for their suitability for *in vivo* testing.

Table of Contents

List of tables and figures

Chapter 4 - Assessing the therapeutic potential of micellar nanocarriers containing curcumin and/or DFO in a cellular model of PD

Chapter 5 - Assessing the therapeutic potential of P68+DQA nanocarriers to deliver NAC and HT alone or in combination with DFO in a cellular PD model

Chapter 6 - Assessing the ability of the nanoformulations to cross a hCMEC/D3 cellular BBB model, target mitochondria and protect against rotenone-induced oxidative stress

HT (10 and 20 µM) and combined HT and DFO (10 and 20 µM HT + 50 and 100 µM DFO, respectively).

Chapter 7- Overview and future directions

Acknowledgements

Firstly, I would like to thank all my supervisors, Professor M. Gulrez Zariwala, Dr Satyanarayana Somavarapu (University College London), and Professor Brendon Noble for all their advice and encouragement throughout my PhD.

I would like to thank Dr Voni Blesia for helping to train me in cell culture at the start of my PhD and for helping to ensure the smooth running of the lab.

I would like to acknowledge Stefanie Chan and Andrew Western from University College London for their assistance with the initial characterisation of the nanoformulations as well as Dr Simon McArthur from Queen Mary University of London and Dr Amy Maclatchy from University of Westminster for kindly gifting the hCMEC/D3 cells for my Transwell® experiments.

Thank you to all my fellow PhD students who provided crucial moral support over the years and helped to keep me motivated, even during the COVID-19 pandemic.

Last but by no means least, I would like to thank my husband Oliver Plank for being so supportive for the duration of my studies and for enabling me to complete my thesis by going part-time in his job following the arrival of our daughter Eva Marie Plank.

Publications

Published abstracts from poster presentations:

A potential neuroprotective approach for Parkinson's disease using novel micellar nanocarriers to co-deliver deferoxamine and curcumin - 8th Congress of the International BioIron Society (2019), EMBL Heidelberg, Germany

A novel nanocarrier antioxidant delivery system to counter iron induced skin cellular oxidative stress - 8th Congress of the International BioIron Society (2019), EMBL Heidelberg, Germany

A novel nanocarrier delivery system for curcumin and deferoxamine as a potential neuroprotective strategy for Parkinson's disease - 5th World Parkinson Congress - WPC 2019 at the International Conference Center in Kyoto, Japan

A Novel Plant Polymer Based Nanocarrier Delivery System for Curcumin to Counter Cellular Oxidative Stress - Spices and Medicine 2018 Annual Autumn Symposium "Exploring Natural Products: Visions for the Future", UCL School of Pharmacy, UK

Published papers:

Mursaleen, L., Noble, B., Somavarapu, S., & Zariwala, M. G. (2021). Micellar Nanocarriers of Hydroxytyrosol Are Protective against Parkinson's Related Oxidative Stress in an In Vitro hCMEC/D3-SH-SY5Y Co-Culture System. *Antioxidants*, *10*(6), 887.

Mursaleen, L., Noble, B., Chan, S. H. Y., Somavarapu, S., & Zariwala, M. G. (2020). N-Acetylcysteine nanocarriers protect against oxidative stress in a cellular model of Parkinson's disease. *Antioxidants*, *9*(7), 600.

Mursaleen, L., Somavarapu, S., & Zariwala, M. G. (2020). Deferoxamine and Curcumin Loaded Nanocarriers Protect Against Rotenone-Induced Neurotoxicity. *Journal of Parkinson's Disease*, *10*(1), 99-111.

Tiekou Lorinczova, H., Fitzsimons, O., **Mursaleen, L**., Renshaw, D., Begum, G., & Zariwala, M. G. (2020). Co-Administration of Iron and a Bioavailable Curcumin Supplement Increases Serum BDNF Levels in Healthy Adults. *Antioxidants*, *9*(8), 645.

Barker, R. A., Bjorklund, A., Gash, D. M., Whone, A., Van Laar, A., Kordower, J. H., Bankiewicz, K., Kieburtz, K., Saarma, M., Booms, S., Huttunen, H., Kells, A., Fiandaca, M., Stoessl, A. J., Eidelberg, D., Federoff, H., Voutilainen, M. H., Dexter, D., Eberling, J., Brundin, P., Isaacs, L., **Mursaleen, L**., Bresolin, E., Carroll, C., Coles, A., Fiske, B., Matthews, H., Lungu, C., Wyse, R., Stott, S., Lang, A. (2020). GDNF and Parkinson's Disease: Where Next? A Summary from a Recent Workshop. *Journal of Parkinson's Disease*, *10*(3), 875-891.

Published magazine articles:

Improving natural antioxidants for the treatment of neurodegenerative

diseases - Catalyst Magazine (issue 35), 2019

Author's declaration

I declare that all the material contained in this thesis is my own work.

Abbreviations

6-OHDA	6-hydroxydopamine
ABAP	2,2'-Azobis(2-methylpropionamidine) dihydrochloride
ABCB7A	ATP-binding cassette protein
ARE	Antioxidant response element
ATCC	American Type Culture Collection
ATP	Adenosine triphosphate
BBB	Blood-brain barrier
BMVEC	Brain microvascular endothelial cells
BSA	Bovine serum albumin
CAA	Cellular antioxidant activity
CoQ	Coenzyme Q10
Cp	Ceruloplasmin
CSF	Cerebral spinal fluid
CytC	Cytochrome C
DCF	2',7'-Dichlorofluorescin
DCFH-DA	2',7'-Dichlorofluorescin diacetate
DFO	Deferoxamine
DFP	Deferiprone
DFX	Deferasirox
DMEM	Dulbecco's modified eagle medium
DMSO	Dimethyl sulfoxide
DMT1	Divalent metal transporter 1
DPBS	Dulbecco's phosphate buffered saline
DQA	Dequalinium
ECL	EMD Millipore™ Immobilon™ Western Chemiluminescent HRP Substrate
EDTA	Ethylenediaminetetraacetic acid
FADH	Flavin adenine dinucleotide

FBS	Foetal bovine serum
FDA	U.S. Food and drug administration
FLVCR1	Feline leukemia virus subgroup C cellular receptor
FRAP	Ferric iron antioxidant power
FTIR	Fourier-transform infrared spectroscopy
GA	Gentamicin
GAPDH	Glyceraldehyde 3-phosphate dehydrogenase
GDNF	Glial cell-derived neurotrophic factor
HBBS	Hank's buffered saline solution
hCMEC/D3	Human cerebral microvascular endothelial cell D3
hFGF-B	Human basic fibroblast growth factor
HT	Hydroxytyrosol
IL	Interleukin
IREB	Iron-responsive element-binding protein
IREs	Iron response elements
Keap1	Kelch-like ECH-associated protein 1
L-dopa	Levodopa
MCU	Mitochondrial calcium uniporter
MEM	Minimum essential media
MHRA	Medicines and healthcare products regulatory agency
MPPþ	1-methyl-4-phenylpyridinium
MPTP	1-methyl-4-phenyl-1, 2, 3, 6-tetrahydropyridine
MTT	3-(4,5-dimethylthiazol-2-yl)-2,5-diphenyl-2H-tetrazolium bromide
NAC	N-acetylcysteine
NAcc	Nucleus accumbens
NADH	Nicotinamide adenine dinucleotide
NeuN	Neuronal nuclear protein
Nramp1	Natural resistance-associated macrophage protein 1
Nrf2	Nuclear factor erthroid 2-related factor 2

Nurr1	Nuclear receptor related 1
NVU	Neurovascular unit
P68	Pluronic® F68
PD	Parkinson's disease
PFC	Prefrontal cortex
PLGA	Poly(lactic-co-glycolic acid)
R3-IGF-1	Human recombinant insulin-like growth factor
S.D.	Standard deviation
SN	Substantia nigra
SNpc	Substantia nigra pars compacta
SWI	Susceptibility weighted imaging
TBA	Thiobarbituric acid
TBARS	Thiobarbituric acid reactive substances
TBS	Tris-buffered saline
TBS-T	Tris-buffered saline with tween 20
TEER	Trans-endothelial electrical resistance
TEM	Transmission electron microscopy
TEMED	N,N,N',N'-Tetramethylethylenediamine
TH	Tyrosine hydroxylase
TNF	Tumour necrosis factor
TMRM	tetramethylrhodamine methyl ester
TPP	triphenylphosphonium
TrkB	Tropomysin receptor kinase B
UVA	Ultraviolet A-rays
UV-Vis	Ultraviolet visible
VEGF	Vascular endothelial growth factor
VTA	Ventral tegmental area
XRD	X-ray diffraction
α-syn	Alpha synuclein

Chapter 1 - General Background

1.1. Introduction

Parkinson's disease (PD) is the second most common progressive neurodegenerative disease (Russo & Nestler, 2013; Bissonette & Rosche, 2016; Mursaleen & Stamford, 2016; Van der Merwe et al., 2017). Although the aetiology of PD is not yet fully understood, there is evidence to suggest an interaction between genetic and environmental risk factors (Yamada-Fowler & Söderkvist, 2015). Numerous genes, including SNCA, LRRK2, parkin, PINK1 and DJ-1, have been associated with hallmarks of the disease such as misfolding and aggregation of the protein alpha-synuclein (α-syn), mitochondrial dysfunction and oxidative stress (Trinh & Farrer, 2013).

In both genetic and sporadic forms of the disease, PD is characterised by a marked and continued loss of dopaminergic neurons in the substantia nigra (SN) of the brain (Russo & Nestler, 2013; Bissonette & Rosche, 2016). Dopamine is a neurotransmitter that is involved numerous processes, from mood, attention and the reward system to the coordination, initiation and termination of voluntary movement (Lees et al., 2009). The SN is located within the basal ganglia of the midbrain and basal ganglia circuits that project to the striatum are responsible for the control of movement (Lees et al., 2009). This includes the initiation and termination of movement as well as inhibition of unwanted movement by regulating the activity of upper motor neurons (Lees et al., 2009). Therefore, PD is typically defined as a movement disorder and clinical diagnosis of PD is based on the presence of cardinal motor symptoms; bradykinesia (slowness of movement), tremor, rigidity, and postural instability (Jankovic et al., 2008; Mursaleen & Stamford 2016). That said, motor symptoms are only one aspect of PD, there are a plethora of non-motor symptoms that people with PD may experience that can dramatically affect quality of life. These include sleep disorders (e.g. insomnia, REM sleep disorder), gastrointestinal disturbances (e.g. constipation, nausea), neuropsychiatric symptoms (e.g. anxiety, depression), autonomic dysfunction (e.g. urinary urgency, incontinence), sensory issues (e.g. loss of sense of smell, pain), speech difficulties (e.g. monotone, slurred speech) and fatigue (Mathur et al 2017; Mursaleen et al, 2017).

Most of the treatments currently approved for PD focus on replenishing dopamine to activate the basal ganglia circuits in order to sustain normal movement (Middleton & Strick, 2000). The 'gold standard' treatment of PD today is the same as it was 60 years ago, using Levodopa (L-dopa) based treatments to alleviate the core motor symptoms (Lopez et al., 2001; Mursaleen & Stamford, 2016). L-dopa has a similar chemical structure to dopamine, however unlike dopamine it can pass the blood-brain barrier (BBB) (Nutl & Fellman, 1984). Endogenously, L-dopa is the precursor to dopamine and is produced from the amino acid tyrosine *via* the enzyme tyrosine hydroxylase (Nutl & Fellman, 1984; Xie et al., 2015) (figure 1). It is easily then converted to dopamine in the presence of DOPA decarboxylase (Nutl & Fellman, 1984; Parkinson Study Group, 2004; Thanvi & Lo, 2004) (figure 1).
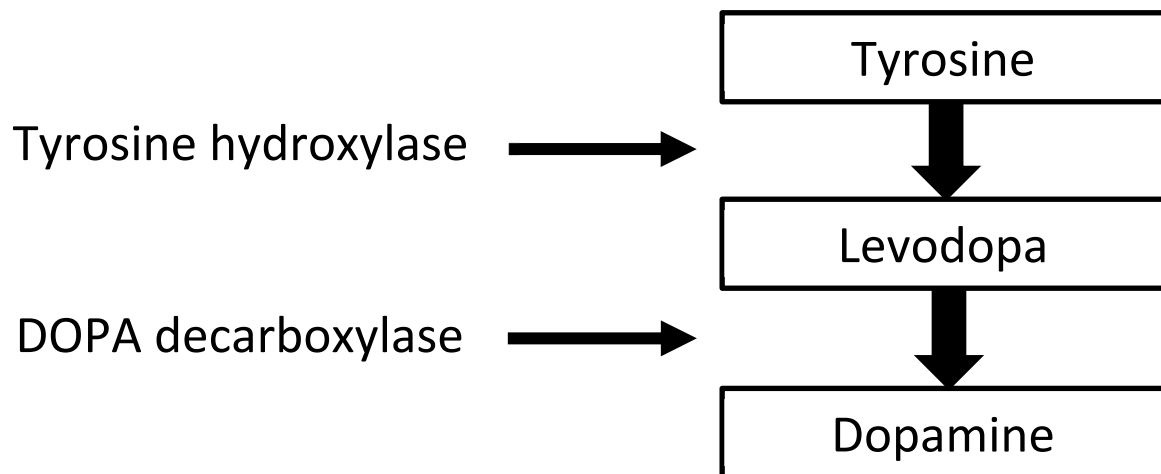
Figure 1. Schematic diagram of the endogenous formation of dopamine from tyrosine adapted from Thanvi & Lo (2004). Tyrosine is converted to L-dopa by the rate limiting enzyme tyrosine hydroxylase. L-dopa is subsequently converted to dopamine via DOPA decarboxylase.

Since currently approved medications only manage the motor symptoms, as the disease progresses patients require higher doses, which, for dopaminergic therapies, increase the possibility of side effects such as dyskinesia (involuntary movements) and impulse control disorders (e.g. excessive gambling) (Thanvi & Lo, 2004). Dyskinesia is the most common side effect of dopamine replacement therapies and can often account for the more serious adverse events that can occur in PD (Mursaleen & Stamford, 2016). For people who experience severe dyskinesia, it is often their most troublesome symptom, dramatically impacting on daily living and making the very basics of life such as eating a meal or doing up buttons extremely difficult (Mathur et al., 2017).

Other side effects more common with dopamine receptor 2 agonist therapy, such as vivid dreams, REM sleep behavioural disorder, hallucinations (auditory, visual and olfactory) and impulse control disorders (including hyper-sexuality, pathological gambling and behavioural stereotypy) also result because none of the current dopaminergic treatments are specifically targeted to the nigrostriatal pathway, where the main therapeutic benefit resides (Thanvi & Lo, 2004; Moore et al., 2014; Zhang et al., 2014; Mursaleen & Stamford, 2016). All dopamine receptors are activated by dopamine receptor agonists and all dopaminergic neurons respond to L-dopa by releasing more dopamine (Mursaleen & Stamford, 2016), therefore it is the unintended activation of the same receptors in the nucleus accumbens (NAcc) and prefrontal cortex (PFC) which result in unwanted psychological side effects. This is because basal ganglia circuits are also key in non-motor operations involved in cognitive and emotional processes (Middleton & Strick, 2000).

The pre-frontal and limbic loops regulate initiation and termination of cognitive and emotional processes (Middleton & Strick, 2000). The balance between information maintenance and flexible adjustment of information that characterises executive function and cognitive processes depends critically on an optimal level of dopamine signalling in the PFC (Goldman-Rakic, 1995). However, with dopaminergic therapy the limbic loop responsible for the regulation of emotion and motivation can become overactive, particularly at the mesolimbic dopamine projections from the ventral tegmental area (VTA) to the NAcc, resembling similarity to the over-activity of the limbic loop exhibited in schizophrenia (Meyer-Lindenberg, 2010) (figure 2).

In normal conditions, PFC pyramidal neurons directly excite mesocortical dopamine neurons in the VTA and indirectly inhibit mesostriatal dopamine neurons through activation of GABAergic neurons in the VTA (Lewis and Gonzalez- Burgos, 2006) (figure 2). In Schizophrenia, the PFC loop is reduced at the mesocortical dopaminergic projections from the VTA to the PFC due to the opposing effects of the PFC projections on dopaminergic cells (Lewis & Gonza´lez-Burgos, 2008). Therefore, the overall reduction in PFC cell activity leads to an excess of dopamine receptor activation in the NAcc (Lewis & Gonza´lez-Burgos, 2008). This functional excess of dopamine neurotransmission results in psychotic features such as hallucinations and delusions which can similarly be achieved with use of dopamine receptor agonists, such as amphetamine which have both high psychogenic propensity and

addictive potential (Carlsson, 2006). Behavioural characteristics consistent with the abuse of psychostimulants, such as amphetamine, can be seen in people with PD following long-term or excessive use of antiparkinsonian medication due to the unintended rise of dopamine in the NAcc (Espana & Jones, 2013; Mursaleen & Stamford., 2016).
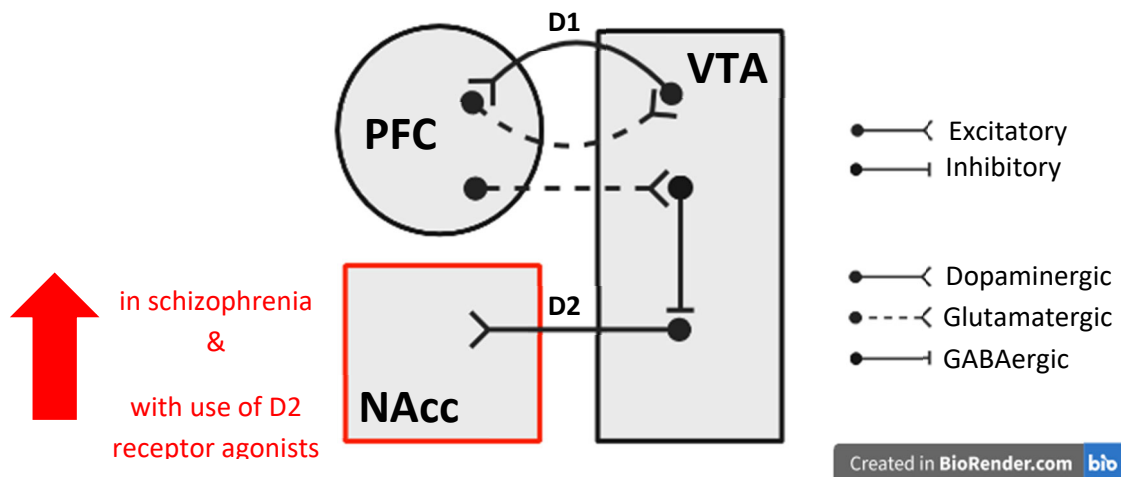
Figure 2. A schematic diagram of a basal ganglia circuit involved in regulation of emotion and motivation, adapted from Carlsson (2006). In schizophrenia there is a decreased level of dopamine in the PFC and decreased glutamatergic activity in the VTA which leads to a reduction in GABAergic activity in the VTA and therefore an increase in dopamine in the NAcc. This increase in dopamine in the NAcc can also be achieved with the use of dopamine receptor 2 agonists and can result in symptoms of psychosis. PFC = prefrontal cortex, VTA = ventral tegmental area, NAcc = nucleus accumbens, D1 = dopamine 1 receptor signalling, D2 = dopamine 2 receptor signalling.

Due to the progressive nature of the disease, symptoms of Parkinson's get worse over time. Although there are evidently medications which can manage the symptoms, such treatments do not come without a long list of potential of side effects and they do not work to modify the course of the disease. As the most recent UK figures suggest a 1 in 37 lifetime risk of being diagnosed with PD (Parkinon's UK, 2018) and an annual cost to the NHS close to three billion pounds (Fineberg et al., 2013), it is imperative that curative therapeutics are investigated. There is increasing evidence showing a marked accumulation of iron in the SN of PD patient brains (Dexter et al., 1987; Griffiths et al., 1999; Graham et al., 2000; Martin et al., 2008; Wallis et al., 2008; Rossi et al., 2013). Such elevated iron levels have been linked to the hallmarks of PD, including mitochondrial dysfunction, inflammation and α-syn misfolding and aggregation (Lewy body pathology), and therefore provides a promising disease-modifying therapeutic approach. This chapter will outline the role of iron within the

body and brain, how iron homeostasis is disrupted in PD and how such disruption is involved in PD progression. It will then go onto discuss research into related therapeutics and what is needed to overcome the pitfalls of previous research by using nanotechnology-based solutions to target treatments.

1.2. Iron homeostasis

1.2.1 Iron uptake and regulation

Iron is a critical nutrient for the majority of living organisms. It is vital for energy production *via* normal respiration as well as its clear role in oxygen transport within the blood (Ganz & Nemeth, 2015). Iron is highly abundant in the atmosphere, yet atmospheric iron is largely insoluble because it exists in the oxidised, ferric form (Ganz & Nemeth, 2015; Dev & Babitt, 2017; Pietrangelo, 2017). Much of the iron within the body is taken up in the diet, however although 12-18 mg of ferric iron is ingested daily, only around 1-2 mg is absorbed by duodenal enterocytes (Dev & Babitt, 2017). Due to the limited access to both atmospheric and dietary iron, the human body maintains normal iron homeostasis by continuously conserving and recycling iron (Pantopoulos et al., 2012; Ganz, 2013; Dev & Babitt, 2017).

In order for enterocytes to take up iron, ferric iron must be reduced to ferrous iron by duodenal cytochrome b ferric reductase (Critchton et al., 2002). The divalent metal transporter 1 (DMT1), located on the apical membrane of enterocytes, then transports ferrous iron into the cell (Ganz & Nemeth, 2015; Knutson 2017). Another iron transporter located on the basolateral membrane of the cell, ferroportin, allows passage of ferrous iron out of the cell into the plasma (Ganz & Nemeth, 2015; Knutson 2017). In order to prevent mass transport of iron into the plasma, much of the ferrous iron that enters the cell is oxidised to ferric iron and stored in ferritin molecules (Critchton et al., 2002). In the plasma, iron is mostly bound to the organic iron chelator transferrin which can strongly bind to two ferric iron molecules in a reversible manner, as a result transferrin receptors mediate iron uptake in the majority of cells within the body (Critchton et al., 2002; Garrick & Garrick, 2009: Ganz & Nemeth, 2015). Binding of iron-saturated transferrin to the transferrin receptor 1 results in the formation of a transferrin-transferrin receptor complex (Critchton et al., 2002; Garrick & Garrick 2009; Elliott & Head, 2012; Dev & Babitt, 2017) (figure 3).
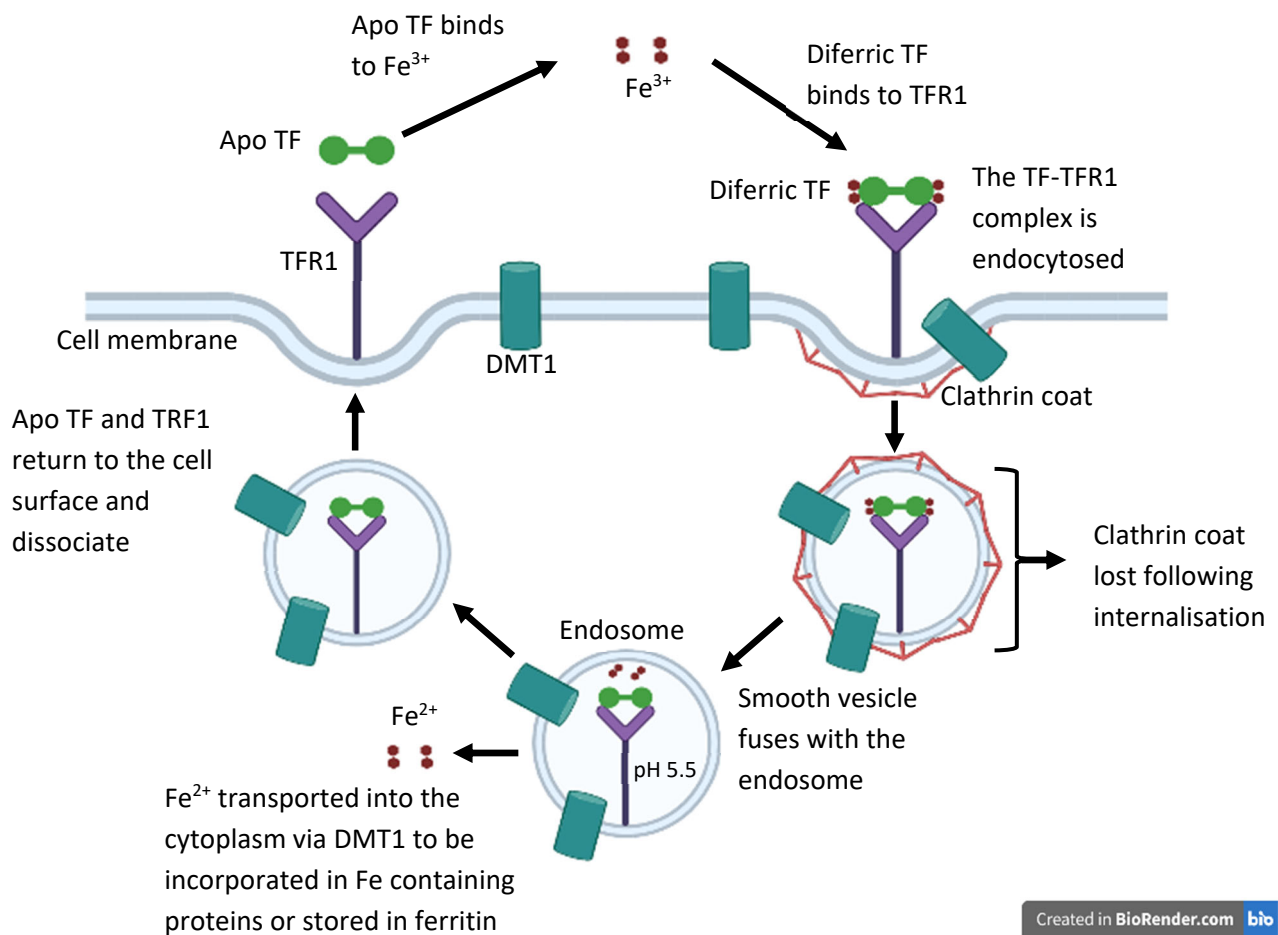
Figure 3. Cellular iron uptake via transferrin-receptor 1 (TFR1) adapted from Elliott & Head (2012). Diferric transferrin (TF) binds to transferrin receptor 1 at the cell surface. Clathrin coated vesicles internalise the complex via endocytosis, losing their clathrin coat in the process. The now smooth vesicle fuses with an endosome to release ferric iron (Fe^{3+}) from TF into the more acidic endosomal lumen. The divalent metal transporter 1 (DMT1) transports the reduced, ferrous iron (Fe^{2+}) into the cytoplasm to become incorporated into essential iron containing proteins or stored in ferritin. The apotransferrin (Apo TF) left bound to the receptor complex is reutilised following its return to the cell surface and released back into circulation.

Following the formation of this complex, clathrin-coated vesicles internalise the complex losing their clathrin-coat in the process (Critchton et al., 2002; Dev & Babitt, 2017) (figure 3). These now smooth vesicles can fuse with endosomes to release ferric iron from transferrin into the endosomal lumen which has a more acidic pH of 5.5 (Bali et al., 1991; Sipe & Murphy, 1991; Critchton et al., 2002; Garrick & Garrick, 2009; Elliott & Head, 2012; Knutson et al., 2017) (figure 3). This is supported by evidence from mammalian cell culture studies which have shown 60-80% of transferrin bound iron to be released into the cell following internalisation of the transferrin-transferrin receptor complex, with the rest being released back into the incubation media which mimics circulation (Ciechanover et al., 1983; Garrick et al., 1993). Once free from the complex, iron is reduced to the ferrous form and DMT1

transports it into the cytoplasm, where it can become incorporated into essential iron containing proteins and used in numerous cellular processes or stored in ferritin (Critchton et al., 2002) (figure 3). The iron-free or apotransferrin left bound to the receptor complex is reutilised following its return to the cell surface and released back into circulation (Critchon et al., 2002; Elliott & Head, 2012) (figure 3). This role of DMT1 in cellular iron uptake has been highlighted in studies using primary reticulocytes from the DMT1 deficient Belgrade rat, where iron released into the cell is reduced by 45-65% due to the lack of ability of such cells to retrieve iron *via* DMT1 from the endosomes (Garrick et al., 1993). As a result, most of the iron remains bound to transferrin and is released back into the treatment media (Garrick et al., 1993).

Numerous cellular proteins require iron as a co-factor, most using haem and iron sulphur cluster iron centres which are predominately synthesised in the mitochondria (Levi et al., 2009). Therefore, following iron uptake into the cell, much of the labile iron is trafficked into the mitochondria where it is utilised in haem and iron-sulphur cluster pathways (Lv & Shang, 2018). Iron sulphur cluster assembly within mitochondria involves numerous proteins, including frataxin which acts as an iron chaperone and donates iron to the cluster (Bulteau et al., 2004; Chiang et al., 2017). Whereas haem is produced from mitochondrial labile iron being inserted into protoporphyrin IX by ferrochelatase (Chiabrando et al., 2014). Haem and iron sulphur clusters are also incorporated into many non-mitochondrial proteins and therefore require transport into the cytosol. Exportation of iron sulphur clusters from mitochondria into cytosol occurs via the ATP-binding cassette protein (ABCB7A) whereas haem is transported into cytosol by the feline leukemia virus subgroup C cellular receptor (FLVCR1b), it is exported out of the cytosol by the FLVCR1a isoform (figure 4). Free iron within mitochondria that is not assembled into haem and iron sulphur clusters is stored in mitochondrial ferritin (Campanella et al., 2009; Lv & Shang, 2018).

Mitochondrial iron homeostasis and cellular iron homeostasis and metabolism are closely linked, and this has been highlighted by numerous *in vitro* and *in vivo* studies (Richardson et al., 2010). For example, Campanella et al (2009) showed that, in mammalian cells, expression of mitochondrial ferritin has a role in regulating both cytosolic and mitochondrial labile iron and leads to iron being trafficked from the cytosol to mitochondria.
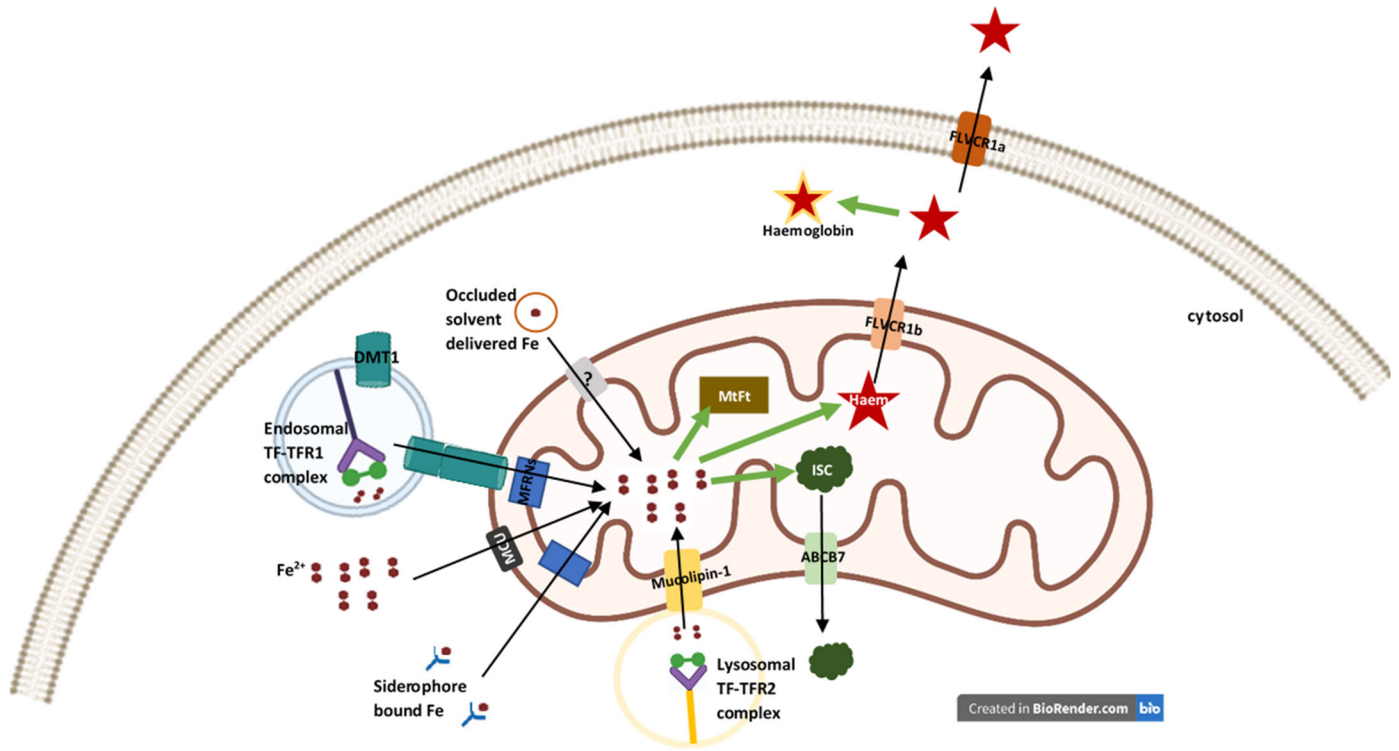
Figure 4. Intracellular iron trafficking to and from mitochondria, adapted from Lv & Shang (2018). Mitochondria can acquire iron from cytosolic labilie iron, from endosomes, from lysosomes and via vascular transport of occluded solvent delivered iron. Mitochondrial labile iron can be used for the synthesis of iron sulphur clusters (ISCs) and haem and can be stored in mitochondrial ferritin (MtFt). Haem and ISCs are utilised in a number of proteins both inside and outside of mitochondria. DMT1 = divalent metal transporter 1; MFRNs = mitoferrins; MCU = mitochondrial calcium uniporter; ABCB7 = ATP-binding cassette protein; FLVCR1 = feline leukemia virus subgroup C cellular receptor.

Further to this, when mitochondrial haem levels are low, there is an increase in transferrin-bound iron uptake into the cell (Richardson et al., 2010; Lv & Shang et al., 2018). In most cells, mitochondrial iron levels are regulated by mitoferrin 1 and 2, which are localised to the inner mitochondrial membrane (Paradkar et al., 2009). Studies have shown that mitoferrin 2 is the main transporter of iron into mitochondria of non-erythroid cells (Shaw et al., 2006; Hung et al., 2013). There are a number of pathways in which mitochondria are thought to acquire iron (figure 4). (1) iron can be acquired from the cytosolic labile iron pool where low molecular weight ligands bound to cytoplasmic proteins, such as siderophores, can sequester labile iron and mitoferrins can deliver iron to mitochondria (Lv & Shang., 2018). (2) lysosome released labile iron can be transported into the mitochondria *via* the inner mitochondrial calcium uniporter (MCU) (Uchiyama et al., 2008). (3) in erythroid cells, ferrous iron released from the lysosomal diferric transferrin-transferrin receptor 2 complex can enter mitochondria through the cation channel mucolipin-1 (Khalil et al., 2017). (4) in erythroid cells, iron can be directly delivered from transferrin containing endosomes to

mitochondria as DMT1 is found on the outer mitochondrial membrane (Sheftel et al., 2007; Wolff et al., 2014; Wolff et al., 2018). It is thought that endosomal DMT1 interacts with the mitochondrial DMT1 contributing to a 'kiss and run' endocytosis processes of iron into mitochondria (Hamdi et al., 2016; Wolff et al., 2018). (5) solvent occlusion may be used to deliver non-labile iron through vascular transport into mitochondria (Shvartsman et al., 2007). Clearly mitochondria are a major site of iron transport and storage and iron levels must be tightly controlled by iron regulatory proteins to maintain mitochondrial iron homeostasis and avoid damage that can result from free iron, which is highly reactive (Lv & Shang, 2018).

Iron in its free form can be highly reactive and damaging to cell membranes, DNA, and proteins; it is therefore sequestered in proteins such as transferrin, ferritin, and haemoglobin to mitigate this threat (Bratic & Nils-Larsson, 2013; Kandola et al., 2015). In normal conditions more than 50% of total iron within the body is bound to haemoglobin and up to 25% may be stored within hepatocytes or hepatic and splenic macrophages in the form of ferritin (Bratic & Nils-Larsson, 2013; Ganz & Nemeth, 2015; Kandola et al., 2015; Knutson et al., 2017; Dev & Babitt, 2017). Systemic iron regulation is mainly controlled by the liver derived hormone, hepcidin (Ganz & Nemeth, 2015; Knutson et al., 2017). When plasma levels and hepatic stores of iron are high, absorption of iron from the diet is blocked, hepcidin synthesis is increased and hepcidin binds to ferroportin which results in the degradation of ferroportin and reduced export of iron into the plasma, which traps iron in enterocytes and macrophages (Ganz & Nemeth, 2015). Whereas when iron levels are low, there is downregulation of hepcidin and cellular absorption of iron at the gut is activated (Ganz & Nemeth, 2015; Knutson et al., 2017). Apart from the systemic regulation of iron, individual cells have distinct regulatory mechanisms to maintain iron homeostasis based on their individual requirements (Ganz & Nemeth, 2015; Knutson et al., 2017). Yet, most cells obtain iron from the extracellular fluid *via* endocytosis of the transferrin-transferrin receptor complex (Critchton et al., 2002; Garrick & Garrick 2009; Dev & Babitt, 2017). Levels of transferrin and other proteins involved in cellular iron uptake are controlled by iron-responsive element-binding proteins IREB1 and 2 (Ganz & Nemeth, 2015). In response to cellular iron deficiency, activated IREBs bind to mRNA iron response elements (IREs) to regulate the stability and translation of mRNA in order to increase the release of iron from

cytoplasmic ferritin and increase cellular uptake of iron (Ganz & Nemeth, 2015). These mechanisms of iron homeostasis are not dissimilar to that of the brain.

1.2.2. Brain iron homeostasis

Although the brain is known to be an organ with a particularly high concentration of iron, the mechanisms by which iron passes the BBB are still not fully understood (Knutson et al., 2004; McCarthy & Kosman, 2012; Jiang et al 2017). Brain microvascular endothelial cells (BMVECs), astrocytes and pericytes are the three main cellular components of the BBB and together form tight junctions which prevent the uptake of polar molecules from blood (Abbott et al., 2006; Rouault & Cooperman, 2006; McCarthy & Kosman, 2015). Most molecules that can pass the BBB are trafficked transcellularly *via* transport proteins (receptor-mediated or absorptive transcytosis) mainly because BMVECs are not fenestrated and possess tight junctions unlike peripheral vascular endothelial cells which are fenestrated and allow passage of polar molecules. (Abbott et al., 2006; Rouault & Cooperman, 2006). The morphological structure of the BBB results in two clear membranes, one on the blood side (the apical membrane), the other on the brain side (the basal membrane) (McCathy & Kosman, 2015). Located basolaterally to the BMVECs are the astrocytes which are supporting glial cells that protect neurons from oxidative damage (Iadecola, 2004; Oide et al., 2006). Using a human BMVEC cell line, McCarthy & Kosman (2014) showed that efflux of iron from BMVECs is regulated by astrocytes which secrete agents such as ceruloplasmin (Cp) or hepcidin to enhance or reduce iron efflux, respectively. It has been suggested that this is part of the function of the neurovascular units (NVUs), the units of the BBB which consist of neurons linked to astrocytes and BMVECs capable of communicating in a contact-dependent manner (McCarthy & Kosman, 2015). In this theory, such astrocyte signalling is part of the NVU function to respond directly to the requirements of neurons within the NVU, modulating iron traffic across the BBB by signalling from neurons to astrocytes to BMVECs (McCarthy & Kosman, 2015).

The exact mechanism by which iron enters BMVECs is not fully described but evidence suggests that, like in the periphery, DMT1 is present on BMVECs (McCarthy & Kosman, 2015). Using an *in vitro* model of the BBB, Duck et al (2017a) showed a reduction in transferrin movement across the BBB as well as a reduction in the movement of iron across

BMVECs into the basolateral chamber following treatment with the DMT1 inhibitor, XEN602. These results support previous finding from *in vivo* studies using the Belgrade rat which reported that although there were high levels of circulating transferrin, levels of free iron and transferrin brain uptake were reduced by 85% compared to wild type rats (Farcich & Morgan, 1992; Burdo et al., 1999; Moos & Morgan, 2004). As well as DMT1, ferroportin has also been shown to be located in BMVECs, suggesting that ferroportin may be a mechanism for transporting iron out of BMVECs (Yang et al., 2011; McCarthy & Kosman, 2013). As transferrin receptors are present in BMVECs of the rat brain (Yang et al., 2011; Siddappa et al., 2002), it has been further suggested that iron cellular uptake into BMVECs occurs in the same manner as in the periphery, with endocytosis of the transferrin-transferrin receptor complex and, following acidification, the release of ferrous iron from the endosome into the cytoplasm *via* DMT-1 (McCarthy & Kosman, 2015). This is supported by the finding that ferroportin expression in bovine BMVECs was decreased by iron loading (Duck et al., 2017a). Further support for the similar mechanism of iron homeostasis in the brain as in the periphery comes from evidence that incubation of microglia, neurons and astrocytes with hepcidin decreases expression of ferroportin 1 receptors in all groups (Urrutia et al., 2013). As BMVECs have been shown to contain ferritin (Burdo et al., 2004), it is proposed that cytoplasmic ferrous iron can either be stored in ferritin or exported *via* ferroportin where it can then be taken up by neural cells of the NVU (Duck et al., 2017a). As BMVECs have a mechanism for storing iron, it has been posited the BBB may act in part as an iron reservoir which, when signalled, can release iron into the brain (Duck et al., 2017b).

It has long been evident that the brain can resist iron deficiency due to its ability to retain iron with minimal transport of iron out of the brain (Youdim et al., 1989; Bradbury et al., 1997). This is likely because the brain has the highest energy requirements of all parts of the body and iron is essential for respiration processes (Pino et al., 2017) as well as for numerous processes specific to the brain such as myelination of neurons and neurotransmitter synthesis (Youndim & Green, 1978; Hidalgo & Nunez, 2007). For example, iron is required for the synthesis of the neurotransmitter dopamine as well as its neurotransmission (Pino et al., 2017). Iron is also critical for foetal brain development with iron deficiency being associated with impaired physical and cognitive development in children (Rasmussen, 2001; Jáuregui-Lobera, 2014; Cerami, 2017). The storage of iron within

the brain could therefore be an evolutionary adaption in response to the high iron requirements in early development which may have the propensity to become maladaptive when there is an overabundance of iron in the brain. In a similar way to dopamine, iron is heterogeneously distributed throughout the brain (Hill & Switer, 1984; Rouault, 2013), with the striatum, located in the midbrain, being one of the regions with the highest levels of iron that also accumulate with normal ageing (Wayne Martin et al 1998). This is understandable since iron is highly important for dopamine synthesis and transmission and there are high concentrations of dopamine in the striatum in order to regulate movement (Pino et al., 2017). It is perhaps unsurprising considering the close relationship of iron and dopamine that iron dysregulation has been heavily implicated in PD.

1.3. Iron and PD

1.3.1. Iron dysregulation in PD

In PD there is a marked accumulation of iron in the SN, particularly in the SN pars compacta (SNpc) (Martin et al., 2008), which has been demonstrated in both post-mortem analysis of PD patient brains and by measuring iron using magnetic resonance imaging (MRI) techniques (Dexter et al., 1987; Griffiths et al., 1999; Graham et al., 2000; Wallis et al., 2008; Rossi et al., 2013). Excess free iron reacts with hydrogen peroxide *via* the Fenton reaction producing one of the most toxic reactive oxygen species (ROS), hydroxyl (Barbusinski, 2009 Bratic & Nils-Larsson, 2013; Kandola et al., 2015; Costa-mallen et al., 2017) (figure 5). This is usually common at mitochondria where iron is present for its role in respiration and hydrogen peroxide is produced as a natural byproduct of the electron transport chain (Bratic & Nils-Larsson, 2013; Kandola et al., 2015) (figure 5). It has been shown in people with PD that there are excessive levels of non-ferritin bound free iron within dopaminergic SN neurons, particularly in the mitochondria (Wypijewska et al., 2010), as well as reduced glutathione antioxidant levels which would normally convert hydrogen peroxide to water (Kandola et al., 2015) (figure 5). The catabolism of dopamine by monoamine oxidases can also produce hydrogen peroxide which can then be converted into hydroxyl in the presence of free iron (Götz et al., 2004). Increased levels of hydroxyl results in oxidative damage to proteins, lipids and DNA within cells and eventual cell death, and such oxidative stress is thought to be a major contributor to the neurodegeneration observed in PD (Gerlach et al.,

1994; Halliwell et al., 2001). This is supported by studies in animal models where intra-nigral injection of iron in rats induced a PD-like phenotype and pathology (Ben-Shachar et al., 1991). Using susceptibility weighted imaging (SWI), others have also reported that the elevated iron deposition in the SN of people with PD compared to controls was significantly correlated with motor symptoms and some non-motor symptoms such as cognitive, sleep and autonomic issues (Liu et al., 2017). Furthermore, using 6-hydroxydopamine (6-OHDA), a toxin commonly used to induce PD-like neurodegeneration in animal models, iron chelators have been shown protect against neurotoxic effects (Youdim et al., 2004). Similarly, in patients, recent clinical trials of the iron chelator deferiprone (DFP) showed that DFP was able to reduce iron levels and that this was correlated with a decrease in the Unified Parkinson's Disease Rating Scale (UPDRS) score for motor symptoms, a clinical rating scale used to measure PD symptom severity (Devos et al., 2014).

Normally, most iron in the SN is bound to ferritin (Gałązka-Friedman et al., 1996) and compared to the liver, there is a higher ratio of heavy chain/light chain ferritin in the SN (Gałązka-Friedman et al., 2005). In the early stages of PD there is an increase in striatal ferritin accumulation which has been suggested to be involved in the motor dysfunction seen in people with PD (Videl et al., 2004; Oakley et al., 2007; Simmons et al 2007). Light chain ferritin is involved in storing iron within the shell of ferritin, and in PD patients, although there can be elevated overall levels of ferritin, there is decreased light chain ferritin within the SN (Levi et al., 1994). A reduction in light chain ferritin may allow easier efflux of free iron from ferritin stores which can then be utilised in the Fenton reaction (Koziorowski et al, 2007). It has been shown in PD patients that there are increased ferritin and free iron levels as well as reduced levels of neuromelanin and a marked loss of pigmented dopaminergic neurons in the SN (Gerlach et al., 2006; Lotfipour et al., 2012). In the SN, neuromelanin acts as a non-ferritin store of iron, accounting for roughly 20% of iron within this region (Fasano et al., 2006). Due to decreased levels of neuromelanin in PD patients, it has been suggested that as well as increased release of free iron from ferritin, there is also elevated release from neuromelanin stores (Costa-Mallen et al 2017).

Further evidence suggesting that the elevated levels of iron in PD are involved in the neurodegenerative process comes from the hereditary disease aceruloplasminemia (Costa-Mallen et al 2017). Aceruloplasminemia is an autosomal recessive condition resulting from a

mutation that causes absence or dysfunction ceruloplasmin, a ferroxidase enzyme involved in brain iron regulation (Levi et al., 2014). Such dysfunction in ceruloplasmin causes accumulation of iron in astrocytes resulting in cell death and similar motor symptoms to PD (Levi et al., 2014). Ceruloplasmin activity has also been shown to be reduced in the SN of PD patients (Hochstrasser et al., 2004) and, in PD mouse models, infusions of ceruloplasmin peripherally reduce neurodegeneration (Ayton et al., 2013). Taken together, this suggests that reduced activity of ferroxidases contributes to the accumulation of iron (Costa-Mallen et al 2017) and therefore the neurodegeneration observed in PD.

Although there is much evidence to suggest that there are elevated levels of iron in the SN of PD patients, results from a three year follow up study showed that whilst iron is accumulated in the SNpc, over the same three-year period a reduction in iron levels was observed in the white matter (Ulla et al., 2013). Lowered iron levels in other brain regions have also been found in post-mortem PD brains, with significantly lower iron in the temporal cortex of PD patients compared to controls which has been associated with a reduction of ferroportin, DMT1 and transferrin receptors (Yu et al., 2013). Furthermore, numerous studies have indicated that there are lowered serum levels of iron, (Logroscino et al., 1997; Costa-Mallen et al., 2015), ferritin, transferrin, and iron saturation of transferrin in people with PD compared to controls (Logroscino et al., 1997). In line with this, a reduced risk of developing PD has been associated with genetic mutations resulting in elevated levels of iron within the blood (Pichler et al., 2013), and anaemia (defined as low haemoglobin levels) has been positively correlated with an increased risk of PD (Savica et al. 2009). As iron deficiency is the most common cause of anaemia this suggests that despite having elevated iron in the SN, people with PD may have iron deficiency in the rest of the body. Collectively, such evidence suggests that there may be a systemic dysregulation of iron homeostasis in people with PD (Costa-Mallen et al 2017).

Recent studies have provided further evidence supporting the hypothesis of systemic iron deficiency in PD regardless of there being iron accumulation in the SNpc. Pino et al (2017) mimicked iron deficiency in mice by restricting dietary intake of iron for 30 days which lowered iron and ferritin levels in the liver and serum. Such restriction of dietary iron also affected iron metabolism in the brain, with levels of ferritin being reduced in the hippocampus but increased in the striatum (Pino et al., 2017). This supports similar findings

from Erikson et al (1997), where iron levels were observed to be low in the hippocampus but not in the striatum of rats deficient in dietary iron. Interestingly, it has been shown in multiple studies that an iron deficient diet results in lowered levels of dopamine and metabolites of dopamine in the striatum but not in the hippocampus (Pino et al., 2017; Matek et al., 2016; Unger et al., 2014) which could be a result of the elevated iron levels in the striatum leading to oxidative stress in this region. These findings suggest that the striatum has a distinct ability to counter iron deficiency by increasing ferritin expression and therefore the storage of iron (Pino et al., 2017), which may ultimately lead to excess iron that contributes to the dopaminergic neuronal death evident in PD.

1.3.2. Iron-induced oxidative stress and mitochondrial dysfunction in PD

Oxidative stress and mitochondrial dysfunction are common features of SN dopaminergic neurons in PD, and both have been linked with genetic mutations associated with PD (Schapira, 2007; Barodia et al 2017). However, mitochondrial dysfunction and oxidative stress were implicated in the pathogenesis of PD before genetic forms were identified, as it had been shown that there is partial inhibition of mitochondrial complex 1 activity in the brain, platelets, and skeletal muscles of people with idiopathic PD (Krige et al., 1992; Yoshino et al., 1992). Furthermore, neurotoxins such as rotenone and 1-methyl-4-phenyl-1, 2, 3, 6-tetrahydropyridine (MPTP), that induce a form of parkinsonism in humans, primates and rodents, act by partially inhibiting mitochondrial complex 1 resulting in increased production and accumulation of ROS (Langston, 1987; Jenner & Olanowm, 1996; Zhou et al., 2008; Camilleri & Vassallo, 2014; Gautier et al., 2014; Moon & Paek, 2015). ROS generated under such conditions have been shown to act in a feed-forward manner as both an effect and cause of mitochondrial dysfunction.

As mentioned above, oxidative stress can be defined as damage to proteins, lipids and DNA as a result of toxic oxygen free radicals, ROS (Tutar et al., 2013). Dysregulated levels of iron resulting in excessive iron accumulation or 'iron overload' catalyses hydrogen peroxide into the highly reactive hydroxyl radical *via* the Fenton and Haber-Weiss reactions (Barbusinski, 2009; Thomas et al., 2009; Bratic & Nils-Larsson, 2013) (figure 5).
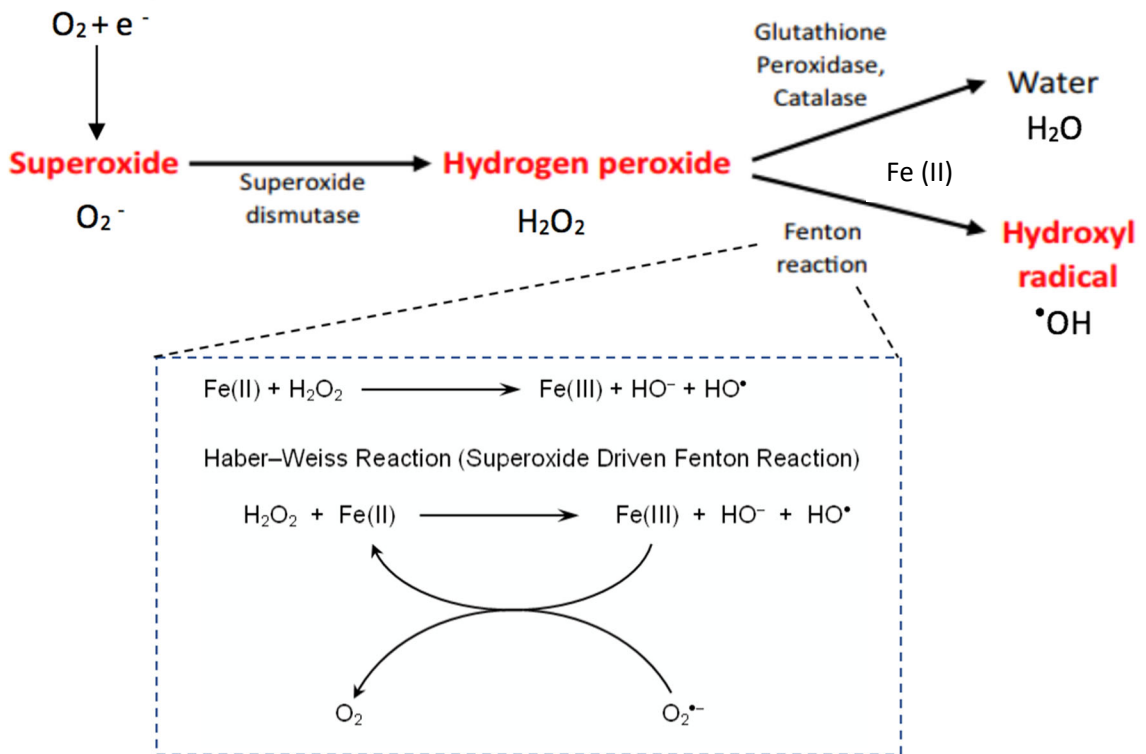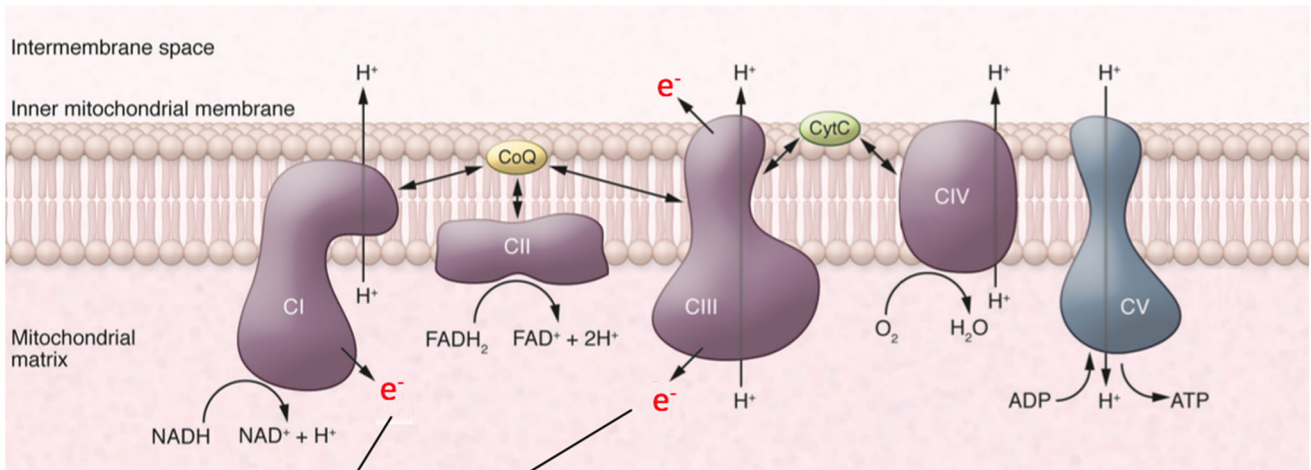
Figure 5. A schematic diagram of the mitochondrial electron transport chain and the generation of ROS adapted from Bratic & Nils-Larsson (2013), Kandola et al (2015) and Barbusinski (2009). Oxidative phosphorylation conducted by the four respiratory chain complexes (CI–CIV) and ATP synthase (CV) located in the inner mitochondrial membrane generates adenosine triphosphate (ATP). The electron transfer from reduced nicotinamide adenine dinucleotide (NADH) and reduced flavin adenine dinucleotide (FADH$_2$) to oxygen (O$_2$) releases energy which is used to pump protons (H$^+$) via complexes CI, CIII, and CIV. ATP production is driven by the proton gradient across the inner mitochondrial membrane via CV. Reactive oxygen species (ROS) are a natural by-product of oxidative phosphorylation. Superoxide is generated by leakage of free electrons (e$^-$) from CI and CIII. Cells are protected against oxidative damage by a variety of endogenous antioxidant enzymes that convert ROS into less harmful by-products. Superoxide is converted to hydrogen peroxide by manganese-containing superoxide dismutase. Hydrogen peroxide is then converted to water, mainly by glutathione peroxidase, which is the most abundant mitochondrial peroxidase. However, in the presence of free ferrous iron (Fe(II)), hydrogen peroxide can be converted to the highly reactive hydroxyl radical via the Fenton reaction. (CytC = cytochrome C; CoQ = coenzyme Q10; Fe (III) = ferric iron; HO$^-$ = hydroxide).

Sustained hydroxyl formation can occur at mitochondria as the precursors and catalysts for the Fenton reaction are co-located within the mitochondrial matrix (Thomas et al., 2009). Superoxide is an example of a ROS which is generated during adenosine triphosphate (ATP) formation *via* oxidative phosphorylation in the mitochondria (Bratic & Nils-Larsson, 2013; Kandola et al., 2015; Zhu et al., 2015), and hydrogen peroxide is formed from superoxide by manganese-containing superoxide dismutase (Thomas et al, 2009; Bratic & Nils-Larsson, 2013) (figure 5). Although these ROS are natural by-products of this essential process of aerobic respiration (of which antioxidant enzymes can usually cope), under conditions of persistent ROS production, during mitochondrial dysfunction and iron overload, enzymes that usually remove ROS can become overwhelmed.

Mechanisms underlying mitochondrial iron overload in PD appear to be linked to reduced mitochondrial iron-sulfer cluster synthesis and concomitant induction of transferrin receptor 2 expression. Reduced iron-sulphur cluster synthesis can result from inhibition of mitochondrial complex 1, which is present in PD (Krige et al., 1992; Yoshino et al., 1992). Mitochondrial complex 1 inhibition using rotenone has been shown to reduce iron-sulphur cluster synthesis, content, and activity of iron-sulphur cluster-containing enzymes (Mena et al., 2011). Transferrin receptor 2 has been found in mitochondria of dopaminergic neurons in the human SN and the transferrin-transferrin receptor 2 pathway has been shown as a mechanism to deliver iron directly to mitochondria complex 1 to be utilised in iron containing proteins (Mastroberardino et al., 2009). The transferrin-transferrin receptor 2 pathway is likely initiated in an attempt to mitigate the reduction in iron-sulphur cluster content and synthesis apparent in PD. However, this pathway is redox-sensitive and the excessive ROS production, caused by incomplete electron transfer as a result of complex 1 inhibition in PD, can oxidise transferrin thiols to disulfides as shown by rotenone models of PD (Mastroberardino et al., 2009; Horowitz et al., 2010). This leads to the accumulation of oxidised transferrin inside the mitochondria of dopaminergic neurons and eventually to the release of ferrous iron from transferrin which is then available to generate hydroxyl via Fenton chemistry (Mastroberardino et al., 2009; Horowitz et al., 2010). ROS resulting from complex 1 inhibition can also promote the release of ferrous iron directly from iron-sulphur cluster proteins in the mitochondrial respiratory chain (Horowitz et al., 2010; Zucca et al.,

2017). Together such accumulation of highly reactive ferrous iron within mitochondria results in sustained mitochondrial hydroxyl formation.

Located within all cells, mitochondria are double membraned organelles which are essential for energy production *via* oxidative phosphorylation (Da Poian, 2000). Each mitochondrion contains two – ten replicates of the mitochondrial genome and there are multiple copies of mitochondria within a single cell (Youle et al., 2012). ATP, the energy source for all cells, is generated *via* oxidative phosphorylation, enabled by the electron transport chain located on the mitochondrial inner membrane (Elston et al., 1998; Birch-Machin, 2006; Birch-Machin & Swalwell, 2009; Bratic & Nils-Larsson, 2013) (figure 4). The electron transport chain consists of five complexes of proteins, complexes 1 and 2 utilise products from glycolysis and the kreb/TCA cycle (the previous stages of aerobic respiration) such as nicotinamide adenine dinucleotide (NADH) and flavin adenine dinucleotide (FADH) (Birch-Machin, 2006; Bratic & Nils-Larsson, 2013) (figure 5). During this process, NADH and FADH are oxidised which releases electrons that are then transferred through each protein complex down the electron transport chain (Birch-Machin, 2006; Bratic & Nils-Larsson, 2013; Kandola et al., 2015) (figure 5). Although essential for all living cells, mitochondria are also the principal site for ROS generation, with mitochondria being the site of 90% of total cellular ROS production (Barbusinski, 2009; Bratic & Nils-Larsson, 2013; Kandola et al., 2015). During oxidative phosphorylation, free electrons leak from the protein complexes of the electron transport chain, when these electrons combine with molecular oxygen, superoxide radicals are generated (Birch-Machin, 2000; Birch-Machin, 2006) (figure 5). It is common for superoxide to be generated as a by-product of this process and therefore there are well established defence mechanisms to minimise oxidative stress following ROS generation (Bratic & Nils-Larsson, 2013; Kandola et al., 2015). As well as endogenous antioxidants, such as superoxide dismutase, glutathione peroxidase and catalase, which counter ROS (figure 5), toxic products such as ROS can be transferred to a single mitochondrion within the cell *via* fission-fusion and this mitochondrion can then be targeted for destruction by mitochondrial specific autophagy (mitophagy), to prevent widespread damage to mitochondria within the cell (Youle et al., 2012). As well as the elimination of dysfunctional mitochondria, it is thought that low level ROS production also promotes mitochondrial biogenesis and repair mechanisms for dysfunctional mitochondria, however as mitochondria are the primary site

for oxidative damage, high levels of ROS can lead to the accumulation of damaged mitochondria (Jiang et al., 2017). Following high level ROS production, the accumulation of mitochondrial dysfunction can prevent proper signalling for mitophagy which in turn increases ROS production and decreases ATP production eventually resulting in cellular apoptosis and necrosis (Kroemer & Reed, 2000; Simpkins & Dykens, 2008; Jiang et al., 2017).

This phenomenon is particularly highlighted in forms of autosomal recessive familial PD where there is loss of function in the genes encoding Parkin and PINK1 (Barodia et al., 2017). Parkin, an E3 ubiquitin ligase, and PINK1, a mitochondrial-targeted kinase, function together to induce mitophagy and remove dysfunctional mitochondria (Narendra et al., 2008; Matsuda et al., 2010). Loss of function of PINK1 and/or Parkin results in an accumulation of mitochondrial dysfunction, ROS production and eventual dopaminergic neuronal death as seen in patients with PINK1 and parkin mutations (Barodia et al., 2017). Parkin has also been implicated in sporadic PD as it is extremely sensitive to oxidative stress (Greene et al., 2005). This has been highlighted in brain analysis of sporadic PD patients where oxidative damage to parkin has been observed (Chung et al., 2004; Yao et al., 2004). Oxidative damage to parkin can inactivate parkin, therefore it has been suggested that oxidative stress and the resulting parkin loss of function in dopaminergic neurons may contribute to the onset and/or progression of idiopathic PD (LaVoie et al., 2005).

The most toxic cellular ROS is hydroxyl (Critchton & Ward, 2013; Dlouhy & Outten, 2013), it can cause a range of DNA lesions either by directly damaging both nuclear and mitochondrial DNA (Melis et al, 2013) or altering DNA expression *via* epigenetic processes (Kwok, 2010). It can also cause protein carbonylation by modifying amino acid residues (Dalle-Donne et al 2003a, b). This has been linked with functional alterations in both structural and enzymatic proteins which inevitably lead to the removal or accumulation of the altered protein, both of which can be extremely catastrophic to cells (Dalle-Donne et al 2003a). As well as its affects on DNA and proteins, in lipids hydroxyl can promote peroxidation of the polyunsaturated fatty acids in membranes resulting in membrane alterations, leakage and eventually functional loss of membranes (Catala, 2009). Lipid peroxidation is particularly detrimental because it forms secondary aldehyde by-products which are also highly reactive, like ROS these can cause irreversible modifications resulting in loss or impaired function of phospholipids, proteins, and DNA (Dalle-Donne et al., 2003a,

b; Perluigi et al., 2012). Although, elevated levels of iron induce hydroxyl formation, excessive ROS can also promote the release of iron from iron-sulphur cluster proteins in the mitochondrial respiratory chain (Zucca et al 2017). This increase in free iron within the mitochondria is then available to be utilised in the Fenton reaction perpetuating the formation of hydroxyl resulting in a continuous cycle of damaging oxidative stress (Zucca et al., 2017).

The brain is the organ which requires the most intensive oxidative metabolism, brain cells are therefore particularly sensitive to ROS due to their propensity to generate large amounts of ROS from the high levels of oxidative phosphorylation necessary to meet its energy demands (Jiang et al., 2017). In normal conditions, there are elevated basal levels of oxidative stress in the SN and this is markedly increased in PD (Jiang et al., 2017). The increased levels of free iron in dopaminergic neurons found in PD can result from the release of iron from ferritin, haem proteins (e.g. haemoglobin, cytochrome c) and from iron-sulphur clusters and can result in continuous ROS production (Reif, 1992). In PD, ROS production is further heightened due to the impairment of the mechanisms for removing ROS (e.g. superoxide dismutase, glutathione peroxidase and catalase), this coupled with the excessive levels of free iron, induces ongoing oxidative stress, cell dysfunction and ultimately cell death (Kroemer & Reed, 2000; Simpkins & Dykens, 2008; Jiang et al., 2017). It has been reported that glutathione levels in the SN of people with PD are reduced by up to 40% compared to healthy controls (Sian et al, 1994). Glutathione is regulated by the nuclear factor erthroid 2-related factor 2 (Nrf2) – Kelch-like ECH-associated protein 1 (Keap1) pathway which is responsible for regulating the expression of many of the endogenous antioxidants (Magesh et al., 2012). In normal conditions, when ROS is present, Nrf2 becomes active causing it to dissociate from Keap1 and translocate to the nucleus so it can bind to the antioxidant response element (ARE) in the promotor region of antioxidant genes (Nguyen et al., 2009). As well as the resulting upregulation of genes involved in antioxidant production, this process has also been shown to promote the expression of genes involved in mitochondrial protection (Lee & Johnson, 2004; Petri et al., 2012). In PD, there is a reduction in Nrf2-Keap1 signalling resulting in lowered levels of antioxidant defences (Bavarsad Shahripiour et al., 2014). In sporadic PD, it is thought that the reduced Nrf2-Keap1 signalling and marked reduction in glutathione may be a result of the existing iron-induced

oxidative stress and mitochondrial dysfunction (Bavarsad Shahripiour et al., 2014) and that this vicious cycling combination likely promotes the progressive nature of the disease.

1.3.3. Iron and inflammation in PD

Active inflammatory processes are another hallmark of PD (Hunot & Hirsch 2003; Ong & Farooqui, 2005; Cahill et al., 2009; Sian-Hulsman et al., 2011, von Bernhardi & Eugenin, 2012) that are also associated with elevated levels of iron. In the brain, inflammation is mediated by the secretion of inflammatory cytokines such as interleukin (IL)-1, IL-6, and tumour necrosis factor (TNF)-α from microglia and astrocytes (Kaushal & Schlichter, 2008; Smith et al., 2012). Post-mortem studies have shown that people with PD have elevated levels of IL-1β, IL-2, IL-4, IL-6 and TNF-α (Mogi et al., 1994a, b, 1996). Such proinflammatory cytokines have been shown to regulate DMT1 expression in numerous cell types, for example the expression of DMT1 is upregulated by TNF-α, increasing iron uptake into bronchial epithelial cells (Wang et al, 2005; Paradka & Roth, 2006; Hanke & Kielian 2011; Wajant & Scheurich, 2011). Moreover, during infection conditions, inflammatory cytokines have been shown to stimulate hepcidin synthesis (Wrighting & Andrews., 2006; Gnana-Prakasam et al., 2008; Frazier et al., 2011; Ganz & Nemeth., 2012). In studies using aged rats, microglia activation, ferritin expression and total iron content were increased following injections of the inflammatory stimuli lipopolysaccharide (LPS) into the striatum (Hunter et al., 2008). Urrutia et al (2013) also found that inflammatory stimuli increased the expression of DMT1 in neurons, astrocytes and microglia as well as increasing the expression of hepcidin in astrocytes and microglia but not in neurons. Taken together, such evidence suggests that inflammatory processes have a key role in iron homeostasis.

Although there is much evidence to suggest that inflammatory processes regulate iron levels in the body and the brain, when microglia are cultured with excess iron, there is increased nuclear factor kappa-light-chain-enhancer of activated B cells (NF-κB) excretion of inflammatory cytokines within the microglia (Saleppico et al., 1996). This suggests that iron accumulation can also enhance the toxic effects of inflammatory cytokines (Urrutia et al., 2013). Other *in vitro* studies have also shown that microglia are activated in response to elevated iron levels and release free radicals including superoxide, hydrogen peroxide and nitric oxide as well as inflammatory factors such as IL-1β, TNF-α and prostaglandin, all of

which can contribute to the progressive dopaminergic neurodegeneration apparent in PD (Zhang et al., 2014). Liu et al (2017) investigated iron levels and inflammatory factors in people with PD compared to controls using SWI and by measuring iron metabolism related proteins and inflammatory factors in cerebral spinal fluid (CSF) and serum. As described in previous studies, results showed that the SN was the main region of excess iron deposition in both PD patients and controls, however in the PD group ferritin levels were significantly elevated in the CSF and reduced in the serum compared to controls (Liu et al., 2017). This was correlated with increased levels of IL-1β in the CSF, suggesting that IL-1β is an inflammatory cytokine produced by excess iron in the SN (Liu et al., 2017). As there is a clear relationship between the characteristic inflammation of PD and elevated iron in the SN, this further cements the importance of iron dysregulation in the pathology of PD.

1.3.4. Iron and protein misfolding and aggregation in PD

Iron accumulation has also been implicated in one the most widely acknowledged pathological features of PD, the presence of Lewy pathology; Lewy bodies and Lewy neurites which are intra neural protein inclusions within cell bodies and axons, respectively (Hare & Double, 2016; Brundin et al., 2017). Such protein inclusions are primarily the accumulation of abnormal, misfolded aggregations of α-syn, the non-amyloid component of the amyloid precursor protein (Hare & Double, 2016; Chan et al., 2017). Evidence of the involvement of α-syn in the pathogenesis of PD stems back to over 50 years ago where post-mortem analyses of PD brains showed accumulation of α-syn and Lewy pathology (Duffy & Tennyson, 1965; Forno & Norville 1976; Watanebe et al., 1977; Hayashida et al., 1993). Since then, the discovery of the association of point mutations and multiplications of the α-syn gene (SNCA), resulting in misfolding and excessive production of α-syn with increased risk of PD, has further implicated α-syn in PD (Chan, 2017). Although α-syn aggregation seems to be involved in PD pathology, SNCA mutations are rare and so α-syn is unlikely to be the sole contributor to degeneration in PD (Double & Hare 2016).

α-syn is mainly localised in the presynaptic terminals of neurons and accounts for about 1% of total protein in neurons, however the exact role of α-syn is unclear (Brundin et al., 2017). It has been shown that there is an IRE on the unsaturated 5' region of α-syn mRNA and therefore it has been suggested that α-syn may be involved in intracellular iron homeostasis

(Friedlich et al., 2007). Double & Hare (2016) suggest that α-syn might play a role in iron storage and binding and that, like other endogenous iron chelators, there may be leakage of free iron as α-syn iron binding sites become saturated. In normal conditions α-syn is a soluble, unfolded monomer usually bound to synaptic vesicle membranes (Brundin et al., 2017). Whereas in pathological conditions, like in PD, α-syn misfolds forming insoluble amyloid fibrils which can then aggregate together (Brundin et al., 2017). Due to its presence on vesicles containing neurotransmitters, it has been suggested that α-syn could also be involved in packaging dopamine into vesicles, and that mutations or misfolding of the protein may result in gradual leakage of reactive dopamine into the cytoplasm (Lotharius & Brundin, 2002). Such dopamine can be readily oxidised or react with free iron; both these effects result in toxic dopamine species which can cause irreversible damage to cells (Lortharis & Brundin, 2002; Asanuma et al., 2003). As α-syn aggregation has also been shown to occur mainly in the presence of iron and dopamine (Ostrerova-Golts et al., 2000), it has also been suggested that other PD-specific molecular events are required to trigger misfolding and aggregation such as, oxidative stress, mitochondrial dysfunction, lysosomal dysfunction and inflammation (Chan et al, 2017).

It has been shown that abnormal accumulation of free iron leads to aggregation of α-syn (Golts et al 2002; Das et al., 2010), and it is thought that the ability of free iron to induce oxidative stress by generating free radicals could lead to such aggregation (Zecca et al., 2004; Belaidi & Bush, 2015). It has also been proposed that oxidation by iron-related ROS and dopamine may result in the protein being unrecognisable to the ubiquitin-proteasome degradation pathway, leading to the formation of toxic oligomers (Anderson et al., 2004; Saha et al., 2004). Normal α-syn is degraded by both the autophagy-lysosome and ubiquitin-proteosome systems, whereas toxic oligomeric α-syn is mainly cleared by the autophagy-lysosome system (Lee et al., 2004). In PD the autophagy-lysosome system is dysfunctional and therefore clearance of toxic α-syn is impaired (Usenovic et al., 2012; Rothaug et al., 2014). It is thought that such dysregulation in α-syn clearance is a result of excess iron levels in the SN of people with PD, as it has been shown that iron inhibits the activity of lysosomal cathepsins, the main lysosomal protein involved in the degradation of α-syn in rat liver cells (Misaka & Tappel, 1971), human retinal pigment epithelial cells (Chen et al., 2009) and Nramp-deficient macrophages and microglia (Wu et al., 2017). Nramp1 (natural resistance-

associated macrophage protein 1) is a lysosomal iron transporter and its expression has recently been reported to be increased in post-mortem striatum tissues of people with PD, compared with controls (Wu et al., 2017). This may be because Nramp1 expression is known to be up-regulated in response to infection, inflammation (Govoni et al., 1997) and hypoxia (Bayele et al., 2007) which have all been implicated in PD pathology. In addition, due to mitochondrial dysfunction there is also decreased expression of vacuolar H+-ATPase in PD (Werner et al., 2008) and it is this pump that drives the proton gradient of lysosomes (Ohkuma et al., 1982), suggesting that mitochondrial dysfunction in PD may lower the acidity of lysosomes leading to a reduced efflux of Nramp1-mediated iron (Wu et al., 2017). Therefore, the increased expression of Nramp1 in brain tissues of PD patients might be a compensatory protective response against increased toxic α-syn resulting from insufficient Nramp1-mediated iron efflux (Wu et al., 2017). Evidently, there is accumulating evidence to suggest that iron and iron-induced oxidative stress are involved in α-syn aggregation and therefore PD pathology.

Although α-syn has recently been suggested to be involved in normal axonal transport (Toba et al., 2017), such aggregation of toxic oligomeric α-syn evident in PD has been shown to result in axonal transport dysfunction (Volpicelli-Daley, 2017). Data suggests that axonal transport defects precede degeneration in PD (Chung et al., 2009; Chu et al., 2012; Lamberts et al., 2015) and this may be a result of iron associated aggregation of α-syn. In PD, α-syn aggregates in axon terminals are associated with accumulation of synaptic vesical proteins (Galvin et al., 1999). Further evidence for the role of axonal transport dysfunction in PD comes from the finding that molecular motor levels that are associated with axonal transport are lowered in PD brains (Chu et al., 2012). For example, kinesin (an enabler of anterograde axonal transport from the soma to presynaptic terminals), has been shown to be reduced in the SNpc of PD brains before loss of dopaminergic neurons (Volpicelli-Daley, 2017). Furthermore, Chu et al (2012) found a reduction in the abundance of motor proteins in neurons containing α-syn aggregates, which also suggests that toxic α-syn aggregates induce alterations in motor proteins effecting axonal transport that precedes neurodegeneration in PD.

In late stage PD, retrograde axonal transport has also been shown to be reduced (Volpicelli-Daley, 2017). Studies using neurotoxin models of PD such as MPTP and 6-OHDA have shown

that the neurotrophic factors glial cell-derived neurotrophic factor (GDNF) and neurturin protect against neurodegeneration, however clinical trials of neurtrin failed to produce significant benefits (Olanow et al., 2015) and similar trials of GDNF have had limited success (Volpicelli-Daley, 2017; Whone et al., 2019). Impaired axonal transport may have contributed to the inability of neurotrophic factors to promote neuronal survival and enhance outgrowth. This is because axonal transport of neurotrophin receptors in signalling endosomes is required to deliver signalling molecules to the neuronal soma where they can translocate to the nucleus and activate gene transcription factors important for neuronal differentiation and survival (Volpicelli-Daley, 2017). Disrupted axonal transport likely impairs signalling of growth factors which may contribute to degeneration in PD. For example, the formation of Lewy neurite-like inclusions in neurons can impair the transport of the neurotrophin receptor tropomyosin receptor kinase B (TrKB) causing an accumulation of signalling molecules in the cytoplasm (Volpicelli-Daley et al., 2014). This is supported by the finding that GDNF treatment was not protective in the AAV α-syn model of PD suggesting that pathogenic α-syn disrupts neurotrophic signalling (Decressac et al., 2011; Decressac et al., 2012). Whereas, overexpression of the nuclear receptor related 1 protein, Nurr1, has been shown to be protective in α-syn models and this is likely because direct expression of Nurr1 in the nucleus does not require retrograde transport of the GDNF ret receptor (Volpicelli-Daley, 2017). Retrograde transport dysfunction may also be implicated in other aspects of PD as it is responsible for transporting degradative organelles such as endosomes and autophagosomes, which are required for targeting proteins and damaged organelles for degradation in the lysosomes located in the soma (Maday & Holzbaur, 2016). Therefore, impaired retrograde transport may prevent targeting of toxic α-syn aggregates as well as dysfunctional mitochondria to lysosomes (Sacino et al., 2016), highlighting another toxic cycle of disease pathology in PD.

Together this evidence suggests that iron-related aggregation of α-syn can lead to axonal transport dysfunction and that this may be an early event in PD pathogenesis as well as involved in the ongoing progression of the disease.

1.3.5. Iron and dopamine in PD

As previously described, PD is characterised by the loss of dopaminergic neurons which regulate voluntary movement, located in the SN of the brain (Lees et al., 2009). Clearly iron plays a role in such dopaminergic neuronal loss, through its involvement in oxidative stress, mitochondrial dysfunction, inflammation and α-syn aggregation. Although overall dopamine levels are low in the SN of people with PD, dopamine can also be neurotoxic as it can be readily oxidised by non-enzymatic reactions generating reactive molecules such as dopamine quinone (Lortharis & Brundin, 2002; Asanuma et al., 2003). Similar to how the abnormal accumulation of free iron leads to aggregation of α-syn (Golts et al 2002; Das et al., 2010), oxidative dopamine metabolites are also known to promote aggregation of toxic oligomergic α-syn (Lortharis & Brundin, 2002; Yamakawa et al., 2010). Many of the neurotoxic species produced from dopamine metabolism are dependent on iron (Hare et al., 2014). Vesicular dopamine metabolites are usually protected against oxidation in neurons which have a high concentration of iron as the formation of toxic dopamine metabolites primarily occurs in the cytoplasm (Exner et al., 2012). However, in the SN the end-product of dopamine metabolism is neuromelanin following the conversion of dopamine to o-quinones (Zucca et al., 2015), and neurotoxic intermediates can be formed by iron-facilitated reactions with o-quinones (Hare & Double, 2016). Unlike the SN, there are some regions of the brain that are affected by PD (highlighted by α-syn pathology) that do not result in catastrophic neuronal loss despite evident elevated iron levels (McCann et al., 2015), suggesting that additional factors are required to induce such devastating neurodegeneration.

Hare & Double (2016) suggest the major difference in the SNpc, resulting in the marked degeneration of dopaminergic neurons, is the interaction between iron and dopamine to produce neurotoxic species specific to this region. In the SNpc, dopamine is thought to be oxidised by iron and oxygen to form dopamine quinone and 6-OHDA, the commonly used neurotoxin for PD models (Hare et al., 2013). In the presence of ROS, which are elevated in PD in response to excess iron, quinones can promote protein oxidation by alkylating thiol and amine groups and such changes disrupt the integrity of the cell membrane, eventually resulting in cell death (Hare & Double, 2016). 6-OHDA, the other by-product of iron-induced oxidation of dopamine, can form ROS and potentially inhibit mitochondrial complex 1 and 4

(Glinka et al., 1997). Therefore, elevated levels of 6-OHDA can result in the loss of structural integrity of mitochondria leading to mitochondrial dysfunction, a reduction in ATP production and eventual cell death.

It has also been suggested that in the presence of hydrogen peroxide, the reduction of ferric iron to ferrous iron in SNpc dopaminergic neurons results in the formation of a dopamine-iron complex intermediate which produces hydroxyl (Pezzella et al., 1997). The intermediate complex is thought to be an unstable 6-OHDA quinone which has been supported by *in vitro* studies showing that unlike iron chelation with Ethylenediaminetetraacetic acid (EDTA), antioxidant enzymes and radical scavengers do not influence 6-OHDA production (Hare & Double, 2016). 6-OHDA has also been shown to free iron from ferritin (Monteiro & Winterbourn 1989; Double et al., 1998), increasing the labile pool of iron available for use in Fenton reactions, creating a cycle that can overwhelm the compensatory endogenous antioxidant mechanisms (Hare et al., 2013). The reaction between iron and dopamine can therefore not only produce toxic radicals directly but also indirectly exacerbate iron-induced oxidative stress and together promote neurodegeneration in PD.

Overall, it is clear that the accumulation of iron in the SNpc in PD is associated with multiple mechanisms of the disease. Finally, with the recent discovery of ferroptosis, the non-apoptotic iron-mediated cell death pathway, iron has been further implicated in the neurodegeneration process of PD (Hare & Double, 2016). Interestingly, the antioxidant glutathione peroxidase 4 has been shown to inhibit the ferroptosis pathway (Dixon et al., 2012). Glutathione peroxidase 4 is significantly reduced in the SN of PD patients compared to controls and may be partly responsible for the accumulation of hydroxyl radicals as glutathione peroxidases are responsible for the reduction of hydrogen peroxide into water *via* the oxidation of reduced glutathione (Bellinger et al., 2011). Mitochondrial glutathione peroxidase 4 is covalently modified by dopamine quinone (Hauser et al., 2013). This inactivates its activity, compromising both its ability to scavenge free radicals and inhibit ferroptosis (Hare & Double, 2016). In mouse models, genetic ablation of glutathione peroxidase 4 initiates rapid degeneration of motor neurons (Chen et al., 2015) suggesting an inability to prevent ferroptotic cell death. Together, this evidence suggests that elevated iron in the SNpc is not only involved in most of the hallmarks of PD that are associated with

dopaminergic cell death but that iron-mediated pathways may also be directly responsible for some level of neurodegeneration seen in PD.

1.4. Research into therapeutic strategies to combat iron-induced oxidative stress in PD

Since iron and iron-induced oxidative stress are clearly implicated in the neurodegeneration seen in PD, there has been increasing research into the therapeutic benefit of iron chelators and antioxidants for PD. Several iron chelators such as DFP, deferoxamine (DFO), and deferasirox (DFX) are clinically available but are mainly utilised to treat peripheral iron overload disorders such as thalassaemia and haemochromatosis (Mobarra et al., 2016; Kontoghiorghes & Kontoghiorghes, 2020). Metal ions, including those of iron, are positively charged and can easily bind with ligands containing carbonyl, hydroxyl, or thiol groups (Kontoghiorghes & Kontoghiorghes, 2020). It is through this mechanism that iron chelators work, for example DFO has numerous hydroxyl and carbonyl groups (figure 6), and these can coordinate with ferric iron *via* the donation of electrons (Morbarra et al., 2016).
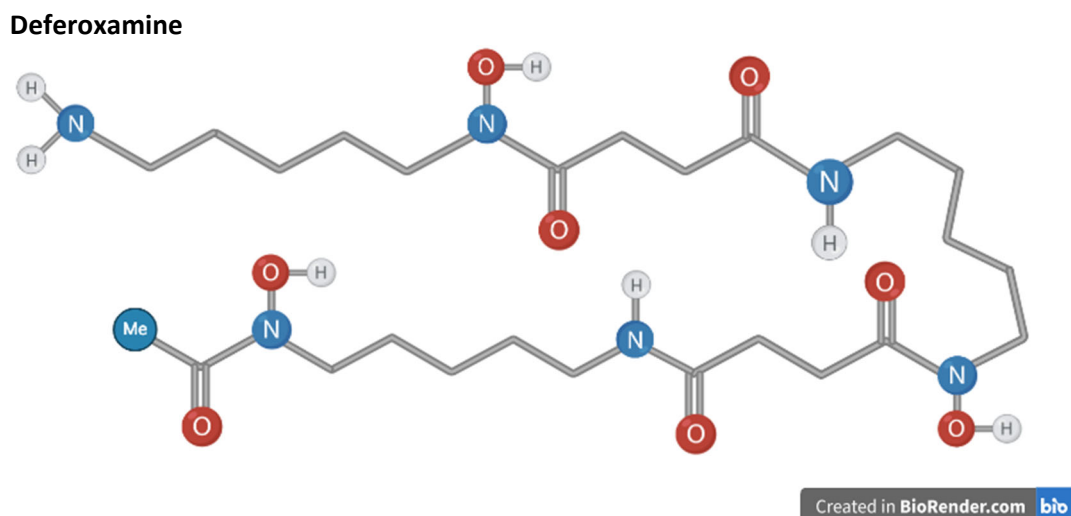
Deferoxamine

Figure 6. Chemical structure of Deferoxamine

Both DFO and DFP are able to oxidise free ferrous iron to prevent it from engaging in chemical reactions involved in ROS formation, such as the Fenton reaction, and can form a water-soluble complex with ferric iron which can then be excreted in the urine and/or faeces (Mobarra et al., 2016; National Center for Biotechnology Information, 2020).

Ward et al (1995) were the first group to demonstrate that DFP and DFO were able to remove excess brain iron in animal models of brain iron overload. Subsequently, Dexter et al (2011) showed that these chelators are neuroprotective in a 6-OHDA rat model of PD,

where neuroprotection was observed as protection of dopaminergic neuronal integrity and preservation of striatal dopamine content in the SN. Clinically, studies assessing tolerability of iron chelation have been carried out utilising DFP in Friedreich ataxia patients (Boddaert et al., 2007), where a gene mutation causes under expression of the mitochondrial protein frataxin which is involved in assembly of iron-sulphur proteins and protection of the mitochondria from iron-mediated oxidative stress (Gakh et al., 2006). This leads to the accumulation of mitochondrial iron, mitochondrial respiratory inhibition, and oxidative stress (Gakh et al., 2006). In the 6-month Friedreich ataxia study carried out by Boddaert et al (2007), DFP at 20-30mg/kg/day was well tolerated by the patients and resulted in a reduction in labile iron. Chelator treatment caused no apparent haematological or neurological side effects while reducing neuropathy and ataxic gait (Boddaert et al., 2007). These positive results in Friedreich ataxia suggest that DFP may be able to access the brain and have prompted multiple clinical trials in early-stage PD (Martin-Bastida et al., 2017; ClinicalTrials.gov, 2018a, b).

For example, Martin-Bastida et al (2017) assessed brain iron chelation by DFP for 6 months in a small phase 2 randomised double-blinded placebo controlled clinical trial in 22 people with early PD (less than 5 years since diagnosis). Overall, DFP was well tolerated by PD patients and was able to remove iron from a variety of brain regions. Although not statistically significant, the results also indicated a trend for improved motor symptoms and quality of life in patients treated with 30 mg/kg DFP (Martin-Bastida et al., 2017). Importantly, 6-months of DFP did not appear to cause a generalised lowering of iron levels in the brain and therefore did not seem to implicate other neurological functions which involve iron such as mood and cognitive processes (Martin-Bastida et al., 2017). What's more, DFP therapy seemed to be most effective in patients with low initial serum levels of iron (Martin-Bastida et al., 2017), supporting the idea that in PD when there is high iron in the SNpc, there are low levels in the serum. Nonetheless, an overall reduction in serum levels of iron was observed in patients treated with DFP (Martin-Bastida et al., 2017) which with long term use may be detrimental to those patients who already had low serum iron. Surprisingly, a reduction of iron in the SNpc following DFP treatment was only observed in three patients (Martin-Bastida et al., 2017), much lower than expected considering that the SNpc is where iron levels are significantly elevated in people with PD and has been

associated with neurodegeneration of dopaminergic neurons. It is argued by the authors that this could be because iron is tightly bound to neuromelanin in the SNpc (Sian-Hülsmann et al., 2011; Zucca et al., 2014) which is much less chelatable than iron from ferritin, and therefore longer-term use of DFP may be required to lower iron levels in the SNpc (Martin-Bastida et al., 2017). Based on such finding there are two larger long-term clinical trials of DFP currently underway to evaluate its efficacy as a disease modifying therapy for PD (ClinicalTrials.gov, 2018a, b).

Although there is accumulating evidence that iron chelation may be of benefit for PD, the rationale used by Martin-Bastida et al (2017) to explain why DFP was not successful at lowering iron in the SNpc directly conflicts with evidence suggesting that there is elevated ferritin levels and free iron in the SNpc of people with PD (Gerlach et al., 2006; Lotfipour et al., 2012). Therefore, it might be more plausible that DFP was unable to significantly lower iron in the SNpc of the majority of patients because DFP is actively metabolised following administration and as it is not targeted to that region, which is deep within the brain, it is unable to reach the SNpc at therapeutic concentrations. In line with this, although it is reported that DFP is more permeable to the BBB compared to other chelators (Ward et al., 1995), it may not be the most suitable chelator because it is much more toxic than DFO and has a risk of serious adverse side effects such as agranulocytosis and neutropenia (Galanello, 2007; Morbarra et al., 2016). Unlike DFP which is bidentate chelator that can bind ferric iron in a 3:1 ratio, DFO is a hexadentate iron chelator which forms a 1:1 DFO:ferric iron complex at physiological pH (Mobarra et al., 2016; Kontoghiorghes & Kontoghiorghes, 2020). This is advantageous because less drug is required to achieve the same effect. Although both can chelate iron from ferritin, DFO does not readily chelate iron from transferrin or haemoglobin (National Center for Biotechnology Information, 2020; Kontoghiorghes & Kontoghiorghes, 2020). As a result, DFO is far more tolerable than DFP and for this reason it remains the first line treatment for Beta-thalassemia even though it requires continuous subcutaneous injections compared to the oral administration of DFP (Morbarra et al., 2016). Therefore, if the brain penetrance of DFO could be improved it may also be more favourable for the treatment of excess iron in PD. Nevertheless, the effects of long-term continuous use of any of these chelators are unknown in PD and, due to their non-specific nature, the side effects could be serious since iron is an essential part of numerous cellular processes such as

respiration (Pino et al., 2017) and neurotransmitter synthesis (Youndim & Green, 1978; Hidalgo & Nunez, 2007).

Another approach to combat iron-induced oxidative stress is by using antioxidants to counter the ongoing production of ROS in the presence of excess free iron. One of the most widely studied antioxidants as a potential therapeutic is curcumin. Curcumin is commonly used in Chinese medicine, it is a polyphenol extract from the herb Curcuma longa L (Ammon and Wahl, 1991; Tsai et al., 2011). There are three functional groups within curcumin, two phenolic groups and one diketone moiety (Priyadarsini 2013) (figure 7). The hydroxyl groups within the structure of curcumin enables it to act as free radical chain-breaker, reacting with free radicals by donating hydrogen to ROS (Priyadarsini, 2014; Ferrari et al., 2014; Salem et al., 2014; Tu et al., 2017) (figure 7). The diketo/enol moiety of curcumin (figure 6b) is capable of accepting as well as donating hydrogen and can therefore participate in Michael addition reactions as either a Michael acceptor or donor (Dinkova-Kostova et al., 2001; Balogun et al., 2003; Priyadarsini, 2014; Ferrari et al., 2014). This is because Michael addition occurs between unsaturated ketones as acceptors and anions of hydroxyl, cysteine and selenol groups as donors (Priyadarsini, 2014).

Curcumin
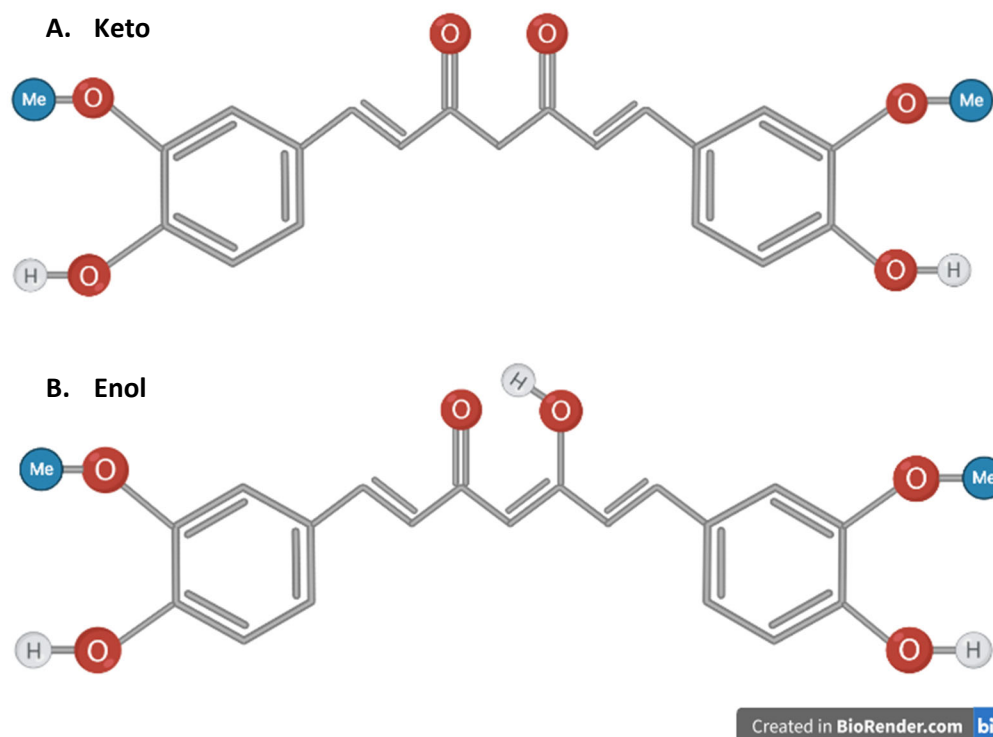
Figure 7. A. Chemical structure of Curcumin in keto form. B. Chemical structure of Curcumin in enol form.

However, it is the ability of curcumin to act as a Michael acceptor which accounts for its indirect antioxidant effects *via* the inhibition of the Keap1-Nrf2 interaction (Dinkova-Kostova et al., 2001; Balogun et al., 2003; Magesh et al., 2012; Tu et al., 2017). Michael acceptors react with the cysteine thiolate groups within keap1 which enables the dissociation of Nrf2 and translocation to the nucleus where it can induce the expression of ARE mediated endogenous antioxidant enzymes (Luo et al., 2007; Nakamura & Miyoshi, 2010; Tu et al., 2017). It is the diketone group which also accounts for the reported metal chelator properties of curcumin in its enol form; in general curcumin can bind to metals in a 2:1 ratio where the enolic proton is replaced by the metal ion and the phenolic moieties stay intact within the curcumin-metal complex (Priyadarsin, 2014) (figure 7b). It is through all these mechanisms that curcumin is thought to have potential as a therapeutic agent for PD.

In both *in vitro* and *in vivo* PD models, curcumin has been able to protect against dopaminergic neurodegeneration. For example, in a cellular rotenone-induced neurotoxin model of PD, curcumin reduced ROS and cytotoxicity as well as inhibited caspase 3 and 9 activation, preventing apoptosis (Liu et al., 2013). Similarly, in a mutant A53T α-syn cellular model of PD curcumin pre-treatment reduced cell death as well as levels of mutant α-syn (Jiang et al., 2013). In an *in vivo* drosophila model of PD, curcumin not only reduced cell death but also ameliorated PD-like symptoms (Liu et al., 2013). Furthermore, recent evidence suggests that curcumin is also protective against mitochondrial dysfunction. Van der Merwe et al (2017) showed curcumin to be protective in a PINK1 knock down model of PD; PINK1 has an intrinsic role in the removal of dysfunctional mitochondria and mutations in PINK1 result in early-onset autosomal recessive PD. Although there is supportive preclinical evidence for the benefit of curcumin as a potential therapeutic for PD, curcumin is rapidly eliminated from the body and therefore has limited retention time in circulation (Yang et al., 2007). This suggests that curcumin cannot access the brain with real therapeutic efficacy. Studies which have altered the formulation of curcumin such as encapsulation in glycerol monooleate have increased the half-life of curcumin (Mohanty and Sahoo et al., 2010). Tsai et al (2011) used a poly(lactic-co-glycolic acid) (PLGA) liposome nanoformulation, which is approved by the U.S. Food and Drug Administration (FDA) for pharmaceutical application, to encapsulate curcumin and found that these could pass the BBB and enter brain tissues such as the cerebral cortex and the hippocampus. However, the PLGA

formulations of curcumin were also found in other organs such as the spleen and the liver (Tsai et al, 2011). Zupančič et al (2014) developed a novel nanoformulation of curcumin using DQAsomes, vesicles formed from the amphiphile dequalinium (DQA), which was able to specifically target mitochondria. This is particularly beneficial since mitochondria are the main site of intracellular free radical formation (Thomas et al., 2009; Bratic & Nils-Larsson, 2013; Kandola et al., 2015; Costa-mallen et al., 2017). However, this nanoformulation of curcumin was not developed to get into the brain or treat neurodegeneration and therefore would need to be assessed in relevant PD models in order to evaluate its potential benefit for PD.

Although the bioavailability, brain penetrability and targeting of curcumin has been improved by encapsulation using different nanoformulations, these have yet to be tested in PD models. Furthermore, a nanoformulation which incorporates all the preferred characteristics relevant for it to become a successful therapeutic for PD, such as high BBB penetrance and targeting to the mitochondria within dopaminergic neurons of the SNpc, has yet to be designed. Until further research is carried out to find the most appropriate formulation of curcumin, curcumin is unlikely to move forward into clinical testing for PD.

Hydroxytyrosol (HT) is another natural phenolic compound that has generated interest in PD research due to its antioxidant properties. HT is a major component of olive oil and therefore prominent in the Mediterranean diet (Khalatbary, 2013; Yu et al., 2016), which has been related to lower mortality (Trichopoulou et al., 2003; Trichopoulou, 2004), improved cardiovascular health (Barzi et al., 2003; Granados-Principal et al., 2014) and slower cognitive decline (Feart et al., 2009). Research also supports a protective role of HT against neurodegeneration (Hashimoto et al., 2004; Han et al., 2007; González-Correa et al., 2008; Wu et al., 2009; Ristagno et al., 2012; Pasban-Aliabadi et al., 2013). Like curcumin, the phenolic group provides ROS scavenging properties through the ability of the benzene ring-bound hydroxyl groups to donate either an electron or hydrogen atom to stabilise the ROS (Amic et al., 2007; Sandoval-Acuña et al., 2014; Lombard et al., 2018) (figure 8a).

In PD related cellular models, HT protects dopaminergic neurons against cell death following oxidative stress (Hashimoto et al., 2004). Animal studies have shown resistance to oxidative stress *via* reduced lipid peroxidation in dissociated brain cells following administration of 100 mg/kg HT for 12 days (Schaffer et al., 2007). This suggests that HT can access the brain,

however, other studies show that although it can cross the BBB, brain uptake of HT is lower than uptake in other organs (D'Angelo et al., 2001). Wu et al (2009) showed that, in a cellular model, HT was protective against dopamine and 6-OHDA induced cell death but had no significant protective effect in another commonly used model of PD, 1-methyl-4-phenylpyridinium (MPPþ)-induced degeneration. This suggests that HT is protective against ROS and dopamine induced oxidative stress but not mitochondrial dysfunction as, unlike dopamine and 6-OHDA, MPPþ is solely an inhibitor of mitochondrial complex 1 and does not directly form ROS (Wu et al., 2009; Schapira, 2010). Furthermore, recent data suggests that HT decreases dopamine synthesis likely due to the negative feedback of tyrosine hydroxylase (Laschinski et al., 1986), an enzyme vital for the synthesis of dopamine (figure 1). It has therefore been suggested that HT may not be the most suitable antioxidant for PD as PD is characterised by a marked reduction in dopamine.

Taken together, preclinical data suggests that HT is protective against some forms of oxidative stress but not against mitochondrial dysfunction. Although it can pass the BBB (D'Angelo et al., 2001), clinical studies of HT in people with PD are unlikely to commence due to its potential for lowering dopamine levels. Further research is required to understand the antioxidant effects of HT as it would be expected that if it was potently protective against iron-induced oxidative stress that it would have some effect against MPPþ because ROS is mainly generated in the mitochondria and mitochondrial dysfunction increases ROS production. The lack of effect in against MPPþ (Han et al., 2007; Wu et al., 2009), might be due to the lack of target specificity of HT and therefore limited uptake by mitochondria within PD effected neurons.

A. Hydroxytyrosol **B. N-acetylcysteine**
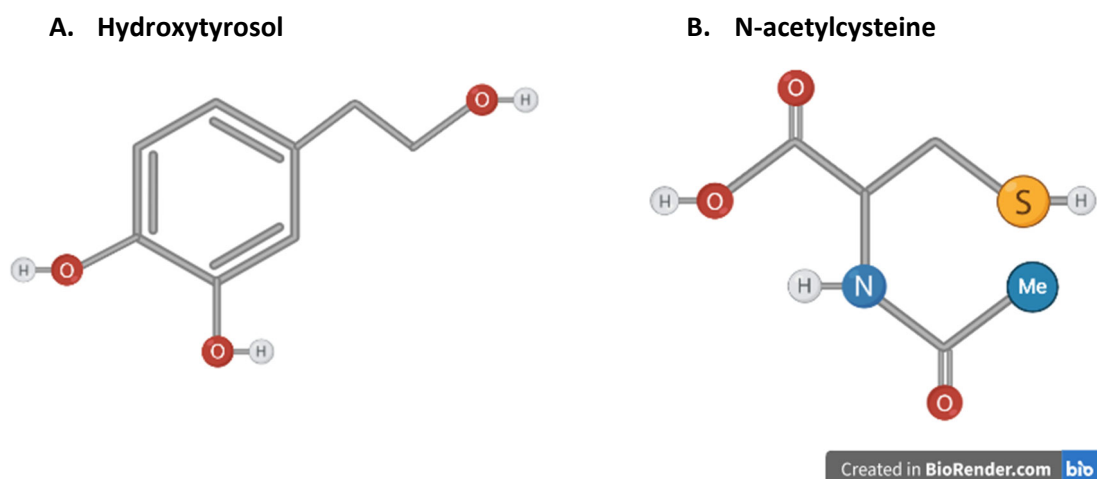
Figure 8. A. Chemical structure of Hydroxytyrosol. B. Chemical structure of N-acetylcysteine.

A recent study has suggested that N-acetylcysteine (NAC), which acts as a precursor to endogenous glutathione, is superior to HT as a potential disease-modifying therapeutic for PD since NAC is not only a potent antioxidant but has been shown to increase tyrosine hydroxylase activity (Goldstein et al 2017). NAC is FDA approved to treat paracetamol overdose and is also marketed as a dietary supplement in the US (Goldstein et al., 2017). As a derivative of cysteine, NAC primarily exhibits its antioxidant properties indirectly, through the production of glutathione (Samuni et al., 2013) (figure 8b). However, being a thiolic compound it can also take part in Michael addition reactions as an electron pair donor and donate hydrogen atoms to ROS such as hydroxyl (Samuni et al., 2013; Aldini et al., 2018) (figure 7b).

Preclinical studies of NAC in PD models have shown that it is protective against dopaminergic cell death induced by rotenone (Rahimmi et al., 2015) and 6-OHDA (Soto-Otero et al., 2000) as well as MPTP (Perry et al., 1985; Chen et al., 2007; Park et al., 2004; Sharma et al., 2007), unlike HT. Clark et al (2010) demonstrated that NAC can also protect against toxic α-syn aggregates in transgenic mice, with glutathione levels increased within 5-7 weeks of NAC treatment. These elevated glutathione levels, however, were not maintained at 1 year (Clark et al., 2010). This might be related to the presence of dopamine quinone in dopaminergic neurons affected by PD as dopamine quinone has been shown to inhibit glutathione peroxidase 4 (Hauser et al., 2013; Hare & Double, 2016) and therefore glutathione present may not be fully utilised leading to its eventual downregulation. Numerous clinical trials have been carried out or are underway testing NAC as a therapy for various neurological and psychiatric disorders (Slattery et al., 2015), these along with the mounting preclinical evidence has triggered the clinical investigation of whether NAC can slow PD progression (Monti et al., 2016).

Human studies suggest that NAC does enter the brain as oral NAC administration increases the concentration of NAC to about 10 μM in the CSF (Katz et al., 2015; Reyes et al., 2016). However, the ability of NAC to pass the BBB has been disputed in studies where brain uptake has not been evident, these discrepancies are likely due to differences in dose and mode of administration (Bavarsad Shahripour et al., 2014). For example, oral administration of 200 mg NAC is less than 5% bioavailable (Bavarsad Shahripour et al., 2014) and it is largely undetectable following ingestion (Cotgreave & Moldeus, 1987). Moreover, at high

concentrations, which may be required to get therapeutically relevant concentrations into SNpc, there is evidence that NAC lowers dopamine synthesis as gluthathione overproduction has been reported to be cytotoxic in dopaminergic neurons (Garrido et al., 2011). Although there have been multiple clinical trials of NAC for different aspects of PD, with another planned (Clinicaltrials.gov, 2018c), research into different formulations of NAC is needed to increase BBB passage and targeting to the SNpc in order to reduce the dose required to provide therapeutic value and prevent cytotoxicity associated with high doses. It is worth conducting such research because NAC is a direct precursor to glutathione, an antioxidant which is lowered in dopaminergic neurons within the SNpc in PD (Kroemer & Reed, 2000; Simpkins & Dykens, 2008; Jiang et al., 2017). That being said, as glutathione peroxidase 4 is also lowered in PD (Hauser et al., 2013; Hare & Double, 2016) partly due to inhibition from dopamine quinone (Lortharis & Brundin, 2002; Yamakawa et al., 2010), this could reduce the therapeutic effect of NAC for people with PD due to a reduced ability to oxidise glutathione necessary to convert hydrogen peroxide into water. Therefore, the best strategy may be to administer NAC in combination with a drug that can reduce dopamine quinone levels such as an iron chelator (Hare & Double, 2016). A combination of an iron chelator alongside an antioxidant targeted to the dopaminergic neurons within the SN may be more successful in combating the neurodegenerative process in PD, especially in early PD where such a therapy could potentially stop the progressive loss of dopaminergic neurons.

1.5. Nanoformulation for targeted delivery of drugs across the BBB

The BBB prevents the passage and activity of 98% of potential neuropharmaceuticals (Dove, 2008). Although, some of the drugs discussed above may be able to pass the BBB, none of these are able to target the mitochondria within the dopaminergic neurons effected in PD, where the majority of hydroxyl is formed. Moreover, as these drugs have not been designed for use in PD, they are not targeted to the brain and although they may be able to pass the BBB, the level of drug that reaches the brain is very low.

Unlike many other methods that attempt to specifically target treatments, nanotechnology is one of the least invasive. For example, one method used in a recent clinical trial of PD was a novel convection-enhanced diffusion delivery system which meant patients had to undergo brain surgery to fit the delivery system directly through the skull (Pardridge et al.,

2007; Gimenez et al., 2011; T.G. Study Group, 2017; Whone et al., 2019). Direct targeting in this manner has the benefit of bypassing the BBB, however such invasive methods incur risks both during the procedure and after, as proper maintenance is required in order to prevent infection. Other less invasive methods that have been explored include nasal delivery and the most conventional method, chemical alteration of the drug in question.

Nasal delivery can increase passage of small lipid-soluble molecules into the brain as shown by higher concentrations of drug found in the CSF than in the plasma (Kumar et al., 1982). This indicates that certain drugs can move directly from the nasal submucal space into the CSF compartment of brain, bypassing the digestive system and therefore reducing the rate at which the drug is metabolised (Pardridge et al., 2007). Lipid-soluble small molecules that have been nasally delivered enter the blood *via* absorption of CSF at the superior sagittal sinus (Pardridge et al., 2007). Nasal delivery of current PD drugs may be beneficial as it would prevent the interaction with protein and other foods that has been reported by numerous patients to affect the ability of PD medications to work properly (Parkinson Québec, 2015; Mathur et al., 2017). Also, due to the fast access to the brain it would allow the effects of symptomatic drugs to work more quickly, preventing long periods where people with PD have to wait for their drugs to 'kick in'. It is therefore unsurprising that this method is being researched for some current PD medications, for example CVT-301 is an inhaled formulation of L-dopa (Acorda, 2017). Although nasal delivery may be a good route of administration for some existing PD treatments most drug candidates to treat brain disorders are not lipid-soluble small molecules, most are water soluble or have large molecular weights (>400 Da) and therefore cannot freely cross the nasal mucosa (Pardridge et al., 2007). What's more, where nasal delivery can support access into the brain, it does not aid the specific targeting of the drug to the location where it is required.

Chemical modification of drugs, on the other hand, could provide the targeting. Most chemical modification approaches to targeted delivery of drugs across the BBB have attempted to congregate the drug to a BBB transporter by creating prodrugs using chemical modifications such as pegylation, cyclisation, methylation, halogenation, or addition of unnatural bonds (Juillerat-Jeanneret et al., 2008). This requires the drug to mimic an endogenous ligand in order to be successful because most transporters at the BBB are highly selective (Juillerat-Jeanneret et al., 2008). For example, an anti-inflammatory agent,

ketoprofen, has undergone successful chemical modification to target the LAT1 transporter by linking it to the phenolic hydroxyl group of the amino acid tyrosine *via* ester bonds (Gynther et al., 2008). In theory, therefore, it would be possible to alter the chemical structure of iron chelators, such as DFP and DFO, and antioxidants such as curcumin, HT and NAC, in order for them to pass the BBB and target mitochondria. However, this process is highly time consuming and involves much trial and error to find the correct modification for targeting that does not alter the overall desired effect of the drug (Juillerat-Jeanneret et al., 2008). Further to this, the new prodrug created would have to undergo rigorous safety and preclinical testing to ensure that the modifications are not harmful. Therefore, when there is interest in existing drugs which already have a long-standing safety profile, such as DFP and DFO, this may not be best option in terms of fastest route to clinical translation.

Nanotechnology approaches in formulation science are increasingly being researched for targeted delivery and passage across the BBB as they provide a versatile approach that can retain the potency of entrapped molecules while enhancing passage across biological membranes and targeting to neurons (Masserini et al., 2013) and mitochondria (Zupančič et al., 2014). Many drug-loaded nanoparticles also have the added benefit of being able to utilise nasal delivery due to their small size and often lipid-permeable structure, allowing faster access into the brain (Pardridge et al., 2007). One example are the mitochondrial-targeted DQAsomes developed by Zupančič et al (2014) for nasal delivery, to treat acute lung injury. When nanocarriers are developed from chemicals with known safety profiles or from non-synthetic, natural materials and encapsulate existing non-modified drugs, there is more existing safety data for the constituent parts of the nanoformulation compared to chemically modified prodrugs. Therefore, nanotechnology-based solutions have the potential not only to pass the BBB and successfully target drugs to neuronal mitochondria, but when using already licenced drugs such as DFP or DFO, they may also be closer to clinical translation then targeting methods that alter chemical structure.

1.6. Scope of project

The primary aim of this project is to develop novel nanoformulations of iron chelators and antioxidants that can pass the BBB and target mitochondria within dopaminergic neurons, to reduce oxidative stress and dopaminergic neuronal death in a cellular PD model.

This can be sub-divided into the following individual objectives:

- Develop and characterise nanoformulations of iron chelators and antioxidants

- Develop and characterise a cellular model of PD

- Assess the therapeutic potential of nanoformulations against oxidative stress and dopaminergic cell death in a cellular PD model

- Develop and characterise a cellular BBB model in co-culture with a cellular PD model

- Assess the ability of nanoformulations to cross the cellular BBB model and target the mitochondria within dopaminergic neurons

Chapter 2 – Materials and methods

2.1. Materials

Unless otherwise stated, all chemicals were analytical grade or cell culture grade where applicable. SH-SY5Y cells were purchased from the American Type Culture Collection (ATCC CRL-2266, USA). hCMEC/D3 cells were kindly gifted from Dr Simon McArthur (Senior Lecturer in Clinical Neuroscience and Pharmacology, Queen Mary University of London, UK) at passage 31, previously purchased from VHBio Ltd (Gateshead, UK) (Hoyles et al., 2018).

EGM -2 MV Microvascular Endothelial Cell Growth Medium-2 BulletKit™, fibronectin (bovine plasma), collagen from calf skin, Dulbecco's phosphate buffered saline (DPBS), Hank's Buffered Saline Solution (HBSS) and HEPES Buffer (1 M) were purchased from Lonza (UK). Methanol (HPLC grade), L-glutamine, foetal bovine serum (FBS), Dulbecco's Modified Eagle Medium (DMEM) Glutamax®, Minimum Essential Media (MEM), 100X antibiotic-antimycotic, poloxomer 68 (Pluronic® F68) and Kolliphor® HS 15 (Solutol®) were supplied by Fisher Scientific, UK. The Pierce BCA protein assay kit, MitoTracker™ Red CMXRos kit and NucBlue™ Live ReadyProbes™ reagent were also purchased from Fisher Scientific, UK. Dequalinium chloride hydrate (95%), Curcumin (≥94% curcuminoid content, ≥80% curcumin), Deferoxamine mesylate salt (92.5%), N-Acetyl-L-cysteine (99%), 3-Hydroxytyrosol (≥98%), Rotenone (≥95%), Protease inhibitor cocktail (cat no. P8340), Thiazolyl Blue Tetrazolium Blue (MTT), Dimethyl sulfoxide (DMSO), 2',7'-Dichlorofluorescin diacetate (DCFH-DA), 2,2'-Azobis(2-methylpropionamidine) dihydrochloride (ABAP) and 2, 4, 6-tripyridyl-s- triazine and iron(III) Chloride Hexahydrate were purchased from Sigma-Aldrich, UK. The ferrous sulphate (20% iron), ferrozine, ammonium acetate, ascorbic acid, potassium permanganate and hydrochloric acid used for the ferrozine assay were also purchased from Sigma-Aldrich, UK. All chemicals used for immunoblotting were also purchased from Sigma-Aldrich and Fisher Scientific (UK). The Mini-PROTEAN® Tetra Vertical Electrophoresis Cell, 4-gel, for 1.0 mm thick handcast gels, with PowerPac™ Basic Power Supply (product no. #1658025FC) was purchased from Bio-Rad, UK. The anti-Tyrosine Hydroxylase (Cat. No. AB152) and anti-NeuN, clone A60 (cat no. MAB377) were purchased from Merck Millipore, USA. Anti-GAPDH antibody [6C5] loading control (cat no. ab8245), goat anti-rabbit IgG H&L

(HRP) (cat no. ab6721) and goat anti-mouse IgG H&L (HRP) (cat no. ab6789) were purchased from Abcam biotechnology company (UK). The mitochondrial hydroxyl radical detection assay kit (cat no. ab219931) was also purchased from Abcam, UK. The Ferritin ELISA kit (product code S-22) was from ATI Atlas (Chichester, UK). The TBARS Parameter Assay Kit (product code KGE013) was purchased from R&D Systems, Parameter TM, UK. Experimental reagents were prepared using Milli-Q water (water purified through a 0.22 μm membrane filter with a resistivity of 18.2 MΩ). Sterile filters were from Millex-MP, Millipore, Ireland. Flasks were from Nunc (Denmark) and all culture plates, pipettes, stripettes and eppendorf tubes were from Corning, UK.

2.2. Development and characterisation of the nanoformulations

2.2.1. Preparation of antioxidant and/or iron chelator micellar nanoformulations

All nanoformulations were prepared using a modified thin-film hydration method (Weissig et al., 1998, Zupančic et al, 2014). Briefly, P68 and Sol nanocarriers with or without DQA were dissolved in 10 ml of methanol along with the antioxidant (curcumin, NAC, or HT) and/or iron chelator (DFO) of interest at certain ratios (table I, chapters 3 and 5). Using a rotary evaporator (Hei-VAP Advantage Rotary Evaporator, Heidolph, Germany) the methanol was then evaporated at 200 rpm and 80°C, under vacuum until a thin film was obtained. The resultant thin film was hydrated with 10 ml of distilled water and mixed thoroughly at 80°C for 1-2 min and sonicated using a VWR Ultrasonic cleaner bath USC300T (VWR International Limited, UK) for a further 1 min until the film was fully removed and dissolved in the water. In order to remove any unloaded antioxidant and/or iron chelator, the obtained solution was filtered through a sterile 0.22 μm filter. To enable storage of samples for further analysis, some samples were freeze dried (lyophilized) using a Virtis AdVantage 2.0 BenchTop freezedryer (SP Industries, UK).

2.2.2. Size and surface charge of the nanoformulations

The particle size and surface charge of nanoformulations were measured using the Zetasizer Nano ZS (Malvern Instruments, UK). Size distribution was measured *via* photon correlation spectroscopy as Z-Ave hydrodynamic diameter and polydispersity index. Transmission electron microscopy (TEM) analysis was performed to analyse morphology (size and shape)

of the nanoformulation complexes using a FEI CM 120 BioTwin transmission electron microscope (Philips Electron Optics BV, Netherlands) at acceleration voltage 120.0 kV. Approximately 40 μl of the nanoparticle dispersion was placed on a Formvar/carbon coated copper grid and negatively stained with 1% uranyl acetate. Digital images were taken at 13,500, 17,500, 46,000, and 65,000 times magnification.

2.2.3. Determination of drug loading and encapsulation efficiency

UV-Visible (UV-Vis) spectroscopy was employed to study drug loading and encapsulation efficiency of the nanoformulations based on the calibration curves of the free drugs. Methanol and water were added in a 1:1 ratio to dissolve the carrier in order to release the drug and achieve a theoretical concentration of each drug (10 μg/ml curcumin, 20 μg/ml DFO, 20 μg/ml HT and 1 mg/ml NAC). Curcumin, DFO, NAC and HT content were calculated using UV-Vis spectroscopy at 423 nm, 204 nm, 234 nm, and 280 nm, respectively. The percentage of drug loading and encapsulation efficiency were calculated using the following equations:

- Drug loading (%) = (determined mass of drug within nanocarriers / mass of drug-loaded nanocarriers) X 100

- Encapsulation efficiency (%) = (determined mass of drug within nanocarriers / theoretical mass of drug within nanocarriers) X 100

2.2.4. Structural analysis

Using an X-ray diffractometer (Rigaku MiniFlex600, Miniflex, Japan), X-ray diffraction (XRD) patterns were obtained for pure curcumin, DFO, NAC, HT, DQA, P68, Sol and lyophilized P68, P68+DQA, Sol and Sol+DQA formulations of curcumin, NAC, HT and/or DFO to determine the atomic and molecular structure. All samples were analysed at room temperature in the angle range 5–35° with a step size of 0.01° and scanning rate 2°/min.

The chemical structure of the pure drugs, nanocarriers alone, their physical mixtures and lyophilized drug-loaded nanocarriers was analysed using a PerkinElmer Spectrum 100 Fourier-transform infrared (FTIR) spectrometer (PerkinElmer, USA) from 650 to 4000 cm^{-1} at a resolution of 4 cm^{-1}.

2.2.5. Antioxidant power of the antioxidant nanoformulations

The potential antioxidant activity of drug-loaded nanoparticles was determined using the modified ferric iron reducing antioxidant power (FRAP) assay and compared to the FRAP results of the corresponding free drug as previously described (Zupančič et al., 2014). To prepare the FRAP reagent, acetate buffer (pH 3.6), tripyridyl triazine, and iron (III) chloride were mixed. The concentrations of drug within the nanoparticles were spectrophotometrically measured using a microtilter plate reader (VersaMax, Molecular Devices, USA) as described above. To analyse the antioxidant activity, samples of the nanoformulations and drug stock solutions were added to the FRAP reagent and incubated at 25°C for 30 min. The samples were read at absorbance 593 nm. The blank comparator was FRAP reagent without the addition of any drugs or nanoformulations. The absorbance values were normalised as trolox equivalent antioxidant capacity as trolox is a recommended baseline antioxidant reference point for multiple antioxidant assays (Anon, 2012; Yusof et al., 2018).

2.2.6. SH-SY5Y cell culture and cytotoxicity testing of the nanoformulations

SH-SY5Y cells were grown in DMEM - Glutamax®, pH 7.4 supplemented with 10% FBS and 1% antibiotic/antimycotic in a 5% CO_2 environment at 37°C. SH-SY5Y cells were thawed and left to grow in plastic T75 (75 cm^2) flasks until they reached 70% confluence. Adherent cells were then detached from the surface of the flasks *via* trypsinisation, counted and seeded at 1,000,000 cells/cm^2 into 6 or 96-well plates according to the bioassay being performed.

In order to evaluate the toxicity of drug-loaded nanoformulation, SH-SY5Y cells were treated with free curcumin, NAC, HT and/or DFO or the corresponding concentrations of each drug-loaded nanoformulation for between 24, 48 and 72 h. Cell viability was assessed using the MTT assay based on the reduction of the yellow thiazolyl blue tetrazolium bromide salts (3-(4, 5-dimethylthiazol-2-yl)-2, 5-diphenyltetrazolium bromide, MTT) to the purple formazan by mitochondrial dehydrogenases. Briefly, SH-SY5Y cells were grown at a seeding density of 1,000,000 cells/cm^2 in 96 well plates until confluent. The cells were treated with either free or nanoformulated curcumin, NAC, or HT with or without the combination of DFO at varying concentrations for up to 72 h. The cells were then incubated with an additional 20 µl of 5

mg/ml solution of MTT DPBS solution for 4 h at 37°C. Following aspiration, 100 µl of DMSO was added to each well to dissolve the formazan crystals. To ensure DMSO was mixed well, plates were placed on a shaker at 75 rpm for 15 min and the absorbance was read at 570 nm on a spectrophotometer.

2.3. Assessing the therapeutic potential of the nanoformulations compared to free drug preparations against a rotenone cellular model of PD

2.3.1. SH-SY5Y cell culture, rotenone treatment and lysate harvesting

The human neuroblastoma SH-SY5Y cell line was used to create an *in vitro* model of PD (reviewed in Xicoy et al., 2017). As described above, SH-SY5Y cells were grown in DMEM - Glutamax®, pH 7.4 supplemented with 10% FBS and 1% antibiotic/antimycotic in a 5% CO_2 environment at 37°C. SH-SY5Y cells were thawed and grown in plastic T75 flasks until they reached 70% confluence. Adherent cells were then detached from the surface of the flasks *via* trypsinisation and seeded into well plates at specific numbers according to the bioassay being performed (6-well or 96-well plates).

Based on methods previously described (Kim et al., 2011; Martins et al., 2013), cells were treated with rotenone (in MEM) at concentrations ranging from 5 µM to 100 µM for 24 h with the aim to reduce cell viability by approximately 50%.

Where necessary, cells were grown in 6 well plates until confluent and lysed at 4°C as previously described by Zariwala et al (2013), using 350 µl ice-cold lysis buffer (50 mM NaOH supplemented with 1 ug/ml protease inhibitor cocktail) whilst rocking gently for 40 min in ice trays on a plate shaker (8 rpm). Cell lysates were collected using sterile cell scrapers, passed through a 25G needle and aliquoted into microcentrifuge tubes ready for further analysis. For each experiment requiring the use of cell lysate, the total protein content was determined using the Pierce BCA kit following the manufacturer's protocol (as previously described by Kim et al., 2011), using the bovine serum albumin (BSA) stock (2 mg/ml) provided in the kit as the standard.

2.3.2. The ability of the nanoformulations to protect against rotenone induced reduction in cell viability

The protective properties of drug-loaded nanocarriers against rotenone-induced reduction in cell viability was assessed using the MTT Assay. As described above, SH-SY5Y cells were grown at a seeding density of 1,000,000 cells/cm^2 in 96 well plates until confluent. The cells were pre-treated for 3 h with either free or nanoformulated curcumin, DFO, NAC, HT or curcumin, NAC or HT combined with DFO at a range of concentrations, or with corresponding unloaded, blank formulations. SH-SY5Y cells were then treated with 100 μM rotenone for 24 h, each well containing a total volume of 200 μl. Rotenone only and MEM only treatments, without any pre-treatments, were used as controls. The cells were then incubated with an additional 20 μl of 5 mg/ml solution of MTT DPBS solution for 4 h at 37°C. Following aspiration, 100 μl of DMSO was added to each well to dissolve the formazan crystals. To ensure DMSO was mixed well, plates were placed on a shaker at 75 rpm for 15 min and the absorbance was read at 570 nm on a spectrophotometer.

2.3.3. Western blot analysis

Western blot analysis was carried out to identify the presence of the dopamine marker, tyrosine hydroxylase and the neuronal marker NeuN following 24 h 100 μM rotenone treatment, with or without 3 h pre-treatment with the free drug or nanoformualtion conditions. SH-SY5Y cells were lysed at 4°C and the total protein content was determined using the BCA assay as described above. The samples were diluted with sample buffer containing 62.5 mM Tris (pH 6.8), 25% glycerol, 0.01% coomassie blue, 2% sodium dodecyl sulfate (SDS) and 5% β-mercaptoethanol to ensure equal protein concentrations for gel loading and to enable protein tracking through the gel during electrophoresis. The 1.0 mm gels were cast manually using the Bio-Rad mini-format handcast system using two thirds 12% running gel solution and one third 4% stacking gel solution (table 1). The running gel was added between the glass plates and left to set for ~ 10 minutes until polymerised before the stacking gel was added. A comb was placed into the stack to provide wells for sample loading.

Table 1. List of reagents for making up the running and stacking gel solutions.

Reagents	Running gel (12%)	Stacking gel (4%)
Distilled H_2O	3345 µl	6060 µl
Running gel solution (1.5 M Tris-HCl pH 8.8)	2500 µl	-
Stacking gel solution (0.5 M Tris-HCl pH 6.8)	-	2500 µl
10% SDS	100 µl	50 µl
30% acrylamide/bisacrylamide	4000 µl	1330 µl
10% ammonium persulphate (APS)	50 µl	50 µl
N,N,N',N',Tetramethylethylenediamine (TEMED)	5 µl	10 µl

Samples containing 10 µg of protein were loaded and proteins were separated by gel electrophoresis using running buffer containing 25 mM Tris-base, 192 mM glycine and 0.1% SDS, at 200 V for 45 min. The proteins were then transferred to a nitrocellulose membrane at 4°C, 110 V for 65 min using 6X transfer buffer diluted in methanol and distilled water (1:3.33 ratio), containing a final concentration of 31 mM Tris-base and 50 mM glycine. The membrane was blocked for 1 h at room temperature with TBS-T 5% BSA (BSA in tris-buffered saline with Tween 20 (10 mM Tris–HCl, 150 mM NaCl and 0.1% Tween 20, pH 7.5)). The membrane was then washed three times for 5 min in TBS-T and incubated with either 1:1000 anti-tyrosine hydroxylase (rabbit) or 1:100 anti-NeuN (mouse) and 1:500 anti-GAPDH (mouse) primary antibodies over-night at 4°C on a plate rocker (40 rpm). Following three 5 min washes in TBS-T, the membrane was incubated for 2 h at room temperature with the relevant secondary antibody (1:3000 goat anti-rabbit IgG H&L or goat anti-mouse IgG H&L). The protein bands were then detected using EMD Millipore™ Immobilon™ Western Chemiluminescent HRP Substrate (ECL) for 10 min and the membrane was exposed and visualised using the Azure Biosystems 600 imager. Western blot analysis was carried out using Image J using equal sized rectangular 'regions of interest' for each band to quantify the intensity of each band in relation to the background.

2.3.4. Total iron content and ferritin analysis

Cell harvesting and iron content experiments were carried out using the method previously described by Zariwala et al (2013). SH-SY5Y cells were grown in 6-well plates and pre-treated with free drug or drug-loaded nanoformulations for 3 h at 37°C before treatment with rotenone for 24 h. Following this, cells were washed with DPBS and lysed as described above.

Total iron was quantified using a modified version of the ferrozine colorimetric assay used in Zariwala et al (2013). Briefly, 200 µl of 0.1 M HCL was added to 200 µl of sample lysate. The iron standards were prepared using analytical grade $FeSO_4$. Samples were then incubated in the dark with 200 µl of iron releasing agent (1.4 M HCL and 4.5% $KMnO_4$ in water) for 2 h at 60°C under a fume hood. Samples were then cooled to room temperature before being incubated for 30 min with 60 µl of iron detection reagent (6.5 mM ferrozine, 2.5 M ammonium acetate, 1 M ascorbic acid). Equal volumes (200 µl) of the test and standard samples were aliquoted into 96-well microplates in duplicate and absorbance was read at 550 nm using a microplate reader (VersaMax, Molecular devices, USA).

Cell lysate samples were also assessed for ferritin concentration using a spectrophotometric sandwich ELISA kit. 30 µl of each sample and standard were loaded in duplicate into a 96-well plate coated with rabbit antihuman spleen ferritin. Incubation steps were carried out as described in the manufacturers protocol (S-22; ATI Atlas, UK). Briefly, samples and standards were incubated in 200 µl of the conjugate for 2 h at 195 rpm, 37°C. The samples and standards were then washed three times with MiliQ water before they were incubated with 200 µl of the substrate solution for 30 min at room temperature. Following incubation, 100 µl of potassium ferricyanide solution was added to each sample and standard, and the absorbance was read at 495 nm and 630 nm using a microplate reader (VersaMax, Molecular devices, USA). All samples were assayed in duplicate. The ferritin and ferrozine concentrations were standardised against the total protein concentration.

2.3.5. Lipid peroxidation assessment

The thiobarbituric acid-reactive-substances (TBARS) assay was used to assess ROS generated oxidative stress, specifically lipid peroxidation (Dutta et al., 2012; Chakraborti et al., 2017).

Malondialdehyde (MDA) is a secondary end-product of the oxidation of polyunsaturated fatty acids and is therefore considered a marker of lipid peroxidation (Dutta et al., 2012; Chakraborti et al., 2017). The TBARS assay is a measure of MDA by reacting it with thiobarbituric acid (TBA) in a colorimetric reaction to form TBARS. Briefly, SH-SY5Y cells were grown in 6-well plates until confluent. Following pre-treatment with the relevant free or nanoformulated conditions, the cells were incubated with 100 μM rotenone for 24 h. Cells were then washed once with DPBS and lysed at 4°C as described above. The TBARS assay was carried out in accordance with the manufacturer guidelines (R&D Systems, Parameter TM, UK). Briefly, freshly prepared TBA was added to TBARS acid-treated cell lysate which was incubated at 60°C for 2.5 h. The samples were read at absorbance 532 nm before and after incubation to estimate the formation of TBARS.

2.3.6. Cellular antioxidant activity assessment

The cellular antioxidant activity was measured based on the method described by Chen et al (2015) which is a slightly modified version of the assay developed by Wolfe et al (2007) and Hu et al (2013). SH-SY5Y cells were seeded in black-walled, clear-bottom 96-well microplates. Once confluent, cells were washed with DPBS and treated with 200 μl of different concentrations of drug-loaded nanocarriers or drug solution for 1 h at 37°C. Cells were then washed with MEM and treated with 200 μl of the fluorescent probe DCFH-DA (100 μM) and incubated for a further 30 min at 37°C. Following aspiration, each well was treated 100 μl of prooxidant dissolved in MEM (600 μM ABAP, 100 μM rotenone or 200 μM free iron). The assay was modified to also test rotenone and iron as the prooxidant in order more closely mimic iron-induced oxidative stress present in PD. The fluorescence of the cells was read every 5 min for 1 h at 528 nm and 485 nm emission and excitation (respectively) on the Fluostar Optima Fluorescence Plate Reader. The CAA unit was calculated using the following equation:

CAA Unit = 100-(Area under the curve (AUC) of the treatment / AUC of control) X 100

$AUC = (1 + (RFU1 / RFU0) + (RFU2 / RFU0) …)$

where RFU0 is the relative fluorescence value of point zero and RFUx is the relative fluorescence of each time point (e.g. RFU5 is relative fluorescence value at minute 5).

2.3.7. Mitochondrial hydroxyl radical detection

The mitochondrial hydroxyl radical detection assay is a fluorometric assay which detects intracellular hydroxyl radical using an OH580 probe that selectively reacts with hydroxyl radicals present in live cells. Such reaction generates a red fluorescence signal that can be read at 540/590 nm excitation/emission. The assay was carried out according to the manufacturer's protocol (ab219931; Abcam, UK). Briefly, SH-SY5Y cells were seeded in black-walled, clear-bottom 96-well microplates until confluent. Cells were then washed with DPBS and treated with different concentrations of drug-loaded nanocarriers or free drug at a volume of 200 μl for 3 h at 37°C. Following this, cells were washed with DPBS and treated with 100 μl of 6.25X OH580 probe for 1 h at 37°C. 100 μl of 200 μM rotenone (final concentration 100 μM) was then added to each well and cells were incubated for 24 h at 37°C. Cells were then washed with DPBS and the fluorescence was read on the Fluostar Optima Fluorescence Plate Reader.

2.4. Development and characterisation of a cellular BBB model

2.4.1. hCMEC/D3 cell culture

The hCMEC/D3 cerebral microvascular endothelial cell line was used to create an *in vitro* model of the BBB as previously described (Cristante et al., 2013; Weksler et al., 2013; Maggioli et al., 2016; Weksler et al., 2015; Paradis et al., 2016; Hoyles et al., 2018). hCMEC/D3 cells were grown in a 5% CO_2 environment at 37°C in Microvascular Endothelial Cell Growth Medium-2 BulletKit^{TM} (EGM-2 MV) which is supplemented with 5% FBS, 0.04% hydrocortisone, 0.4% hFGF-B (human basic fibroblast growth factor), 0.1% VEGF (vascular endothelial growth factor), 0.1% R3-IGF-1 (human recombinant insulin-like growth factor), 0.1% ascorbic acid and 0.1% GA (gentamicin sulfate-amphotericin). The hCMEC/D3 cells were thawed and left to grow in plastic T75 flasks until sufficiently confluent (~70%). The adherent cells were then detached from the surface of the flasks using trypsin, the cells were then counted and seeded at 300,000 cells/cm^2 into the 3.0 μm pore polycarbonate membrane inserts of 6 and 96-well Costar Transwell® plates precoated with 1:20 type 1

collagen from calf skin: DPBS (1 h) and 1:100 fibronectin from bovine plasma: DPBS (1 h). To promote tight junction formation, the hCMEC/D3 cells were exposed to VEGF-free media for 72 h prior to testing (Cristante et al., 2013; Maggioli et al., 2016; Hoyles et al., 2018; Gonzalez-Carter et al., 2019).

2.4.2. Trans-endothelial electrical resistance assessment

Trans-endothelial electrical resistance (TEER) was measured to assess the resistance of the BBB model as previously described by Burkhart et al (2016). TEER values were read using an epithelial Volt-Ohm meter and sterile Chopstick Electrodes and expressed as $\Omega.cm^2$ (resistance of the tissue (Ω) x membrane area (cm^2). High TEER values are desired as the presence of tight junctions increases the resistance (Paradis et al., 2016). In the presence of hydrocortisone TEER values of hCMEC/D3 cells have been shown to reach 300 $\Omega.cm^2$ (Weksler et al., 2013; Molino et al.,2014; Gonzalez-Carter et al., 2019), TEER values were therefore measured each day post seeding into Transwell® plates, until a resistance of close to 300 $\Omega.cm^2$ was reached before carrying out any of the BBB passage experiments.

2.4.3. BBB membrane permeability

The integrity of the BBB model was also assessed using the Lucifer yellow permeability assay (as previously described by Molino et al.,2014; Qosa et al., 2017; Setiadi et al., 2019). The lithium salt Lucifer yellow CH is a small (MW 457 Da) hydrophilic dye that is retained by the BBB and therefore presence of Lucifer yellow passing through the BBB model indicates a weak, leaky model (Molino et al., 2014). Once a TEER value of 300 $\Omega.cm^2$ was reached, hCMEC/D3 cells were incubated at 37°C for 1 h with 1.5 ml 0.1 mg/ml lucifer yellow in HBSS+10 mM HEPES in the apical upper compartment and 2.5 ml of HBBS in the lower basolateral chamber. Following this, the medium in the basolateral compartment and samples from the treatments added to the apical compartment were aliquoted in duplicate into a black 96 well plate in order to carry out fluorometric analysis using the Fluostar Optima Fluorescence Plate Reader (excitation 485nm, emission at 535nm). The results are expressed in terms of permeability in 10^{-3} cm/min with the aim of achieving a permeability between 1.2 and 0.6 x 10^{-3} cm/min as previously reported (Paolinelli et al., 2013; Förster et al., 2008; Eigenmann et al., 2013) because it is above this point when the barrier is

considered permeable or open. The permeability coefficient (Pc) was calculated from the following equation: Pc (cm/min) = (Vb × Cb) / (Ca × A × T) where Vb is the volume in the basolateral side (µl), Cb is the final basolateral concentration of Lucifer yellow (µM), Ca is the initial apical concentration of lucifer yellow (µM), A is the membrane growth area (cm^2), and T is the time of transport (min) (Molino et al., 2014; Qosa et al., 2017).

2.5. Assessing the ability of nanoformulations to cross the cellular BBB model, target mitochondria and protect against a rotenone model of PD

2.5.1. Assessment of nanocarrier passage across the hCMEC/D3 BBB model

A transport assay was carried out to assess the flux of nanoformulations across the model BBB as previously described (Bressler et al., 2013; Åberg et al., 2016). Each chamber was washed three times with phenol red-free HBSS carefully to avoid disturbing the hCMEC/D3 monolayer. 1 ml and 2.5 ml HBSS was then added to the apical and basolateral chambers (respectively) and incubated at 37 °C for 10 min. Following aspiration, the apical chamber was treated for 1 h at 37 °C with 1.5 ml nanoformulated or corresponding free curcumin, NAC, HT and/or DFO treatments (in HBSS) at a range of concentrations. The basolateral chambers were then sampled and curcumin, DFO, NAC and HT content were calculated using UV-Vis spectroscopy at 423 nm, 204 nm, 234 nm and 280 nm (respectively) as described in 2.23 above. TEER measurements were taken immediately after each transport assay to assess the stability of the BBB model and potential toxicity of each treatment.

2.5.2. hCMEC/D3 and SH-SY5Y co-culture

The hCMEC/D3 cells were grown in T75 flasks until sufficiently confluent (~70%). The adherent cells were then seeded at 300,000 cells/cm^2 into the 3.0 µm pore polycarbonate membrane inserts of 6 and 96-well Costar Transwell® plates precoated with 1:20 type 1 collagen from calf skin: DPBS (1 h) and 1:100 fibronectin from bovine plasma: DPBS (1 h) (as described above). In parallel, SH-SY5Y cells were grown in T75 flasks until 70% confluent and then seeded into 6 or 96-well plates (as described above). Once both sets of cells were fully confluent and the hCMEC/D3 cells reached a membrane potential of 300 Ω.cm^2, the relevant Transwell® inserts were place into the 6 or 96-well plates containing the confluent SH-SY5Y cells ready for immediate treatment (figure 1).
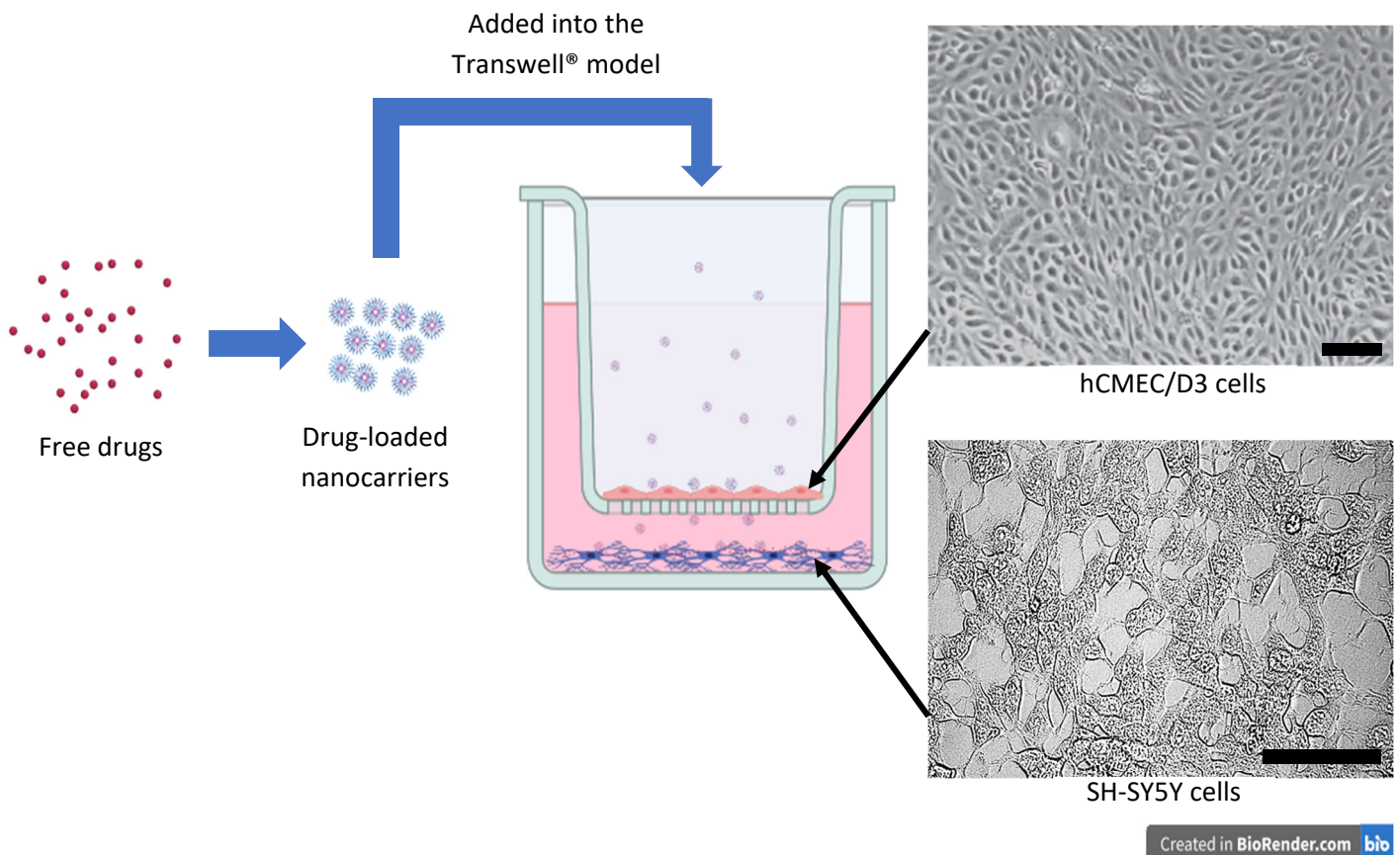
Figure 1. Schematic diagram of the Transwell® BBB co-culture model. Scale bars: hCMEC/D3 cells = 50μm, SH-SY5Y = 75 μm.

2.5.3. Assessment of the ability of nanocarriers to pass the BBB and target mitochondria

The ability of the curcumin nanoformulations to target mitochondria was assessed as previously described by Zupančič et al (2014). The basolateral chamber of the 6-well co-culture system containing confluent SH-SY5Y cells was treated with 2.5 ml MEM. The apical chamber containing hCMEC/D3 cells was treated with 1.5 ml nanoformulated or corresponding free curcumin treatments (in HBSS) at a range of concentrations and incubated for 1 h at 37°C in a humidified incubator containing 5% CO_2. The basolateral inserts were then removed and the SH-SY5Y cells were incubated for a further 2 h at 37°C to allow the treatments to be internalised. Following the incubation, the treatment media was aspirated and cells were washed with DPBS and incubated for 30 min with 100 nM solution of red fluorescent mitochondrial dye Invitrogen™ MitoTracker™ Red CMXRos in MEM. The cells were then washed with DPBS and cell nuclei were stained with NucBlue™ Live ReadyProbes™ reagent diluted in MEM. The samples were examined under a fluorescent microscope (EVOS™ FL Auto 2 – Invitrogen, Fisher Scientific, UK) to assess mitochondrial

71

targeting properties of curcumin-loaded nanocarriers. These experiments were carried out using curcumin and curcumin-loaded nanocarriers only due to the ability of curcumin to auto-fluoresce and be identified using a fluorescent microscope. The nuclei, mitochondria and curcumin were visualised using the DAPI (excitation: 357/44 nm, emission: 447/60 nm), CY5 (excitation: 628/40 nm, emission: 685/40 nm) and GFP (excitation: 470/22 nm, emission: 525/50 nm) objectives, respectively.

2.5.4. Assessment of the ability of nanocarriers to pass the BBB and protect against rotenone

The basolateral chamber of the 96-well co-culture system containing confluent SH-SY5Y cells was treated with 200 μl MEM. The apical chamber containing hCMEC/D3 cells was treated with 150 μl nanoformulated or corresponding free curcumin, NAC, HT and/or DFO treatments (in HBSS) at a range of concentrations and incubated for 1 h at 37 °C (figure 1). The inserts were then removed and the SH-SY5Y cells were incubated at 37°C for a further 2 h. SH-SY5Y cells were then treated with 100 μM rotenone for 24 h. The MTT and mitochondrial hydroxyl assays (as described above) were then carried out to assess the ability of the treatments to protect against reduced cell viability and oxidative stress after passing the BBB model.

2.6. Statistical analysis

For all experiments the mean of six replicates was calculated for each treatment, and the data were expressed as mean ± standard deviation (S.D.). The MTT, ferrozine, TBARS, mitochondrial hydroxyl assays and ferritin ELISA results were statistically analysed using one-way analysis of variance (ANOVA) followed by the Dunnett's T3 post hoc test. A two-way ANOVA followed by the Tukey's multiple comparisons post hoc test was used to analyse the FRAP and CAA assays as well as the western blot analysis and a two-way ANOVA followed by the Šidák multiple comparisons post hoc test was used to analyse the TEER and BBB passage data. (PRISM software package, Version 8, Graphpad Software Inc., San Diego, USA).

Chapter 3 - Development & characterisation of micellar nanocarriers containing curcumin and/or DFO

3.1. Introduction

Nanocarriers have demonstrated potential as targeted delivery systems to improve stability of labile molecules and enhance delivery across biological membranes, including the BBB, whilst retaining the potency of entrapped molecules (Masserini et al., 2013; Zupančič et al., 2014). Nanotechnology derived approaches may therefore provide a useful strategy for antioxidant and iron chelator therapies for PD as the therapeutic potential of such compounds are currently restricted due to issues such as instability, low bioavailability, and limited brain penetrance (Yang et al., 2007; Martin-Bastida et al., 2017, detailed in chapter 1).

Lipid-based nanoparticles (such as liposomes and solid lipid nanoparticles) as well as polymer-based nanoparticles (such as micelles) have been developed to overcome the issues of poor solubility, stability, and bioavailability of antioxidants, such as curcumin, in order to promote their utilisation as potential disease therapeutics (Ma et al., 2008; Yu et al., 2011; Zong et al., 2011; Doggui et al., 2012, Kumar et al., 2014, Hong et al., 2017, Liu et al., 2017, Davis et al., 2018; Wang et al., 2018) . Lipid-based nanoparticles are considered to be the least toxic for drug delivery purposes since such nanoparticles are usually composed of naturally occuring molecules allowing for biocompatibility and biodegradability (Ganesan et al., 2017; Rakotoarisoa and Angelova, 2018). However, polymeric micelles are considered more advantageous for brain delivery due to characteristics such as small particle size (10-200 nm) within the ideal range for brain penetrance, high water-solubility as well as low toxicity (Gaucher et al., 2005; Batrakova & Kabanov 2008, Kataoka et al., 2012; Elezaby et al., 2017; Rakotoarisoa and Angelova, 2018). Other benefits of micelles include high encapsulation efficiency, ease of sterilisation due to the small particle size, and self-assembling properties which allow for relative ease of preparation, handling, and incorporation of hydrophobic drugs (Zhang et al., 2012, Elezaby et al., 2017; Rakotoarisoa and Angelova, 2018). Due to the hydrophilic shell of micelles, there is also reduced interaction with plasma proteins and reduced uptake by the reticuloendothelial system which, along with the ability to target specific regions of the brain using various ligands and

surface modifications, aids delivery to the desired location (Zhang et al., 2012, Elezaby et al., 2017; Rakotoarisoa and Angelova, 2018). In the case of conventional micelles which have soft cores, such as pluronic micelles, there is no interaction between the drug and polymer (Saxena & Hussain et al., 2013; Liu et al., 2014). Hydrophobic drugs are therefore easily incorporated into the core of conventional micelles *via* direct mixing methods such as thin-film hydration where vacuum aided evaporation of an organic solvent, containing both the polymer and the drug, produces a film and resulting drug-loaded micelles following hydration and agitation (Saxena & Hussain et al., 2013; Liu et al., 2014).

Many studies have shown the benefits of encapsulating antioxidants such as curcumin within micellar nanocarriers, for example Hu et al (2014) reported that encapsulation of curcumin within micelles resulted in a 45-fold increase in bioavailability in plasma of rats and Hagl et al (2015) showed administration of micellar curcumin in mice resulted in a 10-fold increase in brain curcumin concentration. Similarly, there are also benefits of incorporating iron chelators such as DFO in micelles, as although DFO is commonly used to treat iron-overload disorders, in its native form its lack of target specificity and potential cytotoxicity limits its wider clinical use (Liu et al., 2017). The amphiphilic polymers Pluronic® F68 (P68) and Solutol® HS 15 (Sol) have been successfully used to develop micellar nanocarriers of numerous compounds (Hörmann & Zimmer 2016, Liu et al., 2016; Lee et al., 2018; Desfrançois et al., 2018) including curcumin and DFO for other indications (Shaikh et al., 2009, Zhao et al., 2012, Deo et al., 2012; Kumar et al., 2014, Hong et al., 2017; Liu et al., 2017, Davis et al., 2018; Wang et al., 2018; Welzel et al., 2019).

Mitochondrial targeting of antioxidants and iron chelators may provide a potent therapeutic strategy for PD as mitochondria are the main site of intracellular iron-induced free radical formation and resultant oxidative stress (Thomas et al., 2009; Bratic & Nils-Larsson, 2013; Kandola et al., 2015; Costa-mallen et al., 2017). Numerous mitochondrial targeters have been developed to aid the delivery of iron chelators and antioxidants to mitochondria. For example, Reelfs et al (2016) developed a tricatechol-based, mitochondria-targeted hexadentate iron chelator linked to mitochondria-homing SS-like peptides (short cell-permeant signal peptides that mimick mitochondrial import sequence) to protect against ultraviolet A-rays (UVA)-induced oxidative damage and cell death. Such aromatic-cationic peptides are concentrated in depolarized mitochondria (Doughan & Dikalov, 2007; Cerrato

et al., 2015) and are not therefore taken up due to mitochondrial membrane potential unlike other mitochondria-targeted agents such as the antioxidant MitoQ, ubiquinone targeted to the mitochondria by attachment to a lipophilic cation, triphenylphosphonium (TPP) (Reelf et al., 2016). Although the SS-like peptide approach has demonstrated potent protection of skin fibroblasts against UVA through the ability to target mitochondria and chelate iron, it has been developed via the synthesis of a completely new peptide which requires extensive preclinical safety testing before it can be clinically evaluated. For nanocarrier delivery systems, the packing of lipophilic cations into the formulation is a common method to achieve mitochondria-targeted delivery of associated compounds (Wang et al., 2011; Bae et al., 2018). This is because of the highly negative electric potential across the mitochondrial inner membrane which allows positively charged compounds to preferentially accumulate in the mitochondrial matrix against their concentration gradient (Weiss et al., 1987; Weissig, 2015; Shi et al., 2018). Various lipophilic cations such as rhodamine, TPP and dequalinium (DQA) have been associated with bioactive compounds of interest in order to improve their mitochondrial uptake (Weissig et al., 1998; Lyrawati et al., 2011; Wang et al., 2011; Santos et al., 2014; Sun et al., 2019). This method is relatively simple compared to other more complex strategies such as the conjugation of protein transduction domains or mitochondrial targeting sequences (Kawamura et al., 2013; Yamada & Harashima, 2013; Sandoval-Acuña et al., 2016; Paparidis et al., 2018) and therefore may be less time consuming and expensive. Although rhodamine has long been used as a mitochondria stain in living cells (Weiss, 1984) and TPP has been used to develop the antioxidant supplements MitoQ and MitoVitE which have also shown some protective effects in Friedreich Ataxia fibroblasts (Jauslin et al., 2003), DQA is bola-amphiphile which is doubly positively charged due to the presence of two delocalised cation centres and therefore possesses both hydrophilic and lipophilic properties beneficial for passing membranes and delivering hydrophobic drugs (Weiss et al., 1987; Weissig, 2015; Shi et al., 2018). DQA has traditionally been used as an antimicrobial agent in over-the-counter lozenges and mouthwashes and is approved to treat bacterial vaginosis in the UK (Weiss et al., 1987; Weissig, 2015; NICE, 2020). Further to this, since mitochondrial targeting of lipid-based nanocarriers using DQA has been well established (Weissig et al., 1998, Lyrawati et al., 2011; Wang et al., 2011; Bae et al., 2018; Shi et al., 2018), including in nanoformulations

of curcumin (Zupančič et al., 2014), it is a good potential candidate for clinical use within nanoformulations.

This study therefore aimed to develop micellar nanocarrier delivery systems for curcumin and/or DFO using the amphiphilic polymers, P68 and Sol with or without DQA with the relevant characteristics to allow for BBB penetrance before being tested for therapeutic effects in an *in vitro* PD model.

3.2. Results

All P68 and Sol nanoformulations demonstrated high encapsulation efficiency (66-96%) (table 1). DFO-loaded P68 nanocarriers had the highest mean encapsulation efficiency (95%), curcumin-loaded nanocarriers had 79% and the combined curcumin (67%) and DFO (66%) nanocarriers had the lowest encapsulation efficiencies (table 1). The mean P68 nanocarrier size was <200 nm in all cases, however curcumin-loaded nanocarriers had the largest particle sizes (table 1). Sol drug-loaded nanocarriers generally had smaller particle sizes than the corresponding P68 nanocarriers but, in both cases, curcumin-loaded nanocarriers had the largest particle sizes (table 1).

Table 1. Hydrodynamic Diameter (d), Polydispersity Index (PDI), Surface Charge, Drug Loading (DL) and Encapsulation Efficiency (EE) of blank and drug-loaded P68 and Sol nanoformulations prepared at 80°C (mean ± S.D. n=6).

Sample	Contents (mg/ml)		d (nm)	PDI	Charge (mV)	DL (%)	EE (%)
P68 (Blank)	P68:	10	12.5 ± 4.5	0.243 ± 0.050	-3.78 ± 6.69	-	-
P68 - Curcumin	P68: Curcumin:	10 2	184.3 ± 12.6	0.124 ± 0.040	-5.88 ± 5.74	13.49 ± 3.17	78.57 ± 21.26
P68 - Curcumin + DFO	P68: Curcumin: DFO:	10 0.28 5	177.2 ± 14.9	0.068 ± 0.029	-0.44 ± 2.72	Curcumin: 1.40 ± 0.25 DFO: 24.26 ± 3.18	Curcumin: 66.91 ± 10.40 DFO: 65.63 ± 11.10
P68 - DFO	P68: DFO:	10 2	73.1 ± 12.5	0.217 ± 0.021	-2.22 ± 2.08	15.98 ± 0.92	95.17 ± 6.54
Sol (Blank)	Sol:	10	15.3 ± 3.1	0.136 ± 0.061	-4.84 ± 7.02	-	-
Sol - Curcumin	Sol: Curcumin:	10 2	173.3 ± 12.1	0.201 ± 0.021	-8.33 ± 8.69	14.27 ± 0.61	83.25 ± 4.15
Sol - Curcumin + DFO	Sol: Curcumin: DFO:	10 0.28 5	13.9 ± 1.3	0.161 ± 0.064	-0.36 ± 1.01	Curcumin: 1.42 ± 0.16 DFO: 30.47 ± 2.94	Curcumin: 74.71 ± 8.25 DFO: 89.88 ± 12.31
Sol - DFO	Sol: DFO:	10 2	16.9 ± 4.4	0.144 ± 0.072	-1.52 ± 1.67	16.13 ± 0.77	96.20 ± 5.41

All P68 and Sol nanoformulations had low polydispersity as represented by mean polydispersity indices <0.22 suggesting that the majority of the nanocarriers within the formulation are of a similar size (table 1). The P68 and Sol nanocarriers had similar low negative surface charges (-0.36 to -8.33 mV) for each condition, with curcumin nanocarriers in both cases having the most negative charge and combined curcumin and DFO nanocarriers having the least (table 1).
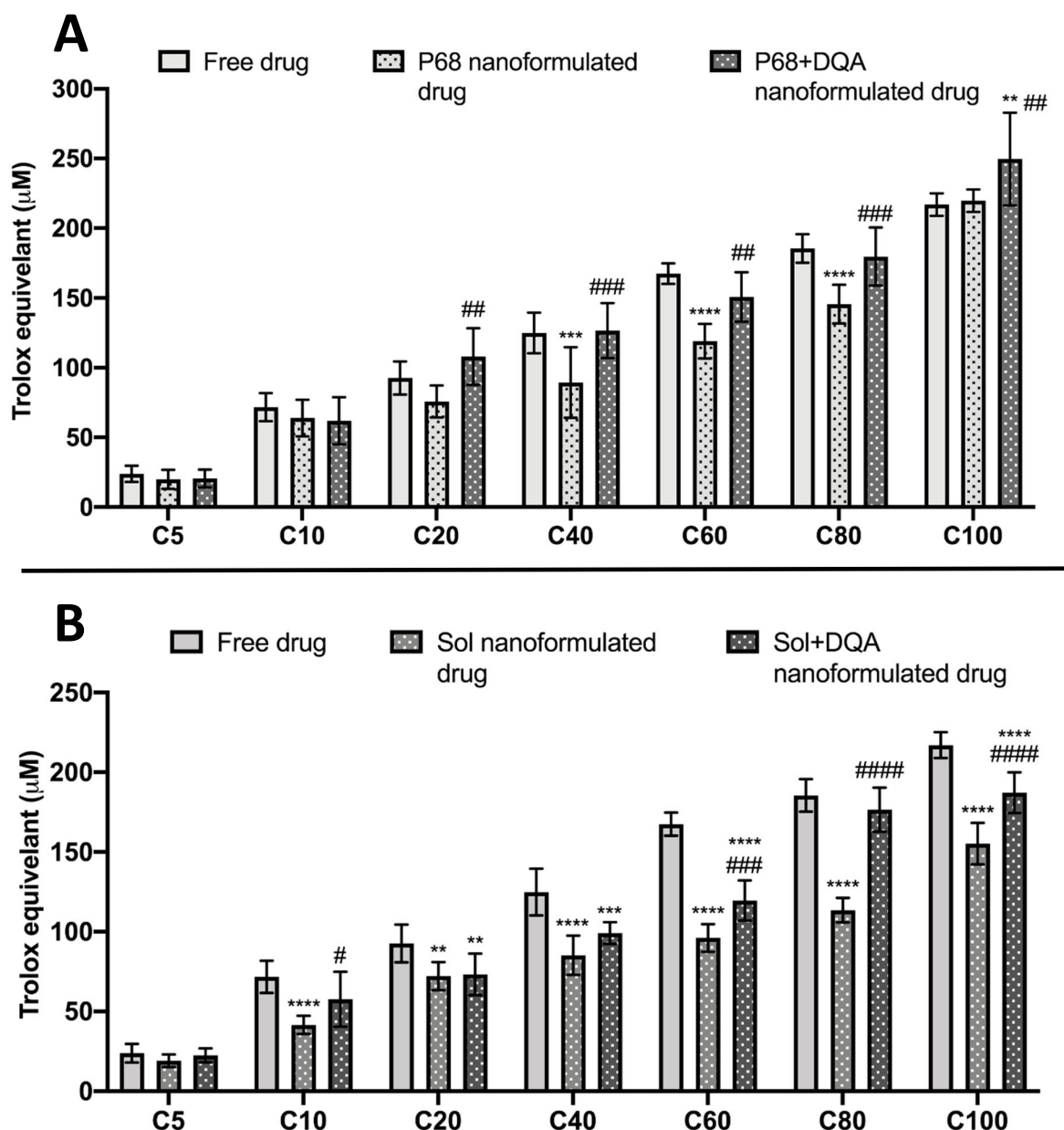
Figure 1. A. Antioxidant activity of free, P68 and P68+DQA nanoformulated $5 - 100$ μM curcumin measured by the FRAP assay (mean ± S.D., n=6). B. Corresponding FRAP assay results for free, Sol and Sol+DQA nanoformulated curcumin. * represents significance values of nanoformulated drug compared to free drug within the same treatment condition (**** $p < 0.0001$, *** $p < 0.001$, ** $p < 0.01$). In A. # represents significance values of P68 compared to P68+DQA nanoformulated drug within the same treatment condition (### $p < 0.001$, ## $p < 0.01$). In B. # represents significance values of Sol compared to Sol+DQA nanoformulated drug within the same treatment condition (#### $p < 0.0001$, ### $p < 0.001$, # $p < 0.05$).

In order for the nanocarriers to be able to target mitochondria, DQA was added to each of the P68 and Sol curcumin nanoformulations at a low enough concentration to aid targeting but to prevent toxicity (as previously described in Zupančič et al., 2014) (table 2). The antioxidant power of each formulation was compared to the corresponding free curcumin at a range of concentrations (5 - 100μM) using the FRAP assay (figure 1). The antioxidant capacity of DFO was not assessed because it is an iron chelator and not an antioxidant.

When comparing the free, P68 and P68+DQA nanoformulated curcumin significant differences in mean trolox equivalent antioxidant capacity were observed between the different concentrations of curcumin treatments ($F_{(6, 105)}$= 352.5, $p < 0.0001$) and the different treatment preparation types ($F_{(2, 105)}$ = 29.12, $p < 0.0001$) (figure 1). All concentrations of the P68+DQA curcumin nanocarriers had similar antioxidant capacity as the corresponding free drug concentrations of curcumin and was significantly higher at 100 μM curcumin ($p = 0.0035$) (figure 1A). However, at between 40 μM and 80 μM, free curcumin exhibited higher antioxidant capacity than the corresponding P68 curcumin concentrations (40 μM - $p = 0.0004$, 60 μM - $p < 0.0001$, 80 μM - $p < 0.0001$) (figure 1A). In most cases, the P68+DQA nanoformulations also had higher antioxidant capacity than the P68 nanoformulations, between 14% and 43% (20 μM - $p = 0.0015$, 40 μM - $p = 0.0002$, 60 μM - $p = 0.0018$, 80 μM - $p = 0.0007$, 100 μM - $p = 0.0035$) (figure 1A). The highest difference was observed at 20 μM where P68+DQA curcumin exhibited 43% higher antioxidant capacity than P68 curcumin (figure 1A). The addition of DQA to the Sol curcumin formulations also increased antioxidant capacity of the Sol formulations at the majority of curcumin concentrations by between 21% and 56% (10 μM - $p = 0.0261$, 60 μM - $p = 0.0006$, 80 μM - $p < 0.0001$, 100 μM - $p < 0.0001$) (figure 1B). However, at all concentrations between 20 μM and 40 μM, free curcumin exhibited significantly higher antioxidant capacity than both Sol and Sol+DQA formulations ($p < 0.0001$ in all cases except 20 μM Sol - $p = 0.0031$, 20 μM Sol+DQA – $p = 0.0054$ and 40 μM Sol+DQA - $p = 0.0002$) (figure 1B).

To find the optimal concentration of curcumin and DFO to use in the drug-loaded nanocarriers, various concentrations of free curcumin (5 μM – 100 μM) and DFO (10 μM – 200 μM) were tested on SH-SY5Y cells to assess cytotoxicity (figure 2, 3).
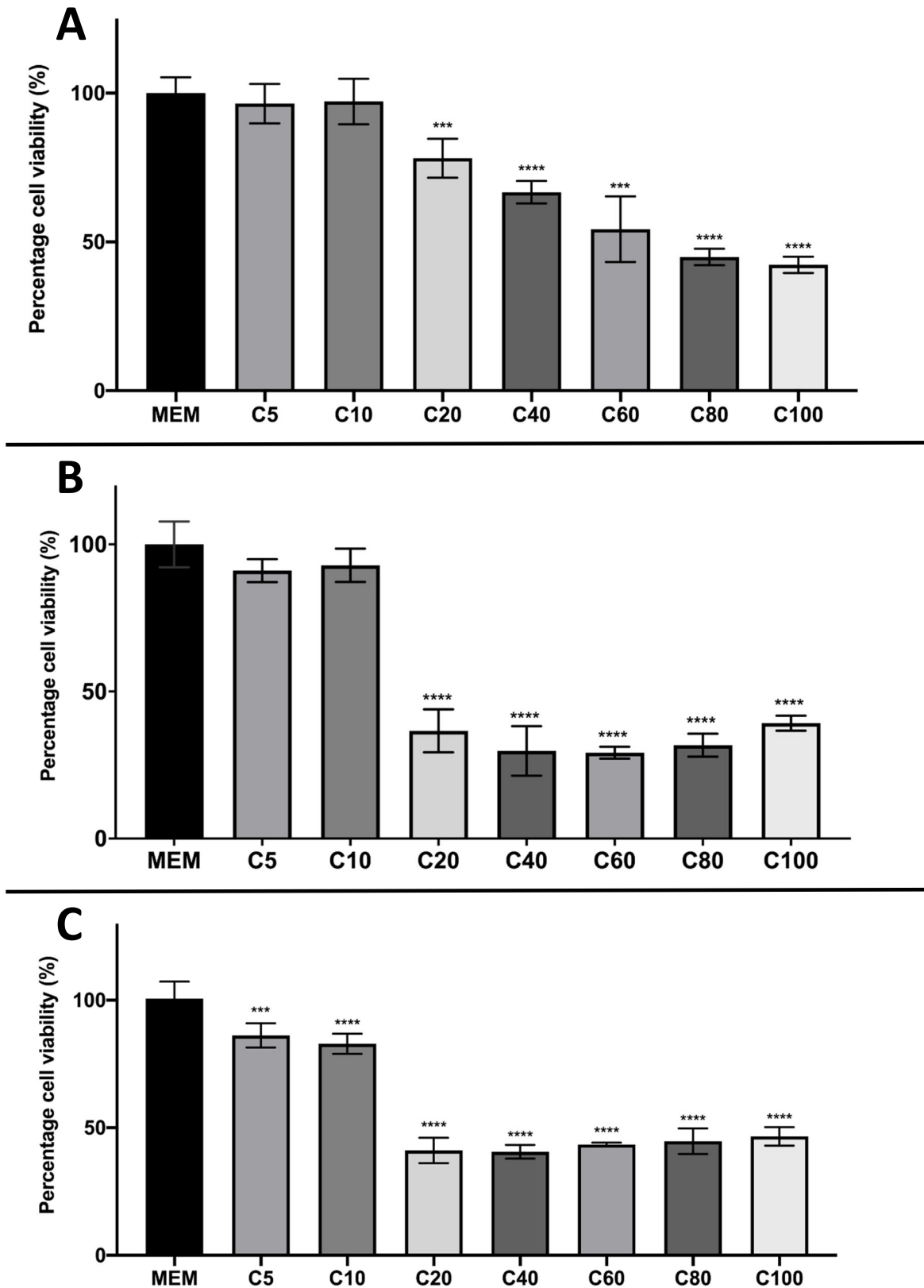
Figure 2. A. MTT assay results of 24 h 5 μM – 100 μM curcumin treatment. MEM represents the control condition where cells were only treated with media (mean ± S.D., n=6). B. Corresponding MTT assay results for 48 h curcumin treatments. C. Corresponding MTT assay results for 72 h curcumin treatments * represents significance values of the treatment conditions compared to the control condition (**** p < 0.0001, *** p < 0.001).
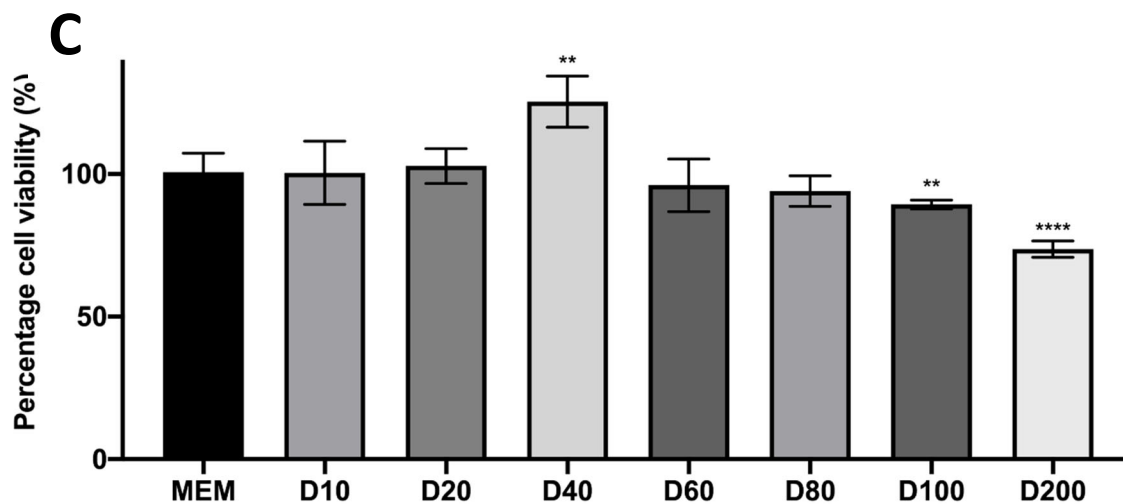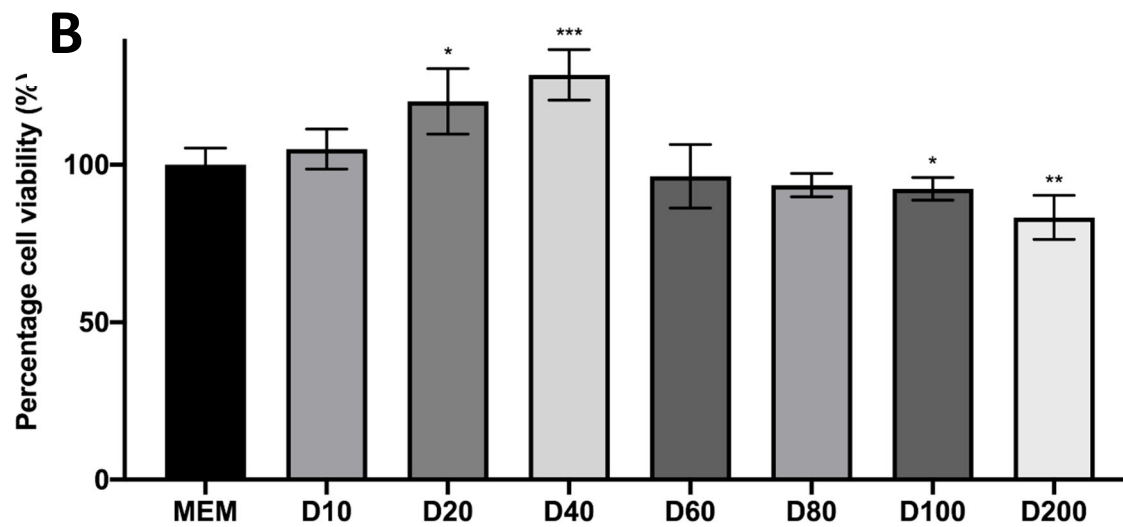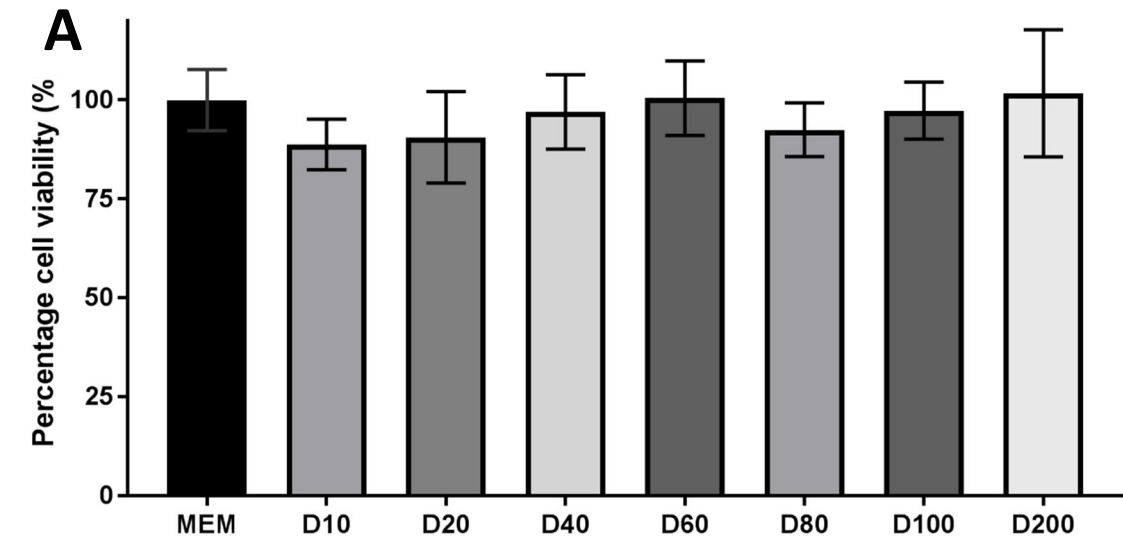
Figure 3. A. MTT assay results of 24 h 10 μM – 200 μM DFO treatment. MEM represents the control condition where cells were only treated with media (mean ± S.D., n=6). B. Corresponding MTT assay results for 48 h DFO treatments. C. Corresponding MTT assay results for 72 h DFO treatments. * represents significance values of the treatment conditions compared to the control condition (**** $p < 0.0001$, *** $p < 0.001$, **$p < 0.01$, * $p < 0.05$).

Significant differences in mean cell viability were observed between the different curcumin concentrations at 24 h ($F_{(7, 22.84)}$ = 98.7, $p < 0.0001$), 48 h ($F_{(7, 40)}$ = 3.019, $p = 0.0121$) and 72 h ($F_{(7, 36.79)}$ = 250.2, $p < 0.0001$) (figure 2). Similarly, significant differences were also observed between the different DFO concentrations at the 48 h ($F_{(7, 27.87)}$ = 25.97), $p < 0.0001$) and 72 h ($F_{(7, 25.72)}$= 24.71, $p < 0.0001$) time points but not at 24 h ($F_{(7, 40)}$ = 0.1488, $p = 0.1488$) (figure 3). 5 μM and 10 μM curcumin both maintained cell viability at control levels whereas concentrations of 20 μM and above significantly reduced cell viability to levels below 80% following treatment for 24 h ($p < 0.0001$) (figure 2A). In contrast all concentrations of DFO (10 μM – 200 μM) maintained cell viability compared to control, with no evidence of toxicity after 24 h treatment (figure 3A). A similar pattern was observed for both curcumin and DFO following 48 h (figure 2B, 3B) and 72 h treatment (figure 2C, 3C). Although by 72 h, there was also a significant reduction in cell viability at 10 μM and 20 μM curcumin as well as with 100 μM and 200 μM DFO ($p < 0.0001$). The highest concentrations of free curcumin (5 μM and 10 μM) and DFO (100 μM) that exhibited no cytotoxicity (defined as cell viability below 80%) at each time point were then assessed in the P68 and Sol nanoformulations.

Figure 4 shows the effects of the P68 and Sol nanoformulated curcumin (5 μM and 10 μM) and/or DFO (100 μM) and corresponding blank formulations on SH-SY5Y cell viability following 24 h treatment, in comparison with the corresponding free curcumin and/or DFO conditions. No significant differences in mean cell viability were observed between the P68 and free curcumin and/or DFO conditions ($F_{(12, 65)}$ = 0.8932, $p = 0.5581$) (figure 4A), whereas significant differences were observed between the Sol and free curcumin and/or DFO conditions ($F_{(12, 65)}$ = 2.836, $p = 0.0035$) (figure 4B). All P68 nanocarriers (drug-loaded and corresponding blank formulations) maintained cell viability at control levels (figure 4A). In general, there was marginally less toxicity following P68 nanocarrier 24 h treatments compared to the free drug conditions and, with the combination of 10 μM curcumin and 100 μM DFO, the formulation into P68 nanocarriers appears to protect against the toxicity induced by the combination of the free drugs ($p = 0.0001$) (figure 4A). In contrast, only the curcumin-loaded Sol nanocarriers were able to maintain cell viability at control levels, with the DFO and combined curcumin and DFO treatment conditions resulting in significant toxicity ($p < 0.0001$) (figure 4B). Similarly, to the P68 nanocarriers, the 5 μM and 10 μM

curcumin-loaded Sol nanocarrier treatments resulted in marginally higher cell viability than the corresponding free drug conditions (p = 0.0273 and p = 0.0097, respectively) (figure 4B). As a result, loading of curcumin and/or DFO was continued in the P68 and P68+DQA nanocarriers for further assessment but only curcumin was used for the Sol and Sol+DQA nanocarriers.
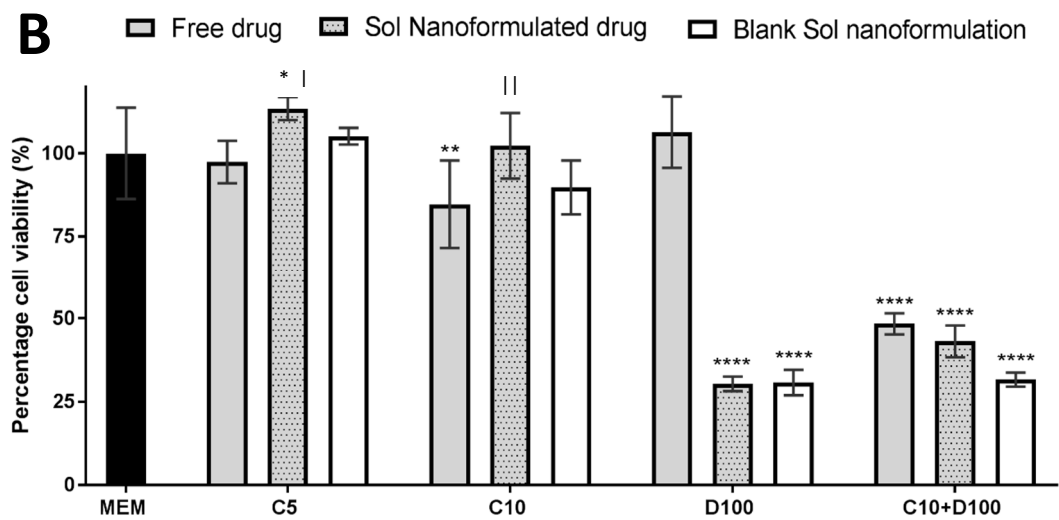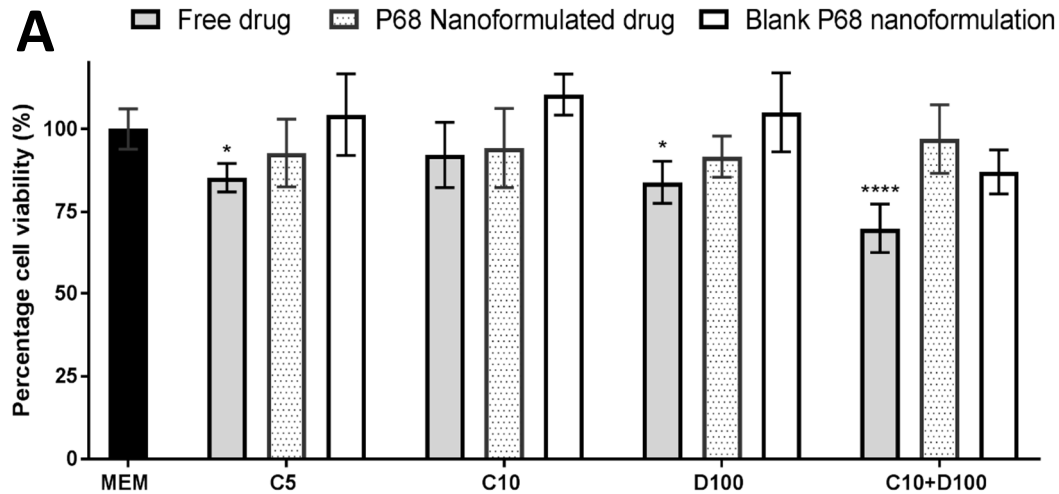
Figure 4. A. MTT assay results of 24 h treatment with free drug, P68 nanoformulated or corresponding blank preparations of either 5 μM or 10 μM curcumin (C5, C10), 100 μM DFO (D100) or combined 5 μM or 10 μM curcumin with 50 μM or 100 μM DFO (C5+D50, C10+D100). MEM represents the control condition where cells were only treated with media (mean ± S.D., n=6). B. Corresponding MTT assay results for 24 h free drug, Sol nanoformuated drug or corresponding blank treatments (mean ± S.D., n=6). * represents significance values of treatment conditions compared to the control condition (**** $p < 0.0001$, ** $p < 0.01$, * $p < 0.05$). | represents significance values of nanoformulated drug compared to free drug within the same treatment condition (|| $p < 0.01$, | $p < 0.05$).

The addition of DQA to aid mitochondrial targeting of these nanocarriers did not significantly change the particle size of the P68 or Sol nanocarriers (table 1 and 2). However, it did result in more positive surface charges (0.02 to 9.29 mV) and appears to have resulted in increased encapsulation efficiency in some cases, for example with combined curcumin and DFO P68 nanocarriers from 67% and 66% to 86% and 96%, respectively (table 1 and 2).

Table 2. Hydrodynamic Diameter (d), Polydispersity Index (PDI), Surface Charge, Drug Loading (DL) and Encapsulation Efficiency (EE) of blank and drug-loaded P68+DQA and Sol+DQA nanoformulations prepared at 80°C (mean ± S.D. n=6).

Sample	Contents (mg/ml)		d (nm)	PDI	Charge (mV)	DL (%)	EE (%)
P68+DQA (Blank)	P68: DQA:	9 1	25.52 ± 10.3	0.24 ± 0.04	0.78 ± 0.80	-	-
P68+DQA - Curcumin	P68: DQA: Curcumin:	9 1 2	182.6 ± 31.5	0.099 ± 0.09	4.27 ± 4.15	14.68 ± 1.55	86.17 ± 10.58
P68+DQA - Curcumin + DFO	P68: DQA: Curcumin: DFO:	9 1 0.28 5	191.8 ± 45.3	0.078 ± 0.04	9.29 ± 5.12	Curcumin: 1.01 ± 0.19 DFO: 31.77 ± 1.80	Curcumin: 81.78 ± 10.16 DFO: 95.56 ± 7.83
P68+DQA - DFO	P68: DQA: DFO:	9 1 2	50.44 ± 33.1	0.246 ± 0.05	0.02 ± 1.62	16.10 ± 0.43	95.94 ± 3.07
Sol+DQA - Curcumin	Sol: DQA: Curcumin:	9 1 2	141.3 ± 26.9	0.186 ± 0.02	4.65 ± 1.32	16.05 ± 0.72	93.03 ± 0.15

TEM analysis shows generally spherical morphology with characteristically small particle size typical of micelles (10 - 200 nm) for all P68 and P68+DQA drug-loaded nanocarriers imaged. The particle sizes shown in the TEM images are consistent with the mean zeta-average particles sizes for each formulation, which ranged from 50 – 184 nm (figure 5, table 1 and 2).

	DFO	DFO + Curcumin	Curcumin

P68 nanocarriers

500 nm
HV = 120.0 kV, Direct Mag: 17500x

500 nm
HV = 120.0 kV, Direct Mag: 17500x

500 nm
HV = 120.0 kV, Direct Mag: 13500x

P68 + DQA nanocarriers

500 nm
HV = 120.0 kV, Direct Mag: 17500x

500 nm
HV = 120.0 kV, Direct Mag: 33500x

500 nm
HV = 120.0 kV, Direct Mag: 17500x
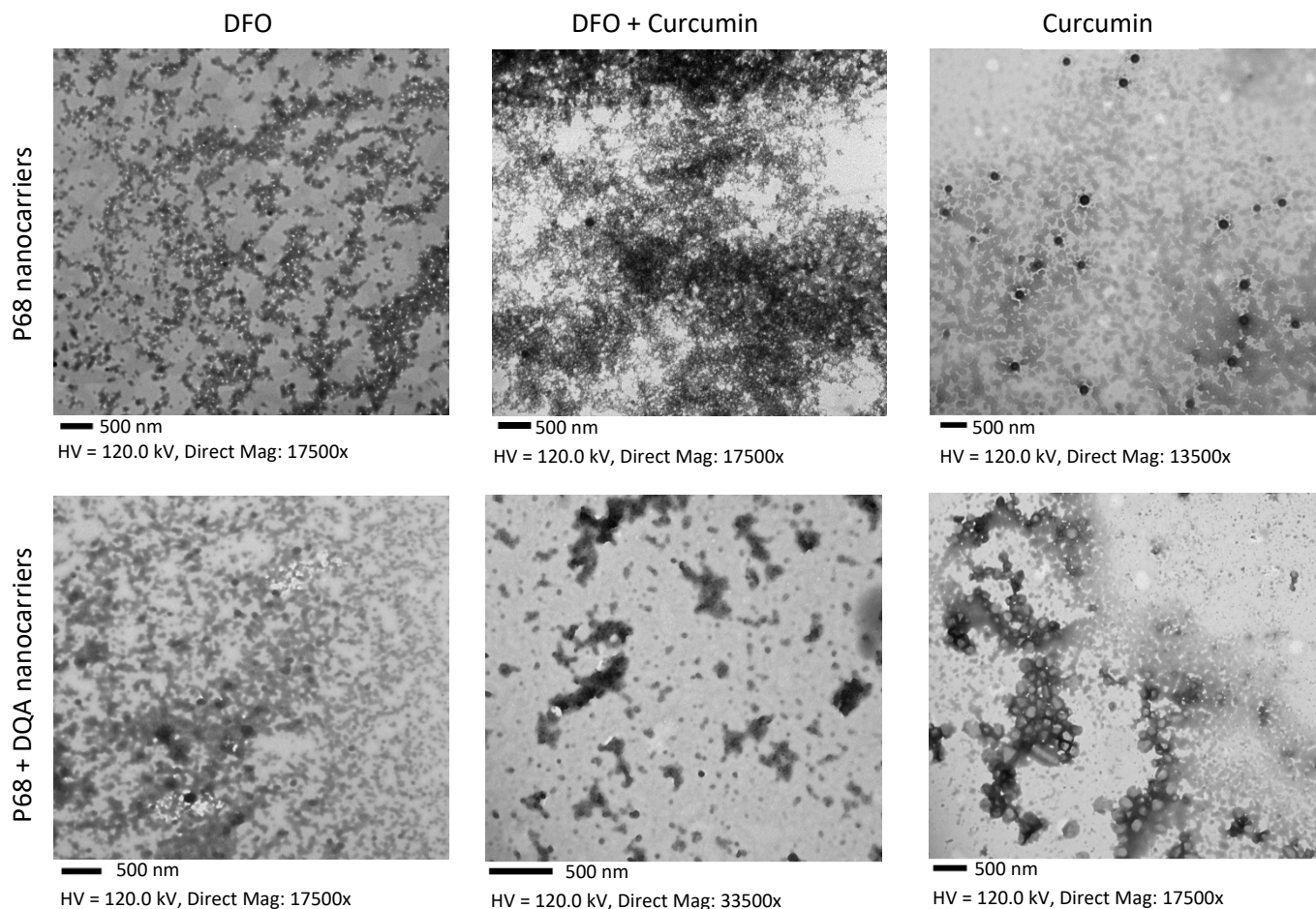
Figure 5. TEM images of P68 and P68+DQA drug-loaded nanocarriers. Scale = 500 nm in all cases.

Figure 6 presents the XRD patterns of free curcumin, free DFO, P68, DQA, Sol and the lyophilized formulations of curcumin and/or DFO-loaded P68, P68+DQA, Sol and Sol+DQA nanocarriers. The spectrum of curcumin shows the main peaks at 8.98, 12.28, 14.60, 17.28, 18.22, 19.56, 21.30, 23.42, 25.62, 27.44, 29.14 and 44.4°, indicating a high level of crystallinity (figure 6(i)A, (ii)A, (v)A-(viii)A). The spectrum of DFO also shows a high level of crystallinity with main peaks at 11.44, 14.16, 17.60, 18.20, 20.76, 20.94, 22.56, 25.20, 27.58, 33.22 and 44.38° (figure 6(iii)A, (iv)A, (v)B, (vi)B). The P68 spectrum exhibits fewer peaks than DFO and curcumin, the main ones being at 18.94, 23.08, 26.80 and 44.24° showing some crystalline features (figure 6(i-iv)B, (v-vi)C).
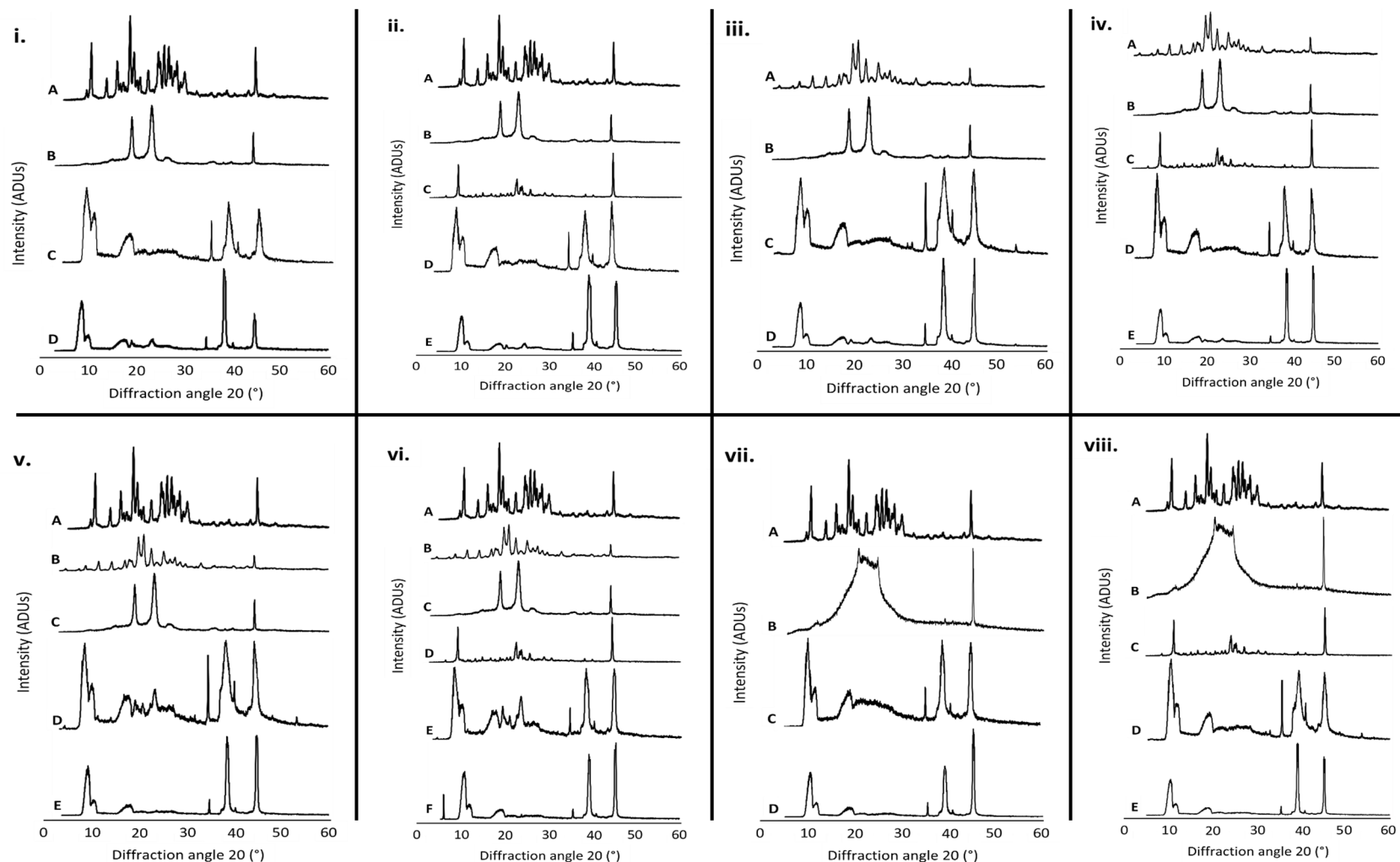
*Figure 6. **(i) P68 curcumin.** XRD patterns of (a) curcumin, (b) P68, (c) a physical mixture of P68, DQA and curcumin in the same ratio as the nanoformulation and (d) lyophilized P68 curcumin nanoformulation. **(ii) P68+DQA curcumin.** XRD patterns of (a) curcumin, (b) P68, (c) DQA, (d) a physical mixture of P68, DQA and curcumin in the same ratio as the nanoformulation and (e) lyophilized P68+DQA curcumin nanoformulation. **(iii) P68 DFO.** XRD patterns of (a) DFO, (b) P68, (c) a physical mixture of P68 and DFO in the same ratio as the nanoformulation and (d) lyophilized P68 DFO nanoformulation. **(iv) P68+DQA DFO.** XRD patterns of (a) DFO, (b) P68, (c) DQA, (d) a physical mixture of P68, DQA and DFO in the same ratio as the nanoformulation and (e) lyophilized P68+DQA DFO nanoformulation. **(v) P68 curcumin+DFO.** XRD patterns of (a) curcumin, (b) DFO, (c) P68, (d) a physical mixture of P68, curcumin and DFO in the same ratio as the nanoformulation and (e) lyophilized P68 curcumin+DFO nanoformulation. **(vi) P68+DQA curcumin+DFO.** XRD patterns of (a) curcumin, (b) DFO, (c) P68, (d) DQA, (e) a physical mixture of P68, DQA, curcumin and DFO in the same ratio as the nanoformulation and (f) lyophilized P68+DQA curcumin+DFO nanoformulation. **(vii) Sol curcumin.** XRD patterns of (a) curcumin, (b) Sol, (c) a physical mixture of Sol and curcumin in the same ratio as the nanoformulation and (d) lyophilized Sol curcumin nanoformulation. **(viii) Sol+DQA curcumin.** XRD patterns of (a) curcumin, (b) Sol, (c) DQA, (d) a physical mixture of Sol, DQA and curcumin in the same ratio as the nanoformulation and (e) lyophilized Sol+DQA curcumin nanoformulation.*

85

DQA spectrum results also show crystallinity with the main peaks at 9.42, 22.64, 23.98, 25.72 and 44.5° (figure 6(ii)C, (iv)C, (vi)C, (viii)C). The Sol spectrum data, however, shows a different profile with one larger peak between 18.96 and 23.16° and a single peak at 44.24° (figure 6(vii-viii)B). The spectra of lyophilized P68 (figure 6 (i)D, (iii)D, (v)E), P68+DQA (figure 6(ii)E, (iv)E, (vi)F), Sol (figure 6(vii)D) and Sol+DQA (figure 6(viii)E) drug-loaded formulations revealed far fewer peaks than its constituent components with generally only 3 main peaks at around 8.6, 34.5, 38.2 and 44.6° indicating a more amorphous state for all components. This reduction of peaks was not observed for any of the physical mixtures of the formulation components (figure 6).

Figure 7 shows the FTIR spectrum for each of the P68 and P68+DQA curcumin and/or DFO lyophilized formulations as well as the Sol and Sol+DQA curcumin lyophilized formulations, the individual components of each formulation and the physical mixture of these components. The curcumin FTIR spectrum (figure 7ia, iia, v-viiia) highlight the presence of hydroxyl groups (OH) with the sharp peak at 3510 cm^{-1} and broad peak at 3300 cm^{-1}. The peak at 1626 cm^{-1} results from the vibrations of the C=C bonds and the strong peak at 1505 cm^{-1} represents the stretching vibrations of the aromatic ring. The stretching of the enol hydroxyl group directly bonded to an alkene (C=C) and carbonyl (C=O) groups are represented by peaks at 1204 cm^{-1} and 962 cm^{-1}, respectively. The FTIR spectrum for DFO (figure 7iiia, iva, vb, vib) includes stretching vibrations of characteristic bonds for OH (3324, 1472, 1386 cm^{-1}), C=O (2864, 1652, 1536, 974 and 897 cm^{-1}), NH$_2$ (1598 cm^{-1}) and N-H (3115, and 1608 cm^{-1}). The FTIR spectrum for P68 (figure 7ib-ivb, vc, vic) shows characteristic peaks at around 2880, 1060, 841 cm^{-1}, representing the vibrations of the hydroxyl groups and the stretching vibrations of the symmetrical C-O and asymmetrical C-O of the ether groups, respectively. A vibration of the methylene group (CH$_2$) is also observable at 1279 cm^{-1}. Whereas the spectrum for Sol (figure 7viib, viiib) showed characteristic hydroxyl and ester (a carbon atom bound to a carbon *via* single bond, an oxygen *via* double bond, and an oxygen *via* single bond) groups at 2924 and 1732 cm^{-1}, respectively. The DQA spectrum (figure 7iic, ivc, vid, viiic) shows the absorption peaks for the two primary amine groups for N-H stretches, asymmetrical and symmetrical, at 3342 and 3264 cm^{-1}. The sharp peak at 1605 cm^{-1} represents the vibration of aromatic C=C bonds and the peaks at 2928 and 2847 cm^{-1} represent methyl group stretching and deformation.
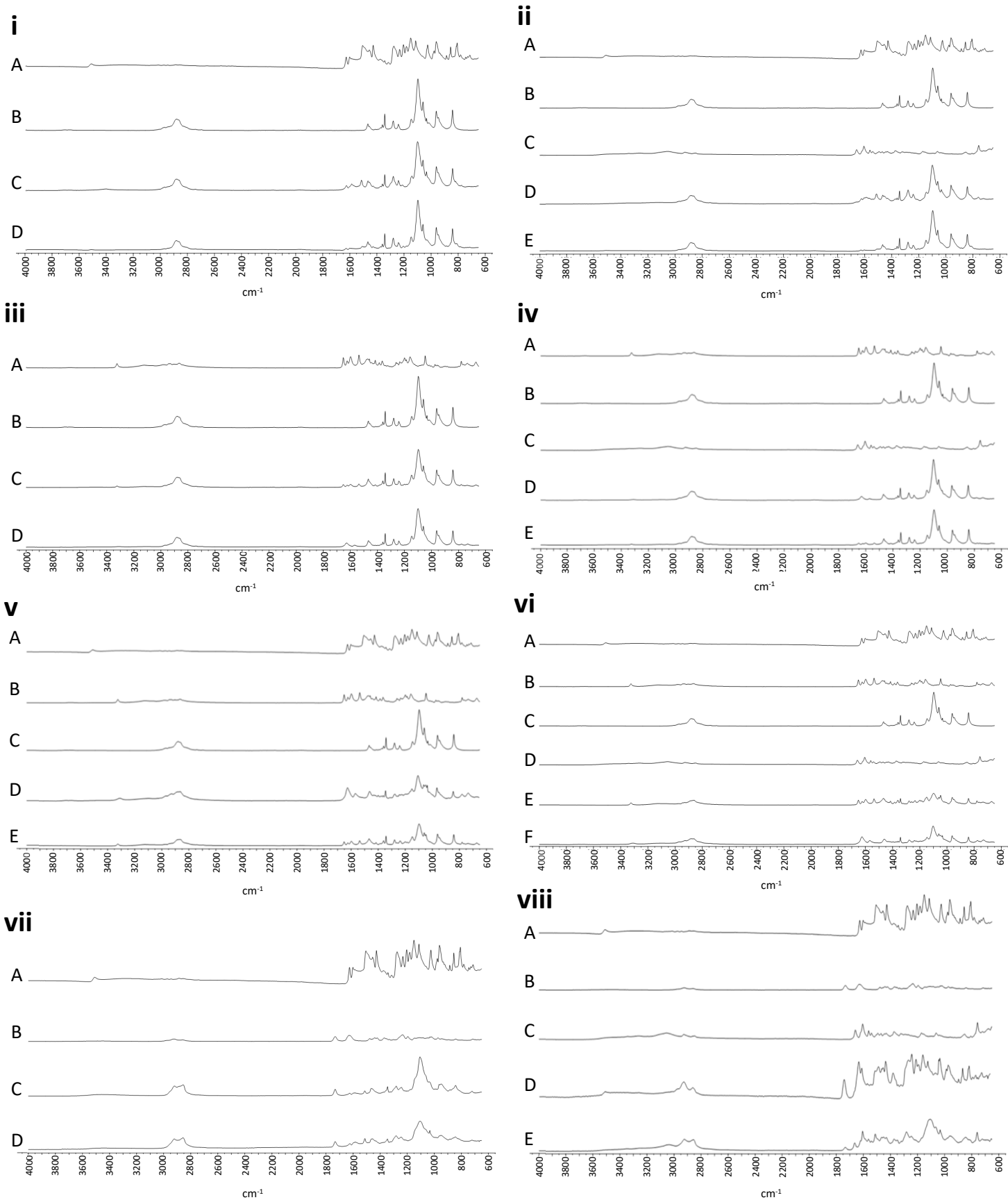
*Figure 7 **(i) P68 curcumin**. FTIR spectra for (a) curcumin, (b) P68, (c) a physical mixture of P68, DQA and curcumin in the same ratio as the nanoformulation and (d) lyophilized P68 curcumin nanoformulation. **(ii) P68+DQA curcumin.** FTIR spectra for (a) curcumin, (b) P68, (c) DQA, (d) a physical mixture of P68, DQA and curcumin in the same ratio as the nanoformulation and (e) lyophilized P68+DQA curcumin nanoformulation. **(iii) P68 DFO.** FTIR spectra for (a) DFO, (b) P68, (c) a physical mixture of P68 and DFO in the same ratio as the nanoformulation and (d) lyophilized P68 DFO nanoformulation. **(iv) P68+DQA DFO.** FTIR spectra for (a) DFO, (b) P68, (c) DQA, (d) a physical mixture of P68, DQA and DFO in the same ratio as the nanoformulation and (e) lyophilized P68+DQA DFO nanoformulation. **(v) P68 curcumin+DFO.** FTIR spectra for (a) curcumin, (b) DFO, (c) P68, (d) a physical mixture of P68, curcumin and DFO in the same ratio as the nanoformulation and (e) lyophilized P68 curcumin+DFO nanoformulation. **(vi) P68+DQA curcumin+DFO.** FTIR spectra for (a) curcumin, (b) DFO, (c) P68, (d) DQA, (e) a physical mixture of P68, DQA, curcumin and DFO in the same ratio as the nanoformulation and (f) lyophilized P68+DQA curcumin+DFO nanoformulation. **(vii) Sol curcumin.** FTIR spectra for (a) curcumin, (b) Sol, (c) a physical mixture of Sol and curcumin in the same ratio as the nanoformulation and (d) lyophilized Sol curcumin nanoformulation. **(viii) Sol+DQA curcumin.** FTIR spectra for (a) curcumin, (b) Sol, (c) DQA, (d) a physical mixture of Sol, DQA and curcumin in the same ratio as the nanoformulation and (e) lyophilized Sol+DQA curcumin nanoformulation.*

The physical mixtures for each formulation (figure 7ic, iid, iiic, ivd, vid, viic, viiid) show peaks corresponding to the constituent parts within the mixture. However, in most cases the peaks of the curcumin and/or DFO components appear less intense within the physical mixtures. The FTIR spectrum for each of the lyophilized formulations are similar to those of the physical mixtures but with decreased intensity in most cases (figure 7ic-d, iid-e, iiic-d, ivd-e, vd-e, vie-f, viic-d, viiid-e).

3.3. Discussion

Nanocarriers were developed using the amphiphilic polymers P68 and Sol as they have been successfully used to develop micellar nanocarriers of numerous compounds (Hörmann & Zimmer 2016, Lee et al., 2018; Desfrançois et al., 2018) including curcumin and DFO for other indications (Shaikh et al., 2009, Zhao et al., 2012, Kumar et al., 2014, Hong et al., 2017). The use of micelles in particular was primarily based on the known ability of micelles to cross the BBB with low toxicity (Gaucher et al., 2005; Batrakova & Kabanov 2008, Kataoka et a., 2012; Elezaby et al., 2017; Rakotoarisoa and Angelova, 2018). Mitochondrial targeting of nanocarriers using DQA has been established (Weissig et al., 1998, Lyrawati et al., 2011) therefore the addition of DQA to the nanoformulation was used to assess whether mitochondrial targeting would result in increased potency since mitochondria are the primary site for iron-induced oxidative stress (Bratic & Nils-Larsson, 2013; Kandola et al., 2015).

Curcumin and/or DFO were successfully incorporated into P68, Sol, P68+DQA and Sol+DQA nanocarriers, with high loading efficiency (table 1, 2). This is consistent with reports that micelles have high encapsulation efficiencies (Zhang et al., 2012, Elezaby et al., 2017; Rakotoarisoa and Angelova, 2018). The FRAP results suggested a relationship between increased concentration of curcumin and increased antioxidant power (figure 1), this is in line with previous findings from Ak & Gülçin (2008) which also showed that increasing concentrations of curcumin resulted increased ferric reducing ability. Generally, of all the nanoformulations tested, the P68+DQA curcumin nanoformulations were the only formulations to consistently exhibit antioxidant power comparable or higher than the corresponding free curcumin, at all concentrations (figure 1). However, at the 5 μM and 10 μM concentrations which were later selected for treatment in SH-SY5Y cells, all

formulations apart from Sol curcumin at 10 μM exhibited antioxidant power at least as high as free curcumin (figure 1). These results suggest that in the majority of cases these nanoformulations should perform at least as well as free curcumin at protecting against oxidative stress. Ultimately the 5 μM and 10 μM concentrations of curcumin were selected for further evaluation as these were the highest concentrations of free curcumin that resulted in no cytotoxicity of SH-SY5Y cells after treatment for up to 72 h (figure 2). The antioxidant capacity of DFO was not assessed because it is not an antioxidant but also because it is an iron chelator and the assay components contain iron in the ferric tripyridyl triazine complex. The antioxidant capacity is therefore calculated by the ability of a compound to reduce this complex to the ferrous form, measured by a colorimetric reaction and if iron is chelated and bound to DFO no such reaction can be expected to occur. The range of concentrations of DFO (10 – 200 μM) were therefore only evaluated for cytotoxicity. As with curcumin, 100 μM DFO was selected as it was the highest concentration of DFO that did not exhibit cytotoxicity in SH-SY5Y cells following treatment for 24 – 72 h (figure 3). Such results are consistent with previous studies which suggest 5-10 μM curcumin and 100 μM DFO as the optimal concentrations for treatment in PD models using SH-SY5Y cells (Wu et al., 2010; van der Merwe et al., 2017; Guerzoni et al., 2016). However, when combined, free curcumin and DFO (10 μM and 100 μM, respectively) exhibited toxicity (figure 4A). The corresponding combined curcumin and DFO P68 nanocarriers were able to mitigate this toxicity (figure 4A), retaining cell viability at control levels and in general P68 nanocarriers were less toxic than the corresponding free drug conditions across the board (figure 4A). Treatment with Sol nanocarriers of DFO as well as combined curcumin and DFO, on the other hand, resulted in significant toxicity (figure 4B). This prevented such nanoformulations from being progressed for further testing.

The mean size of both P68 and P68+DQA as well as Sol and Sol+DQA nanocarriers was fairly consistent, in all cases curcumin-loaded nanocarriers had a larger mean size than DFO-loaded nanocarriers, and the addition of DFO to curcumin further increased nanocarrier size but all were under 200 nm. These results are consistent with the ability to cross the BBB (Cruz et al., 2016; Grabrucker et al., 2016). The mean surface charge of the P68 and Sol nanocarriers was relatively neutral, between -0.36 and -8.33 mV (table 1). This may also be beneficial for brain penetrance because most nanocarriers with a low to moderate surface

charge between -1 mV and -15 mV have been shown to pass the BBB (Choi et al., 2010; Wiley et al., 2013; Huang et al., 2011; Bramini et al., 2014). The addition of DQA to the formulations resulted in a moderate alteration in charge to a more positive state (+0.02 to +9.29 mV), consistent with previous use of DQA in lipid-based formulations (Vaidya et al.25; Zupančic et al., 2014), however to a much lesser extent as such studies reported charges up to +50 mV. This slight increase in charge is more suitable for brain delivery as it provides a large enough shift in charge to potentially improve physical stability (Zupančic et al., 2014), whilst remaining relatively neutral compared to highly positive charges which are known to cause toxicity to the BBB (Lockman et al., 2004). Further to this, drugs are more likely to be able to pass the BBB if they are not rapidly cleared from the bloodstream (Saraiva et al., 2016), and neutral nanocarriers have been shown to have longer circulation time in the bloodstream compared to those that are very negatively or very positively charged (Arvizo et al., 2011).

Generally, the TEM images showed that all P68 and P68+DQA drug-loaded nanocarriers were spherical with moderately uniform particle sizes <200 nm, which supports the zeta-average particles size data (figure 3, table 1, 2). The spherical dimensions of these nanocarriers may be beneficial as form and dimensions are known to affect biological responses to nanoparticles; for example, spherical nanoparticles have lower adhesion towards the blood vessel walls than non-spherical nanoparticles (Godin et al., 2012; Barua & Mitragotri, 2014), which may aid delivery to remote regions of the body. The XRD studies revealed that the incorporation of curcumin and DFO within all nanocarriers suppressed the crystallization of the drugs resulting in a more amorphous state. This is also advantageous as it is well-known that crystalline to amorphous transformation generally results in increased solubility and stability (Shi et al., 2018). Similarly, the FTIR analysis also indicates the incorporation of curcumin and/or DFO within each of the relevant nanocarriers as well as suppression of the crystalline nature of each drug due to the decrease in intensity of these components within the relevant lyophilized formulations compared to the physical mixtures (figure 7). However, importantly there were no major shifts in the peaks of the FTIR spectra when comparing the lyophilized formulations and physical mixtures. This highlights that there was no conjugation or interaction between any of the chemical groups within the formulations since conformational change of a substance can be represented by shifts in

peaks within the FTIR spectrum as it interacts with the other compounds present in the sample (Bourassa et al., 2010; Zupančic et al., 2014).

Overall, taken together, these results suggest that P68 and P68+DQA curcumin and/or DFO nanocarriers as well as Sol and Sol+DQA curcumin nanocarriers have the relevant characteristics to access the brain without producing cytotoxicity.

3.4. Conclusion

In summary, these results demonstrate the successful formulation of P68 and P68+DQA curcumin and/or DFO nanocarriers, as well as Sol and Sol+DQA curcumin nanocarriers, with the necessary characteristics to improve stability, pass the BBB, and aid combination therapy without inducing toxicity. This strategy may thus provide a novel approach to fully utilise their therapeutic benefit for PD. Further work described in the next chapters will test these nanocarriers in an *in vitro* PD model to assess their ability to protect against iron-induced oxidative stress and the cell death associated with PD.

Chapter 4 - Assessing the therapeutic potential of micellar nanocarriers containing curcumin and/or DFO in a cellular model of PD

4.1. Introduction

As discussed in chapter 1, abnormalities in iron homeostasis and mitochondrial dysfunction are common features of many neurodegenerative disorders including PD, and oxidative stress, particularly within mitochondria, has been highlighted as a key constituent of such neurodegeneration. In PD, as well as elevated free iron levels within mitochondria (Dexter et al., 1987; Griffiths et al., 1999; Graham et al., 2000; Martin et al., 2008; Wallis et al., 2008; Rossi et al., 2013), there are also reduced levels of the natural antioxidant glutathione (Sian et al., 1994; Bavarsad Shahripiour et al., 2014). Together, this can drive accumulation of toxic hydroxyl radicals resulting in sustained oxidative stress and cellular damage (Kandola et al., 2015; Costa-mallen et al., 2017). Studies have shown that PD-like phenotype and pathology can be induced by intra-nigral injection of iron in rats (Ben-Shachar et al., 1991), and that there is a significant correlation between elevated SN iron depositions and the motor symptoms and non-motor symptoms observed in people with PD (Liu et al., 2017). This suggests that iron-induced oxidative stress may play a key role in the initiation and progression of PD (Halliwell et al., 2001; Gerlach et al., 1994; Dexter et al., 1987). Antioxidants and iron chelators therefore hold promise as potential neuroprotective therapies for PD.

The free radical scavenging properties of antioxidants such as curcumin and the potential of iron chelators such as DFO to limit the availability of detrimental free iron may be a promising mechanism to limit the degenerative process in PD. Numerous studies have indicated neuroprotective effects of DFO and curcumin (Youdim et al., 2004; Dexter et al., 2011; Devos et al., 2014; Liu et al., 2013; Jiang et al., 2013; Van der Merwe et al., 2017), and the combination of iron chelators and antioxidants may have even more potent effects as together they can completely restore brain function impaired by iron overload in animal models (Sripetchwandee et al., 2014). That said, few studies have investigated the potential of combining antioxidants and iron chelators for PD as combination therapies are

challenging due to the distinct pharmacokinetic profiles of each drug (Anselmo & Mitragotri, 2016). Furthermore, the therapeutic value of these two compounds is limited as curcumin is unstable with low bioavailability and both are unlikely to access the brain at therapeutic concentrations (Yang et al., 2007; Martin-Bastida et al., 2017). Furthermore, long-term effects of continuous iron chelator use are unknown in PD and due to the non-specific nature of such chelators the side effects could be serious since iron is an essential part of numerous cellular processes such as respiration (Pino et al., 2017) and neurotransmitter synthesis (Youndim & Green, 1978; Hidalgo & Nunez, 2007).

Using nanocarriers to deliver antioxidants and iron chelators such as curcumin and DFO, may provide an effective strategy to overcome the limitations of such compounds as they can improve stability of labile molecules and enhance delivery across membranes including the BBB, whilst retaining the potency of entrapped molecules (Masserini et al., 2013; Zupančič et al., 2014). Nanocarriers are also beneficial for combination therapies to ensure that the drugs are delivered together for synergistic effect (Anselmo & Mitragotri, 2016). Polymeric micelles may be particularly advantageous for the combination of curcumin and DFO for PD as the small particle size (10-200 nm) of such nanocarriers is within the ideal range for brain penetrance (Gaucher et al., 2005; Batrakova & Kabanov 2008, Kataoka et al., 2012; Elezaby et al., 2017; Rakotoarisoa and Angelova, 2018). Following successful loading of curcumin and/or DFO into P68, P68+DQA, Sol and Sol+DQA nanocarriers with the relevant characteristics for brain penetrance (described in chapter 2), these formulations need to be tested in a model of PD to assess their potential therapeutic ability against oxidative stress and cell death.

Rotenone is a pesticide and insecticide that is commonly used to induce the characteristic features of PD in both *in vitro* and *in vivo* models (Xicoy et al., 2017). Rotenone is a strong inhibitor of mitochondrial complex 1 and has been linked to the higher incidences of PD in agricultural areas (Tanner et al., 2011). Rotenone inhibits electron transfer from the iron-sulphur clusters in complex I to ubiquinone which blocks oxidative phosphorylation and limits ATP synthesis (Palmer et al., 1968). Such incomplete electron transfer also results in the excessive formation of ROS and together eventually leads to apoptosis of the effected cells (Li et al., 2003; Fato et al., 2009; Heinz et al., 2017). Unlike other neurotoxin models of PD, rotenone models have been shown to produce the most PD-like motor symptoms in

animals as well as most histopathological hallmarks of PD, from iron accumulation and oxidative stress to Lewy body pathology (Betarbet et al., 2006). The SH-SY5Y human neuroblastoma cell line has been the most widely used for *in vitro* models of PD (reviewed in Xicoy et al., 2017). This study therefore aimed to test the micellar P68, P68+DQA, Sol and Sol+DQA nanocarrier delivery systems for curcumin and/or DFO developed in chapter 2 and their ability to protect against rotenone-induced changes in cell viability and oxidative stress in SH-SY5Y neuronal cells.

4.2. Results

Significant differences in mean cell viability were observed following 24 h rotenone treatment ($F_{(7, 28.2)}$ = 8.557, p < 0.0001). Treatment with all concentrations of rotenone (5 µM – 100 µM) for 24 h significantly reduced cell viability compared to the control cells treated with MEM (5 µM: p = 0.0292, 10 µM: p = 0.0029, 20 µM: p = 0.0007, 40 µM – 100 µM: p < 0.0001). SH-SY5Y cells treated with 100 µM rotenone consistently resulted in a reduction of cell viability by 40-50% as required for the PD model (figure 1).
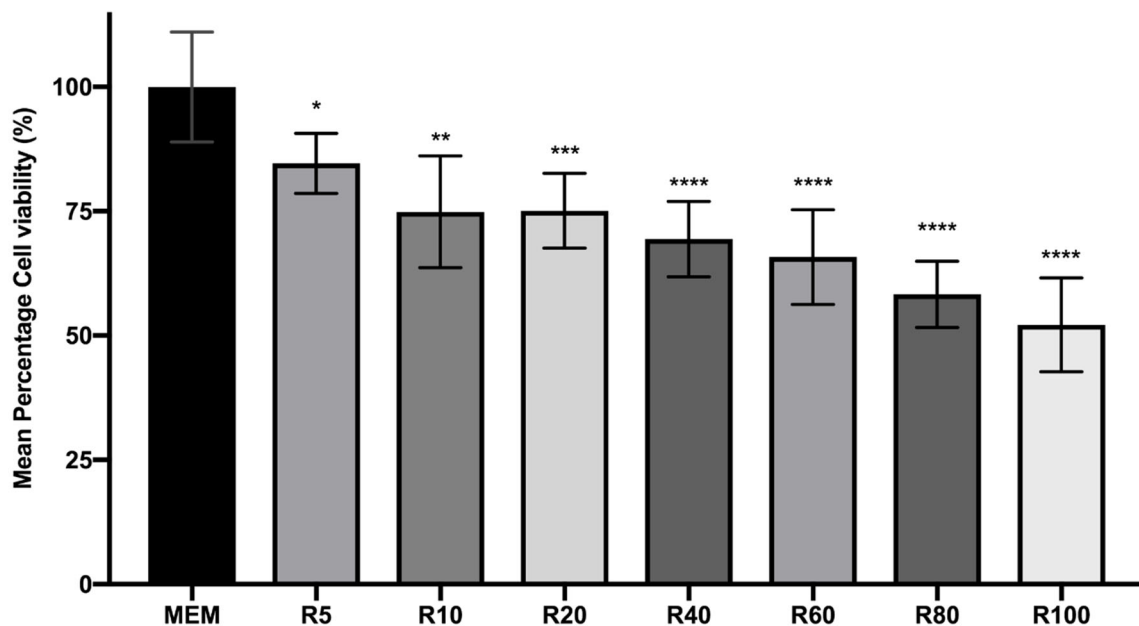
*Figure 1. MTT assay results of 24 h 5 µM – 100 µM rotenone treatment. MEM represents the control condition where cells were only treated with media (mean ± S.D., n=6). * represents significance values of the treatment conditions compared to the control condition (**** p < 0.0001, *** p < 0.001, ** p < 0.01, * p < 0.05).*

When comparing the effects of free drug and P68 nanocarriers on cell viability following rotenone treatment, a significant difference in mean cell viability was observed between the

different treatments (F(16, 94) = 93.97, $p < 0.0001$) (figure 2A). 3 h pre-treatment with P68 nanocarriers of 5 μM and 10 μM curcumin ($p = 0.0039$ and $p = 0.0078$, respectively), 100 μM DFO ($p = 0.0002$) and combined 5 μM curcumin and 50 μM DFO ($p = 0.0029$) significantly protected against the reduction in cell viability induced by 24 h treatment with 100 μM rotenone (figure 2A). Of the P68 nanoformulation conditions which were protective, no single condition was significantly more protective than another. None of the free drug pre-treatment conditions apart from combined 5 μM curcumin and 50 μM DFO ($p = 0.0219$) were able to significantly protect against rotenone, and pre-treatment with the combination of free curcumin (10 μM) and free DFO (100 μM) followed by rotenone treatment appears to be more toxic than rotenone alone ($p = 0.0003$) (figure 2A). There was no significant difference in cell viability following pre-treatment with P68 nanocarriers compared to the corresponding free drug pre-treatments apart from with 10 μM curcumin + 100 μM DFO where pre-treatment with P68 nanocarriers resulted in higher cell viability ($p = 0.0032$), although cell viability remained below 80% in this instance.

Similarly, there was a significant difference in mean cell viability between the different treatments when comparing free drug and P68+DQA nanocarrier pre-treatments followed by rotenone treatment (F(16,60) = 5.639, $p < 0.0001$) (figure 2B). The majority of P68+DQA nanoformulation pre-treatments were able to protect against rotenone (5 μM curcumin ($p < 0.0001$), 10 μM curcumin ($p = 0.0331$), 5 μM curcumin + 50 μM DFO ($p = 0.0104$), 10 μM curcumin + 100 μM DFO ($p = 0.014$)), including the combination for 10 μM curcumin and 100 μM DFO which was not protective in the P68 or free drug conditions (figure 2B). However, P68+DQA nanocarriers of 100 μM DFO did not significantly protect against rotenone. In these results, free 5 μM curcumin pre-treatment was also able to significantly protect against rotenone ($p = 0.0455$). Similar to when using P68 nanocarriers, when comparing P68+DQA nanocarriers with the corresponding free drug pre-treatments, there was only a significant difference found for 10 μM curcumin + 100 μM DFO where pre-treatment with P68+DQA nanocarriers resulted in higher cell viability ($p = 0.004$), however in this case cell viability reached more than 80%.

Figure 2. A. MTT assay results of 3 h pre-treatment with free drug, P68 nanoformulated or corresponding blank preparations of either 5 μM or 10 μM curcumin (C5, C10), 100 μM DFO (D100) or combined 5 μM and 10 μM curcumin with 50 μM and 100 μM DFO (C5+D50, C10+D100) followed by 24 h treatment with 100 μM rotenone (R100) compared to R100 treatment alone. MEM represents the control condition where cells were only treated with media, no pre-treatment nor R100 treatment (mean ± S.D., n=6). B. Corresponding MTT assay results for P68+DQA nanoformulated pre-treatments (mean ± S.D., n=6). * represents significance values of control or pre-treatment conditions compared to treatment rotenone alone (**** p < 0.0001, *** p < 0.001, ** p < 0.01, * p < 0.05). | represents significance values of nanoformulated drug compared to free drug within the same treatment condition (|| p < 0.01).

Likewise, significant differences in mean cell viability were observed between free and Sol+DQA nanoformulated curcumin pre-treatments (F(7, 40) = 3.136, p = 0.0098), however no significant differences were observed between free and Sol nanoformulated curcumin (F(7, 40) = 1.985, p = 0.0814) (figure 3). Both 5 μM and 10 μM curcumin-loaded Sol and

Sol+DQA nanocarrier pre-treatments significantly protected against the reduction in cell viability induced by 24 h treatment with 100 μM rotenone ($p < 0.0001$ in all cases) (figure 3). Although not significant, apart from 5 μM Sol curcumin nanocarriers compared to 5 μM free curcumin ($p = 0.0224$), both Sol and Sol+DQA nanocarriers were generally superior to the corresponding free curcumin conditions (figure 3).
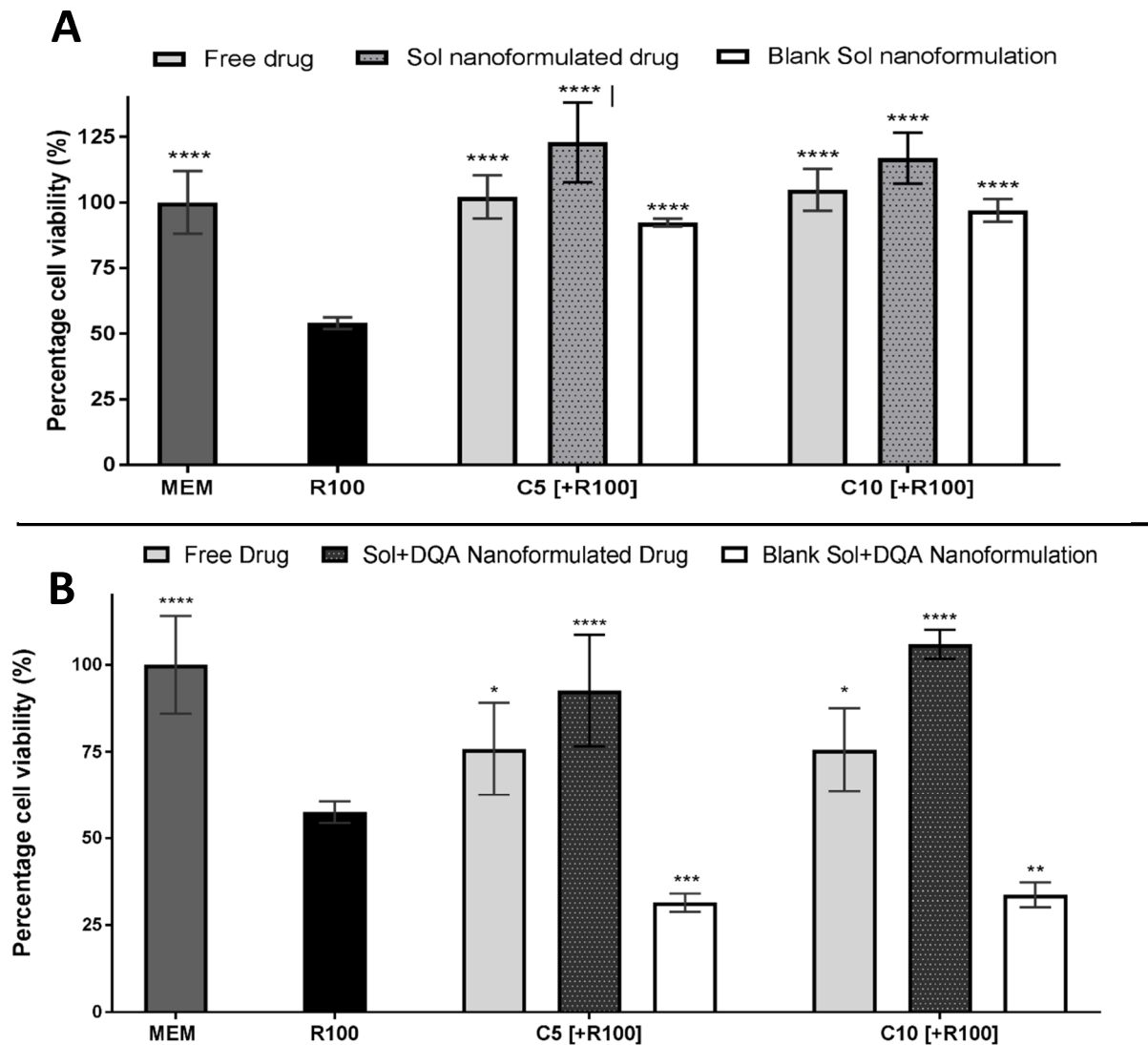
Figure 3. A. MTT assay results of 3 h pre-treatment with free drug, Sol nanoformulated or corresponding blank preparations of 5 μM and 10 μM curcumin (C5, C10) followed by 24 h treatment with 100 μM rotenone (R100) compared to R100 treatment alone. MEM represents the control condition where cells were only treated with media, no pre-treatment nor R100 treatment (mean ± S.D., n=6). B. Corresponding MTT assay results for Sol+DQA nanoformulated pre-treatments (mean ± S.D., n=6). * represents significance values of control or pre-treatment conditions compared to treatment rotenone alone (**** p < 0.0001, *** p < 0.001, ** p < 0.01, * p < 0.05). | represents significance values of nanoformulated drug compared to free drug within the same treatment condition (| p < 0.05).

There was no significant difference between 5 µM and 10 µM curcumin pre-treatments for any preparation (free, Sol or Sol+DQA) (figure 3). Interestingly, the corresponding blank Sol nanocarriers for 5 µM and 10 µM curcumin were also able to significantly protect against 24 h 100 µM rotenone treatment ($p < 0.0001$), however in both cases curcumin-loaded Sol nanocarriers were generally superior (C5: $p = 0.0171$) (figure 3A). No protective effect was observed for the corresponding Sol+DQA blank formulations which, in contrast, appear to be more toxic than rotenone alone ($p = 0.0005$ and $p = 0.0014$, respectively) (figure 3B).
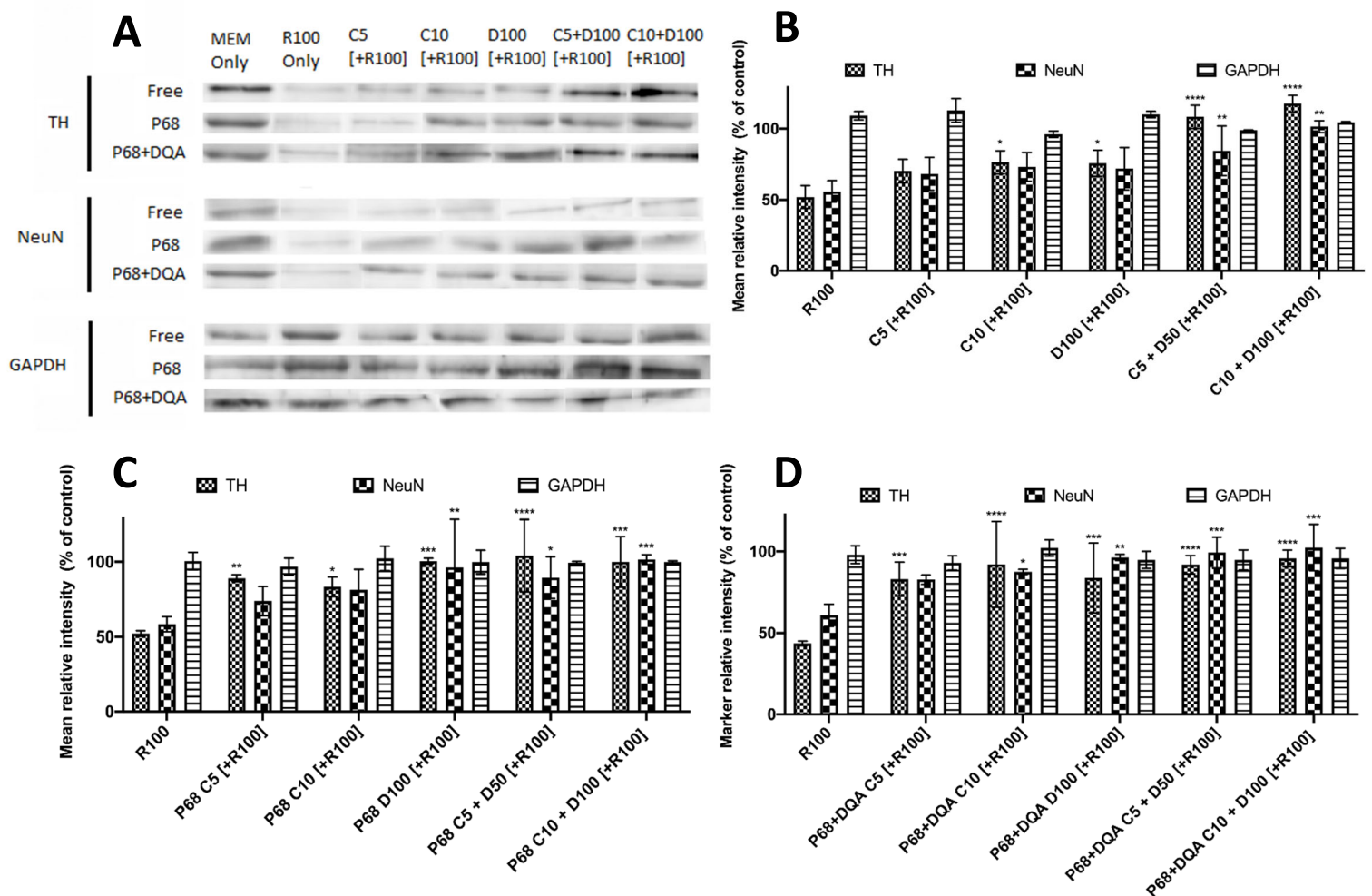
Figure 4. A. Western blot detection of tyrosine hydroxylase (TH) the first rate-limiting enzyme involved in the synthesis of dopamine (~62 kDa), the neuron specific protein NeuN (~48 kDa) and loading control GAPDH (~36 kDa) in 10 µg protein from SH-SY5Y cell lysate. SH-SY5Y cells were treated with MEM media or 100 µM rotenone (R100) only for 24h or pre-treated with free drug, P68 or P68+DQA nanoformulated preparations of either 5 µM, 10 µM curcumin (C5, C10), 100 µM DFO or combined curcumin with 50 µM or 100 µM DFO (C5+D50, C10+D100) (n=3). B. Image J quantification of TH, NeuN and GAPDH proteins detected in SH-SY5Y cell lysate following 3 h pre-treatment with free curcumin, DFO or combined curcumin + DFO or 24 h rotenone treatment only (mean ± S.D., n=3). C. Corresponding Image J quantification of TH, NeuN and GAPDH proteins detected following 3 h pre-treatment with P68 curcumin, DFO or combined curcumin + DFO or 24 h rotenone treatment only (mean ± S.D., n=3). D. Corresponding Image J quantification of TH, NeuN and GAPDH proteins detected following 3 h pre-treatment with P68+DQA curcumin, DFO or combined curcumin + DFO or 24h rotenone treatment only (mean ± S.D., n=3). Quantification is expressed as the percentage of the levels of each marker identified in control cells (lysate of SH-SY5Y cells treated with MEM media only, for 24 h). * represents significance values of pre-treatment conditions compared to rotenone treatment alone for each marker (**** $p < 0.0001$, *** $p < 0.001$, ** $p < 0.01$, * $p < 0.05$).

Western blot analysis of anti-TH and anti-NeuN markers show a significant ability of the different concentrations of the free (F(5, 36) = 19.52, p < 0.0001), P68 (F(5, 36) = 7.855, p < 0.0001), P68+DQA (F(5, 36) = 10.39, p < 0.0001), Sol and Sol+DQA (F(4,30) = 13.47, p < 0.0001) nanoformulated curcumin and/or DFO to protect against the reduction in dopamine and neurons induced by 24 h 100 μM rotenone treatment (figure 4, 5).
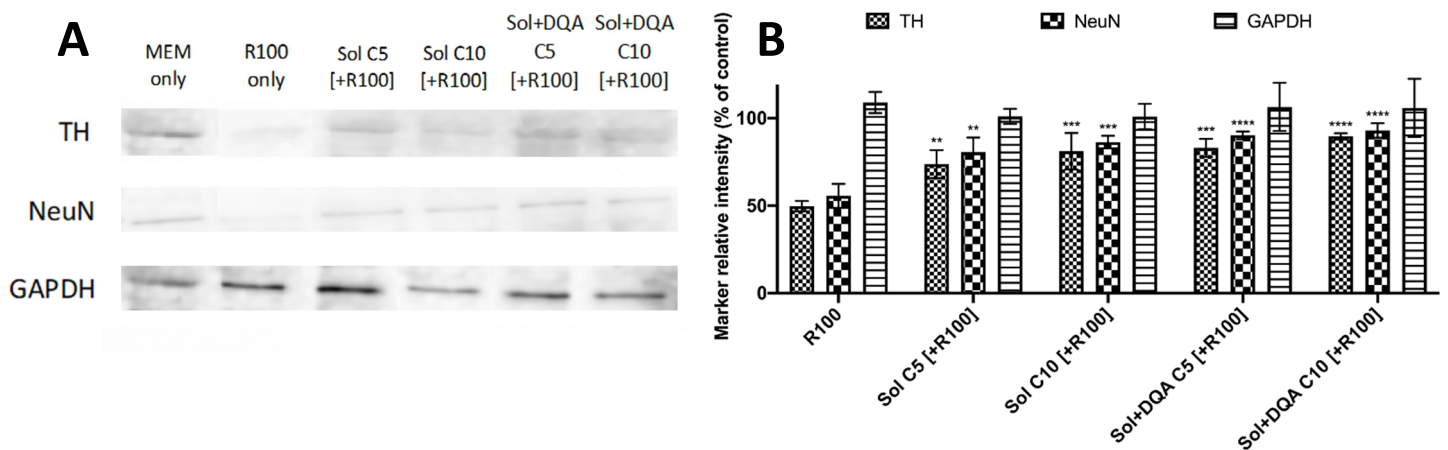
Figure 5. A. Western blot detection of tyrosine hydroxylase (TH) (~62 kDa), NeuN (~48 kDa) and loading control GAPDH (~36 kDa) in 10 μg protein from SH-SY5Y cell lysate. SH-SY5Y cells were treated with MEM media or 100 μM rotenone (R100) only for 24 h or pre-treated with Sol or Sol+DQA nanoformulated preparations of 5 μM or 10 μM curcumin (C5, C10) (n=3). B. Image J quantification of TH, NeuN and GAPDH proteins detected in SH-SY5Y cell lysate following 3 h pre-treatment with Sol or Sol+DQA or 24 h rotenone treatment only (mean ± S.D., n=3). Quantification is expressed as the percentage of the levels of each marker identified in control cells (lysate of SH-SY5Y cells treated with MEM media only, for 24h). * represents significance values of pre-treatment conditions compared to rotenone treatment alone for each marker (**** p < 0.0001, *** p < 0.001, ** p < 0.01).

Treatment with 100 μM rotenone for 24 h reduced the levels of TH by at least 50% and NeuN by at least 40% in SH-SY5Y cells compared to treatment with MEM only (figure 4, 5). 3 h pre-treatment with all conditions , except 5μM free curcumin, significantly protected against the reduction of TH induced by rotenone (5 μM curcumin – P68: p = 0.0081, P68+DQA: p = 0.0004; 10 μM curcumin free: p = 0.0144, P68: p = 0.0358, P68+DQA: p < 0.0001; 100 μM DFO free: p = 0.0182, P68: p = 0.0003, P68+DQA: p < 0.0003; 5 μM curcumin + 50 μM DFO free: p = 0.0001, P68: p < 0.0001, P68+DQA: p < 0.0001; 10 μM curcumin + 100 μM DFO free: p = 0.0001, P68: p = 0.0003, P68+DQA: p < 0.0001) (figure 4). Likewise, all concentrations of P68+DQA curcumin and/or DFO, apart from 5 μM curcumin, significantly protected against the reduction in NeuN induced by rotenone (10 μM curcumin: p = 0.0298; 100 μM DFO: p = 0.0017; 5 μM curcumin + 50 μM DFO: p = 0.0006; 10 μM curcumin + 100 μM DFO: p = 0.0002) but only the treatments containing DFO in the free drug and P68

conditions significantly protected against the reduction in NeuN induced by rotenone (100 µM DFO free: $p = 0.0028$, P68: $p = 0.0062$; 5 µM curcumin + 50 µM DFO; P68: $p = 0.0379$, 10 µM curcumin + 100 µM DFO free: $p < 0.0001$, P68: $p = 0.0014$) (figure 4). The Sol and Sol+DQA curcumin treatments were also able to significantly protect against the rotenone induced reductions of both TH (5 µM - Sol: $p = 0.0065$, Sol+DQA: $p < 0.0001$, 10 µM - Sol: $p = 0.0003$ Sol+DQA: $p < 0.0001$) and NeuN (5 µM - Sol: $p = 0.0047$, Sol+DQA: $p < 0.0001$, 10 µM - Sol: $p = 0.0004$ Sol+DQA: $p < 0.0001$) (figure 5). 3 h pre-treatment with P68+DQA curcumin conditions was at least as protective as the corresponding Sol and Sol+DQA conditions and resulted in up to 16% and 8% more TH and NeuN (respectively) than the corresponding free drug and P68 curcumin conditions (figure 4, 5). In all preparations the combination of 10 µM curcumin + 100 µM DFO exhibited the most protection against rotenone, in terms of both TH and NeuN, retaining levels at a minimum of 96% of control in each case (figure 4). No significant differences in GAPDH levels were identified between cells pre-treated with any free, P68, P68+DQA, Sol or Sol+DQA curcumin and/or DFO condition.

When evaluating iron status using the ferritin ELISA and ferrozine assay, significant differences in mean non-ferritin bound iron were observed between the different free, P68 and P68+DQA pre-treatment conditions containing curcumin and/or DFO compared to treatment with 100 µM rotenone alone for 24 h ($F_{(16, 30.11)} = 33.56$, $p < 0.0001$) (figure 6A). All P68 and P68+DQA nanoformulation pre-treatments of curcumin and/or DFO, except P68+DQA 5 µM curcumin, were able to significantly protect against rotenone induced increased iron levels (5 µM curcumin - P68: $p = 0.0179$; 10 µM curcumin - P68: $p = 0.0287$, P68+DQA: $p = 0.0045$; 100 µM DFO – P68: $p = 0.0057$, P68+DQA: $p = 0.0033$; 5 µM curcumin + 50 µM DFO - P68: $p = 0.0012$, P68+DQA: $p = 0.0089$; 10 µM curcumin + 100 µM DFO – P68: $p = 0.0034$, P68+DQA: $p = 0.0031$) (figure 6A). Although, all free curcumin and/or DFO pre-treatments resulted in lower non-ferritin bound iron concentrations than with rotenone treatment alone, none were able to significantly protect against the rotenone induced increase in non-ferritin bound iron (figure 6A). The P68 and P68+DQA conditions containing DFO resulted in the lowest non-ferritin bound iron concentrations, maintaining levels comparable to control and significantly lower than the corresponding free drug conditions in each case (100 µM DFO – P68: $p = 0.038$ P68+DQA: $p = 0.001$; 5 µM curcumin + 50 µM

DFO - P68: *p* = 0.0135 P68+DQA: *p* = 0.0286; 10 µM curcumin + 100 µM DFO - P68: *p* = 0.0426 P68+DQA: *p* = 0.0141) (figure 6A).
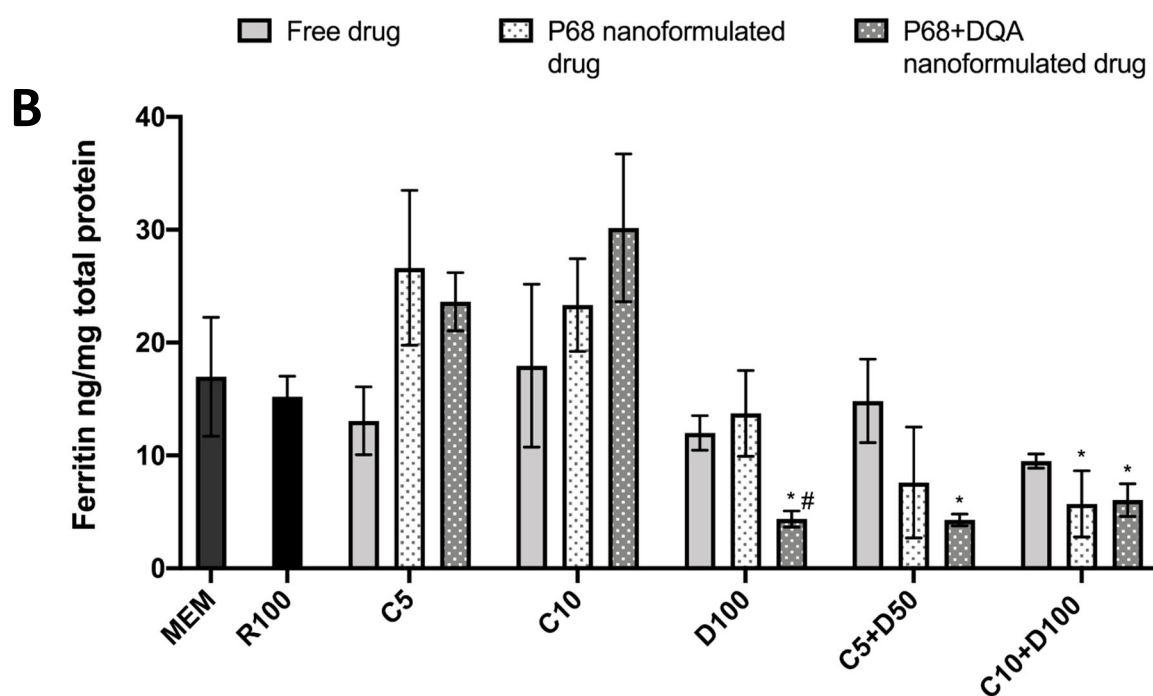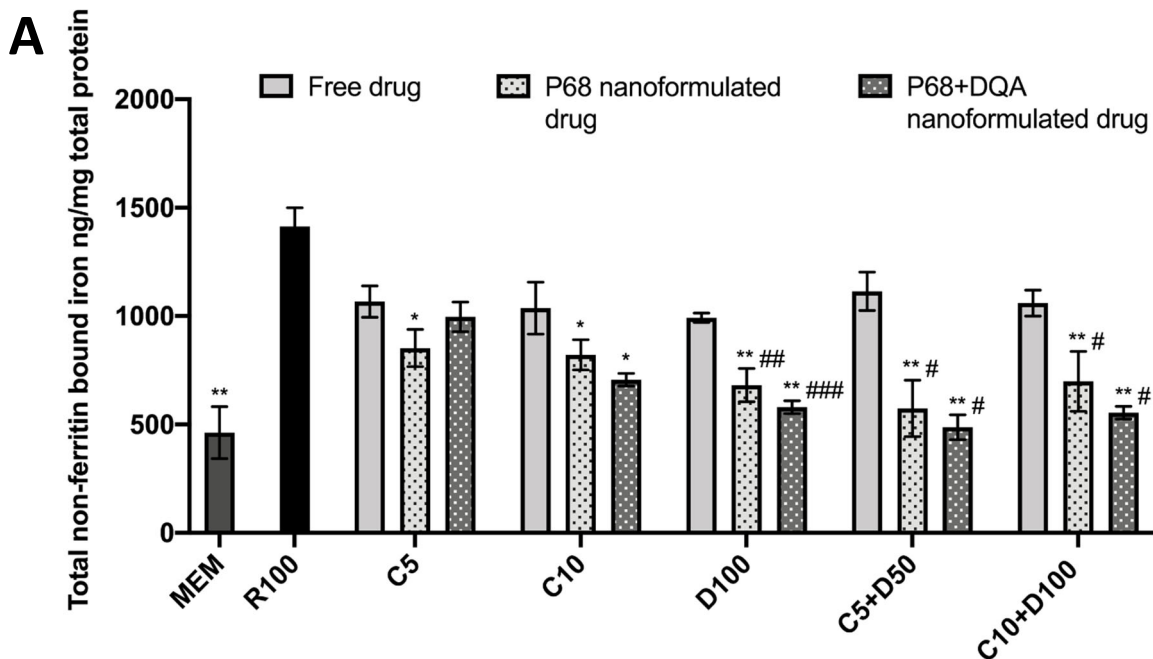
*Figure 6. A. Total non-ferritin bound iron concentrations resulting from 3 h pre-treatment with free drug, P68 or P68+DQA nanoformulated preparations of either 5 µM or 10 µM curcumin (C5, C10), 100µM DFO (D100) or combined curcumin with 50 µM or 100 µM DFO (C5+D50, C10+D100) followed by 24 h treatment with 100 µM rotenone (R100) compared to R100 treatment alone. MEM represents the control condition where cells were only treated with media, no pre-treatment nor R100 treatment (mean ± S.D., n=6). B. Corresponding ferritin ELISA results of 3 h pre-treatment with free drug, P68 or P68+DQA nanoformulated preparations of C5, C10, D100, C5+D50 or C10+D100 followed by 24 h R100 treatment. (mean ± S.D., n=6). Total non-ferritin bound iron (A) was calculated using the total iron concentrations obtained from the ferrozine assay minus the mean ferritin concentrations obtained from the ferritin ELISA (B). * represents significance values of control or pre-treatment conditions compared to rotenone treatment alone (** p < 0.01, * p < 0.05). # represents significance values of P68 or P68+DQA nanoformulated drug compared to free drug within the same treatment condition (### p < 0.001, ## p < 0.01, # p < 0.05).*

101
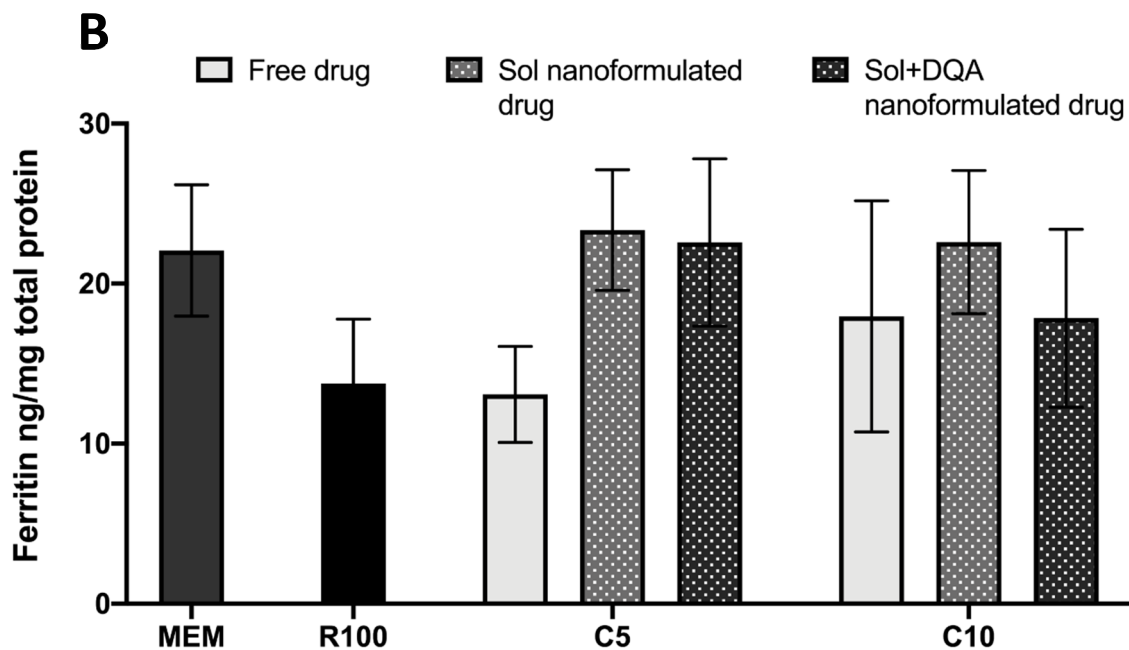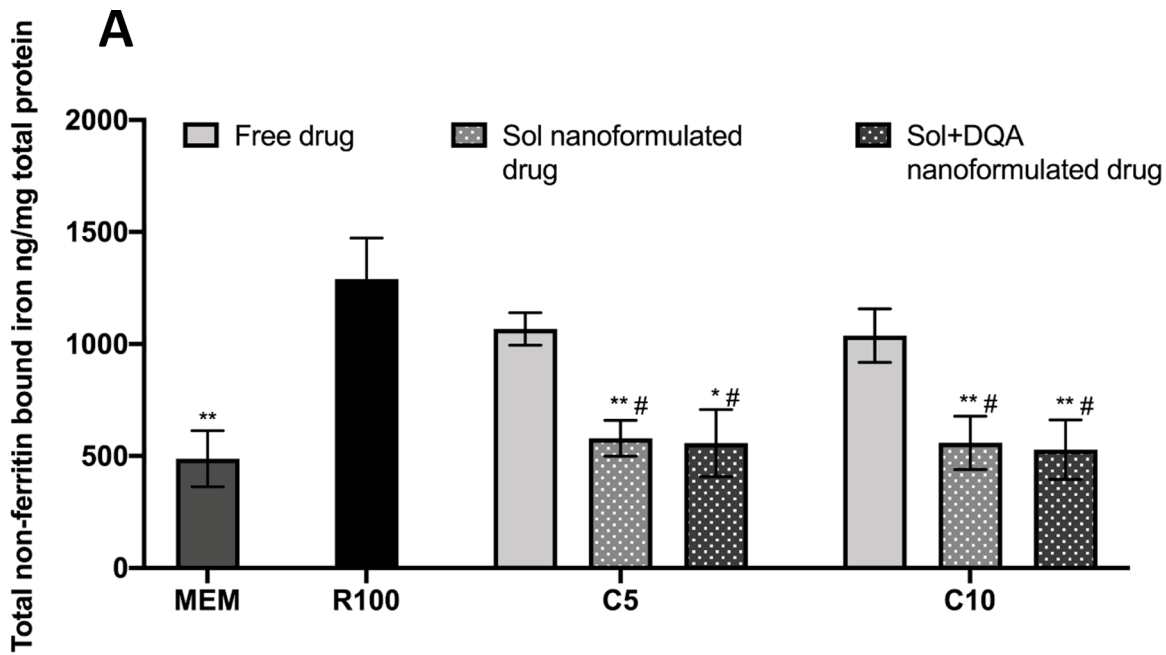
Figure 7. A. Total non-ferritin bound iron concentrations resulting from 3 h pre-treatment with free drug, Sol or Sol+DQA nanoformulated preparations of either 5 μM or 10 μM curcumin followed by 24 h treatment with 100 μM rotenone (R100) compared to R100 treatment alone. MEM represents the control condition where cells were only treated with media, no pre-treatment nor R100 treatment (mean ± S.D., n=6). B. Corresponding ferritin ELISA results of 3 h pre-treatment with free drug, Sol or Sol+DQA nanoformulated preparations of C5 and C10 followed by 24 h R100 treatment. (mean ± S.D., n=6). Total non-ferritin bound iron (A) was calculated using the total iron concentrations obtained from the ferrozine assay minus the mean ferritin concentrations obtained from the ferritin ELISA (B). * represents significance values of control or pre-treatment conditions compared to rotenone treatment alone (** $p < 0.01$, * $p < 0.05$). # represents significance values of Sol or Sol+DQA nanoformulated drug compared to free drug within the same treatment condition (# $p < 0.05$).

Significant differences in mean ferritin concentrations were also observed between the different conditions, when assessing 3 h pre-treatment with free, P68 and P68+DQA curcumin and/DFO compared to 24 h treatment with 100 μM rotenone alone ($F_{(16, 20.73)}$ = 16.01, $p < 0.0001$) (figure 6B). Although there was no significant change in ferritin as a result of 24 h treatment with 100 μM rotenone compared to control, all P68+DQA pre-treatments containing DFO (100 μM DFO - $p = 0.0349$; 5 μM curcumin + 50 μM DFO - $p = 0.0479$; 10 μM curcumin + 100 μM DFO - $p = 0.0425$), and the combination of 10 μM curcumin and 100 μM DFO with the P68 nanoformulations ($p = 0.0384$), significantly reduced ferritin levels by between 60 and 72% compared to control (figure 6B).

Similar to the P68 and P68+DQA nanoformulations, there were significant differences in mean non-ferritin bound iron between the free, Sol and Sol+DQA pre-treatments containing curcumin compared to 24 h treatment with 100 μM rotenone alone ($F_{(7, 18.59)}$ = 27, $p < 0.0001$). 3 h pre-treatment with both 5 μM and 10 μM Sol curcumin ($p = 0.0045$ and $p = 0.0077$) and Sol+DQA curcumin ($p = 0.0221$ in both cases) significantly reduced levels of non-ferritin bound iron induced by 24 h treatment with 100 μM rotenone (figure 7A). Again, none of the free curcumin conditions were able to significantly protect against the increase in total non-ferritin bound iron and, in all cases, pre-treatment with the corresponding Sol and Sol+DQA conditions resulted in significantly lower levels (46 -49%) than with free curcumin (5 μM curcumin – Sol: $p = 0.0158$, Sol+DQA: $p = 0.0481$; 10 μM curcumin – Sol: $p = 0.0419$, Sol+DQA: $p = 0.0285$) (figure 7A). There were no significant difference observed in ferritin concentration between any of the free, Sol and Sol+DQA pre-treatments compared to rotenone treatment alone or between rotenone treatment and control ($F_{(7, 12.47)}$ = 2.648, $p = 0.064$) (figure 7B).

The CAA results of free, free+DQA, P68 and P68+DQA treatments showed significant differences in cellular antioxidant activity between the different treatment preparation types ($F_{(3, 100)}$ = 26.78, $p < 0.0001$) and the different concentrations of treatments ($F_{(4, 100)}$ = 27.78, $p < 0.0001$) (figure 8A, B). P68+DQA nanocarriers had significantly higher cellular antioxidant capability than P68 nanocarriers in all corresponding conditions except 100 μM DFO where there was no significant difference (5 μM curcumin: $p = 0.001$, 10 μM curcumin: $p < 0.0001$, 5 μM curcumin + 50 μM DFO: $p = 0.0012$, 10 μM curcumin + 100 μM DFO: $p = 0.0063$) (figure 8).

Figure 8. A. CAA assay results for free drug, free drug + DQA, P68 and P68+DQA preparations of 5 μM or 10 μM curcumin (C5, C10), 100 μM DFO (D100) and combined curcumin and 50 μM or 100 μM DFO (C5+D50, C10+D100) (mean ± S.D., n=6). * represent significance values between the different drug preparation types within each drug treatment condition (**** p < 0.0001, *** p < 0.001, ** p < 0.01, *p < 0.05). B. A table to show the corresponding significant CAA results between drug conditions of the same treatment preparation.

P68+DQA nanocarriers were also significantly superior in cellular antioxidant activity compared to the corresponding free drug+DQA 5 μM and 10 μM curcumin conditions (p = 0.0003 and p = 0.0022, respectively) (figure 8). There was no significant difference in cellular

antioxidant activity of P68+DQA nanocarriers compared to any of the corresponding free drug alone conditions (figure 8). There was also no significant difference between P68 nanocarriers and free drug+DQA for any of the conditions apart from 10 μM curcumin + 100 μM DFO where free drug+DQA was superior (p = 0.0337) (figure 8). However, in most cases the free drug conditions had a significantly higher cellular antioxidant unit than the corresponding P68 nanocarriers (10 μM curcumin (p = 0.0083), 100 μM DFO (p =0.0343), combined curcumin + DFO for both 5μM + 50μM (p = 0.0203) and 10 μM + 100 μM (p = 0.0082), respectively) (figure 8). In all preparations, free drug, free drug+DQA, P68 and P68+DQA, the combination of 10 μM curcumin and 100 μM DFO had the most antioxidant potential compared to the majority of other conditions (figure 8).

Significant differences between the different treatment preparation types ($F_{(3, 40)}$ = 3.16, p < 0.0001) were observed when assessing the cellular antioxidant activity of free, Sol and Sol+DQA curcumin conditions, however no significant differences were observed between the different concentrations of treatments ($F_{(1, 40)}$ = 0.8404, p = 0.3648) (figure 9).
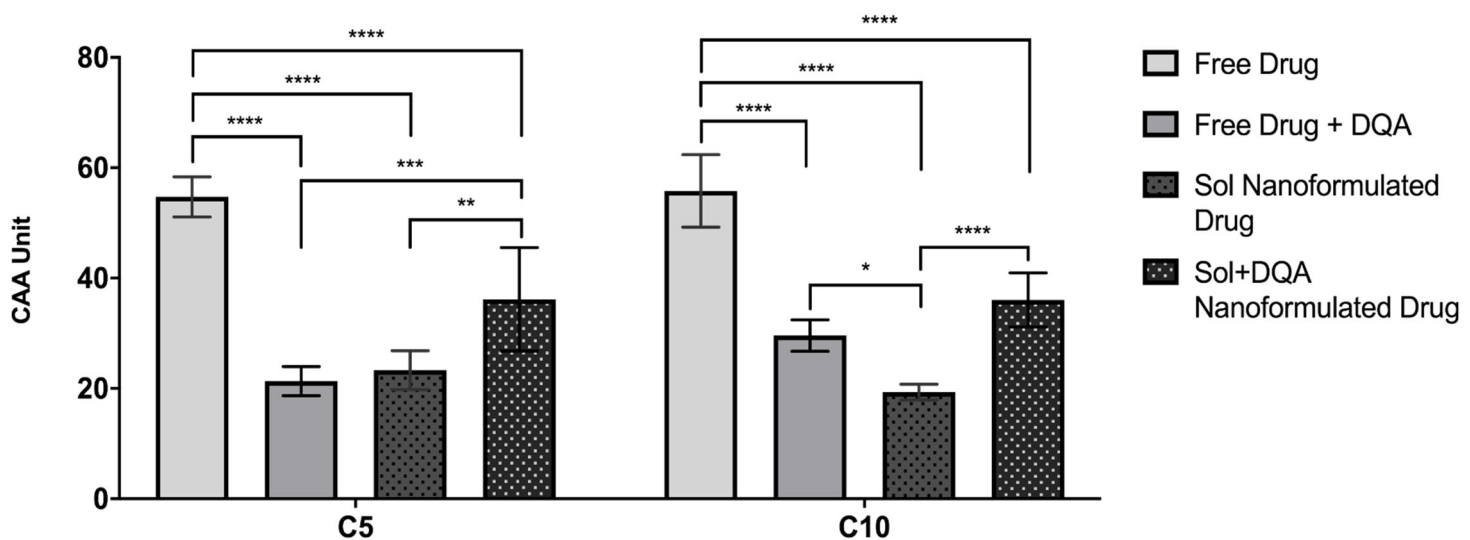
*Figure 9. CAA assay results for free drug, free drug + DQA, Sol & Sol+DQA preparations of 5 μM and 10 μM curcumin (C5, C10) (mean ± S.D., n=6). * represent significance values between the different drug preparation types within each drug treatment condition (**** p < 0.0001, *** p < 0.001, ** p < 0.01, *p < 0.05).*

Sol+DQA nanocarriers had significantly higher antioxidant capability than Sol nanocarriers in both the 5 μM (p = 0.0015) and 10 μM (p < 0.0001) curcumin conditions (figure 9). 5 μM curcumin-loaded Sol+DQA nanocarriers also had significantly superior cellular antioxidant

activity compared to 5 μM free curcumin+DQA (p = 0.0002) (figure 9). However, unlike P68+DQA curcumin-loaded nanocarriers, which in both the 5 μM and 10 μM conditions had up to 10% higher antioxidant activity compared to free curcumin (figure 9), Sol+DQA curcumin-loaded nanocarriers had significantly lower (up to 20%) antioxidant activity compared to corresponding free-curcumin conditions (p < 0.0001). Likewise, in both the 5 μM and 10 μM conditions, free curcumin had significantly higher antioxidant activity compared to free curcumin+DQA (p < 0.0001) and Sol curcumin-loaded nanocarriers (p < 0.0001) (figure 9).

The cellular antioxidant activity of the free, P68, P68+DQA, Sol and Sol+DQA preparations of curcumin and/or DFO were also evaluated using modified versions of the traditional CAA assay (described by Wolfe, et al., 2007; Hu, et al., 2013), where 100 μM rotenone or 200 μM iron were used as the prooxidant instead of ABAP as these results could be more relevant to models of PD and iron-induced oxidative stress. The modified CAA assay results showed significant differences in cellular antioxidant activity between the different free, P68 and P68+DQA preparation types against 100 μM rotenone ($F_{(3, 85)}$ = 309, p < 0.0001) and 200 μM free iron ($F_{(3, 85)}$ = 28.13, p < 0.0001) as well as with the different concentrations of curcumin and/or DFO treatments (rotenone: $F_{(4, 85)}$ = 112.8, p < 0.0001; iron: $F_{(4, 85)}$ = 15.52, p < 0.0001) (figure 10).

All concentrations of the P68+DQA curcumin and/or DFO treatments had significantly higher cellular antioxidant activity against 100 μM rotenone than the free drug preparations (p < 0.0001 in all cases except 5 μM curcumin + 50 μM DFO where p = 0.00214) (figure 10A). The separate curcumin and DFO P68 nanoformulations (but not the combined formulations) also exhibited significantly higher antioxidant activity than the corresponding free drug conditions against rotenone (p < 0.0001 in all cases) (figure 10A). However, in the majority of cases the P68+DQA pre-treatments resulted in significantly higher CAA units (between 32% and 43% higher) than the corresponding P68 pre-treatments (p < 0.0001 in all cases). The highest antioxidant activity against rotenone (mean CAA unit of 34.1) was reached with the P68+DQA preparation of 10μM curcumin + 100μM DFO (figure 10A).
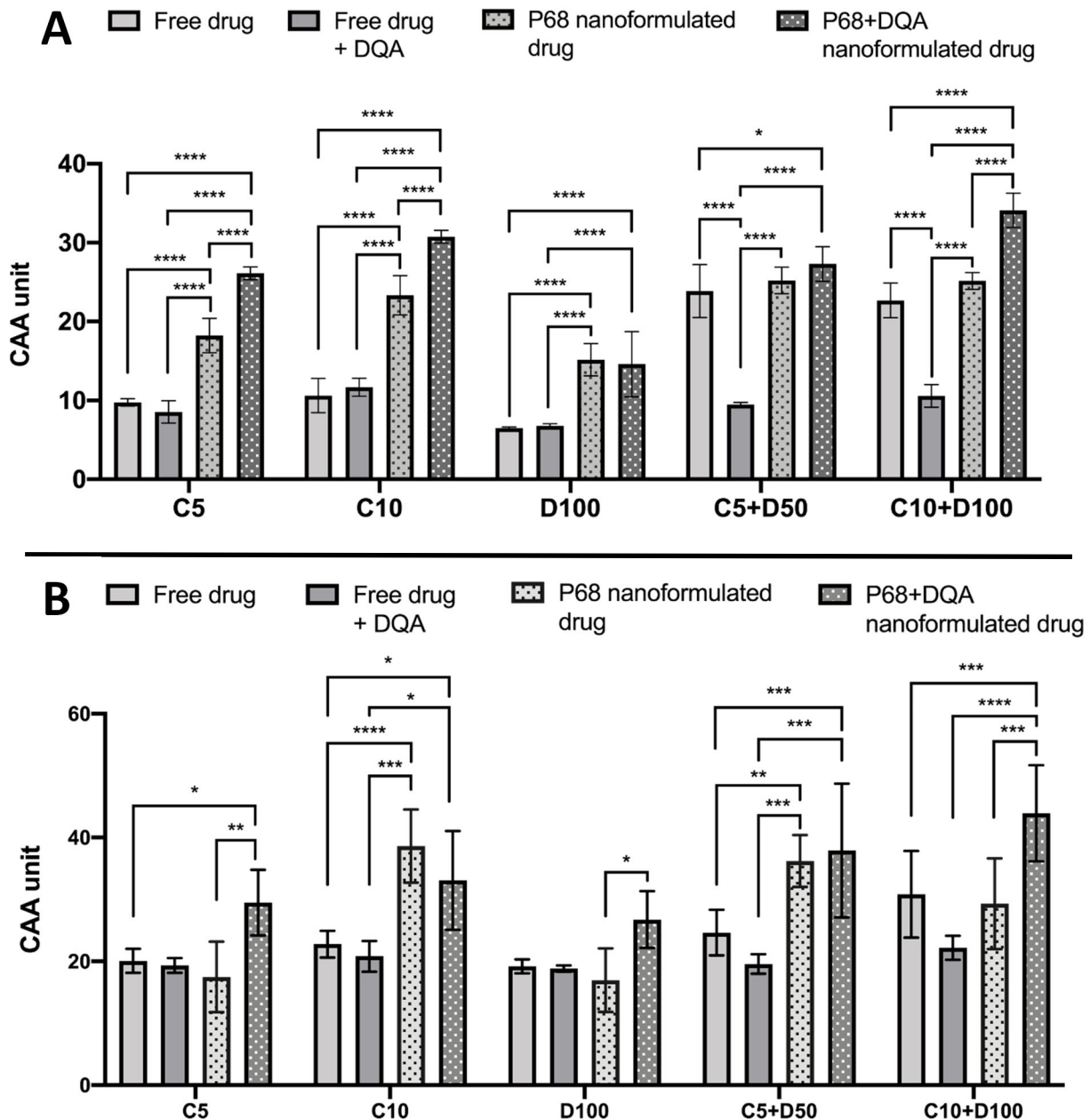
Figure 10. Modified CAA assay results for free drug, P68, P68+DQA nanformulated drug and free drug + DQA preparations of 5 μM or 10 μM curcumin (C5, C10), 100 μM DFO and combined curcumin and 50 μM or 100 μM DFO (C5+D50, C10+D100) when using 100 μM rotenone as the prooxidant (mean ± S.D., n=6). B. Corresponding CAA results when using 200 μM free iron as the prooxidant. * represent significance values between the different drug preparation types within each drug treatment condition (**** p < 0.0001, *** p < 0.001, ** p < 0.01, * p < 0.05).

The P68+DQA nanocarriers of curcumin and/or DFO also consistently had the highest cellular antioxidant activity against 200 μM iron compared to the P68, free drug and free drug+DQA conditions (figure 10B). P68+DQA nanocarriers significantly improved the cellular antioxidative capacity of curcumin and combined curcumin and DFO at both sets of concentrations compared to the corresponding free drug conditions (5 μM curcumin: p = 0.0234; 10 μM curcumin: p = 0.0106; 5 μM curcumin + 50 μM DFO: p = 0.0005; 10 μM

curcumin + 100 μM: p = 0.0006) (figure 9B). This trend was also observed for P68 10 μM

curcumin (p < 0.0001) and combined 5 μM curcumin + 50 μM DFO (p =0.0033) (figure 10B).

Like with rotenone, the highest antioxidant activity against iron (mean CAA unit of 43.92)

was reached with the P68+DQA preparation of 10 μM curcumin + 100 μM DFO (figure 9B).
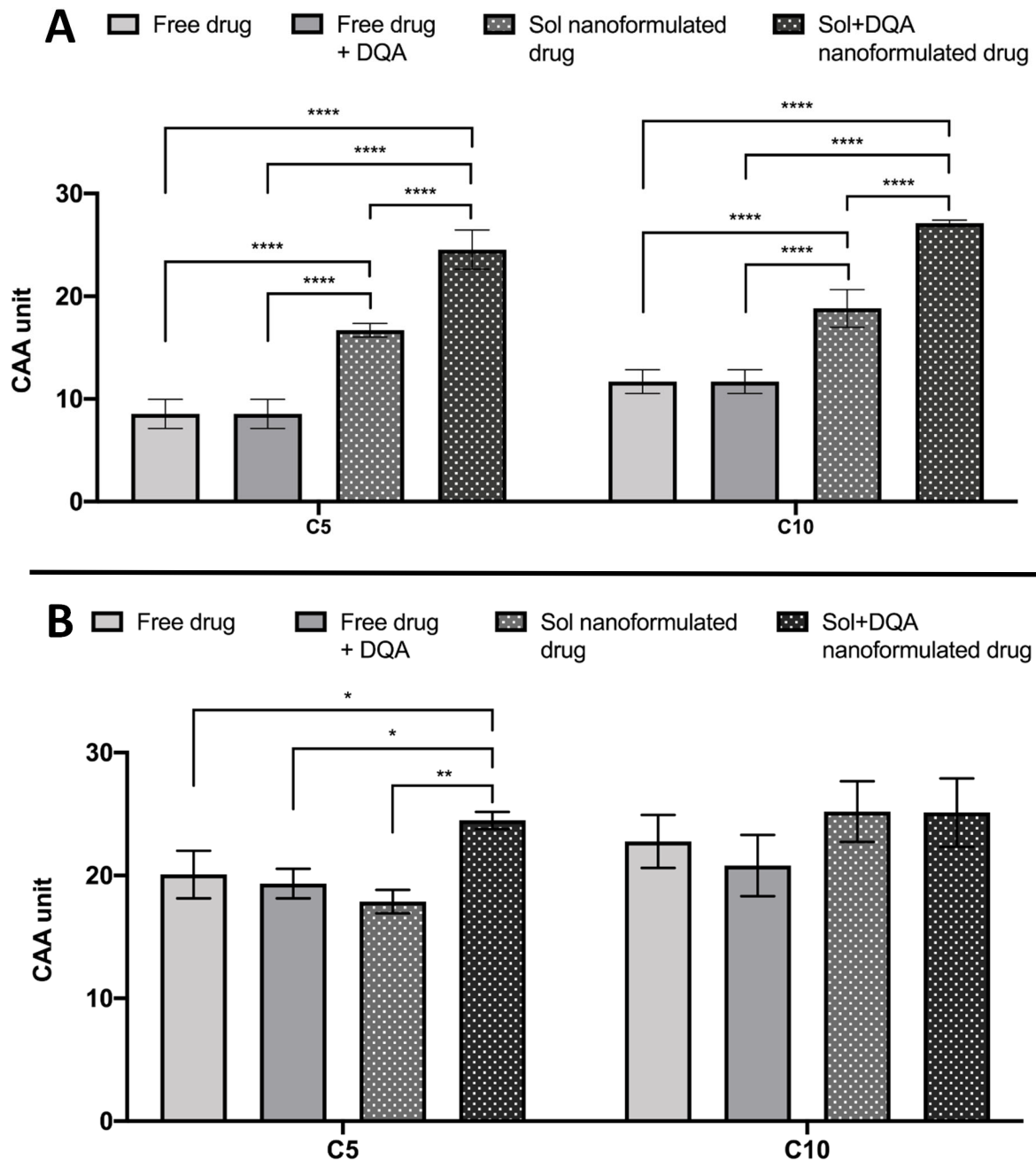
Figure 11. Modified CAA assay results for free drug, Sol, Sol+DQA nanformulated drug and free drug + DQA preparations of 5 μM and 10 μM curcumin (C5, C10) when using 100 μM rotenone as the prooxidant (mean ± S.D., n=6). B. Corresponding CAA results when using 200 μM free iron as the prooxidant. * represent significance values between the different drug preparation types within each drug treatment condition (**** p < 0.0001, ** p < 0.01, * p < 0.05).

Likewise, significant differences between the free, Sol and Sol+DQA preparations of curcumin were observed for cellular antioxidant activity against 100 μM rotenone ($F_{(3, 16)}$ = 189.9, $p < 0.0001$) and 200 μM free iron ($F_{(3, 22)}$ = 6.182, $p = 0.0033$) as well as with the different concentrations of treatments against rotenone ($F_{(1, 16)}$ = 25.36, $p = 0.0001$) and iron ($F_{(1, 22)}$ = 15.83, $p = 0.0006$) (figure 11). Both Sol and Sol+DQA curcumin exhibited higher antioxidant capacity against rotenone than the corresponding free and free+DQA curcumin conditions ($p < 0.0001$ in all cases) (figure 11A). However, at each concentration, the Sol+DQA preparation resulted in the highest cellular antioxidant capacity, 47% and 44% higher than the corresponding Sol conditions of 5 μM and 10 μM curcumin, respectively (figure 11A).

When 200 μM iron was used as the prooxidant, only 5 μM Sol+DQA curcumin exhibited higher antioxidant activity that the corresponding free drug and free drug+DQA curcumin treatments ($p = 0.0237$ and $p = 0.022$, respectively) (figure 11B). Sol+DQA 5 μM curcumin also exhibited significantly higher (37% higher) antioxidant activity against iron compared to 5 μM Sol curcumin ($p = 0.0027$) (figure 11B). However, no significant differences were observed between the different treatment preparations at 10 μM curcumin, with all preparations reaching similarly high CAA units (between 21 and 25) (figure 11B).

When testing the ability to protect against rotenone induce lipid peroxidation, significant differences in mean TBARS concentrations were observed between the different treatments when comparing both P68 ($F_{(16, 84)}$ = 35.36, $p < 0.0001$) and P68+DQA ($F_{(16, 17)}$ = 41.55, $p < 0.0001$) nanocarriers compared to the corresponding free curcumin and/or DFO conditions (figure 12). Treatment with 100 μM rotenone resulted in a 40-45% increase in lipid peroxidation compared to control treated cells. 3 h pre-treatment with free drug, P68 and P68+DQA preparations of all conditions (5 μM curcumin, 10 μM curcumin, 100 μM DFO, 5 μM curcumin + 50 μM DFO, 10 μM curcumin + 100 μM DFO) significantly protected against rotenone-induced lipid peroxidation, measured by TBARS concentration (figure 12). 3 h pre-treatment with P68 nanocarriers of 5 μM and 10 μM curcumin ($p = 0.0012$ and $p = 0.0135$, respectively), 100 μM DFO ($p = 0.0012$) and the combination of 5 μM curcumin and 50 μM DFO ($p = 0.0007$) were significantly more protective against rotenone-induced increase in TBARS concentration compared the corresponding free drug conditions (figure

12A). There was no significant difference in the ability of P68+DQA nanocarriers and the corresponding free drug pre-treatments to protect against rotenone-induced lipid peroxidation (figure 12B).
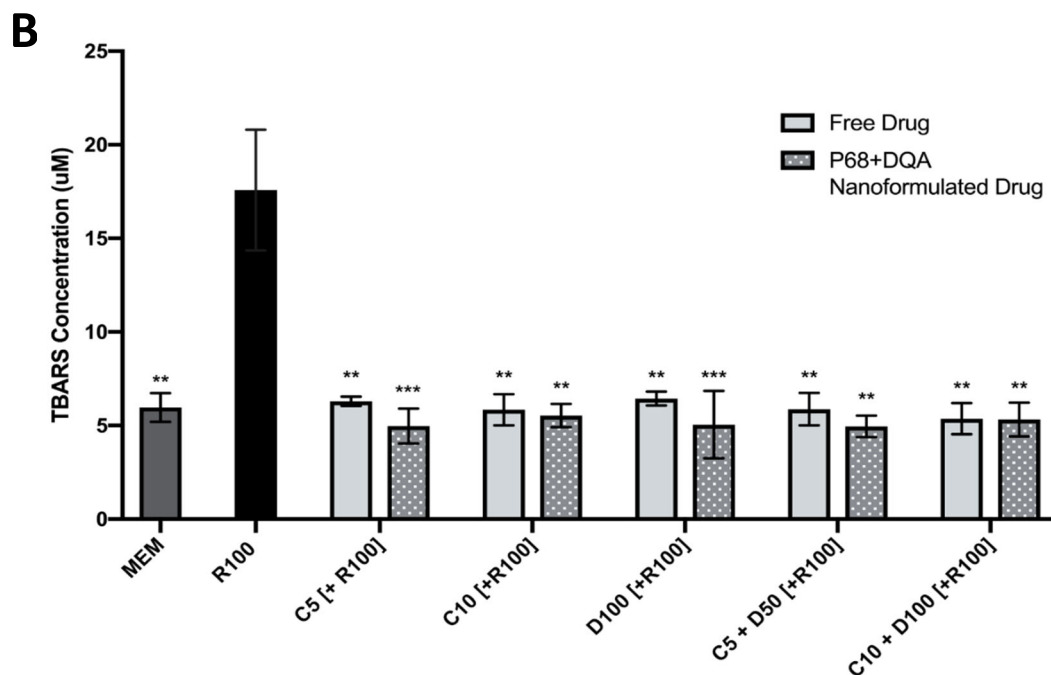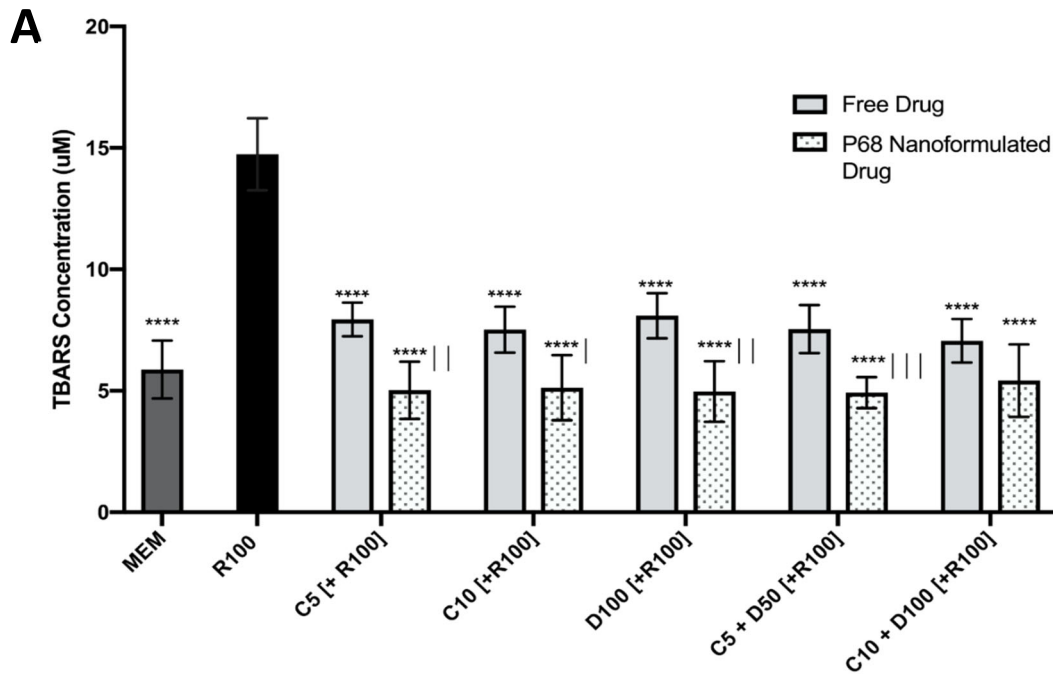
Figure 12. A. TBARS assays results of 3 h pre-treatment with free drug or P68 nanoformulated preparations of either 5 μM or 10 μM curcumin (C5, C10), 100 μM DFO (D100) or combined curcumin with 50 μM or 100 μM DFO (C5+D50, C10+D100) followed by 24 h treatment with 100 μM rotenone (R100) compared to R100 treatment alone. MEM represents the control condition where cells were only treated with media, no pre-treatment nor R100 treatment (mean ± S.D., n=6). B. Corresponding TBARS assay results for P68+DQA nanoformulated pre-treatments (mean ± S.D., n=6). * represents significance values of control or pre-treatment conditions compared to rotenone treatment alone (**** $p < 0.0001$, *** $p < 0.001$, ** $p < 0.01$). | represents significance values of nanoformulated drug compared to free drug within the same treatment condition (||| $p < 0.001$, || $p < 0.01$, | $p < 0.05$).

Significant differences in mean TBARS concentrations were also observed between the different curcumin treatment concentrations when pre-treating for 3 h with either free, Sol or Sol+DQA curcumin conditions ($F_{(7, 23.46)}$, $p < 0.0001$), followed by 24 h rotenone treatment (figure 13). 3 h pre-treatment with 5 μM and 10 μM conditions of both Sol and Sol+DQA curcumin-loaded nanocarriers were also significantly protective against 100 μM rotenone-induced lipid peroxidation ($p < 0.0001$ in all cases) (figure 13). All preparations (free, Sol and Sol+DQA) of both 5 μM and 10 μM curcumin retained TBARS concentration within control range and generally both Sol and Sol+DQA pre-treatments resulted in lower TBARS concentrations than the corresponding free drug conditions (figure 13).
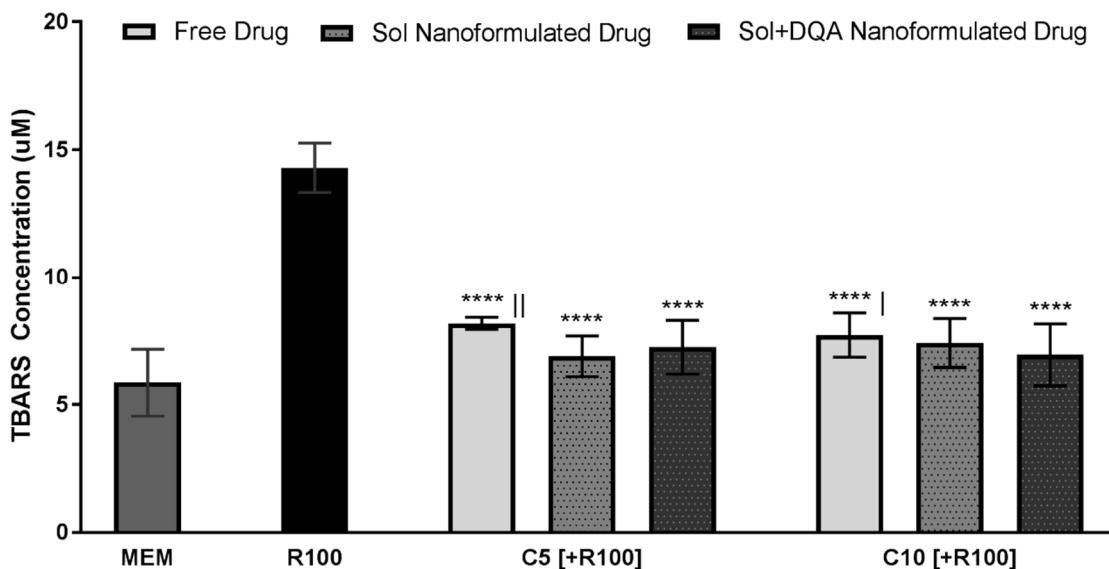
Figure 13. A. TBARS assays results of 3 h pre-treatment with free drug, Sol or Sol+DQA nanoformulated preparations of 5 μM and 10 μM curcumin (C5, C10) followed by 24 h treatment with 100 μM rotenone (R100) compared to R100 treatment alone. MEM represents the control condition where cells were only treated with media, no pre-treatment nor R100 treatment (mean ± S.D., n=6). * represents significance values of control or pre-treatment conditions compared to rotenone treatment alone (**** $p < 0.0001$). | represents significance values of nanoformulated drug compared to free drug within the same treatment condition (||$p < 0.01$, | $p < 0.05$)).

When evaluating the ability of curcumin and/or DFO treatments to protect against increased mitochondrial hydroxyl induced by rotenone, significant differences were observed between the free, P68 and P68+DQA conditions compared to rotenone alone ($F_{(25, 63.21)} = 84.15$, $p < 0.0001$) (figure 14A).
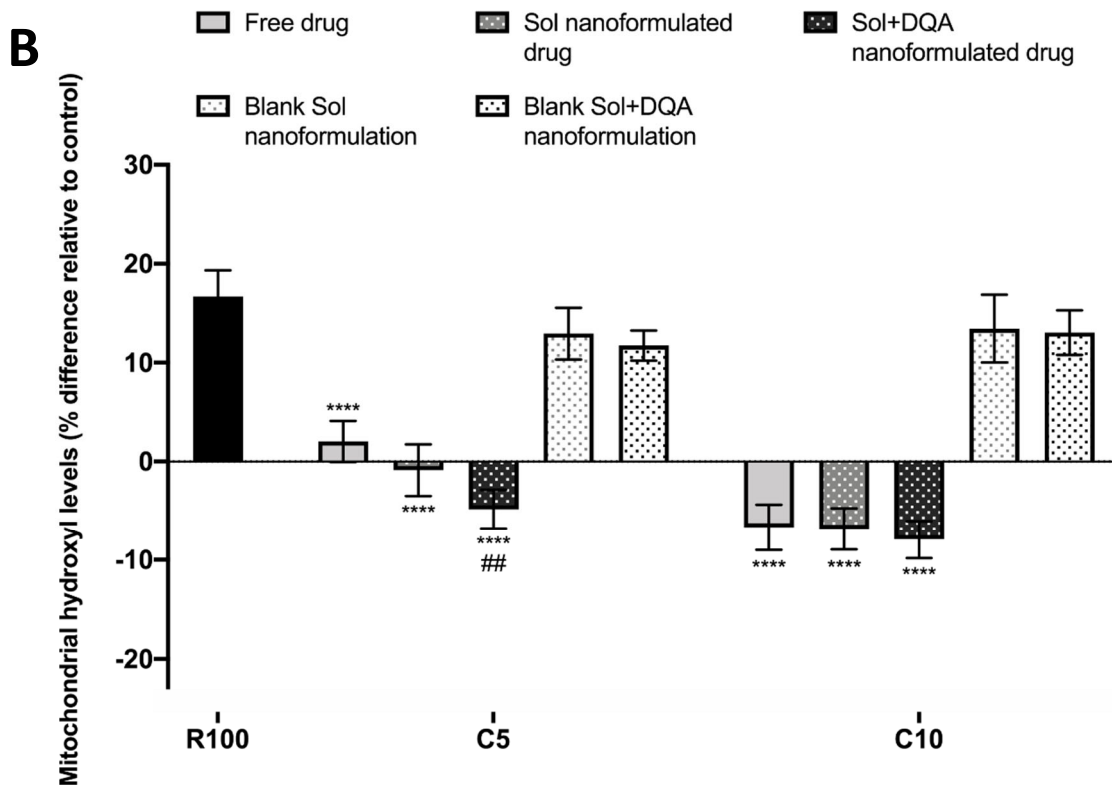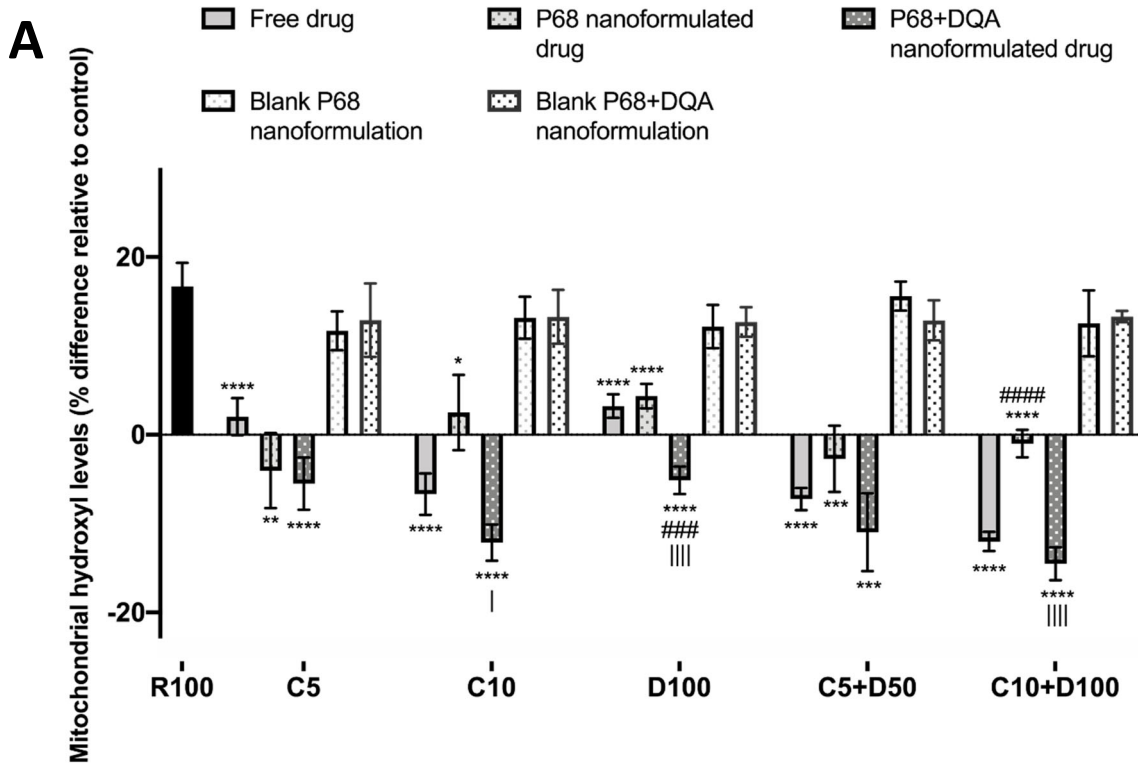
*Figure 14 A. Mitochondrial hydroxyl assay results of 3 h pre-treatment with free, P68, P68+DQA or corresponding blank curcumin (5 μM or 10 μM), DFO (100 μM) or combined curcumin (5 μM or 10 μM) + DFO (50 μM or 100 μM) followed by 24 h treatment with 100 μM rotenone (mean ± S.D., n=6). B. Corresponding mitochondrial hydroxyl assay results for 3 h pre-treatment with free, Sol, Sol+DQA or corresponding blank formulations of curcumin (5 μM or 10 μM) treatments. Mitochondrial hydroxyl levels are expressed as the percentage of hydroxyl identified in control cells (SH-SY5Y cells treated with MEM media only, for 24h). * represents significance values of pre-treatment conditions compared to rotenone treatment alone for each marker (**** p < 0.0001, *** p < 0.001, ** p < 0.01, * p < 0.05). # represents significance values of nanoformulated drugs compared to free drug within the same treatment condition (#### p < 0.0001, ### p < 0.001, ## p < 0.01). | represents significance values of P68+DQA or Sol+DQA nanoformulated drug compared to P68 or Sol nanoformulated drug (respectively) within the same treatment condition (|||| p < 0.0001, | p < 0.05).*

112

3 h pre-treatment with all curcumin and/or DFO conditions significantly protected against the increase in mitochondrial hydroxyl induced by 24 h rotenone treatment, maintaining levels close to or lower than at control ($p < 0.0001$ in all cases except from P68 5 μM and 10 μM curcumin and P68 5 μM curcumin + 100 μM DFO where $p = 0.001$, $p = 0.0111$ and $p = 0.0004$, respectively) (figure 14A). Whereas none of the corresponding blank formulations were able to protect against the increase in hydroxyl induce by rotenone. At 10 μM curcumin ($p = 0.0102$), 100 μM DFO ($p < 0.0001$) and 10 μM curcumin + 100 μM DFO ($p < 0.0001$), P68+DQA pre-treatments resulted in significantly lower mitochondrial hydroxyl levels than the corresponding P68 treatments, reaching levels as low as 14% below control with P68+DQA 10 μM curcumin + 100 μM DFO (figure 14A). In all case, P68+DQA conditions were at least as protective as the corresponding free drug condition against rotenone increased hydroxyl levels and were significantly more protective at 100 μM DFO ($p = 0.0002$). In most cases, there were no significant differences between P68 and free curcumin and/or DFO pre-treatments, but at 10 μM curcumin + 100 μM DFO the free drug was significantly more protective than the corresponding P68 preparation ($p < 0.0001$) (figure 14A).

Significant differences in mitochondrial hydroxyl were also observed between with the free, Sol and Sol+DQA pre-treatments, compared to rotenone alone ($F_{(10, 33)} = 106$, $p < 0.0001$) (figure 14B). 3 h pre-treatment with all free, Sol and Sol+DQA curcumin conditions significantly protected against the increase in mitochondrial hydroxyl induced by 24 h 100 μM rotenone treatment, maintaining levels close to or within 8% lower than at control ($p < 0.0001$ in all cases) (figure 14B). Again, none of the corresponding blank formulations were able to protect against the increase in hydroxyl induced by rotenone (figure 14B). No significant differences were observed between any of the different free, Sol and Sol+DQA pre-treatments of curcumin, except from at 5 μM curcumin where the Sol+DQA pre-treatment resulted in 7% lower hydroxyl than the corresponding free curcumin condition ($p = 0.006$) (figure 14B).

4.3. Discussion

There is much evidence suggesting that curcumin and DFO are protective in numerous models of PD (Youdim et al., 2004; Dexter et al., 2011, Liu et al., 2013, Jiang et al., 2013.,

Devos et al., 2014, Van der Merwe et al., 2017) and that the combination of antioxidants and iron chelators may have even more potent effects (Sripetchwandee et al., 2014). However, the potential of these compounds as possible therapies for PD has been limited due to numerous factors such as brain penetrance, bioavailability, and stability (Yang et al., 2007; Martin-Bastida et al., 2017). Advances in nanotechnology have provided a possible solution to these issues as nanocarriers can be developed to retain the potency of the associated molecule while enhancing targeted delivery and passage across biological membranes (Masserini et al., 2013; Zupančič et al., 2014, Grabrucker et al., 2016; Saraiva et al., 2016). The aim of this study was to assess the ability of the curcumin and/or DFO micellar nanocarriers (developed and characterised in the previous chapter) to protect against reduced cell viability, reduced dopaminergic and neuronal markers, increased non-ferritin bound iron and increased oxidative stress induced by a cellular rotenone model of PD.

P68, P68+DQA, Sol and Sol+DQA nanocarriers were protective against rotenone-induced reductions in cell viability suggesting that they may be able to protect against cell death induced by rotenone (figure 2, 3). It was expected that the combination of the highest tolerable concentrations of curcumin and DFO would be the most effective at protecting against rotenone due to the combination of reduced free iron and increased antioxidants which together should prevent the accumulation of toxic free radicals, which drive oxidative stress. However, pre-treatment with the combination of these free drugs appeared to result in toxicity following rotenone treatment (figure 2). In contrast, following the combined formulation of 10 μM curcumin and 100 μM DFO into P68 and P68+DQA nanocarriers, pre-treatment with the combined drugs not only eliminated the toxicity previously observed but also significantly increased cell viability (figure 2). This effect is likely because once nanoformulated the release characteristics of curcumin and DFO changed to a more gradual, sustained release compared to when loading the cells directly with the free drug forms. Furthermore, micelles release hydrophobic drugs, such as curcumin, more slowly and can therefore reduce the overload and interaction of the associated drugs at the site of the cell (Kwon & Okano, 1996; Hussein & Youssry, 2018), which may account for the cytotoxicity observed when using the higher concentrations of combined free curcumin and DFO. P68 nanocarriers of 10 μM curcumin and 5 μM curcumin + 50 μM DFO were the most successful

at protecting cell viability against rotenone compared to the other drug-loaded P68 nanocarriers, retaining cell viability over 80% (figure 2A). Whereas, increasing concentrations of P68+DQA curcumin and combined curcumin + DFO nanocarriers increasingly protected cell viability, with the pre-treatment of 10 μM curcumin + 100 μM DFO retaining 90% cell viability (figure 2B). Although DFO-loaded P68+DQA nanocarriers did not significantly protect cell viability against rotenone, the addition of 50 μM and 100 μM DFO to 5 μM and 10 μM curcumin-loaded P68+DQA nanocarriers resulted in a modest increase in protection, by 10% and 11% respectively (figure 2B). Both Sol and Sol+DQA preparations of 5 μM and 10 μM curcumin were able to retain at least 90% cell viability following rotenone treatment and neither concentration within each condition was superior to one another (figure 3).

The cell viability data indicates that all nanoformulated treatments tested, but perhaps mostly the combined formulations of curcumin and DFO, could potentially be protective against PD. This is supported by the observations that they were all able to protect against the 50% reduction in cell viability which is representative of the reduction in dopamine nerve terminal density observed (using DAT SPECT imaging) in the SN of people with PD, at diagnosis (EMA, 2018). The western blot analysis further supports the cell viability data that all P68, P68+DQA, Sol and Sol+DQA curcumin and/or DFO conditions exhibit dopaminergic neuronal protection as pre-treatment with all conditions appeared to prevent the significant reduction of tyrosine hydroxylase and NeuN markers induced by 24 h rotenone treatment (figure 4, 5). The western blot data validates the hypothesis that the combination of curcumin and DFO may be an effective strategy to protect against dopamine loss as for each preparation type the combination treatment was seen to result in the most significant protection against rotenone (figure 4). It also highlights that the P68+DQA nanocarriers may be the most suited delivery system as, in most cases, the P68+DQA conditions resulted in higher tyrosine hydroxylase and NeuN levels compared to the P68 nanoformulations and free drug conditions (figure 4). This is likely due to the mitochondrial targeting ability of the P68+DQA nanocarriers as mitochondria within dopaminergic neurons are the main source of elevated free iron which can drive oxidative stress and the resulting cell death (Thomas et al., 2009; Costa-Mallen et al., 2017; Zucca et al., 2017).

As detailed in chapter 1, elevated free iron within the SN is thought to be a central component of PD, with iron-induced oxidative stress, in particular, being linked to both the development and progression of dopaminergic neurodegeneration in PD (Kroemer & Reed, 2000; Schapira, 2007; Simpkins & Dykens, 2008; Kandola et al., 2015; Do Van et al., 2016; Barodia et al 2017; Jiang et al., 2017). Rotenone has been shown to increase levels of free iron in previous studies (Mouhape et al., 2019; Betarbet et al., 2006). This is thought to partially result from the reduction in iron-sulphur cluster synthesis and content as well as activity of iron-sulphur cluster containing enzymes such as, cytosolic aconitase activity, caused by the inhibition of mitochondrial complex 1 (Mena et al., 2011). The reduction of cytosolic aconitase activity, for example, has been associated with an increase in the cytoplasmic labile iron pool due to an increase in iron regulatory protein mRNA binding activity (Mena et al., 2011). Further to this, the excessive ROS production caused by rotenone can also promote the release of iron from iron-sulphur cluster proteins in the mitochondrial respiratory chain (Zucca et al 2017). The iron status data for 24 h rotenone treatment successfully indicates a reproduction of the rise in free iron present in PD and previously reported to be induced by rotenone (Mouhape et al., 2019; Betarbet et al., 2006), as rotenone treatment increased total non-ferritin bound iron by up to 2000% but induced no significant difference in ferritin concentration compared to control cells (figure 6, 7). As ferritin is the most common source of intracellular iron (Ropele et al., 2017), total non-ferritin bound iron can be used as an indicator of free iron.

The majority of the P68 and P68+DQA curcumin and/or DFO pre-treatments protected against the rotenone induced rise in total non-ferritin bound iron, maintaining levels closer to control, however this effect was not observed for any of the free drug treatments (figure 6). As expected, pre-treatment with the P68 and P68+DQA nanoformulations containing the iron chelator DFO resulted in the lowest total non-ferritin bound iron, with the mitochondrially targeted P68+DQA formulations again showing the greatest effect, resulting in up to 66% lower levels when using combined curcumin and DFO compared to rotenone treatment alone (figure 6A). Although it has been suggested that curcumin has a certain level of iron chelator capacity (Jiao et al., 2006), this ability was only realised with P68, P68+DQA, Sol and Sol+DQA nanoformulated curcumin conditions (not free curcumin) and this effect was limited compared to the treatments containing DFO (figure 6, 7). This

suggests that curcumin in isolation, at the tested concentrations does not exert an observable level of iron chelator activity. Although curcumin in its enol form is reported to chelate metal in a 2:1 ratio (Priyadarsin, 2014), at the low treatment concentrations of free curcumin used, in most cases the hydrogen from the diketo group which can be replaced by metal ions, may already be utilised for free radical scavenging due to the extremely high concentrations of ROS induced by rotenone. Whereas the nanoformulations are likely to increase the uptake of curcumin into the cell and into mitochondria, allowing more curcumin to be available for use as an iron chelator. Moreover, it is unsurprising that the addition of DFO increased the effect across the board since DFO has a higher affinity for iron, binding in a 1:1 ratio (Mobarra et al., 2016; Kontoghiorghes & Kontoghiorghes, 2020) and therefore has a higher capacity for chelation compared to curcumin alone. In addition to its ability to chelate free iron, DFO has also been reported to chelate iron from ferritin stores and lower serum ferritin levels (Porter et al, 2014; Hassan and Tolba, 2016; Bou-Abdallah et al., 2018; Kontoghiorghes & Kontoghiorghes, 2020). The mechanism of iron chelation from ferritin is not fully elucidated but it has been proposed that much of this chelation takes place as iron is released by the catabolism of ferritin (Porter, 2014), and as a result of superoxide anions readily diffusing into ferritin and reducing the stored ferric iron into ferrous iron which is released from ferritin and chelated by DFO (Bou-Abdallah et al., 2011). This decrease in ferritin following DFO treatment is partially supported by the ferritin data in this study where, in the majority of cases, only the P68+DQA pre-treatments containing DFO resulted in a significant reduction of ferritin (figure 5B). No significant differences were observed compared to control or rotenone when pre-treating with any of the conditions containing curcumin only (figure 6, 7). Together, this indicates that the combined curcumin and DFO P68+DQA nanoformulations are likely to be the most protective against the increased levels of free iron and the resulting oxidative stress evident in PD.

The CAA assay was used to assess the cellular antioxidant capability of free and formulated curcumin and/or DFO due to its ability to detect the presence of free radicals in physiological conditions. The assay is based on using DCFH-DA as a fluorescent probe that diffuses into cells and is deacetylated by cellular esterases; it is then rapidly oxidised by free radicals to form 2',7'-dichlorofluorescein (DCF) which is highly fluorescent (Wolfe et al.,

2007). The fluorescent intensity is proportional to the levels of cellular ROS and therefore, when using a prooxidant such as ABAP to initiate free radical formation, the antioxidant activity of treatments can be determined by measuring the fluorescent intensity (Wolfe et al., 2007), as outlined in chapter 2. The cellular antioxidant activity results suggest that P68+DQA drug-loaded nanocarriers of all conditions have more potent antioxidant potential than P68 drug-loaded nanocarriers. The addition of DQA to the formulations resulted in a significant increase, between 48% and 65%, in cellular antioxidant activity in all conditions apart from 100 μM DFO where 20% higher antioxidant activity was observed but did not reach statistical significance (figure 8). This suggests that the addition of DQA, which is known to target mitochrondria (Weissig et al., 1998, Lyrawati et al., 2011, Zupančič et al., 2014), significantly improves the antioxidant ability of the formulations. This is also supported by the Sol+DQA cellular antioxidant results which showed an increased antioxidant potential in both 5 μM and 10 μM curcumin conditions compared to the corresponding Sol curcumin conditions. (figure 8). This result was anticipated as mitochondria are the main site of intracellular free radical formation (Thomas et al., 2009; Bratic & Nils-Larsson, 2013; Kandola et al., 2015; Costa-mallen et al., 2017). Unlike the P68+DQA nanocarriers, which in both 5 μM and 10 μM conditions had up to 10% higher antioxidant activity compared to free curcumin (figure 8A), Sol+DQA curcumin-loaded nanocarriers had 20% lower antioxidant activity compared to free-curcumin conditions suggesting a benefit of the P68-based formulation (figure 9). Furthermore, in nearly all preparations, the combination of 10 μM curcumin and 100 μM DFO had the most prominent antioxidant activity (figure 8), suggesting that the combination of increasing antioxidants and decreasing free iron may be the most effective strategy for countering ROS production. Due to the restricted ability of Sol to formulate DFO, as a result of increased cytotoxicity (outlined in chapter 3), this suggests that it is more advantageous to use P68 based micellar nanocarriers, particularly those targeted to mitochondria.

The prooxidant ABAP is used in the CAA assay because it is a highly efficient free radical initiator (Wolfe et al., 2007), however it has no direct physiological relevance to the oxidative stress exhibited in PD. Due to this, a modified version of the traditional CAA assay developed by Wolfe et al (2007) was created and carried out using either rotenone or free iron as the prooxidant in order to more closely mimic iron-induced oxidative stress present

in PD. The results of this modified assay were comparable to those using the traditional method with ABAP, highlighting that both rotenone and free iron can be successfully used as free radical initiators in the CAA assay, to create a more physiologically relevant model. Moreover, as the highest antioxidant activities against both iron and rotenone were also achieved with the P68+DQA preparation of 10 µM curcumin + 100 µM DFO, when comparing all treatments (including Sol and Sol+DQA curcumin) (figure 10, 11), such data further supports the notion that the mitochondrial targeted P68+DQA formulations, of combined curcumin and DFO in particular, may provide the optimal therapeutic strategy for PD.

The TBARS assay was used to assess rotenone-induced lipid peroxidation due to its ability to act as measure of MDA, a secondary product of the oxidation of polyunsaturated fatty acids (Dutta et al., 2012; Chakraborti et al., 2017). When MDA reacts with TBA it forms TBARS in a colorimetric reaction (Dutta et al., 2012; Chakraborti et al., 2017). All P68, P68+DQA, Sol and Sol+DQA drug-loaded nanocarriers protected against rotenone-induced lipid peroxidation, in all cases maintaining TBARS levels equivalent to control conditions (figure 12, 13). Although the results show that only P68 nanocarriers were significantly more protective than the corresponding free drug pre-treatments (figure 12, 13), the actual TBARS concentrations observed for the free drug conditions tested alongside the P68+DQA conditions (figure 12B) were on average 17% lower than those tested alongside the P68 conditions (figure 12A) and although not significant, all P68+DQA conditions show a trend towards reduced lipid peroxidation compared to the corresponding free drug conditions (figure 12B). This could be due to the cells having a higher initial baseline TBARS concentration in the P68 experiment as measured by the control cells which did not receive any pre-treatment or rotenone treatment. The mitochondrial hydroxyl assay results support the observation that all free, P68, P68+DQA, Sol and Sol+DQA curcumin and/or DFO treatments tested can protect against iron-induced oxidative stress, since hydroxyl is the primary oxidant generated by Fenton chemistry in the presence of excess free iron, and mitochondria is the principal source of hydroxyl produced in PD (Thomas et al., 2009; Costa-Mallen et al., 2017; Zucca et al., 2017). Although all conditions were able to protect against the 17% rise in hydroxyl induced by rotenone treatment compared to control, the 10 µM

curcumin + 100 μM DFO P68+DQA pre-treatment was again the most protective, resulting in 15% lower levels of hydroxyl than at control (figure 14).

Overall, these results suggest that all drug-loaded nanocarriers were at least as capable as the corresponding free drug conditions at protecting against reduced cell viability and increased lipid peroxidation induced by rotenone. As the potential therapeutic value of free curcumin and DFO is significantly restricted due to issues such as poor stability, bioavailability, and brain penetrance (Yang et al., 2007; Martin-Bastida et al., 2017), formulating into nanocarrier delivery systems may provide a viable solution, as the physiochemical characterisation data indicated that these formulations would be able to pass the BBB (described in chapter 3). Moreover, the ability to target these non-specific drugs to mitochondria using P68+DQA nanocarriers, in particular, seemed to result in increased cellular antioxidant activity as well as increased protection against rotenone induce dopaminergic cell death and increased mitochondrial hydroxyl levels. The outcome measures of these experiments focused mostly on antioxidant capability therefore it is unsurprising that the curcumin formulations were generally superior to DFO as curcumin is known to obtain antioxidant properties. However, for most experiments the addition of DFO to curcumin resulted in increased effectiveness suggesting that a combination therapy may provide a good approach to combat oxidative stress in PD models. This is another benefit of using nanocarriers as, unlike combination delivery of free drugs which is challenging due to the distinct pharmacokinetic profiles of each drug, nanocarriers can ensure that drugs are delivered together for synergistic treatment (Anselmo and Mitragotri, 2016). Furthermore, since nanocarriers are targeted delivery systems that enhance the delivery across biological membranes (Masserini et al., 2013; Zupančič et al., 2014), their use reduces off target effects and allows for lower doses of the associated drug to be used in order to exhibit the desired therapeutic effect. This is particularly advantageous for compounds like curcumin and DFO which are only likely to reach the brain and produce a therapeutic effect in PD at high concentrations because of their non-specific nature and rapid metabolism (Porter, 2001; Shachar et al., 2004; Yang et al., 2007; Siviero et al., 2015; Martin-Bastida et al., 2017; Nelson et al., 2017) and where, in the case of DFO, high doses have been associated with many systemic toxicities, for example reduced renal and liver function (Brittenham, 2011; Di Nicola et al., 2015; Bayanzay & Alzoebie, 2016).

4.4. Conclusion

In summary, this study demonstrates for the first time the delivery of P68, P68+DQA, Sol and Sol+DQA curcumin and/or DFO nanocarriers to protect against oxidative stress induced by a cellular model of PD. This strategy may thus provide a novel approach to fully utilise their therapeutic benefit for PD. The ability of P68+DQA nanocarriers to target mitochondria appeared to enhance the positive effects of curcumin and DFO to protect against oxidative stress and loss of dopamine induced by rotenone. These nanocarriers could therefore be utilised for other antioxidants that show promise for PD but are also limited by issues of low stability, bioavailability, and limited brain penetrance, such as NAC and HT. The next chapter will outline the development of the P68+DQA nanocarriers for the delivery of NAC and HT, alone and in combination with DFO, and their ability to protect against the rotenone model of PD. Such data will help to identify which of these treatments could be the most potent against iron-induced oxidative stress and which of these formulations could be moved forward into the next stage of testing as potential disease-modifying therapies for PD.

Chapter 5 - Assessing the therapeutic potential of P68+DQA nanocarriers to deliver NAC and HT alone or in combination with DFO in a cellular PD model

5.1. Introduction

As discussed in the previous chapters, nanocarriers can enhance the potency, stability, bioavailability, and the passage across biological membranes of incorporated compounds (Masserini et al., 2013; Zupančič et al., 2014, Zhou et al., 2018; Mursaleen et al., 2020a). Chapters 3 and 4 demonstrated the successful delivery of curcumin and/or DFO from a variety of polymeric micellar nanocarriers in SH-SY5Y cells and the ability of these nanocarriers to protect against reduced cell viability and increased iron related oxidative stress induced by a rotenone model of PD. The P68+DQA nanocarriers were observed to possess the most potential as delivery systems of curcumin and/or DFO for the treatment of PD. This is because they exhibited many of the advantageous characteristics of polymeric micelles that make them suitable for brain penetrance, for example small particle size (<200 nm) and relatively neutral charge (<10 mV) (Gaucher et al., 2005; Batrakova & Kabanov 2008; Huang et al., 2011; Kataoka et al., 2012; Wiley et al., 2013; Bramini et al., 2014; Elezaby et al., 2017; Rakotoarisoa and Angelova, 2018; Zhou et al ., 2018), as well as the ability to target the mitochondria, which are the main sites driving iron-induced oxidative stress and the associated dopaminergic cell death evident in PD (Dexter et al., 1987; Dexter et al., 1987; Gerlach et al., 1994; Griffiths et al., 1999; Graham et al., 2000; Halliwell et al., 2001; Martin et al., 2008; Wallis et al., 2008; Rossi et al., 2013, Kandola et al., 2015; Costa-mallen et al., 2017, Mursaleen et al., 2020a, b).

The P68+DQA nanocarriers could be utilised to deliver numerous other compounds that have shown promise as disease modifying treatments for PD in cellular and animal models but may fall short of providing clinical benefit due to the common stability, solubility and brain penetrance issues mentioned above. NAC and HT are two such antioxidants that have been shown preclinically to protect against models of PD but whose therapeutic properties are likely to be limited clinically. As a precursor of the endogenous antioxidant glutathione, known to be lowered in PD (Kroemer & Reed, 2000; Simpkins & Dykens, 2008; Jiang et al.,

2017), NAC has long been considered as a potential disease-modifying therapeutic for PD. Cellular and animal preclinical assessments of NAC for PD have shown NAC to be protective against dopaminergic cell death resulting from neurotoxin and alpha synuclein models (Perry et al., 1985; Soto-Otero et al., 2000; Chen et al., 2007; Park et al., 2004; Sharma et al., 2007; Clark et al., 2010 Rahimmi et al., 2015; Katz et a;., 2015; Goldstein et al., 2017). There have also been numerous clinical assessments of NAC for neurological conditions, including PD (Bavarsad Shahripour et al., 2014; Slattery et al., 2015; Monti et al., 2016; Reyes et al., 2016; Monti et al., 2019). However, only high doses of free NAC are likely to reach the brain as it has been shown that oral administration of 200 mg NAC results in only 5% bioavailability and NAC is also largely undetectable following ingestion (Cotgreave & Moldeus, 1987; Bavarsad Shahripour et al., 2014). Furthermore, using high doses of NAC is undesirable due to the increased likelihood of off target side effects such as headaches, diarrhoea, and vomiting (Arstall et al., 1995; Ferreira et al., 2011; Tse et al., 2013;). Similarly, preclinical testing of HT has shown promising effects against oxidative stress and dopaminergic cell death in cellular and animal models (Hashimoto et al., 2004; Schaffer et al., 2007; Wu et al., 2009; Schapira, 2010; Yu et al., 2016; Goldstein et al., 2016; Funakohi-Tago et al., 2018) but unlike NAC, HT has yet to be tested in clinical studies for PD. This is likely because HT is rapidly metabolised and therefore unlikely to reach the brain at therapeutic concentrations (Robles-Almazan et al., 2018). Both NAC and HT could therefore benefit from formulation into nanocarriers to achieve their full potential for PD therapeutics.

The curcumin and DFO results, outlined in chapter 4, suggest that combined delivery of antioxidants and iron chelators achieved with the P68+DQA nanocarriers may provide a promising strategy to limit the degenerative process in PD due to the dual approach of free radical scavenging and iron chelation to limit detrimental free iron availability. The aim of this study was therefore to utilise the P68+DQA nanocarriers for NAC and HT alone, or in combination with DFO, and assess their physical characteristics and ability to protect against the rotenone SH-SY5Y model of PD developed in chapter 4.

5.2. Results

All drug-loaded nanoformulations exhibited high encapsulation efficiency (93% - 98%) with both NAC and HT loaded P68+DQA nanocarriers having similar mean encapsulations efficiencies of 93% and 95%, respectively (table 1). All drug-loaded nanocarriers exhibited a significantly higher mean particle size compared to the unloaded blank nanoformulation ($p < 0.0001$) (table 1). The addition of DFO into the formulation, appears to increase the mean encapsulation efficiency of both NAC (5%) and HT (2%), however the mean percentage encapsulation of DFO in the HT formulation was 17.64% lower than in the P68+DQA NAC + DFO formulation, although this was not a significant difference (table 1). The mean size of both the NAC (126 nm) and NAC + DFO (130 nm) loaded P68+DQA nanocarriers were smaller than the HT (166 nm) and HT + DFO (146 nm) loaded nanocarriers (table 1). The addition of DFO to the NAC and HT P68+DQA nanoformulations did not significantly alter particle size (table 1). All nanoformulations had low polydispersity as represented by mean polydispersity indices < 0.24 indicating that the majority of the nanocarriers within each formulation sample were of similar size (table 1). The mean surface charges of all drug loaded nanocarriers were moderately positive (4 mV – 10 mV) but each drug loaded nanoformulation had a higher surface charge compared to the blank unloaded nanoformulation, which exhibited a slightly negative charge (-0.78 mV) (table 1).

Table 1. Hydrodynamic Diameter (d), Polydispersity Index (PDI), Surface Charge, Drug Loading (DL) and Encapsulation Efficiency (EE) of blank and drug-loaded P68+DQA nanoformulations prepared at 80°C (mean ± S.D., n=6).

Sample	Contents (mg/ml)		d (nm)	PDI	Charge (mV)	DL (%)	EE (%)
P68+DQA (Blank)	P68: DQA:	9 1	25.52 ± 10.25	0.24 ± 0.04	0.78 ± 0.80	-	-
P68+DQA: NAC	P68: DQA: NAC:	9 1 20	125.67 ± 9.98	0.23 ± 0.05	3.67 ± 0.46	64.88 ± 1.93	92.74 ± 7.54
P68+DQA: NAC + DFO	P68: DQA: NAC: DFO:	9 1 12.4 5	130.33 ± 11.49	0.24 ± 0.02	6.63 ± 1.44	NAC: 17.53 ± 0.56 DFO: 17.59 ± 0.54	NAC: 98.32 ± 1.44 DFO: 94.36 ± 4.27
P68+DQA: HT	P68: DQA: HT:	9 1 1	166.28 ± 22.41	0.23 ± 0.03	7.43 ± 0.91	8.63 ± 1.16	94.56 ± 13.87
P68+DQA: HT + DFO	P68: DQA: HT: DFO:	9 1 0.24 5	146.26 ± 8.88	0.18 ± 0.07	9.87 ± 1.21	HT: 1.69 ± 0.03 DFO: 27.26 ± 0.30	HT: 97.17 ± 1.81 DFO: 76.72 ± 1.42
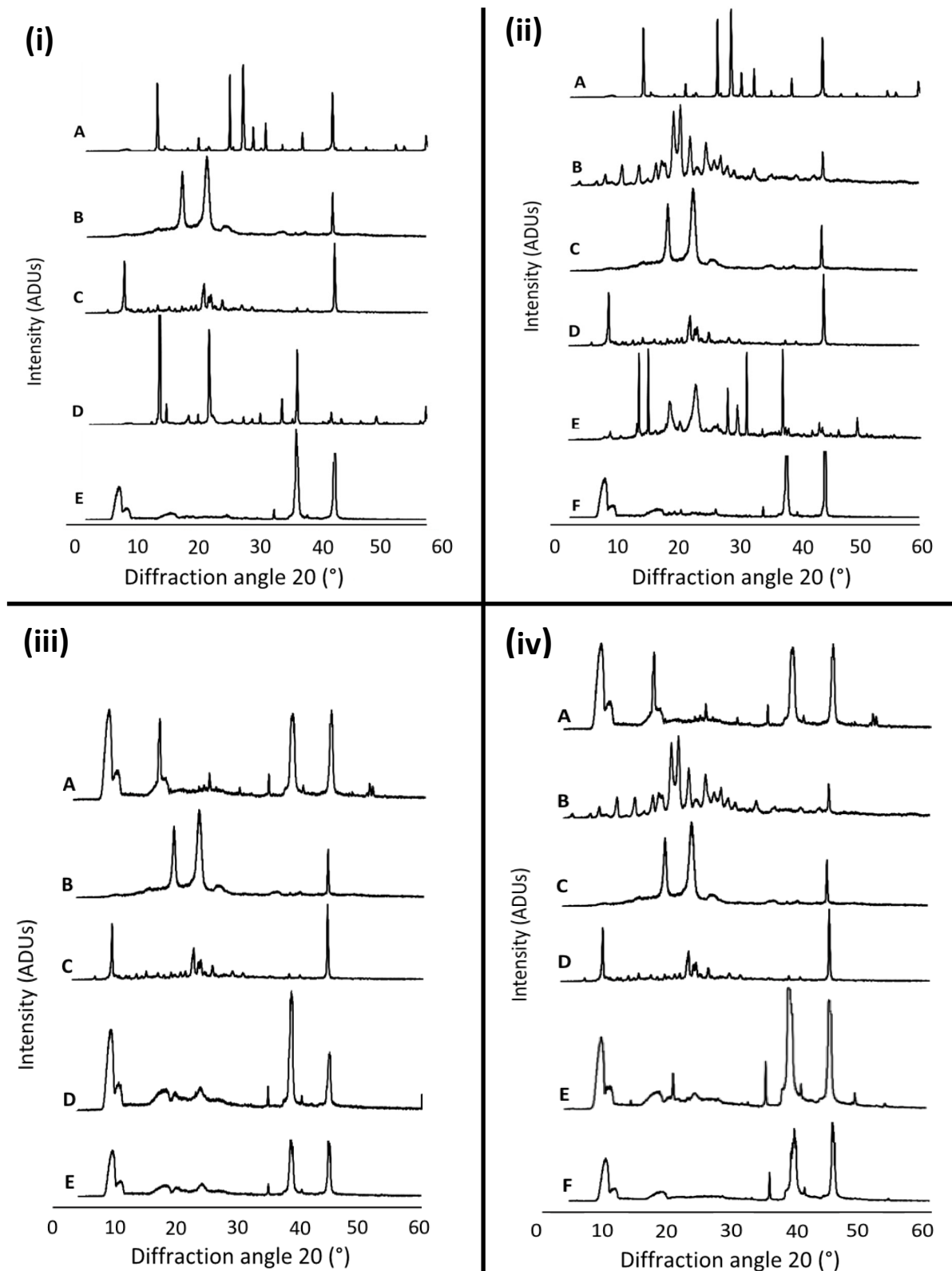
*Figure 1. **(i) P68+DQA NAC**. XRD patterns of (a) NAC, (b) P68, (c) DQA, (d) a physical mixture of P68, DQA and NAC in the same ratio as the nanoformulation and (e) lyophilized P68+DQA NAC nanoformulation. **(ii) P68+DQA NAC+DFO**. XRD patterns of (a) NAC, (b) DFO, (c) P68, (d) DQA, (e) a physical mixture of P68, DQA, NAC and DFO in the same ratio as the nanoformulation and (f) lyophilized P68+DQA NAC+DFO nanoformulation. **(iii) P68+DQA HT**. XRD patterns of (a) HT, (b) P68, (c) DQA, (d) a physical mixture of P68, DQA and HT in the same ratio as the nanoformulation and (e) lyophilized P68+DQA HT nanoformulation. **(iv) P68+DQA HT+DFO**. XRD patterns of (a) HT, (b) DFO, (c) P68, (d) DQA, (e) a physical mixture of P68, DQA, HT and DFO in the same ratio as the nanoformulation and (f) lyophilized P68+DQA HT+DFO nanoformulation.*

Figure 1 presents the XRD patterns of free NAC and HT, the combinations of NAC + DFO and HT + DFO, the lyophilized nanoformulations, the physical mixture of the components of each nanoformulation as well as the individual formulation components (P68 and DQA). The spectrum of NAC shows the main peaks at 14.84, 21.8, 26.94, 29.16, 30.94, 32.94, 39.06, 44.12, 59.82°, indicating a high level of crystallinity (figure 1ia, iia). A high level of crystallinity is also shown with the HT spectrum, with the main peaks at 8.74, 10.2, 16.98, 25,02, 29.98, 34.66, 38.3, 44.9, 51.44, 51.58° (figure 1iiia, iva). DFO also has a crystalline nature with main peaks at 11.44, 14.16, 17.60, 18.20, 20.76, 20.94, 22.56, 25.20, 27.58, 33.22 and 44.38° (figure 1iib, ivb). The P68 spectrum exhibits fewer peaks than NAC, HT and DFO, the main ones being at 18.94, 23.08, 26.80 and 44.24° showing some crystalline features (figure 1ib, iic, iiib, ivc). The DQA spectrum also has fewer peaks than NAC, HT and DFO with the main peaks at 9.42, 22.64, 23.98, 25.72 and 44.5° (figure 1ic, iid, iiic, ivd). The spectra of lyophilized P68+DQA drug-loaded formulations revealed far fewer peaks than its constituent components with generally only 3 main peaks for each formulation, at around 8.9, 34.7, 38.3 and 44.6°, indicating a more amorphous state (figure 1ie, iif, iiie, ivf). This reduction of peaks was not observed for the physical mixtures of the formulation components of those containing NAC (figure 1id, iie), whereas a slight reduction in the number of peaks was observed for the physical mixtures containing HT (figure 1iiid, ive).

Figure 2 shows the FTIR spectrum for the P68+DQA NAC, NAC+DFO, HT and HT+DFO lyophilized formulations, the individual components of each formulation and the physical mixture of these components. The NAC FTIR spectrum (figure 2ia, iia) highlights the presence of the hydroxyl group with a sharp peak at 3374 cm^{-1}. The strong peaks at 1715 and 1532 cm^{-1} results from the stretching vibrations of the C=O bonds. The stretching of the N-H, thiol (SH) and methyl (CH$_3$) groups are represented by peaks at 3374, 2547 and 1228 cm^{-1}, respectively. The HT FTIR spectrum (figure 2iiia, iva) indicates the presence of the characteristic hydroxyl groups with sharp peaks at 3385, 1447 and 1187 cm^{-1}. The strong peak at 1606 cm^{-1} represents the stretching vibrations of the C=C bonds within the aromatic ring. The FTIR spectrum for DFO (figure 2iib, ivb) shows peaks representing stretching vibrations of characteristic bonds for OH (3324, 1472, 1386 cm^{-1}), C=O (2864, 1652, 1536, 974 and 897 cm^{-1}), NH2 (1598 cm^{-1}), N-H (3115, and 1608 cm^{-1}).
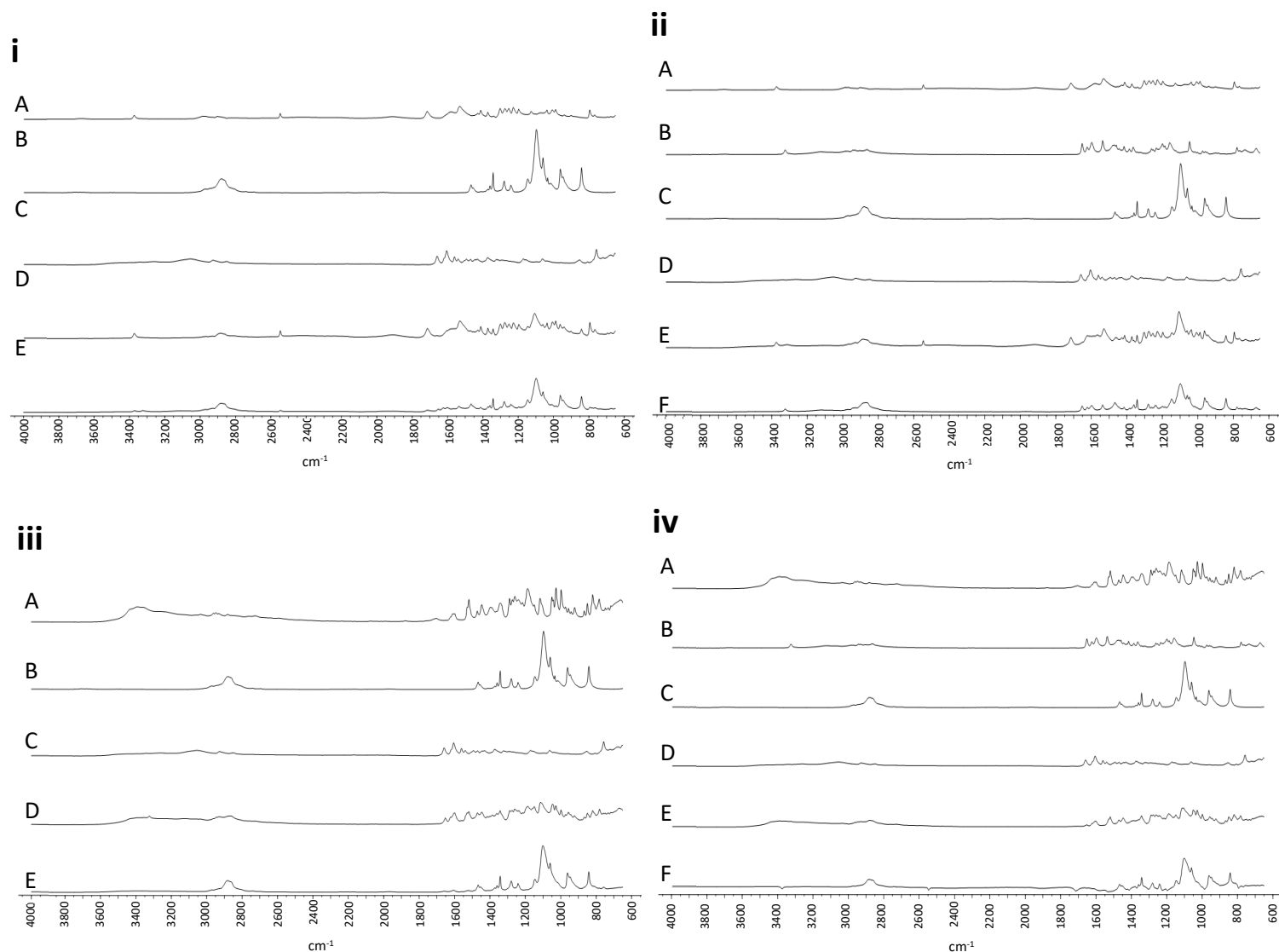
*Figure 2. **(i) P68+DQA NAC**. FTIR spectra for (a) NAC, (b) P68, (c) DQA, (d) a physical mixture of P68, DQA and NAC in the same ratio as the nanoformulation and (e) lyophilized P68+DQA NAC nanoformulation. **(ii) P68+DQA NAC+DFO**. FTIR spectra for (a) NAC, (b) DFO, (c) P68, (d) DQA, (e) a physical mixture of P68, DQA, NAC and DFO in the same ratio as the nanoformulation and (f) lyophilized P68+DQA NAC+DFO nanoformulation. **(iii) P68+DQA HT**. FTIR spectra for (a) HT, (b) P68, (c) DQA, (d) a physical mixture of P68, DQA and HT in the same ratio as the nanoformulation and (e) lyophilized P68+DQA HT nanoformulation. **(iv) P68+DQA HT+DFO**. FTIR spectra for (a) HT, (b) DFO, (c) P68, (d) DQA, (e) a physical mixture of P68, DQA, HT and DFO in the same ratio as the nanoformulation and (f) lyophilized P68+DQA HT+DFO nanoformulation.*

The FTIR spectrum for P68 (figure 2ic, iid, iiic, ivd) shows peaks at around 2880, 1060 and 841 cm^{-1} representing the vibrations of the hydroxyl groups and the stretching vibrations of the symmetrical C-O and asymmetrical C-O of the ether groups, respectively. The sharp peak at 1279 cm^{-1} represents the vibrations of the methylene group. The DQA spectrum (figure 2ic, iid, iiic, ivd) shows the absorption peaks at 3342 and 3264 cm^{-1} which represent the two primary amine groups for the asymmetric and symmetric N-H stretches. The sharp peak at 1605 cm^{-1} represents the vibration of aromatic C=C bonds. Methyl group stretching and deformation is represented by the peaks at 2928 and 2847 cm^{-1}. The physical mixtures for

each formulation (figure 2id, iie, iiid, ive) show peaks corresponding to each constituent within the mixture. However, the HT and DFO peaks appear less intense in the mixtures (figure 2ii, iii, iv) but the NAC peaks remain prominent within the mixtures containing NAC. The FTIR spectrum for each of the lyophilized formulations are similar to those of the physical mixtures but in each case the peaks corresponding to the NAC, HT or DFO elements are less intense (figure 2id-e, iie-f, iiid-e, iv e-f).
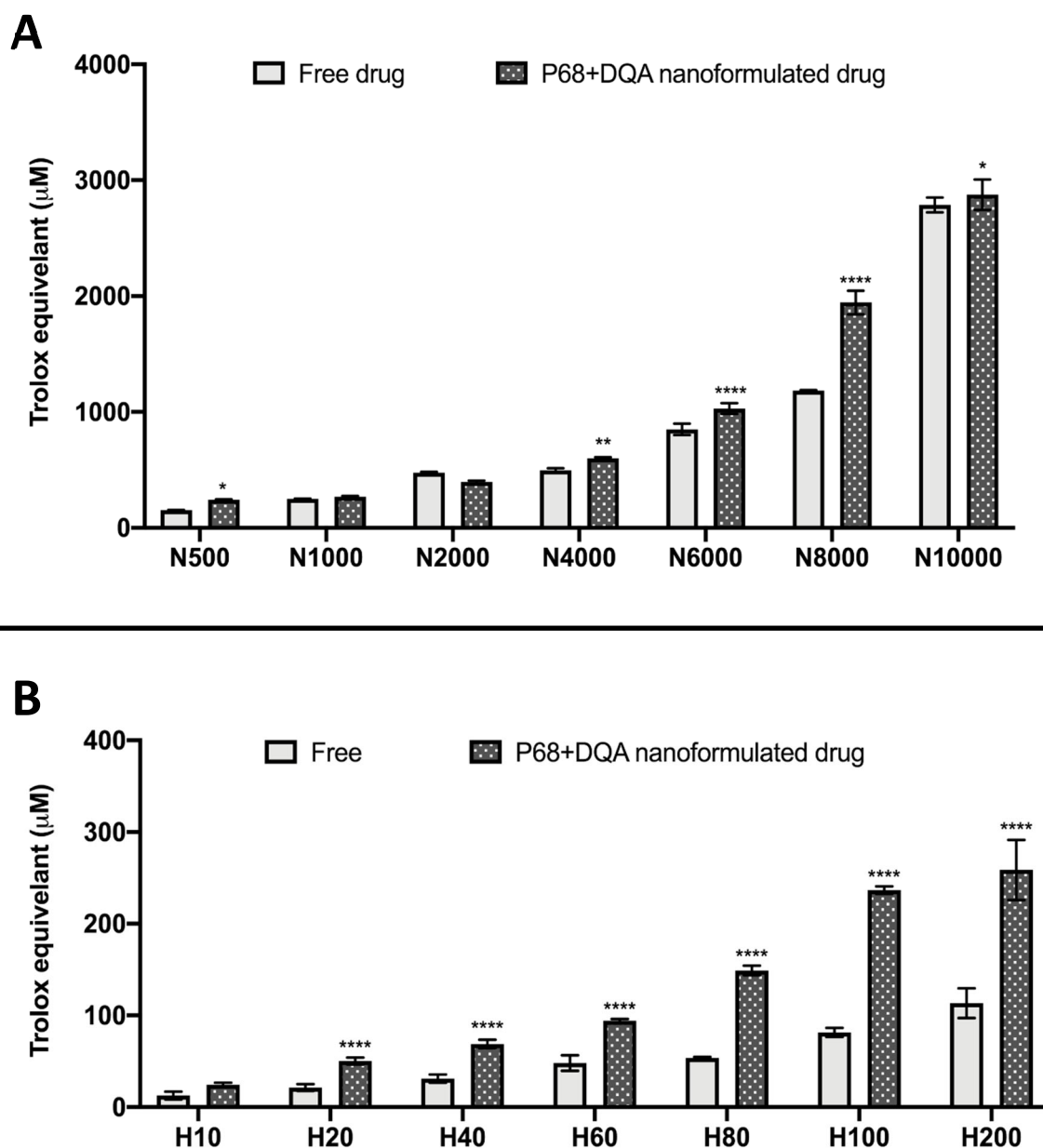
*Figure 3. A. Antioxidant activity of free and P68+DQA nanoformulated 500 - 10,000 μM NAC measured by the FRAP assay (mean ± S.D., n=6). B. Corresponding FRAP assay results for free and P68+DQA nanoformulated HT (10 -200 μM). * represents significance values of nanoformulated drug compared to free drug within the same treatment condition (**** $p < 0.0001$, ** $p < 0.01$, * $p < 0.05$).*

The antioxidant capacity of the NAC (500 – 10,000 μM) and HT (10 – 200 μM) loaded P68+DQA nanoformulations was assessed using the FRAP assay and compared to the corresponding free drug at each concentration (figure 3). In both cases, significant differences in mean trolox equivalent antioxidant capacity were observed between the different concentrations of treatments (NAC: $F_{(6, 70)}$= 4088, $p < 0.0001$, HT: $F_{(6, 70)}$ = 427.5, $p < 0.0001$) and the different treatment preparation types (NAC: $F_{(1, 70)}$ = 219.3, $p < 0.0001$, HT: $F_{(1, 70)}$= 1029, $p < 0.0001$) (figure 3). All concentrations of the P68+DQA NAC nanocarriers had at least the same antioxidant capacity as the corresponding free drug concentrations of NAC (figure 3a). The 500 μM ($p = 0.0222$), 4000 μM ($p = 0.0055$), 6000 μM ($p < 0.0001$), 8000 μM ($p < 0.0001$) and 10,000 μM ($p = 0.0257$) concentrations of P68+DQA NAC exhibited higher antioxidant capacity than free NAC at these concentrations, between 3.19 and 64.15% (figure 3a). The highest notable difference was observed at 8000 μM where P68+DQA NAC exhibited 64.15% higher antioxidant capacity than free NAC (figure 3a). All concentrations of P68+DQA HT, except 10 μM, exhibited significantly higher trolox equivalent antioxidant capacity than the corresponding concentrations of free HT ($p < 0.0001$) (figure 3b). The percentage increase in antioxidant capacity of the P68+DQA HT compared to the free HT preparations were over 100% for the majority of concentrations (20 μM, 40 μM, 80 μM, 100 μM, 200 μM) but all were over 93% (figure 3b).

The same concentration ranges of free and P68+DQA NAC and HT were then tested on the SH-SY5Y cell line to evaluate the cytotoxicity of each concentration, using the MTT assay. When treating SH-SY5Y cells with 500 – 10,000 μM free NAC, P68+DQA NAC and corresponding blank formulations for 24 h, in all cases no significant alteration of cell viability was observed ($F_{(21, 68.61)}$ = 3.123, $p = 0.0002$) (figure 4a). A significant reduction in cell viability compared to control was exhibited at 10,000 μM free NAC ($p = 0.0002$), however cell viability remained above 80% (figure 4a). Following 48 h treatment, a significant reduction in SH-SY5Y cell viability was observed with the 6000 -10,000 μM NAC concentration for both free (38-58%, $p < 0.0001$) and formulated NAC (20-52%, 6000 μM NAC - $p = 0.0471$, 8000 μM and 10,000 μM – $p < 0.0001$) whereas no cytotoxicity was observed for the corresponding blank formulations ($F_{(21, 57.12)}$ = 32.03, $p < 0.0001$) (figure 4b).
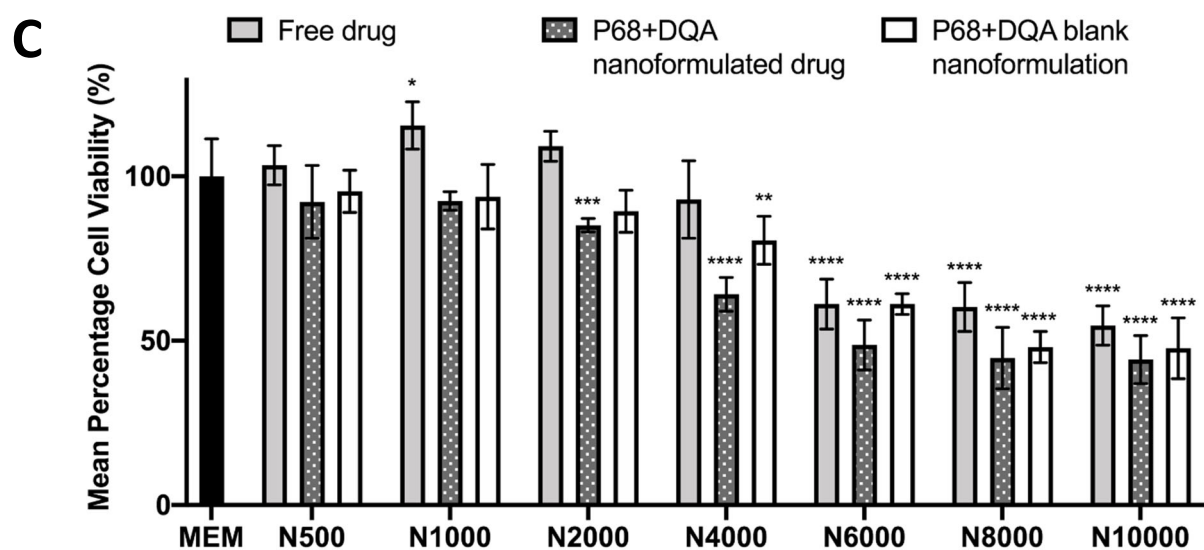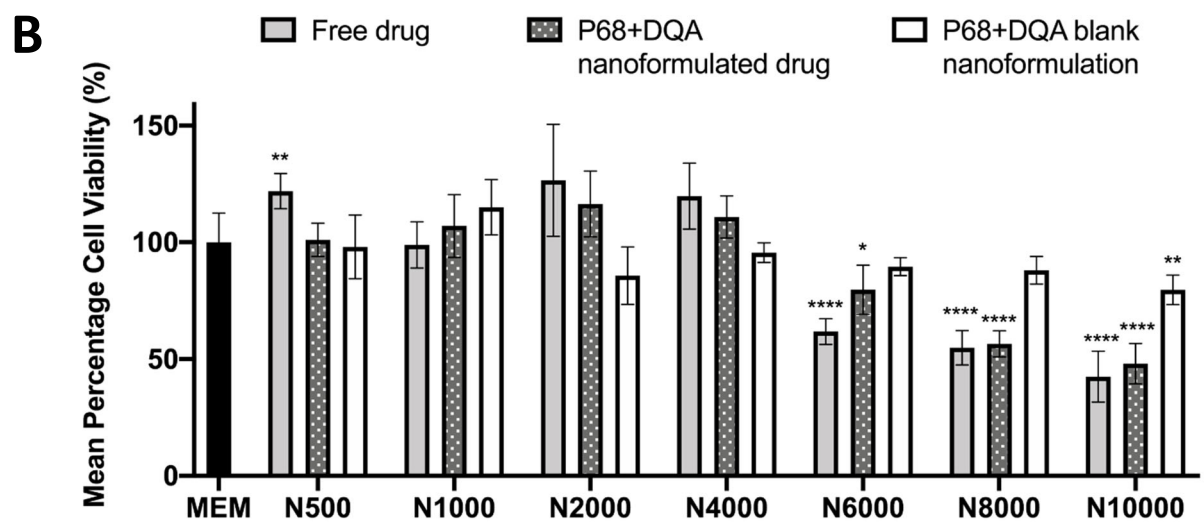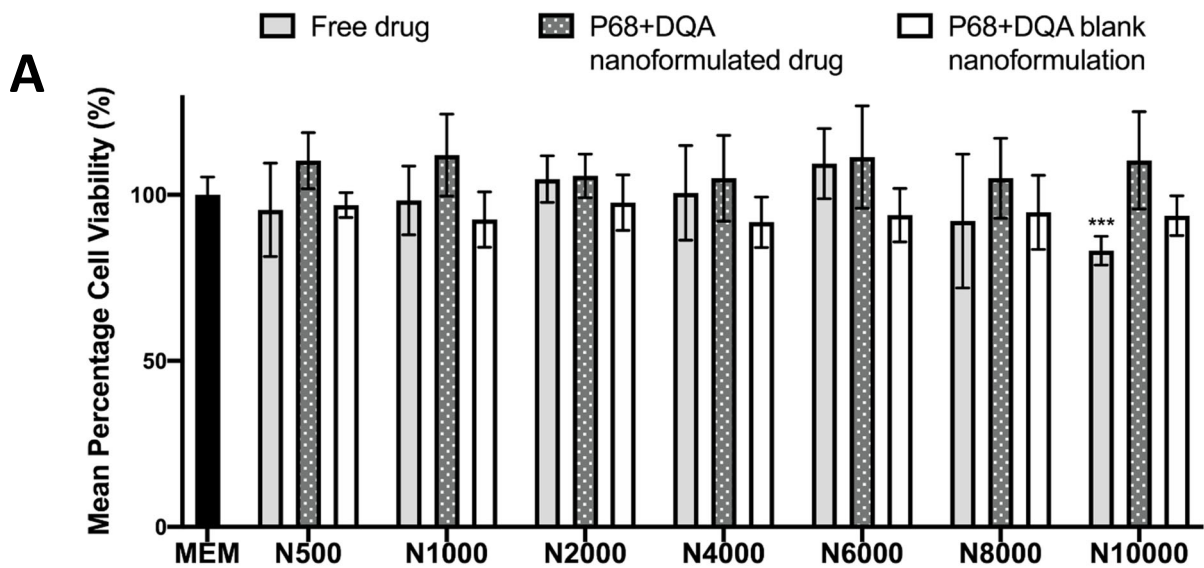
*Figure 4. A. MTT assay results of 24 h 500 μM – 1000 μM NAC treatment. MEM represents the control condition where cells were only treated with media (mean ± S.D., n=6). B. Corresponding MTT assay results for 48 h NAC treatments. C. Corresponding MTT assay results for 72 h NAC treatments * represents significance values of the treatment conditions compared to the control condition (**** p < 0.0001, *** p < 0.001, ** p < 0.01, * p < 0.05).*
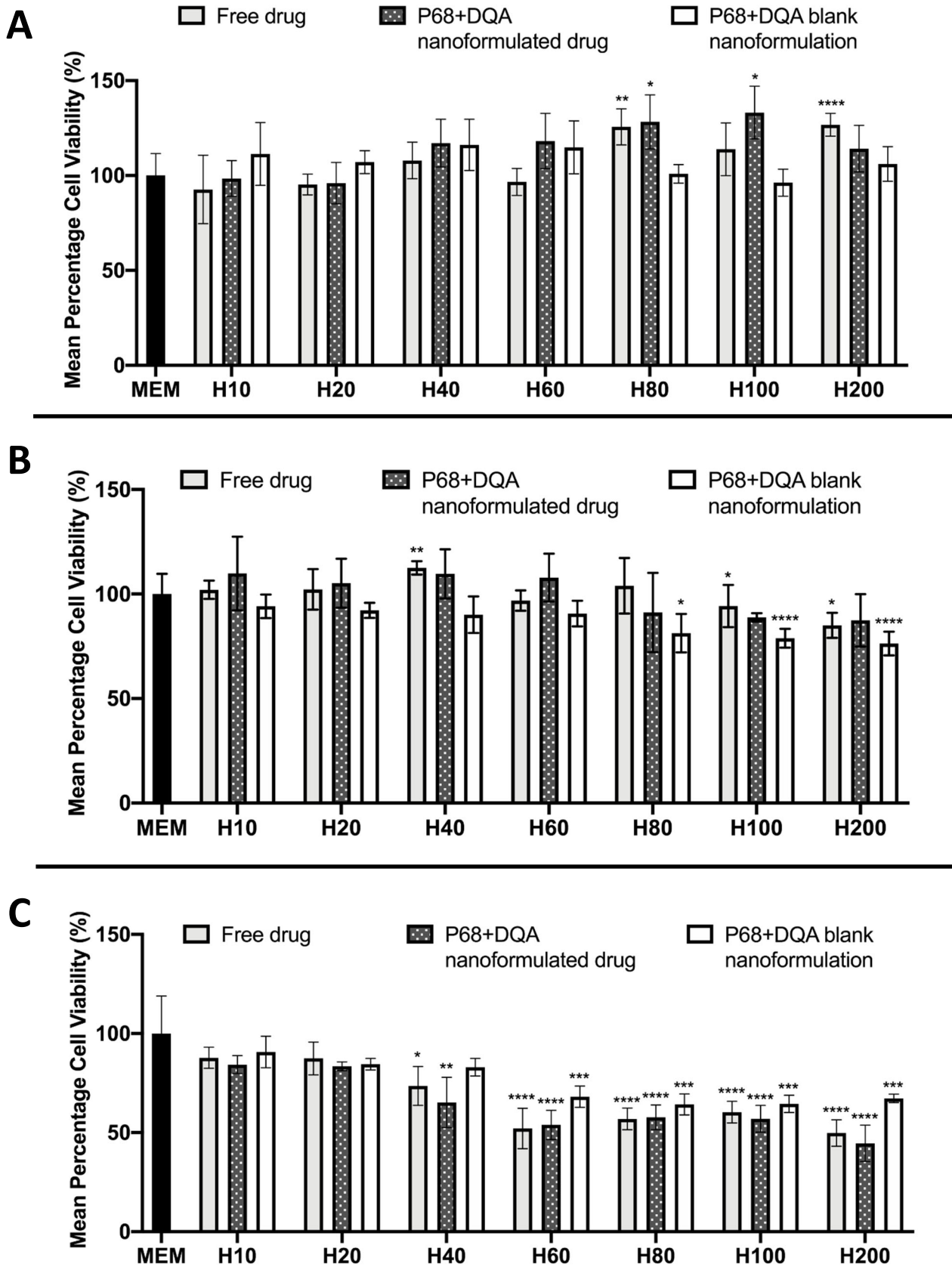
Figure 5. A. MTT assay results of 24 h 10 μM – 200 μM HT treatment. MEM represents the control condition where cells were only treated with media (mean ± S.D., n=6). B. Corresponding MTT assay results for 48 h HT treatments. C. Corresponding MTT assay results for 72 h HT treatments * represents significance values of the treatment conditions compared to the control condition (**** $p < 0.0001$, *** $p < 0.001$, ** $p < 0.01$, * $p < 0.05$).

A similar trend is observed at 72 h treatment with 6000 -10,000 µM NAC free ($p < 0.0001$) and formulated ($p < 0.0001$) NAC (figure 4c). However, by this time point a significant reduction in cell viability, by more than 50%, was also observed for the corresponding blank formulations ($p < 0.0001$ in all cases except 4000 µM blank formulation where $p = 0.0049$). A small reduction in cell viability was also observed with 2000 µM (7.75%, $p = 0.0007$) and 4000 µM (14.85%, $p < 0.0001$) P68+DQA NAC treatment compared to control cells treated with MEM for 72 h ($F_{(21, 84.54)} = 63.35$, $p < 0.0001$) (figure 4c).

Similarly, when assessing the cytotoxicity of a range of concentrations (10 – 200 µM) of free HT, P68+DQA HT and corresponding blank formulations using the MTT assay, cell viability was maintained at control levels or above following treatment for 24 h ($F_{(21, 81.45)} = 6.801$, $p < 0.0001$) (figure 5a). However, no significant reduction in cell viability was observed for any concentration of HT (free or formulated) following 48 h treatment (figure 5b). Although figure 5b shows a significant reduction of cell viability compared to control, when treating with 200 µM free HT ($p = 0.0135$) and the corresponding blank formulations at 80 µM ($p = 0.0338$) and 100 – 200 µM ($p < 0.0001$), cell viability was above 80% in all cases ($F_{(21, 57.30)} = 6.9155$, $p < 0.0001$). By the 72 h time point, a significant reduction in cell viability was observed for free HT at 40 µM ($p = 0.0141$), free and P68+DQA formulated HT at 60 - 200 µM ($p < 0.0001$), and with the corresponding blank formulations ($p < 0.0005$) (figure 5c). However, no cytotoxicity was observed with 40 µM treatment of free and P68+DQA formulated HT ($F_{(21, 73.11)} = 29.41$, $p < 0.0001$) (figure 5c).

The concentrations of free and P68+DQA NAC and HT that exhibited no cytotoxicity at any time point (24 h, 48 h or 72 h) were used in the subsequent evaluation of the protective effects of these antioxidants against various parameters relevant in PD. When comparing the effects of free NAC and P68+DQA NAC nanocarriers on cell viability following 24 h rotenone treatment, significant differences in mean cell viability were observed between the different treatments ($F_{(13, 60.16)} = 25.81$, $p < 0.0001$) (figure 6a). 3 h pre-treatment with P68+DQA nanocarriers of 500 µM and 1000 µM NAC ($p = 0.0002$ and $p = 0.0001$, respectively), combined 500 µM NAC and 50 µM DFO ($p = 0.0029$) and combined 1000 µM NAC and 100 µM DFO ($p = 0.002$) significantly protected against the reduction in cell viability induced by 24 h treatment with 100 µM rotenone (figure 6a).
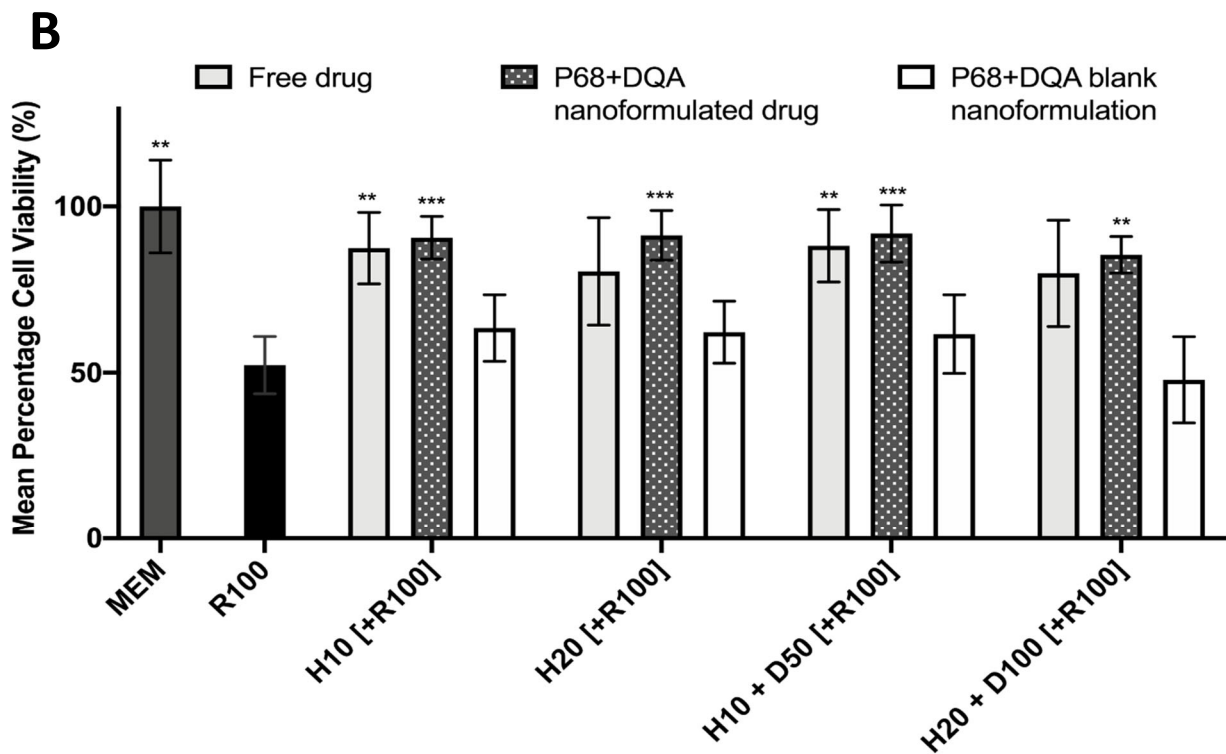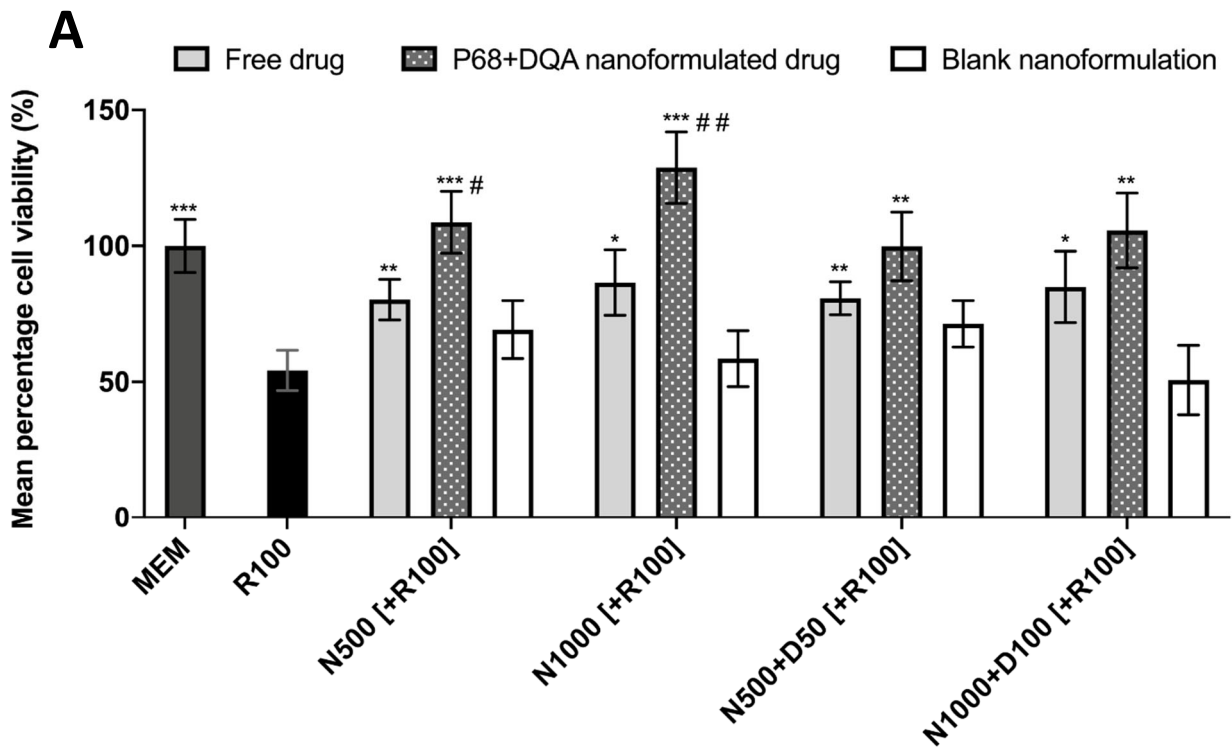
Figure 6. A. MTT assay results of 3 h pre-treatment with free drug, P68+DQA nanoformulated and corresponding blank preparations of either 500 μM or 1000 μM NAC (N500, N1000) or combined NAC with 50 μM or 100 μM DFO (N500+D50, N1000+D100) followed by 24 h treatment with 100 μM rotenone (R100) compared to R100 treatment alone. MEM represents the control condition where cells were only treated with media, no pre-treatment nor R100 treatment (mean ± S.D., n=6). B. Corresponding MTT assay results for the free drug, P68+DQA nanoformulated and corresponding blank pre-treatments of either 10 μM or 20 μM HT (H10, H20) or combined HT with 50 μM or 100 μM DFO (H10+D50, H20+D100) (n=6). * represents significance values of control or pre-treatment conditions compared to rotenone treatment alone (*** p < 0.001, ** p < 0.01, * p < 0.05). # represents significance values of nanoformulated drug compared to free drug within the same treatment condition (## p < 0.01, # p < 0.05).

All the free drug conditions also protected against rotenone induce cytotoxicity (500 µM NAC - p = 0.0068, 1000 µM NAC - p = 0.022, 500 µM NAC + 50 µM DFO - p = 0.0028, 1000 µM NAC + 100 µM DFO - p = 0.0428) but in each case the nanoformulations had a higher mean percentage cell viability and nanocarriers of 500 µM and 1000 µM NAC were significantly more protective than the corresponding concentrations of free NAC (35.42% p = 0.0297 and 48.87% p = 0.0093, respectively) (figure 6a). None of the blank nanoformulations were able to protect against rotenone induced cytotoxicity (figure 6a). Likewise, significant differences in mean cell viability were observed between the different HT and HT + DFO 3 h pre-treatments, when evaluating SH-SY5Y cell viability following 24 h 100 µM rotenone treatment $F_{(13, 52.42)}$ = 13.42, $p < 0.0001$). All HT P68+DQA nanoformulation pre-treatments significantly protected against cytotoxicity induced by 100 µM rotenone (10 µM HT: p = 0.0006 20 µM HT: p = 0.0005, 10 µM HT + 50 µM DFO: p = 0.0007 and 20 µM HT + 100 µM DFO: p = 0.0022) (figure 6b). Whereas, for the free drug pre-treatments, only 10 µM (p = 0.0054) and 10 µM HT + 50 µM DFO (p = 0.0071) were able to significantly protect against the reduction in cell viability induced by rotenone (figure 6b). None of the corresponding blank formulations were protective (figure 6b).

Western blot analysis of anti-TH and anti-NeuN markers reflect the significant ability of the different concentrations of the both free ($F_{(4, 30)}$ = 10.66, $p < 0.0001$) and P68+DQA formulated ($F_{(4, 30)}$ = 40.95, $p < 0.0001$) NAC and NAC + DFO to protect against the reduction in dopamine and neurons induced by 24 h 100 µM rotenone treatment (figure 7). 24 h 100 µM rotenone treatment reduced the levels of TH marker present in SH-SY5Y cells by 40-50% and the levels of NeuN by more than 30% in each case (figure 7, 8). 3 h pre-treatment with 500 µM NAC ($p < 0.0001$ for both), 1000 µM NAC ($p < 0.0001$ and p = 0.0004), 500 µM NAC + 50 µM DFO ($p < 0.0001$ for both) and 1000 µM NAC + 100 µM DFO ($p < 0.0001$ and p = 0.0002) P68+DQA nanoformulations significantly protected against the respective reductions in TH and NeuN induced by rotenone, maintaining TH and NeuN marker levels to at least 99% and 89% of control levels (respectively) (figure 7b).
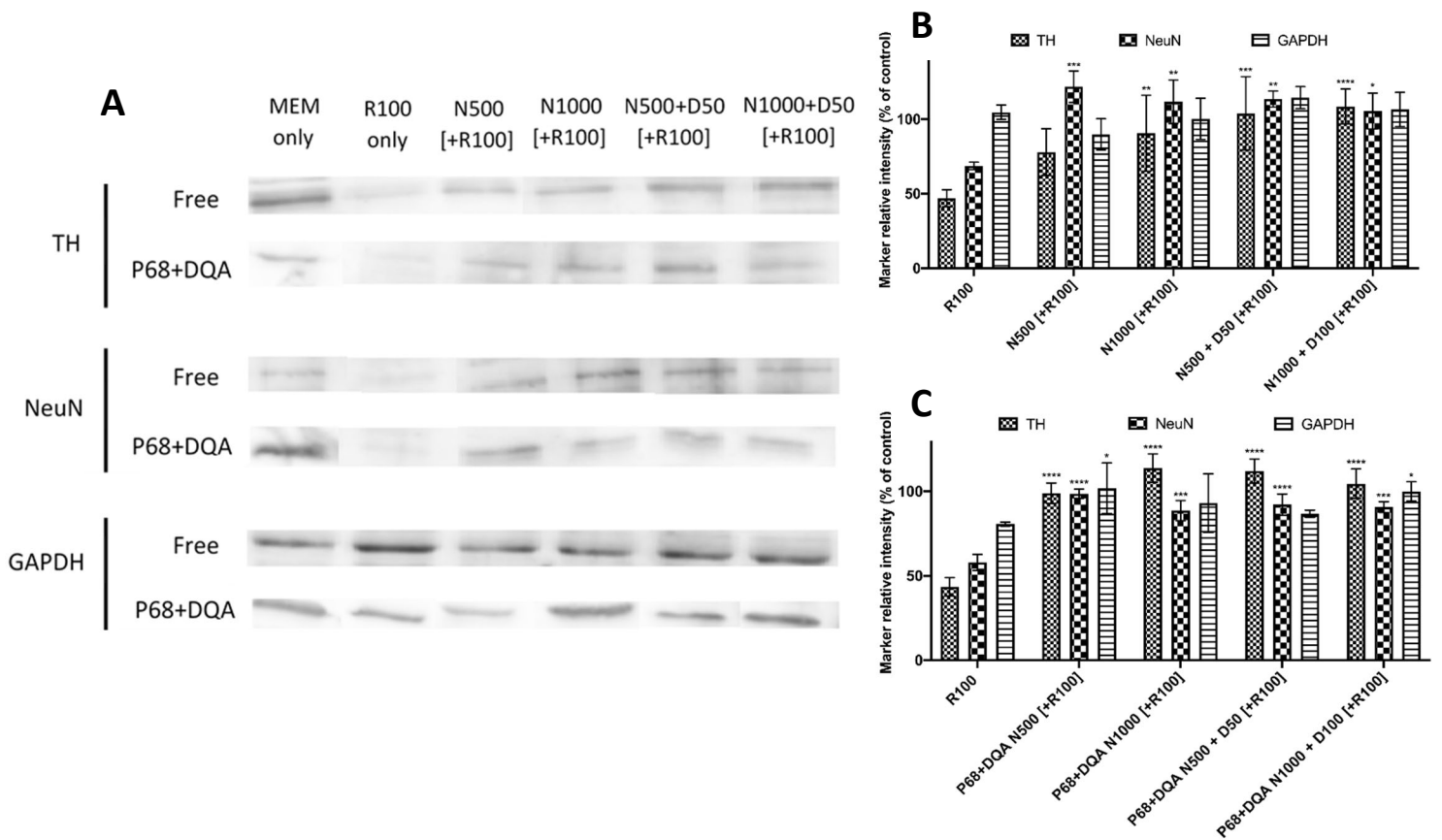
*Figure 7. A. Western blot detection of tyrosine hydroxylase (TH) the first rate-limiting enzyme involved in the synthesis of dopamine (~62 kDa), the neuron specific protein NeuN (~48 kDa) and loading control GAPDH (~36 kDa) in 10 μg protein from SH-SY5Y cell lysate. SH-SY5Y cells were treated with MEM media or 100 μM rotenone (R100) only for 24 h or pre-treated with free drug or P68+DQA nanoformulated preparations of either 500 μM, 1000 μM NAC (N500, N1000) or combined NAC with 50 μM or 100 μM DFO (N500+D50, N1000+D100) (n=3). B. Image J quantification of TH, NeuN and GAPDH proteins detected in SH-SY5Y cell lysate following 3 h pre-treatment with free NAC or combined NAC + DFO or 24 h R100 treatment only (mean ± S.D., n=3). C. Corresponding Image J quantification of TH, NeuN and GAPDH proteins detected following 3 h pre-treatment with P68+DQA NAC or combined NAC + DFO or 24 h R100 treatment only (mean ± S.D., n=3). Quantification is expressed as the percentage of the levels of each marker identified in control cells (lysate of SH-SY5Y cells treated with MEM media only, for 24 h). * represents significance values of pre-treatment conditions compared to R100 treatment alone for each marker (**** p < 0.0001, *** p < 0.001, ** p < 0.01, * p < 0.05).*

This pattern was also observed for the same concentrations of free NAC and NAC + DFO (500 μM NAC: p = 0.059 and p = 0.0003, 1000 μM NAC: p = 0.0034 and p = 0.0039, 500 μM NAC + 50 μM DFO: p = 0.0001 and p = 0.0025 and 1000 μM + 100 μM DFO p < 0.0001 and p = 0.0168), where TH and NeuN marker levels were maintained to at least 78% and 106% of control levels (respectively) (figure 7c). No significant differences in GAPDH levels were identified between cells treated with any free or P68+DQA NAC or NAC + DFO pre-treatments compared to control cells (figure 7b, c), with all pre-treatment conditions resulting in more than 80% of control GAPDH levels. However, the percentage of GAPDH found in the P68+DQA 500 μM NAC and 1000 μM NAC + 100 μM DFO conditions was

significantly higher than in the 100 µM rotenone only condition ($p = 0.0207$ and $p = 0.0411$, respectively) (figure 7c).
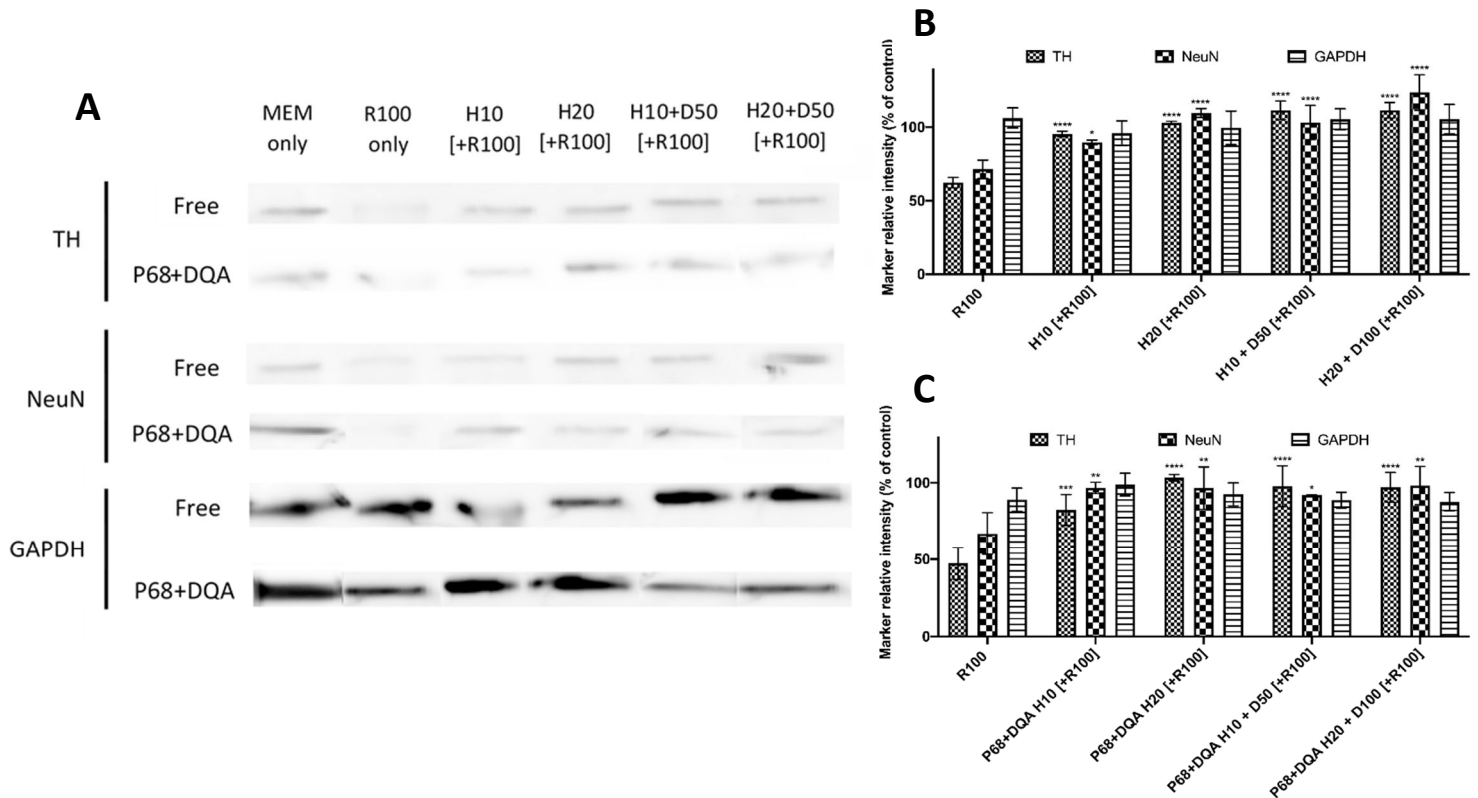
Figure 8. A. Western blot detection of tyrosine hydroxylase (TH) the first rate-limiting enzyme involved in the synthesis of dopamine (~62 kDa), the neuron specific protein NeuN (~48 kDa) and loading control GAPDH (~36 kDa) in 10 µg protein from SH-SY5Y cell lysate. SH-SY5Y cells were treated with MEM media or 100 µM rotenone (R100) only for 24 h or pre-treated with free drug or P68+DQA nanoformulated preparations of either 10 µM, 20 µM HT (H10, H20) or combined HT with 50 µM or 100 µM DFO (H10+D50, H20+D100) (n=3). B. Image J quantification of TH, NeuN and GAPDH proteins detected in SH-SY5Y cell lysate following 3 h pre-treatment with free HT or combined HT + DFO or 24 h R100 treatment only (mean ± S.D., n=3). C. Corresponding Image J quantification of TH, NeuN and GAPDH proteins detected following 3 h pre-treatment with P68+DQA HT or combined HT + DFO or 24 h R100 treatment only (mean ± S.D., n=3). Quantification is expressed as the percentage of the levels of each marker identified in control cells (lysate of SH-SY5Y cells treated with MEM media only, for 24 h). * represents significance values of pre-treatment conditions compared to R100 treatment alone for each marker (**** $p < 0.0001$, *** $p < 0.001$, ** $p < 0.01$, * $p < 0.05$).

3 h pre-treatment with all concentrations of both free ($F_{(4, 30)} = 28.3$, $p < 0.0001$) and P68+DQA ($F_{(4, 30)} = 15.57$, $p < 0.0001$) HT and HT + DFO were also able to protect TH and NeuN, maintaining levels to at least 82% and 90% of control (respectively in both cases) following 24 h 100 µM rotenone treatment (P68+DQA – 10 µM HT: $p = 0.0005$ and $p = 0.0034$, 20 µM HT: $p < 0.0001$ and $p = 0.0036$, 10 µM HT + 50µM DFO: $p < 0.0001$ and $p = 0.0173$ and 20 µM HT + 100 µM DFO: $p < 0.0001$ and $p = 0.002$. Free drug – 10 µM HT: $p < 0.0001$ and $p = 0.0366$, 20 µM HT, 10 µM HT + 50 µM DFO and 20 µM HT + 100 µM DFO: $p < $

0.0001 for both) (figure 8). No significant differences in GAPDH levels were identified between cells treated with any free or P68+DQA HT or HT + DFO pre-treatments compared to control cells or cells treated with 100 µM rotenone only (figure 8b, c).

When evaluating iron status using the ferritin ELISA and ferrozine assay, significant differences in mean non-ferritin bound iron between the different treatment conditions containing NAC ($F_{(9, 14.07)}$ = 84.5, $p < 0.0001$) and HT ($F_{(9, 7.438)}$ = 74.9, $p < 0.0001$) were observed following 24 h 100 µM rotenone treatment (figure 9). All P68+DQA nanoformulation pre-treatments of NAC and NAC + DFO were able to protect against rotenone induced increased iron levels (500 µM NAC (p = 0.004), 1000 µM NAC (p = 0.0054), 500 µM NAC + 50 µM DFO (p = 0.0049), 1000 µM NAC + 100 µM DFO (p = 0.005)) (figure 9a). All concentrations of free NAC and NAC + DFO also significantly protected against increased iron levels resulting from rotenone treatment (500 µM NAC (p = 0.0042), 1000 µM NAC (p = 0.0039), 500 µM NAC + 50 µM DFO (p = 0.0045), 1000 µM NAC + 100 µM DFO (p = 0.004)) (figure 9a). A significantly lower level (40.93%) of non-ferritin bound iron was observed with the P68+DQA formulation at 1000 µM NAC + 100 µM DFO compared to the corresponding free drug (figure 8a). Although there was no significant change in ferritin levels as a result of 100 µM rotenone treatment compared to control, all pre-treatments of free drug and P68+DQA nanoformulations of NAC and NAC + DFO reduced ferritin levels by a range of 43-77% compared to control ($F_{(9, 30.51)}$ = 33.84, $p < 0.0001$) (figure 9b).

3 h pre-treatment with all concentrations of both free and P68+DQA formulated HT and HT + DFO were also able to protect against increased levels of non-ferritin bound iron induced by rotenone (10 µM HT free: p = 0.0022 and P68+DQA formulated: p = 0.0041, 20 µM HT free: p = 0.005 and P68+DQA formulated: p = 0.0042, 10 µM HT + 50 µM DFO free: p = 0.0038 and formulated: p = 0.0037 20 µM HT + 100 µM DFO free: p = 0.0035 and formulated: p = 0.0032) (figure 10a). Only the 20 µM P68+DQA HT pre-treatment resulted in a significantly lower (14.12%) level of non-ferritin bound iron compared to the corresponding free drug pre-treatment (p = 0.0325) (figure 10a). Again, there was no significant difference observed in ferritin concentration between 100 µM rotenone treatment and control but 3 h pre-treatment with 20 µM free and P68+DQA formulated HT ($p < 0.0001$ and p = 0.0031 respectively), P68+DQA 10 µM HT + 50 µM DFO (p = 0.0003) as well as free and P68+DQA formulated 20 µM HT + 100 µM DFO ($p < 0.0001$ and p = 0.0001,

respectively) resulted in a significant reduction in ferritin compared to 100 μM rotenone treatment alone ($F_{(9, 20.86)} = 24.88$, $p < 0.0001$) (figure 10b).
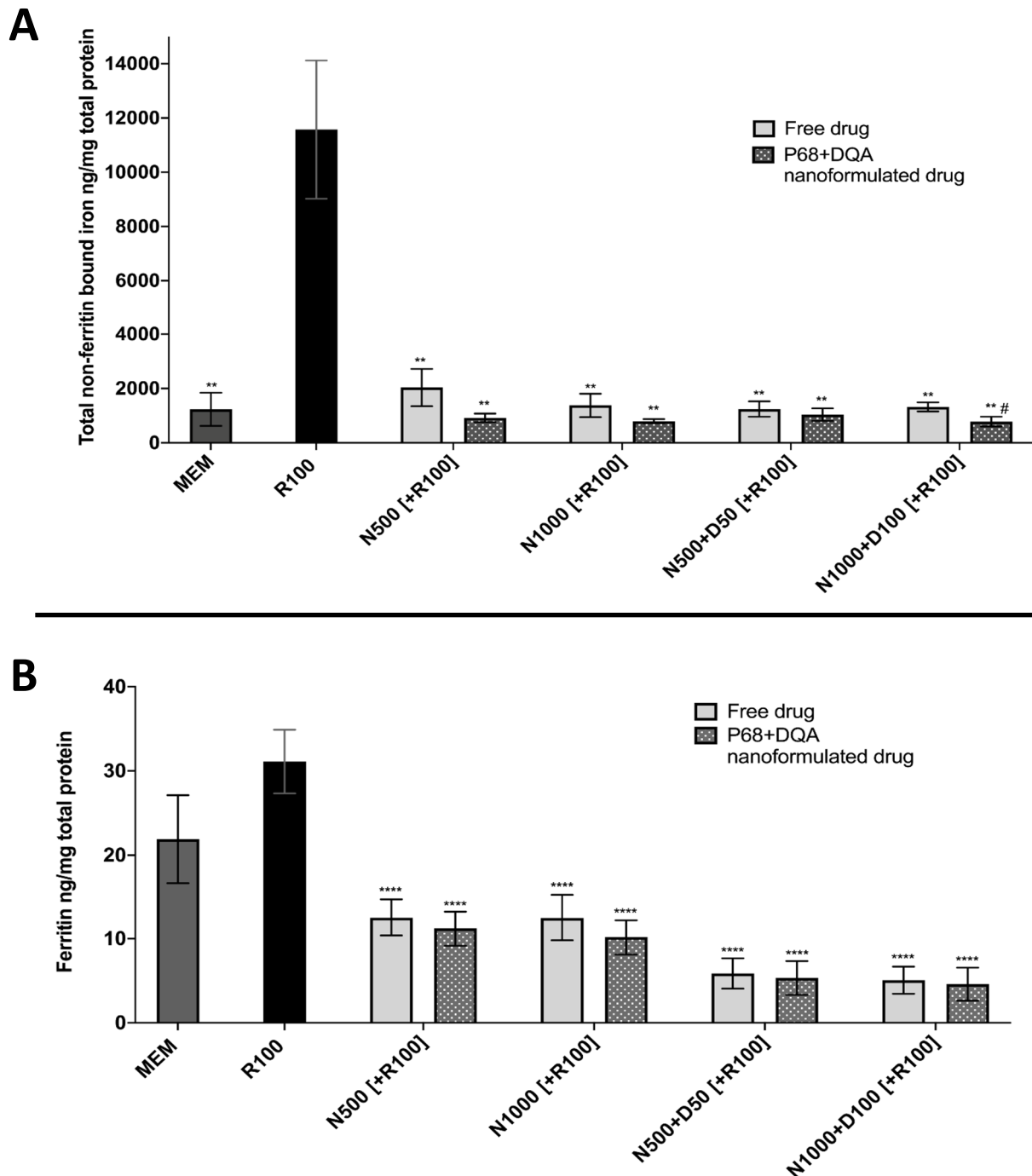
Figure 9. A. Total non-ferritin bound iron concentrations resulting from 3 h pre-treatment with free drug or P68+DQA nanoformulated preparations of either 500 μM and 1000 μM NAC (N500, N1000) or combined NAC with 50 μM or 100 μM DFO (N500+D50, N1000+D100) followed by 24 h treatment with 100 μM rotenone (R100) compared to R100 treatment alone. MEM represents the control condition where cells were only treated with media, no pre-treatment nor R100 treatment (mean ± S.D., n=6). B. Corresponding ferritin ELISA results of 3 h pre-treatment with free drug or P68+DQA nanoformulated preparations of N500, N1000, N500+D50 or N1000+D100 followed by 24 h R100 treatment. (mean ± S.D., n=6). Total non-ferritin bound iron (A) was calculated using the total iron concentrations obtained from the ferrozine assay minus the mean ferritin concentrations obtained from the ferritin ELISA (B). * represents significance values of control or pre-treatment conditions compared to R100 treatment alone (**** $p < 0.0001$, ** $p < 0.01$). # represents significance values of nanoformulated drug compared to free drug within the same treatment condition (# $p < 0.05$).
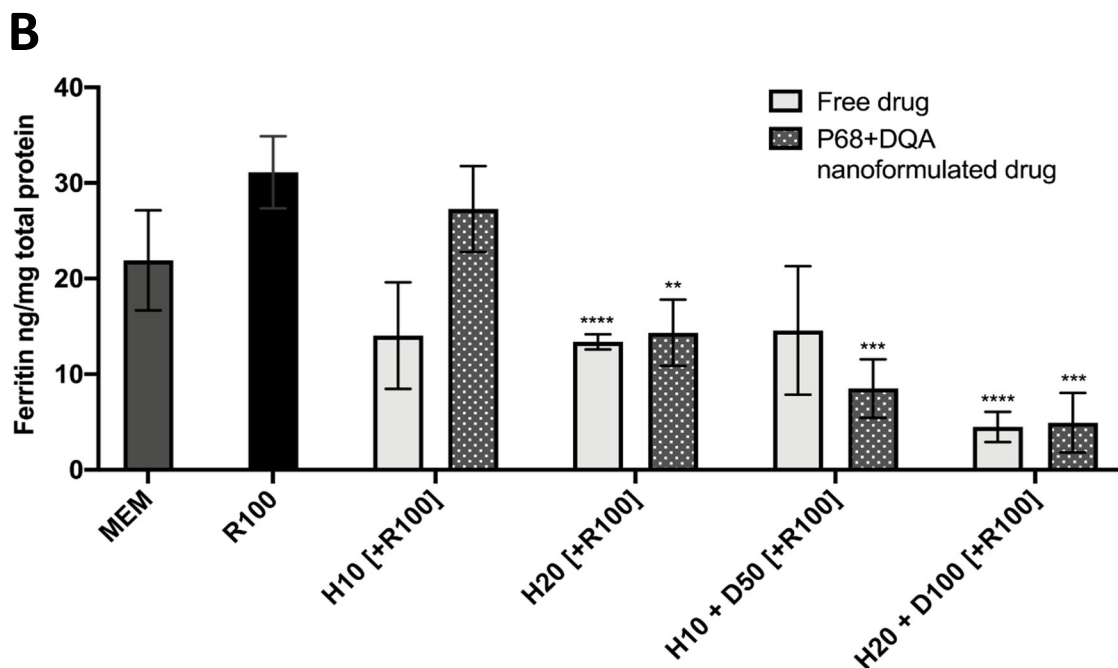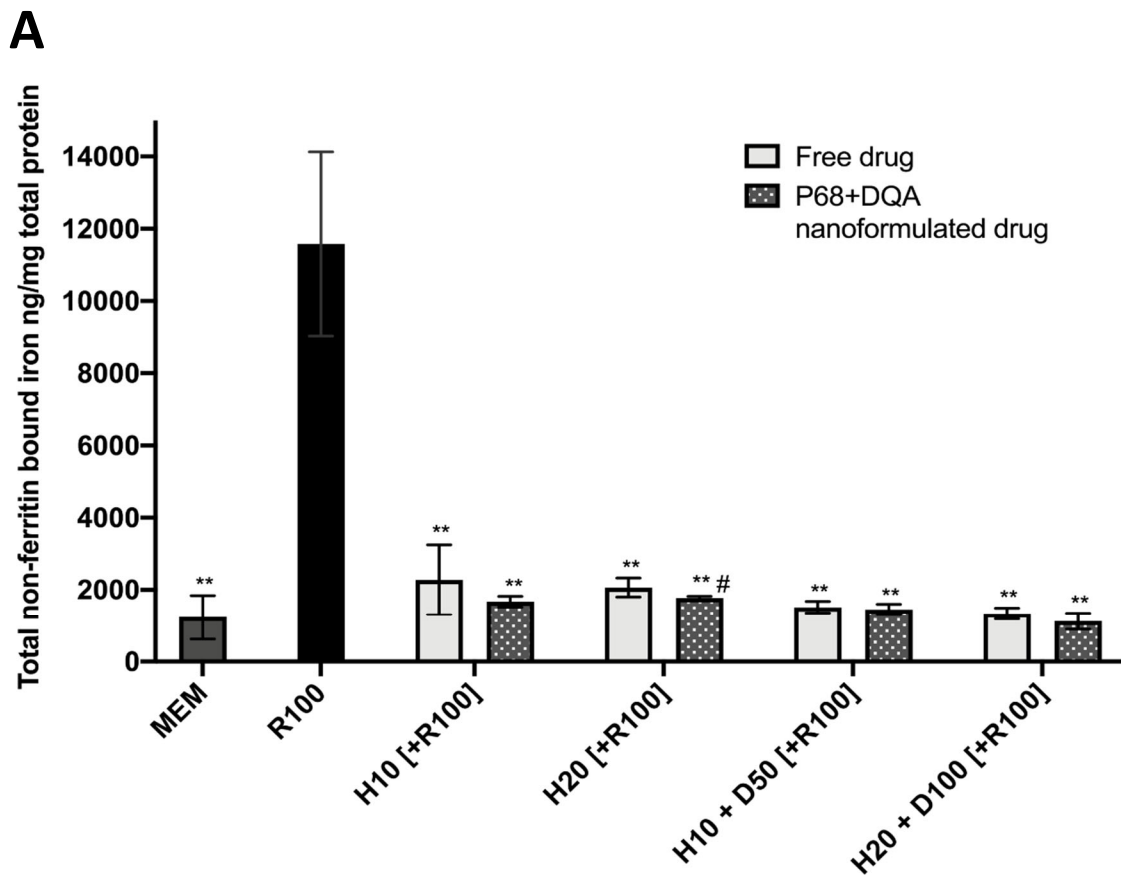
*Figure 10. A. Total non-ferritin bound iron concentrations resulting from 3 h pre-treatment with free drug or P68+DQA nanoformulated preparations of either 10 μM and 20 μM HT (H10, H20) or combined HT with 50 μM or 100 μM DFO (H10+D50, H20+D100) followed by 24 h treatment with 100 μM rotenone (R100) compared to R100 treatment alone. MEM represents the control condition where cells were only treated with media, no pre-treatment nor R100 treatment (mean ± S.D., n=6). B. Corresponding ferritin ELISA results of 3 h pre-treatment with free drug or P68+DQA nanoformulated preparations of H10, H20, H10 + D50 or H20+ D100 followed by 24 h R100 treatment. (mean ± S.D., n=6). Total non-ferritin bound iron (A) was calculated using the total iron concentrations obtained from the ferrozine assay minus the mean ferritin concentrations obtained from the ferritin ELISA (B). * represents significance values of control or pre-treatment conditions compared to R100 treatment alone (**** p < 0.0001, *** p < 0.001, ** p < 0.01). # represents significance values of nanoformulated drug compared to free drug within the same treatment condition (# p < 0.05).*

139

The cellular antioxidant activity of free and P68+DQA NAC, NAC + DFO, HT and HT + DFO was evaluated using variations of the CAA assay, testing the protective effect of these antioxidants against three different prooxidants (100 μM rotenone, 200 μM iron and 600 μM ABAP). ABAP is the traditional prooxidant used for this assay (Wolfe, et al., 2007; Hu, et al (2013) and was therefore used as a control experiment for both NAC and HT evaluations.

The CAA assay results showed significant differences in cellular antioxidant activity between the different treatment preparation types against 100 μM rotenone ($F_{(2, 60)} = 16.79$, $p < 0.0001$), 200 μM free iron ($F_{(2, 60)} = 1036$, $p < 0.0001$) and 600 μM ABAP ($F_{(2, 60)} = 114.6$, $p < 0.0001$) as well as with the different concentrations of NAC and NAC + DFO in the majority of cases (rotenone: $F_{(3, 60)} = 73.77$, $p < 0.0001$; iron: $F_{(3, 60)} = 166.2$, $p < 0.0001$; ABAP: $F_{(3, 60)} = 2.664$, $p = 0.0559$) (figure 11). All concentrations of the P68+DQA preparation of NAC and NAC + DFO had at least as high cellular antioxidant activity against 100 μM rotenone than the free drug preparations and, in all cases, the P68+DQA preparations exhibited significantly higher antioxidant activity (83 – 218%) than the free drug + DQA preparation (500 μM - $p < 0.0001$ and 1000 μM – $p < 0.0001$, 500 μM NAC + 50 μM DFO – $p = 0.0012$ and 1000 μM NAC + 100 μM DFO, $p < 0.0001$) (figure 11a). The highest antioxidant activity against rotenone was reached at 1000 μM NAC for both the free and P68+DQA preparations. P68+DQA nanocarriers of NAC and combined NAC and DFO consistently had significantly higher antioxidant capability (between 8 and 32%) against 200 μM free iron than the corresponding free drug conditions (500 μM NAC - $p = 0.0002$, 1000 μM NAC – $p = 0.0073$, 500 μM NAC + 50 μM DFO – $p = 0.0392$, 1000 μM NAC + 100 μM DFO, $p < 0.0001$) (figure 11b). The highest difference in antioxidant activity between the formulations and free drug preparation was at 500 μM NAC, where the nanocarriers had 32.01% higher antioxidant activity (figure 11b). Likewise, all NAC and NAC + DFO loaded P68+DQA nanocarriers had significantly higher cellular antioxidant activity compared to the corresponding free drug + DQA preparations, by more than 200% in each case ($p < 0.0001$). The P68+DQA preparation of combined 1000 μM NAC and 100 μM DFO had the most antioxidant potential against 200 μM iron compared with all other conditions (figure 11b).
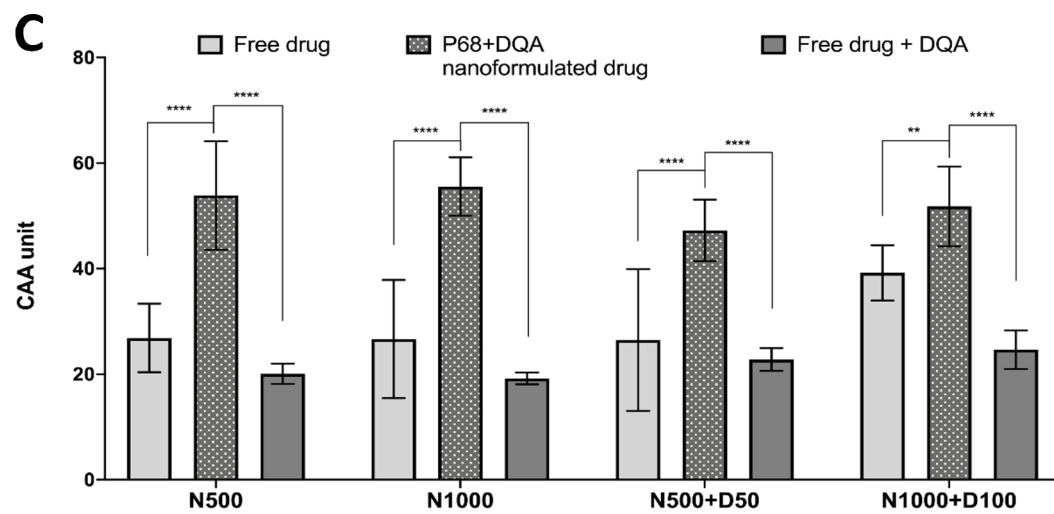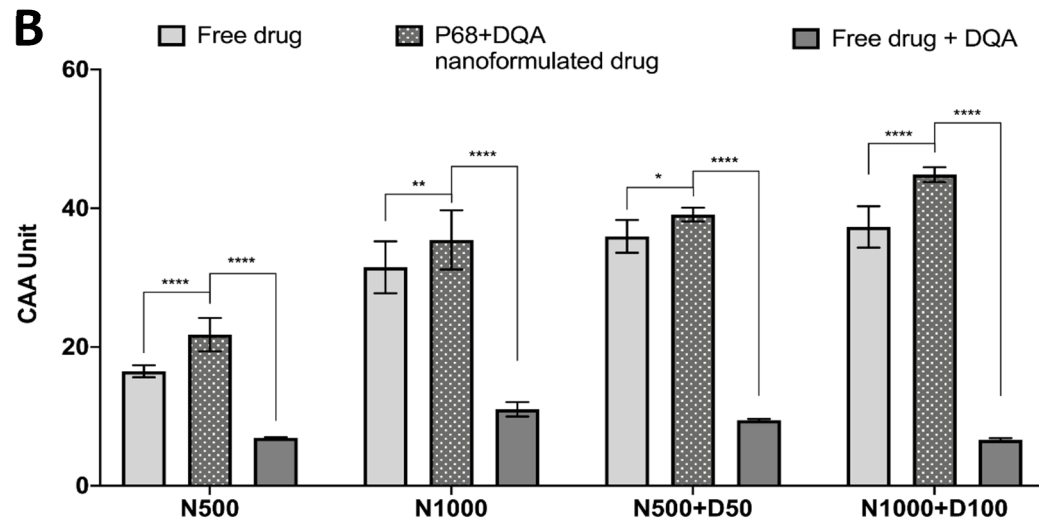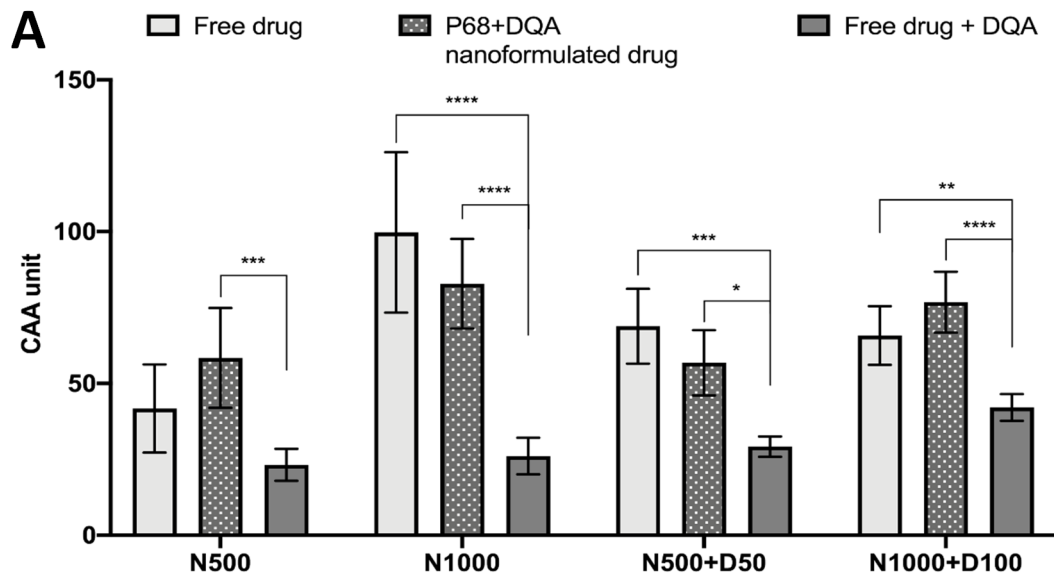
Figure 11. CAA assay results for free drug, P68+DQA nanformulated drug and free drug + DQA preparations of 500 μM or 1000 μM NAC (N500, N1000) and combined NAC and 50 μM or 100 μM DFO (N500+D50, N1000+D100) when using 100 μM rotenone as the prooxidant (mean ± S.D., n=6). B. Corresponding CAA results when using 200 μM free iron as the prooxidant. C. Corresponding CAA results when using 600 μM ABAP as the prooxidant. * represents significance values when comparing the P68+DQA nanoformulated drug to the free drug and free drug + DQA preparations within the same drug condition (**** p < 0.0001, *** p < 0.001, ** p < 0.01, * p < 0.05).

These results are consistent with those seen when using the traditional CAA method, where ABAP was used as the prooxidant, although the P68+DQA preparations of NAC and NAC + DFO have consistently higher CAA units than free preparations when using ABAP as the prooxidant (figure 11c). The cellular antioxidant activity of both free and P68+DQA NAC and NAC + DFO was generally highest when using rotenone as the prooxidant, exhibiting mean CAA units between 42 and 99, compared to 17 and 45 when using iron and 27 and 56 when using ABAP (figure 11).

Likewise, significant differences in cellular antioxidant activity of HT and HT + DFO against 100 μM rotenone ($F(2, 60) = 58.05$, $p < 0.0001$), 200 μM free iron ($F(2, 60) = 415.19$, $p < 0.0001$) and 600 μM ABAP ($F(2, 60) = 54.78$, $p < 0.0001$) were observed between the different treatment preparation types and the different treatment concentrations (figure 12). The cellular antioxidant activity of the P68+DQA preparations of HT and HT + DFO were also at least as high as the free drug preparations at all concentrations when using 100 μM rotenone as the prooxidant, and significantly higher (58.91%) at 10 μM HT ($p = 0.0027$) (figure 12a). All P68+DQA HT and DFO preparations exhibited significantly higher antioxidant activity (80 – 154%) than the free drug + DQA preparation ($p < 0.0001$ in all cases except at 20 μM HT + 100 μM DFO where $p = 0.0003$) (figure 12a). All concentrations of P68+DQA HT and HT + DFO obtained similarly high CAA units, around 60 (figure 12a).

When using 200 μM free iron as the prooxidant, in all cases the P68+DQA nanoformulations of HT and HT + DFO had significantly higher antioxidant capability than the corresponding free drug (63 – 152%) and free drug + DQA (61 - 369%) preparations ($p < 0.0001$) (figure 12b). For both free drug and P68+DQA preparations, the combination of 20 μM HT + 100 μM DFO had the most antioxidant potential compared all other conditions (figure 12b). Free and P68+DQA 20 μM HT and 20 μM HT + 100 μM DFO were much more protective against ABAP than 10 μM HT and 10 μM HT + 50 μM DFO (figure 12c). The overall CAA units of each condition achieved against ABAP were similar to those observed when using iron and rotenone as the prooxidants, but the highest CAA units were again achieved against rotenone, reaching 68 compared to 35 and 39 for ABAP and iron, respectively (figure 12).
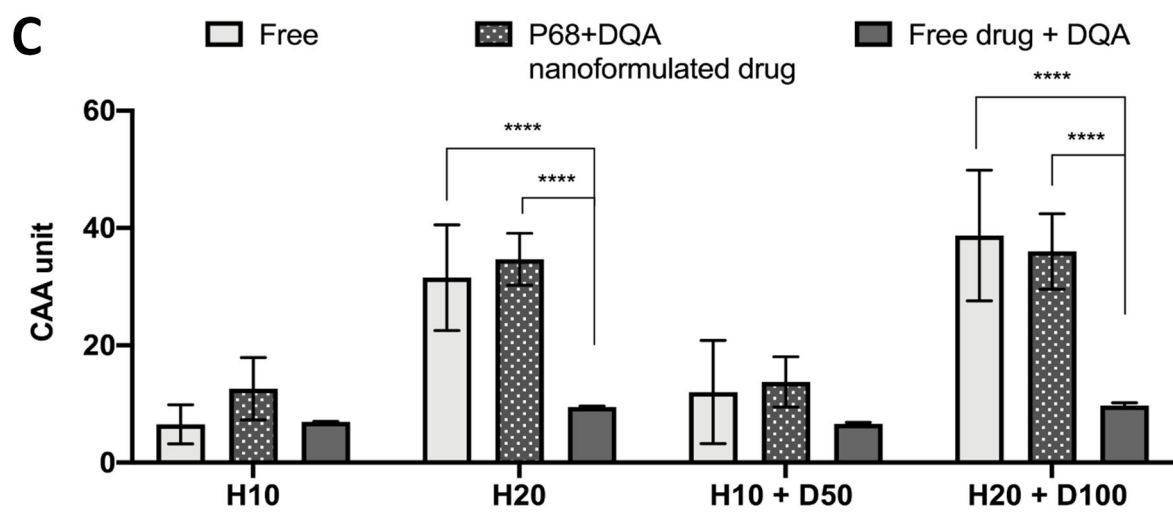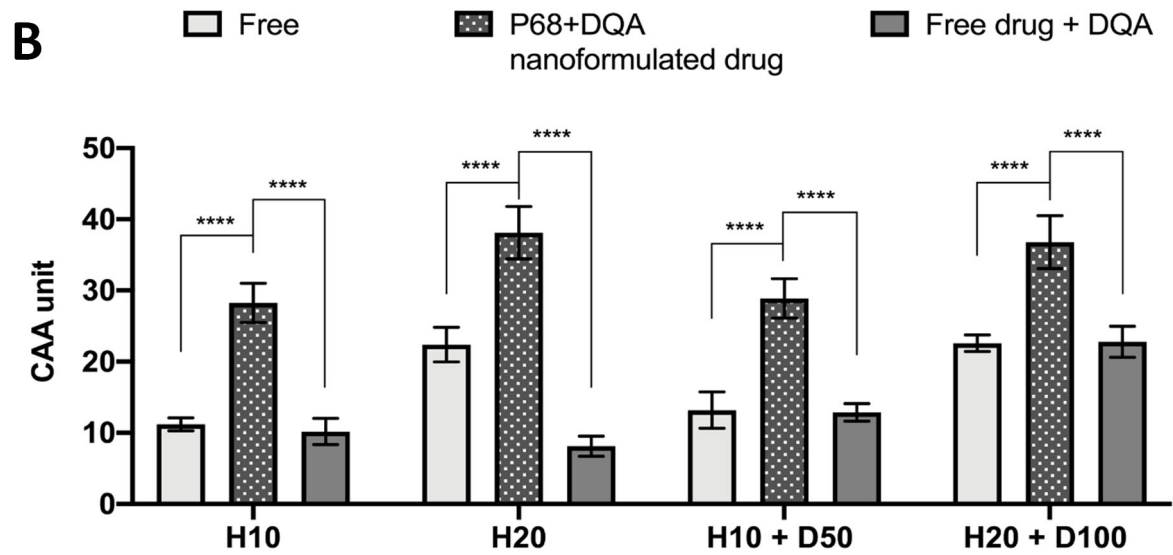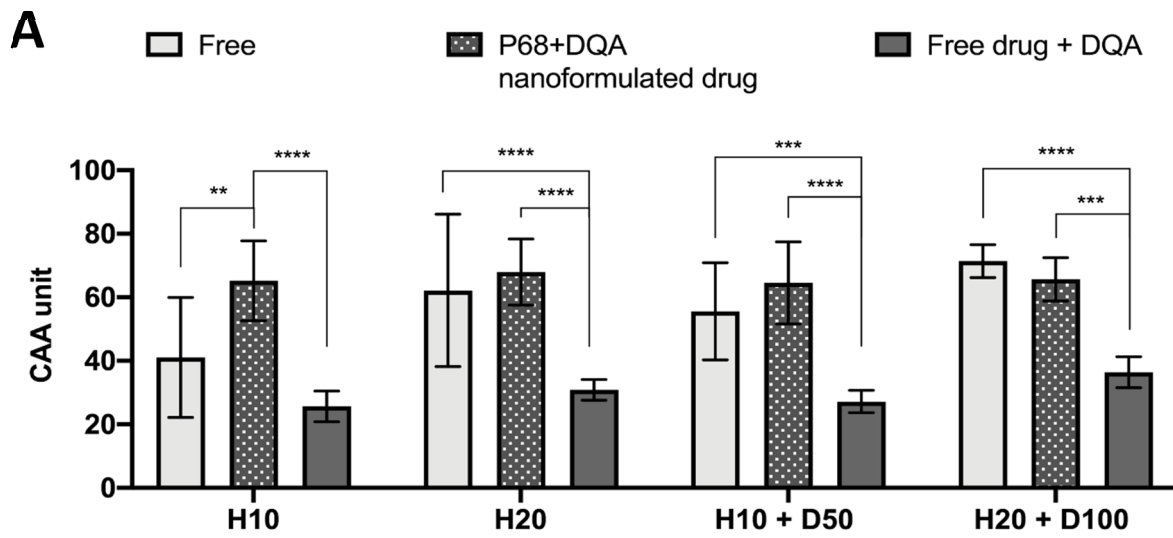
*Figure 12. A. CAA assay results for free drug, P68+DQA nanformulated drug and free drug + DQA preparations of 10 μM or 20 μM HT (H10, H20) and combined HT and 50 μM or 100 μM DFO (H10+D50, H20+D100) when using 100 μM rotenone as the prooxidant (mean ± S.D., n=6). B. Corresponding CAA results when using 200 μM free iron as the prooxidant. C. Corresponding CAA results when using 600 μM ABAP as the prooxidant. * represents significance values when comparing the P68+DQA nanoformulated drug to the free drug and free drug + DQA preparations within the same drug condition (**** p < 0.0001, *** p < 0.001, ** p < 0.01).*
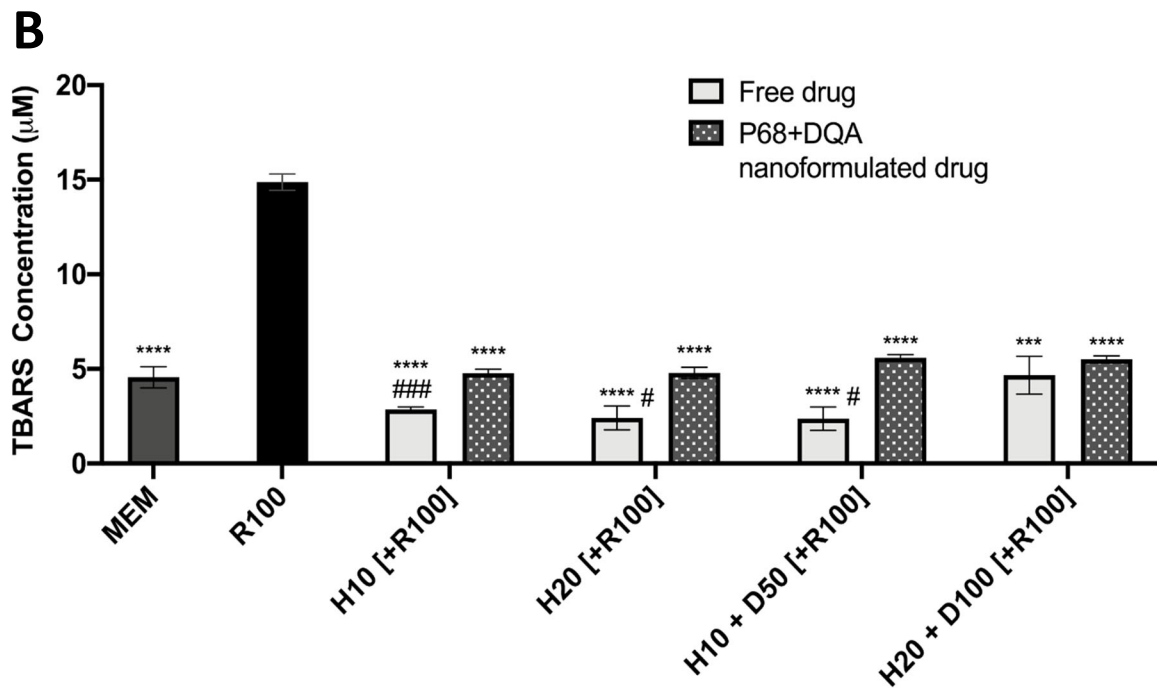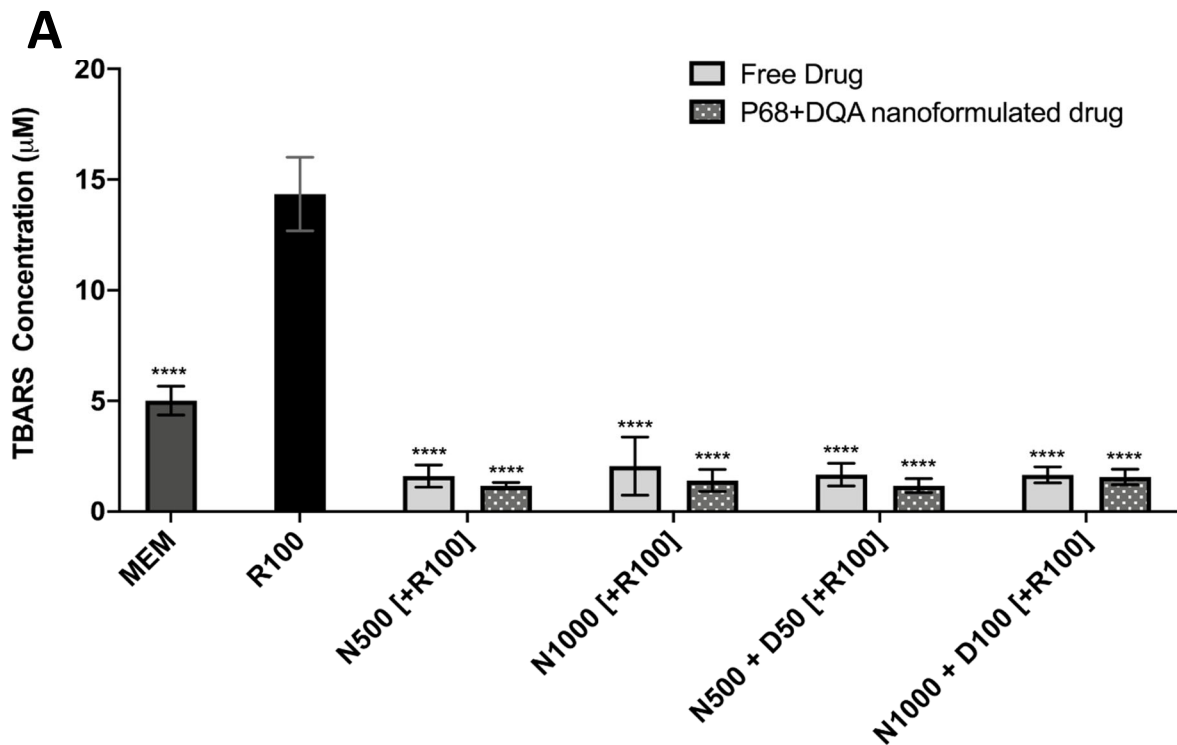
Figure 13. A. TBARS assays results of 3 h pre-treatment with free drug or P68+DQA nanoformulated preparations of either 500 μM or 1000 μM NAC (N500, N1000) or combined NAC and DFO (N500+D50, N1000+D100) followed by 24 h treatment with 100 μM rotenone (R100) compared to R100 treatment alone. MEM represents the control condition where cells were only treated with media, no pre-treatment nor R100 treatment (mean ± S.D., n=6). B. Corresponding TBARS assay results for P68+DQA nanoformulated preparations of 10 μM or 20 μM HT (H10, H20) or combined HT and DFO (H10+D50, H20+D100). * represents significance values of control or pre-treatment conditions compared to R100 treatment alone (**** p < 0.0001, *** p < 0.001). # represents significance values of nanoformulated drug compared to free drug within the same treatment condition (### p < 0.001, # p < 0.05).

When assessing the ability of free drugs and P68+DQA nanocarriers to protect against rotenone induce lipid peroxidation, significant differences in mean TBARS concentrations were observed between the different NAC and NAC + DFO treatments ($F_{(9, 25.92)}$ = 253.5, p < 0.0001) as well as with the HT and HT + DFO treatments ($F_{(9, 12.82)}$ = 209, p < 0.0001) (figure 13).

Significant protection against rotenone-induced lipid peroxidation was observed with 3 h pre-treatment of both free and P68+DQA nanoformulated preparations of NAC and NAC + DFO at all concentrations (p < 0.0001), in each case resulting in between 59% - 68% (free drug preparations) and 69% - 77% (P68+DQA nanoformulations) lower TBARS concentrations than at control (p < 0.0001 in all cases except 1000 μM free NAC where p = 0.0221) (figure 13a). There was no significant difference in the ability of P68+DQA nanocarriers and the corresponding free drug pre-treatments to protect against rotenone-induced lipid peroxidation, however the mean concentration of TBARS following nanocarrier pre-treatment was generally lower (figure 13a). 3 h pre-treatment with all free and P68+DQA formulated HT and HT + DFO concentrations were also able to significantly protect against rotenone induced lipid peroxidation, maintaining control levels (p < 0.0001 in all cases except 20 μM HT + 100 μM DFO where p = 0.0007) (figure 13b). In general, 3 h pre-treatment the free drug preparations of HT and HT + DFO resulted in significantly lower lipid peroxidation compared to the P68+DQA nanoformulations (10 μM HT – 40.18%, p = 0.0004, 20 μM HT - 49.73%, p = 0.0319, 10 μM HT + 50 μM DFO – 57.58%, p = 0.021) (figure 13b).

When evaluating the ability of free and P68+DQA formulated NAC, NAC + DFO, HT and HT + DFO to protect against increased mitochondrial hydroxyl induced by rotenone, significant differences were observed between the different free and formulated treatments for both NAC and NAC + DFO treatments ($F_{(12, 31.78)}$ = 61, p < 0.0001) and HT and HT + DFO treatments ($F_{(12, 39.10)}$ = 32.63, p < 0.0001) (figure 14). Figure 14 shows that 24 h treatment with 100 μM rotenone induced a 12% increase in hydroxyl compared with the control (cells treated with MEM only).
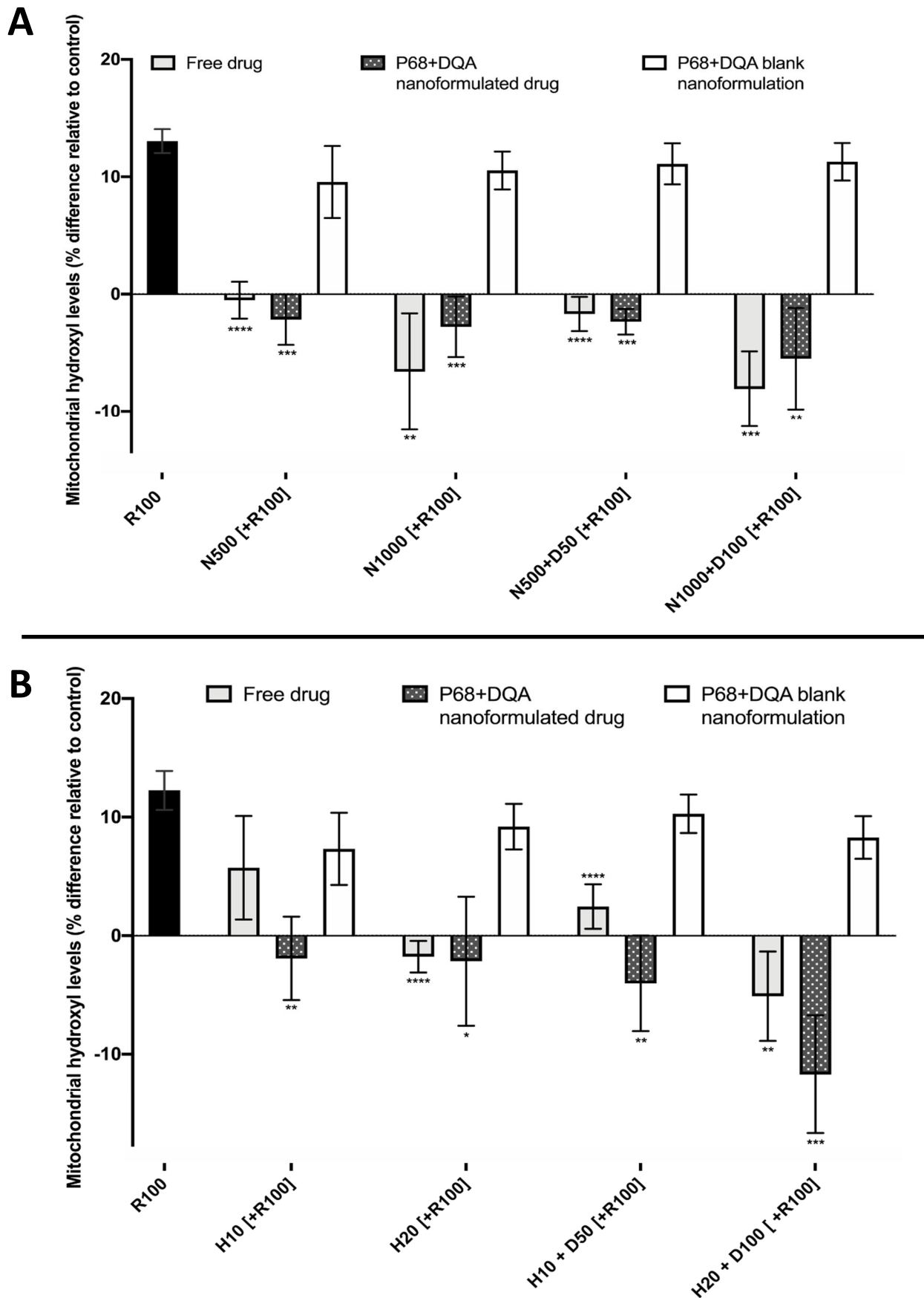
Figure 14 A. Mitochondrial hydroxyl assay results of 3 h pre-treatment with free, P68+DQA or corresponding blank formulations of NAC (500 μM or 1000 μM) or combined NAC (500 μM or 1000 μM) + DFO (50 μM or 100 μM) followed by 24 h treatment with 100 μM rotenone (mean ± S.D., n=6). B. Corresponding mitochondrial hydroxyl assay results for 3 h pre-treatment with free, P68+DQA or corresponding blank formulations of HT (10 μM or 20 μM) or combined HT (10 μM or 20 μM) + DFO (50 μM or 100 μM). Mitochondrial hydroxyl levels are expressed as the percentage of hydroxyl identified in control cells (SH-SY5Y cells treated with MEM media only, for 24 h). * represents significance values of each pre-treatment condition compared to rotenone treatment alone (**** $p < 0.0001$, *** $p < 0.001$, ** $p < 0.01$, * $p < 0.05$).

3 h pre-treatment with all concentrations of free and P68+DQA nanoformuated NAC and NAC + DFO, but none of the corresponding blank formulations, were able to significantly protect against the rotenone induced rise in hydroxyl, maintaining levels equivalent or within 10% lower than at control (500 μM NAC - free ($p < 0.0001$) and P68+DQA ($p = 0.0001$), 1000 μM NAC – free ($p = 0.0053$) and P68+DQA ($p = 0.0002$), 500 μM NAC + 50 μM DFO – free ($p < 0.0001$) and P68+DQA ($p < 0.0001$), 1000 μM NAC + 100 μM DFO, free ($p = 0.0001$) and P68+DQA ($p = 0.0037$)) (figure 14a). No significant differences in hydroxyl levels were observed between the free and P68+DQA NAC and NAC + DFO conditions (figure 14a).

Similarly, protection against rotenone induced mitochondrial hydroxyl was observed following 3 h pre-treatment with nearly all concentrations of free HT and HT + DFO (20 μM HT ($p < 0.0001$), 10 μM HT + 50 μM DFO ($p < 0.0001$) and 20 μM HT + 100 μM DFO ($p = 0.0012$)), and with all concentrations of P68+DQA nanoformuated HT and HT + DFO (10μM HT ($p = 0.0027$), 20μM HT($p = 0.0333$), 10μM HT + 50μM DFO ($p = 0.0025$) and 20μM HT + 100μM DFO ($p = 0.0009$)) (figure 14b). All pre-treatments of free and P68+DQA HT and HT + DFO maintained hydroxyl to levels similar to control, however on average pre-treatment with P68+DQA nanocarriers at 20 μM HT + 100 μM DFO resulted in hydroxyl levels more than 10% lower than the control (figure 14b). No significant differences in hydroxyl levels were observed between the free and P68+DQA HT and HT + DFO conditions and none of the corresponding blank formulations were able to protect against the increase in hydroxyl induced by rotenone (figure 14b).

5.3. Discussion

There is increasing evidence suggesting that NAC and HT are protective in numerous models of PD, as with curcumin and DFO (Soto-Otero et al., 2000; D'Angelo et al., 2001; Park et al., 2004; Hashimoto et al., 2004; Sharma et al., 2007; Schaffer et al., 2007; Chen et al., 2007; Wu et al., 2009; Schapira, 2010; Clark et al., 2010; Rahimmi et al., 2015; Goldstein et al., 2016; Yu et al., 2016; Goldstein et al., 2017; Sarbishegi et al 2018). NAC has also shown promise a potential therapeutic candidate in early clinical trials of PD (Katz et al., 2015; Monti et al., 2019). Yet, as with curcumin and DFO, the full therapeutic potentials of NAC and HT, as disease modifying treatments for PD, are unlikely to be reached due to issues such as low bioavailability and stability, lack of targeted delivery, and limited brain delivery

(Cotgreave & Moldeus, 1987; Yang et al., 2007; Bavarsad Shahripour et al., 2014; Martin-Bastida et al., 2017; Robles-Almazan et al., 2018). Chapters 3 and 4 demonstrated how nanotechnology and formulation science can be utilised to provide a possible solution to these issues by producing nanocarriers that can retain the potency of the entrapped molecule while enhancing targeted delivery and passage across biological membranes. The aim of this study was firstly to assess the ability of the P68+DQA micellar nanocarriers (developed and tested in chapters 3 and 4) to incorporate the antioxidants NAC and HT, alone or in combination with the iron chelator DFO, and secondly, to assess whether these nanoformulations could protect against reduced cell viability, increased free iron and increased oxidative stress induced by a cellular rotenone model of PD. The P68+DQA nanocarriers were chosen specifically based on the evidence that the P68+DQA curcumin and DFO loaded nanocarriers had the most desired characteristics for BBB penetration as well as the highest cellular antioxidant activity compared to the other curcumin and DFO nanocarriers tested in chapters 3 and 4.

NAC and HT, alone or each combined with DFO, were successfully incorporated into P68+DQA nanocarriers with high loading efficiency (table 1). This is consistent with the curcumin and DFO results presented in chapter 3 and supports previous findings that micelles have high encapsulation efficiencies (Zhang et al., 2012, Elezaby et al., 2017; Rakotoarisoa, Angelova, 2018; Mursaleen et al., 2020a). Both NAC and HT P68+DQA nanoformulations exhibited higher encapsulation efficiency than the equivalent curcumin loaded nanoformulations from chapter 3 and reported by Mursaleen et al (2020a), and unlike with curcumin, the addition of DFO to the NAC and HT formulations further increased loading efficiency.

Similar to the curcumin loaded P68+DQA nanocarriers, all P68+DQA nanocarriers containing NAC or HT exhibited consistent particle sizes (polydispersity indices < 0.24) that should be of dimensions sufficient to cross the BBB based on previous reports (Cruz et al., 2016; Grabrucker et al., 2016; Zhou et al., 2018). The mean size of the P68+DQA nanocarriers containing NAC or HT, were however smaller than the nanocarriers containing curcumin, below 170 nm (table 1) compared to 200 nm reported in chapter 3 and by Mursaleen et al (2020a), suggesting they may have increased ability to access the brain. The addition of DFO to the P68+DQA nanocarriers did not significantly increase the size of either NAC or HT

formulations and overall P68+DQA nanocarriers containing NAC yielded the smallest mean particle size, 130 nm or below (table 1). As it is widely accepted that smaller particle size may be advantageous for brain delivery (Cruz et al., 2016; Grabrucker et al., 2016; Zhou et al., 2018), the NAC loaded P68+DQA nanocarriers may be most suited as a treatment where brain penetration is essential, such as with PD.

The mean surface charges of the NAC, NAC + DFO, HT and HT + DFO P68+DQA nanoformulations were similarly neutral like the corresponding curcumin nanocarriers (chapter 3, Mursaleen et al., 2020a), all falling between a mean of +3.67 mV and 9.87 mV (table 1). These relatively neutral surface charges suggest that all NAC and HT P68+DQA nanocarriers, with and without the combination of DFO, should be able to access the brain without causing toxicity to the BBB (Lockman et al., 2004, Choi et al., 2010; Huang et al., 2011; Wiley et al., 2013; Bramini et al., 2014; Zhou et al., 2018). NAC loaded P68+DQA nanocarriers had the lowest surface charge, providing further support that the NAC nanocarriers may be most suited to brain delivery.

Like with curcumin and DFO (chapter 3), XRD studies revealed that the crystalline nature of NAC and HT and their combination with DFO was suppressed by formulation into P68+DQA nanocarriers (figure 1). This more amorphous transformation is of added benefit to these formulations due to the known association with increased solubility and stability (Shi et al., 2018). This suggests that the P68+DQA nanoformulations would be suitable for oral or nasal delivery as they should remain stable once ingested or inhaled and would be more easily absorbed into the blood for systemic or neuronal circulation than free NAC, HT, curcumin or DFO, due to the increased solubility (Savjani et al., 2012). The decrease in intensity of the NAC, HT and DFO peaks, with minimal shifting, in the FTIR spectra for the relevant lyophilized formulations compared to the physical mixtures (figure 2) indicates the incorporation of each of these drugs into the associate NAC, NAC+DFO, HT and HT+DFO P68+DQA nanoformulations, without any conjugation interactions between the chemical groups (Bourassa et al., 2010; Zupančič et al., 2014).

The concentration ranges selected for NAC (500 – 10,000 μM) and HT (10 – 200 μM) and tested in the MTT and FRAP assays were based on and consistent with previous literature (Yamamuro et al., 2006; Yu et al., 2016; Do Van et al., 2016; Goldstein et al., 2017; de las

Hazas et al., 2018; Funakohi-Tago et al., 2018; Ganguly et al., 2019; Martínez et al., 2020). The FRAP results show a correlation between increased concentration and increased antioxidant capacity for both NAC and HT (figure 3). Generally, the P68+DQA HT nanoformulations exhibited significantly higher antioxidant capacity than the corresponding free HT concentrations (figure 3b). This is likely due to the improved stability of HT when loaded into the P68+DQA nanocarriers as low stability is a possible disadvantage for polyphenols such as HT due to the extraction process (Robles-Almazan et al., 2018) whereas NAC is reported to be quite stable but have low bioavailability (Bavarsad Shahripour et al., 2014). Ultimately the 500 μM and 1000 μM concentrations of NAC and the 10 μM and 20 μM concentrations of HT were selected for further evaluation as these were the highest concentrations of both the free drug and P68+DQA nanoformulations that resulted in no observable cytotoxicity in SH-SY5Y cells after treatment for up to 72 h (figure 4 and 5).

All NAC, NAC + DFO, HT and HT + DFO P68+DQA nanocarriers were able to significantly protect to at least the same extent as the corresponding free drug conditions against the 50% reduction in cell viability induced by rotenone (figure 6), suggesting that all treatments could be protective against cell death exhibited in PD. Both concentrations of P68+DQA NAC were significantly more protective (35% and 49%, respectively) than the corresponding free NAC (figure 6a), suggesting that the NAC nanoformulations may be superior to free NAC as a potential protective treatment for PD. Unlike the results seen in chapter 3 where the addition of DFO increased the protective effects exhibited by curcumin formulations, the addition of DFO did not result in further protection of NAC or HT (figure 6). However, the lack of difference observed in both cases could be due to 95-100% cell viability (the same cell viability exhibited by cells treated with MEM media only) being reached in all cases. The western blot analysis further supports that all pre-treatments could protect against PD associated dopaminergic neuronal death as pre-treatment with each concentration of free and P68+DQA NAC, NAC + DFO, HT and HT + DFO resulted in significantly higher levels of the dopaminergic (tyrosine hydroxylase) and neuronal (NeuN) markers compared to with rotenone treatment alone (figure 7, 8).

Iron status (total iron and ferritin bound iron) was evaluated as elevated free iron is thought to be key in the development and progression of PD, mainly due to its ability to drive oxidative stress (Kroemer & Reed, 2000; Schapira, 2007; Simpkins & Dykens, 2008; Kandola

et al., 2015; Do Van et al., 2016; Barodia et al 2017; Jiang et al., 2017). In line with the results described in chapter 4, rotenone treatment resulted in an 838% rise of non-ferritin bound iron compared to control (figure 9a, 10a). There was no significant difference in ferritin levels observed between rotenone treatment and control (figure 9b, 10b). This supports previous reports that rotenone increases levels of free iron by inhibiting mitochondrial complex 1 which indirectly increases the binding activity of iron regulatory protein mRNA (Mena et al., 2011), and generates excessive levels of ROS which promotes the release of iron from iron-sulphur cluster proteins within the mitochondrial respiratory chain (Zucca et al., 2017). As ferritin is the most common source of stored iron intracellularly (Ropele et al., 2017), total non-ferritin bound iron therefore acts as an indicator of free iron. Unlike the curcumin results, where only the formulated treatments were effective, all free and P68+DQA NAC, NAC + DFO, HT and HT + DFO conditions protected against the rise in total non-ferritin bound iron induced by rotenone, maintaining control levels (figure 9a, 10a). Although not significant in most cases, the P68+DQA nanoformulations generally resulted in lower levels of total non-ferritin bound iron compared to the corresponding free drug conditions (figure 9a, 10a). Together, this indicates that the NAC and HT P68+DQA nanoformulations may protect against the increased levels of free iron evident in PD and therefore protect against iron-induced oxidative stress. These results also suggest that the antioxidants NAC and HT possess some inherent iron chelator capacity; this is consistent with previous studies which suggest that NAC can chelate free iron and inhibit the iron-mediated cell death pathway, ferroptosis (Wongjaikam et al., 2017; Do Van et al., 2016; Hjortsrø et al., 1990), and that HT can also chelate from the intracellular labile iron pool (Kitsati et al., 2016; Melidou et al., 2005). Although rotenone treatment did not significantly change control levels of ferritin, the addition of DFO to free and P68+DQA NAC and HT nanoformulations resulted in a significant decrease in ferritin compared to rotenone (53 – 86%) and compared to control (33 – 80%) (figure 9b, 10b). This was not unexpected as DFO has been shown to be able to chelate iron from ferritin (Hassan and Tolba, 2016). Both NAC treatments and 20 μM HT also resulted in significantly lower ferritin levels compared to rotenone but not compared to control (figure 9b, 10b).

The cellular antioxidant activity results support the idea that NAC and HT, alone and combined with DFO, can protect against PD related oxidative stress represented by rotenone (figure 11a, 12a) and iron-induced oxidative stress specifically (figure 11b, 12b), as indicated by the iron status results above. The cellular antioxidant activity against rotenone and free iron, of the P68+DQA preparations of NAC and NAC + DFO, was similar to that of the corresponding free drug in each case (figure 11a, 11b). These results are consistent with those seen when using the traditional CAA method, where ABAP was used as the prooxidant, although the P68+DQA preparations of NAC and NAC + DFO have consistently higher percentage differences compared to the free preparations when using ABAP as the prooxidant (figure 11c). This could be because ABAP may be a less potent prooxidant than rotenone and free iron, since much lower concentrations of iron (200 µM) and rotenone (100 µM) were used to try to achieve a similar level of oxidation compared to ABAP (600 µM). The highest antioxidant activity for both free and P68+DQA NAC and NAC + DFO was observed against rotenone, at 1000 µM NAC in both cases, yielding 167% and 85% higher activity than the treatments with the highest CAA units against iron (1000 µM NAC + 100 µM DFO in both cases), and 154% and 49% higher antioxidant activity than the treatments with the highest activity against ABAP (1000 µM NAC + 100 µM DFO for the free drug preparation and 1000 µM NAC for the P68+DQA nanoformulation), respectively (figure 11). This again supports the notion that NAC may be particularly suited as an antioxidant treatment for PD specifically, since rotenone has been associated with increased incidences of PD in people (Tanner et al., 2011), and is the most common neurotoxin model of PD (Xicoy et al., 2017). Unlike the results reported with curcumin in chapter 4, the addition of DFO to the NAC P68+DQA nanoformulations did not significantly increase cellular antioxidant capacity against rotenone or ABAP (figure 11a, 11c). The addition of DFO did however increase antioxidant activity against free iron where it would be expected that DFO would provide the most benefit being an iron chelator specifically (figure 11b). The ability of NAC to generally match the antioxidant ability of NAC + DFO at both concentrations may be because NAC not only acts as an antioxidant *via* the glutathione mechanism, converting hydrogen peroxide into water, but it can also chelate iron to some extent directly reducing the formation of hydroxyl *via* the Fenton reaction (Hjortsrø et al., 1990; Do Van et al., 2016; Wongjaikam et al., 2017).

Likewise, there was no difference in cellular antioxidant activity against rotenone when comparing P68+DQA and free HT and HT + DFO in most cases (figure 12a). Unlike with NAC and NAC + DFO, the P68+DQA conditions of HT and HT + DFO resulted in higher antioxidant activity against free iron, but not ABAP, compared to the corresponding free drug conditions (figure 12b, 12c). Again, unlike the curcumin results from chapter 4, the addition of DFO to the HT P68+DQA nanoformulations did not increase cellular antioxidant activity in any case, not even when using free iron as the prooxidant (figure 12a, 12b, 12c). This provides further support to the iron status results that, like NAC, HT may also exhibit some iron chelator capacity. Like NAC and NAC + DFO, the overall cellular antioxidant activity of both free and P68+DQA formulated HT and HT + DFO treatments were highest against rotenone, 200% and 78% higher than the highest treatments with iron, and 84% and 89% higher than those with ABAP as the prooxidant, respectively (figure 12). This suggests that they may also be suitable as treatments for PD specifically. Overall, all treatments containing NAC were superior to the treatments containing HT in terms of cellular antioxidant activity against all prooxidants (figure 11, 12), reaching a peak CAA unit of 99 with 1000 µM P68+DQA NAC compared to a peak CAA unit of 68 with 20 µM P68+DQA HT against rotenone (figure 11a, 12a).

Similarly, both free and P68+DQA nanoformulations of NAC and NAC + DFO were superior to those of HT and HT + DFO at lowering lipid peroxidation, measured by TBARS concentration (figure 13). Although all free and P68+DQA nanoformulated HT and HT + DFO pre-treatments maintained control levels, protecting against the 226% increase in lipid peroxidation induced by rotenone (figure 13b), all the pre-treatments containing NAC resulted in lower lipid peroxidation than observed in the control cells (figure 13a). Although not significantly, the P68+DQA NAC and NAC + DFO nanoformulations generally resulted in lower lipid peroxidation (between 6 and 32%) than the corresponding free drug conditions (figure 13a). Whereas in most cases free HT and HT + DFO resulted in lower lipid peroxidation compared to P68+DQA HT and HT + DFO, although the formulated conditions were able to maintain lipid peroxidation at control levels (figure 13b). The mitochondrial hydroxyl assay results support the ability of these P68+DQA nanocarriers to protect against oxidative stress as both free and P68+DQA nanoformulated NAC, NAC + DFO, HT and HT + DFO were able to significantly protect against the 12% rise in mitochondrial hydroxyl

following rotenone treatment (figure 14). This further indicates that NAC and HT are also effective against iron-induced oxidative stress specifically as mitochondrial hydroxyl is the primary oxidant produced by the Fenton reaction in the presence of excess free iron (Costa-Mallen et al., 2017; Zucca et al., 2017; Thomas et al., 2009). The P68+DQA 20 μM HT + 100 μM DFO nanoformulation was the most protective treatment, not only protecting against the rise in hydroxyl induced by rotenone but also further reducing hydroxyl levels to 15% lower than at control (figure 14b). All free and P68+DQA NAC and NAC + DFO conditions were also able to further reduce mitochondrial hydroxyl beyond control levels but to a slightly lesser and not significant extent, between 2 and 8% compared to the 3 – 15% reduction exhibited by the free and P68+DQA HT and HT + DFO conditions (figure 14). Again, no difference was observed between the NAC and NAC + DFO conditions at the same NAC concentrations supporting the idea that NAC does not benefit from the addition of an iron chelator.

Taken together, these results suggest that P68+DQA NAC, NAC + DFO, HT and HT + DFO nanocarriers have the relevant characteristics to access the brain without producing cytotoxicity but that the NAC and NAC + DFO loaded nanocarriers may have the most favourable characteristics for brain penetrance. Similar to the curcumin results, these results suggest that all NAC, NAC + DFO, HT and HT + DFO drug-loaded nanocarriers were at least as capable as the corresponding free drug conditions at protecting against reduced cell viability, reduced levels of dopamine and neuronal markers, increased iron, increased lipid peroxidation and increased mitochondrial hydroxyl levels induced by rotenone. However, in most cases 1000 μM P68+DQA NAC exhibited the strongest ability to protect against rotenone in the majority of parameters, suggesting that NAC might be preferential as a potential disease modifying treatment of PD. This is supported by the results of Goldstein et al (2017) which also suggested that NAC may be more suited as a PD treatment than HT based on data in PC12 cells that, unlike HT, NAC does not feedback and inhibit tyrosine hydroxylase, a key enzyme in the synthesis of dopamine.

As described in chapters 1, 3 and 4, the potential therapeutic value of free antioxidants such as curcumin, NAC, and HT are limited due to issues of stability, solubility, bioavailability, and their limited ability to access the brain (Cotgreave & Moldeus, 1987; Yang et al., 2007; Bavarsad Shahripour et al., 2014; Martin-Bastida et al., 2017; Robles-Almazan et al., 2018).

The results in this chapter further support the concept that the P68+DQA nanocarrier delivery system may provide a viable solution as the particle size and charge data indicated that these formulations would be able to pass the BBB, and the XRD data suggests improved stability and solubility. Unlike the curcumin results in chapter 4, in general the addition of DFO to the NAC and HT P68+DQA formulations did not improve the ability of these treatments to protect against rotenone induced reduction in cell viability and dopamine levels or increased oxidative stress. This could be because NAC and HT have more potent antioxidant scavenging capacity than curcumin and/or because NAC and HT possess some direct iron chelator capacity higher than that of curcumin. Thus, there is little added value in adding DFO to NAC or HT based on the antioxidant parameters assessed in this study, although the addition of DFO may still be beneficial against other iron-related underlying mechanism of PD, for example alpha synuclein accumulation or neuroinflammation.

5.4. Conclusion

In summary, this study demonstrates the successful incorporation of NAC, NAC + DFO, HT and HT + DFO into the novel P68+DQA nanocarriers developed in chapter 3, and, for the first time, successful delivery of these nanocarriers to protect against oxidative stress induced by a rotenone cellular PD model. These results provide further support that this nanocarrier strategy may thus provide an effective approach to fully utilise the therapeutic benefit of antioxidants for PD. In order to provide further supportive evidence that these P68+DQA nanocarriers could be progressed as potential disease modifying treatments of PD, the next steps will be to assess the ability of these P68+DQA nanocarriers compared to the corresponding free drugs to pass across a model of the BBB and target the mitochondria. Such additional data will help to cement the need for the nanoformulation of curcumin, NAC, HT and DFO to fully utilise their potential therapeutic effects.

Chapter 6 - Assessing the ability of the nanoformulations to cross a hCMEC/D3 cellular BBB model, target mitochondria and protect against rotenone-induced oxidative stress

6.1. Introduction

So far, it has been shown that the free and nanoformulated preparations of curcumin, NAC, and HT antioxidants, alone and each in combination with the iron chelator DFO, are protective against rotenone induced oxidative stress and cytotoxicity in SH-SY5Y cells (chapters 4 and 5). However, as the treatments were added directly onto SH-SY5Y cells it is important to establish whether the effects would be replicated *in vivo*, where the ability of drugs to treat neurological conditions are often limited due to the presence of the BBB.

The BBB prevents the passage of 98% of potential neuropharmaceuticals (Dove, 2008) and although curcumin, DFO, NAC, and HT have all been shown to penetrate the brain to some extent, none so far have been shown to do this at sufficiently high levels to have a significant effect on PD progression. As outlined in the previous chapters, nanoformulation is a strategy used to enhance the passage of drugs across biological membranes, including the BBB, by associating the drug of interest with carriers of nano-metre size (Masserini et al., 2013; Zupančič et al., 2014). The results outlined in chapters 3 and 5 suggest that all the P68, P68+DQA, SOL and SOL+DQA nanoformulations tested had a suitable particle size (< 200 nm) to pass the BBB and that the relatively neutral change of the nanoformulations would be particularly suited for brain penetrance. The enhanced ability of the formulations containing DQA to protect against the rise in mitochondrial hydroxyl also suggested that DQA acts as a mitochondrial targetter as expected based on previous reports (Weissig et al., 1998; Lyrawati et al., 2011; Zupančič et al., 2014). However, these results need to be confirmed in a more comprehensive model before the nanoformulations can be evaluated in *in vivo* models.

The human derived brain endothelial cell line, hCMEC/D3, has been used to model the BBB to indicate whether drugs are likely to access the brain *in vivo* in more than 150 publications (Helm et al., 2016). hCMEC/D3 cells benefit from the ability to form a monolayer of

elongated cells on type 1 collagen and express many of the structural and scaffolding proteins associated with the tight junctions present in the BBB, such as VE-cadherin and ß-catenin as well as proteins associated with the apical-basal polarity and junctional tightness of the BBB such as Par-3/Par-6/PKCz and claudin-5, respectively (Weksler et al., 2005; Schrade et al., 2012; Paolinelli et al., 2013; Artus et al., 2014). These cells can be cultured using permeable cell culture plate inserts not only to test the passage of drugs across the membrane but also to enable co-culture to evaluate the effectiveness of treatments. This has been previously described by Pucci et al (2020) where such a system was used to test the ability of their nanovectors to cross a BBB model and target glioblastoma cells. Permeable cell culture plate inserts, such as the Corning Transwell® system, could therefore be utilised to evaluate whether drugs can pass through the hCMEC/D3 cellular barrier and still have a biological effect in the SH-SY5Y rotenone-induced PD model.

This chapter aims to test whether the nanoformulations improve the ability of curcumin, NAC, and HT (alone and each combined with DFO) to access the brain and target mitochondria in a more robust manner by evaluating the effects of each drug in a combined Transwell® hCMEC/D3 BBB and SH-SY5Y cellular model. It will also evaluate whether the protective effects of the free and formulated drugs against rotenone induced cytotoxicity and oxidative stress are retained following passage across the BBB model.

6.2. Results

The mean TEER of hCMEC/D3 cell monolayers grown on Transwell® inserts was shown to peak at 320 $\Omega.cm^2$ on day five post seeding, falling to 304 $\Omega.cm^2$ by day seven (figure 1). On day five post seeding, the permeability of the hCMEC/D3 monolayers were consistently below 1.2×10^{-3} cm/min ($0.91 \pm 0.13 \times 10^{-3}$ cm/min).
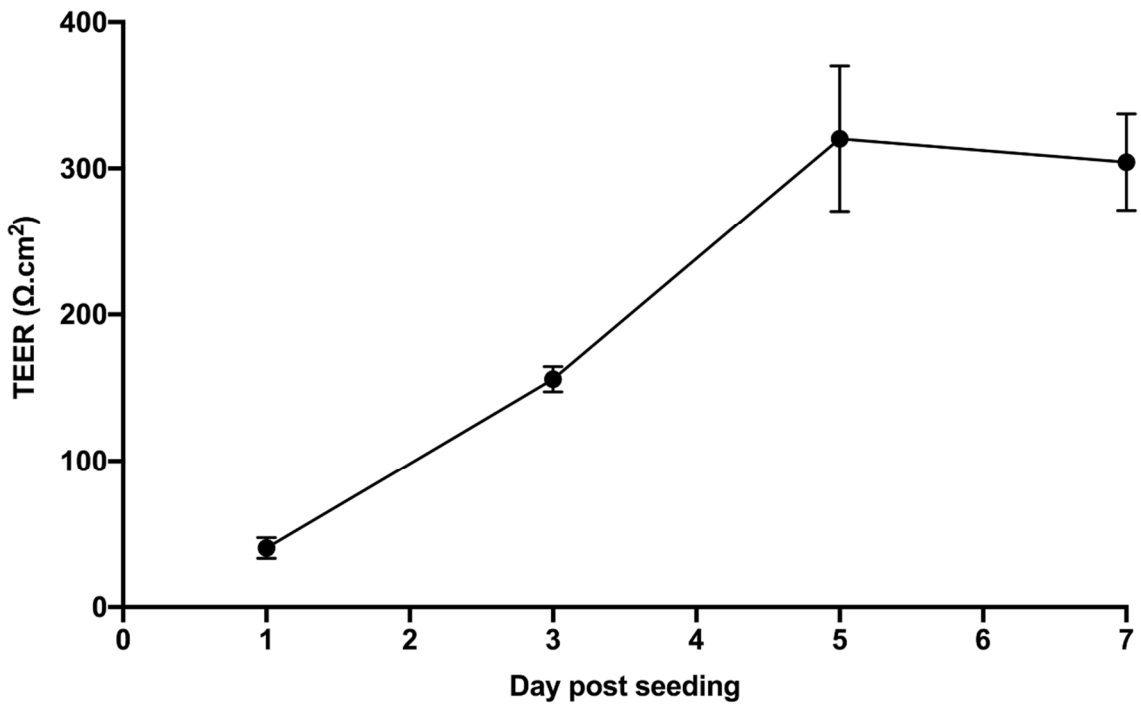
Figure 1. Mean TEER of hCMEC/D3 cell monolayers grown on 3.0 μm Transwell® inserts on days 1, 3, 5 and 7 post cell seeding.
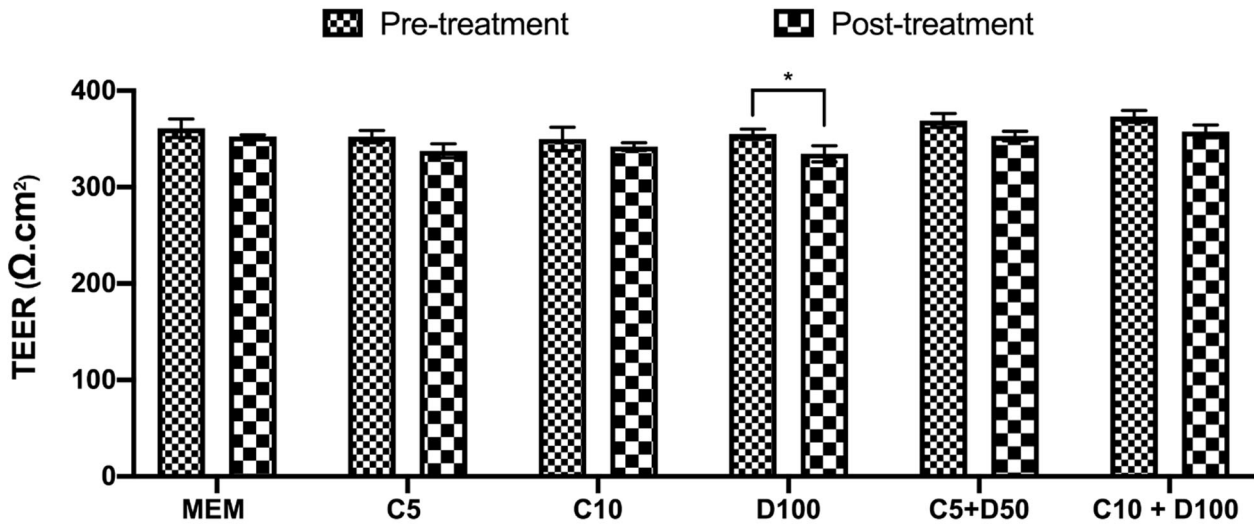
*Figure 2. Mean TEER of hCMEC/D3 cell monolayers on day 5 post seeding before (pre-treatment) and after (post-treatment) treatment with free curcumin, DFO and combined treatments. * represents significance values when comparing the pre- and post-treatment TEER values for a given treatment condition (* p < 0.05).*

A significant reduction in TEER was observed following treatment with 100 µM free DFO (p = 0.0108, figure 2) and 10 µM SOL+DQA formulated curcumin (p = 0.0118, figure 3D). There was no significant change in TEER following treatment with any other free or nanoformulated versions of curcumin or DFO (figure 2, 3). Similarly, no significant difference in TEER was observed following any of the free and nanoformulated NAC and HT treatments (figure 4, 5).
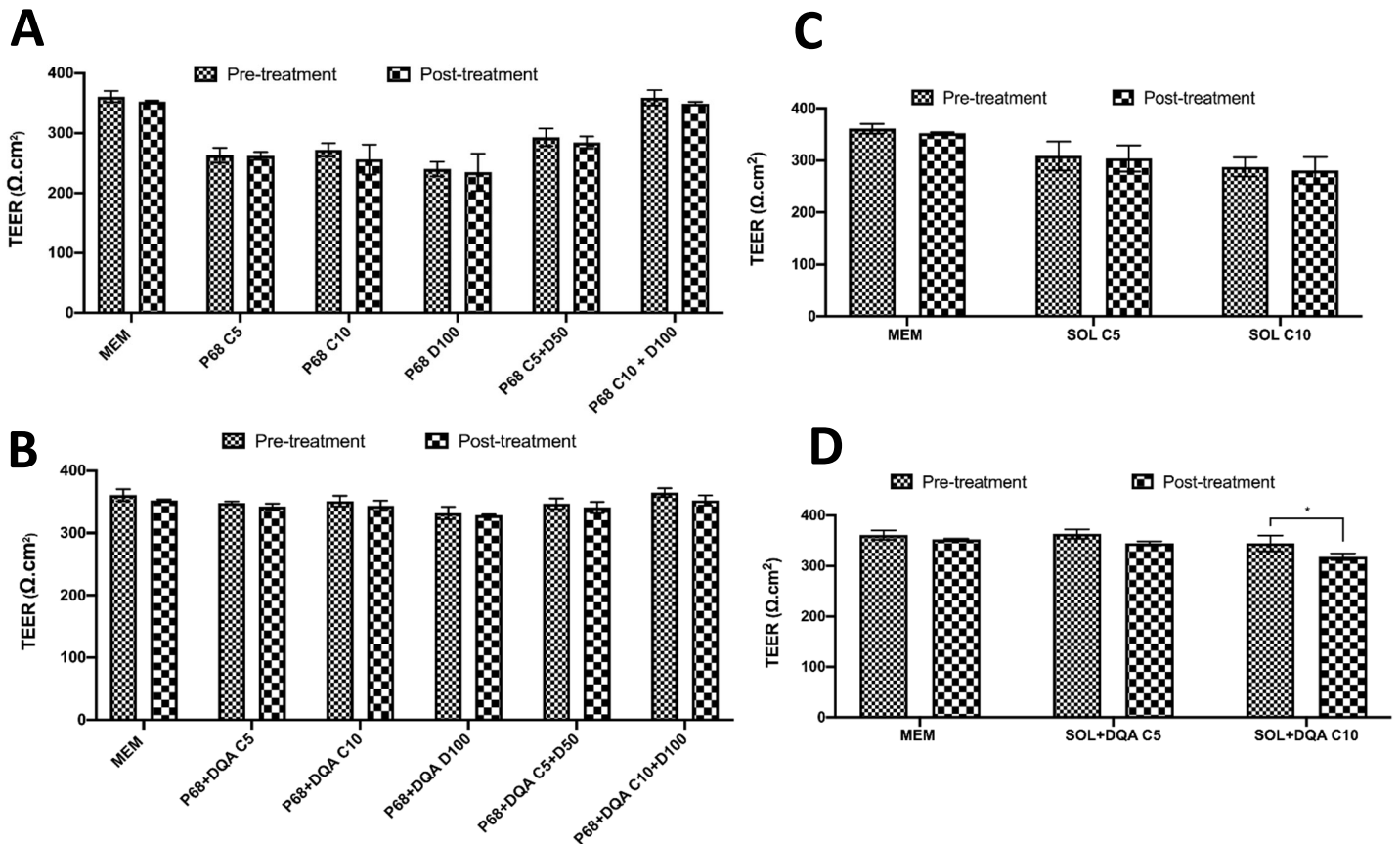
Figure 3. A. Mean TEER of hCMEC/D3 cell monolayers on day 5 post seeding before (pre-treatment) and after (post-treatment) treatment with P68 nanoformulated curcumin, DFO and combined treatments. B. Corresponding TEER results pre- and post-treatment with P68+DQA nanoformulations of curcumin, DFO and combined curcumin and DFO. C. Corresponding TEER results for SOL nanoformulations of curcumin. D. Corresponding TEER results of SOL+DQA curcumin nanoformulations. * represents significance values when comparing the pre- and post-treatment TEER values for a given treatment condition (* $p < 0.05$).
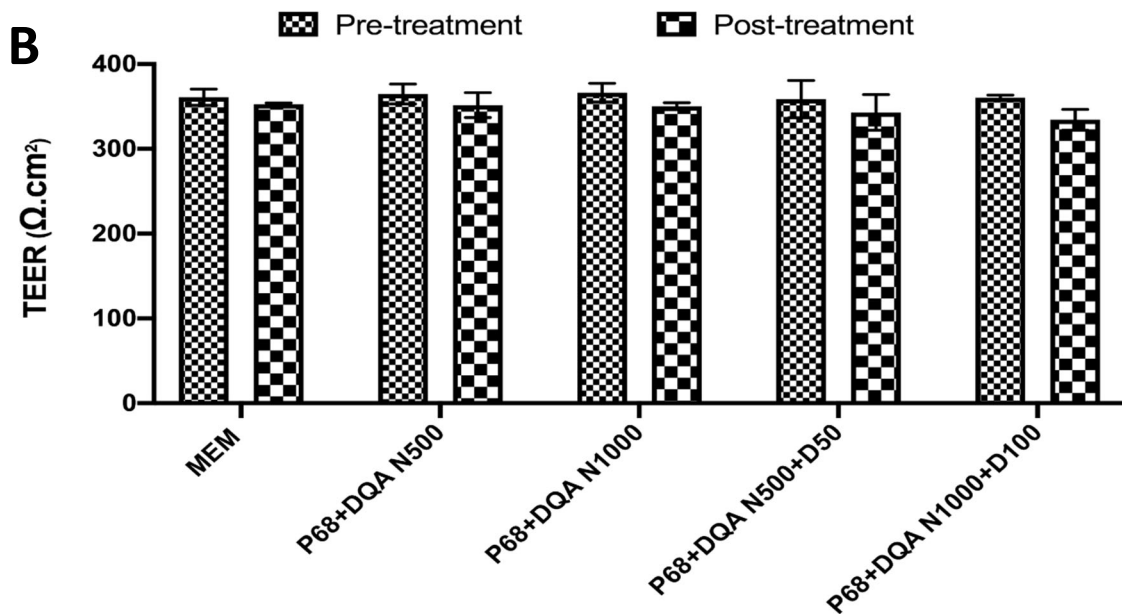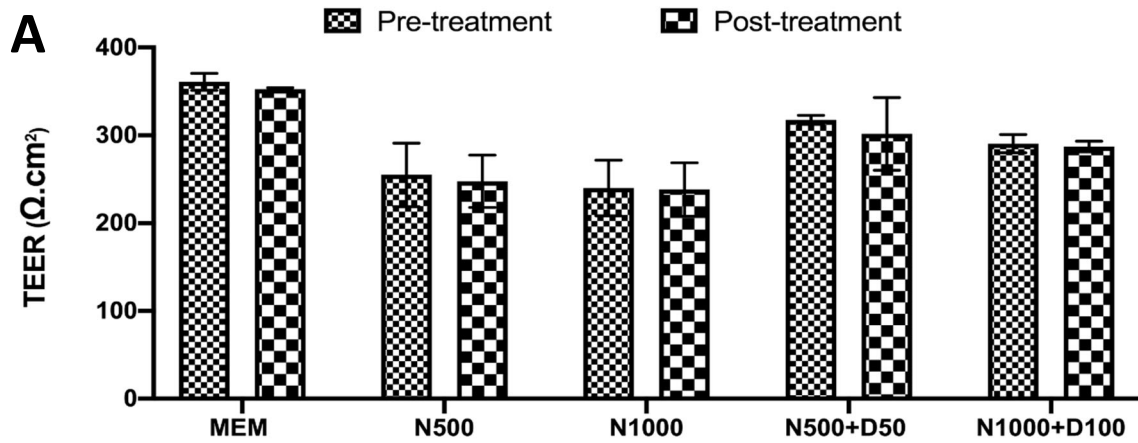
Figure 4. A. Mean TEER of hCMEC/D3 cell monolayers on day 5 post seeding before (pre-treatment) and after (post-treatment) treatment with NAC and combined NAC and DFO free drug treatments. B. Corresponding TEER results for the P68+DQA nanoformulated NAC and NAC+DFO treatments.

When assessing the percentage of curcumin able to pass through the hCMEC/D3 monolayers, significant differences were observed between the different treatment preparations when comparing free, P68 and P68+DQA nanoformulated curcumin ($F_{(2, 52)} = 126.2$, $p < 0.0001$) and when comparing free, SOL and SOL+DQA nanoformulated curcumin ($F_{(2, 30)} = 77.99$, $p < 0.0001$) (figure 6). In most cases, significantly higher percentages of curcumin were reached with the P68 and P68+DQA nanoformulations compared to free curcumin and curcumin + DFO treatments ($p < 0.0001$ in all cases, except with P68+DQA 5 µM curcumin + 50 µM DFO where $p = 0.007$ and P68 5 µM curcumin + 50 µM DFO which was not significant), with the formulations resulting in between 8.6 – 48.8% more curcumin

compared to the free drug treatments (figure 6a). The largest differences between the formulations and free drug treatments were observed at 10 µM curcumin where the P68 and P68+DQA formulations resulted in 46.1% and 48.8% more curcumin (respectively) compared to treatment with free curcumin (figure 6a). However, the highest percentage of curcumin passing the hCMEC/D3 monolayer was achieved using the P68+DQA nanoformulations, reaching more than 80% with the 5 µM curcumin and 10 µM curcumin + 100 µM DFO treatments and this was significantly more than when using the P68 formulations (p = 0.005 and p = 0.0079, respectively) (figure 6a).
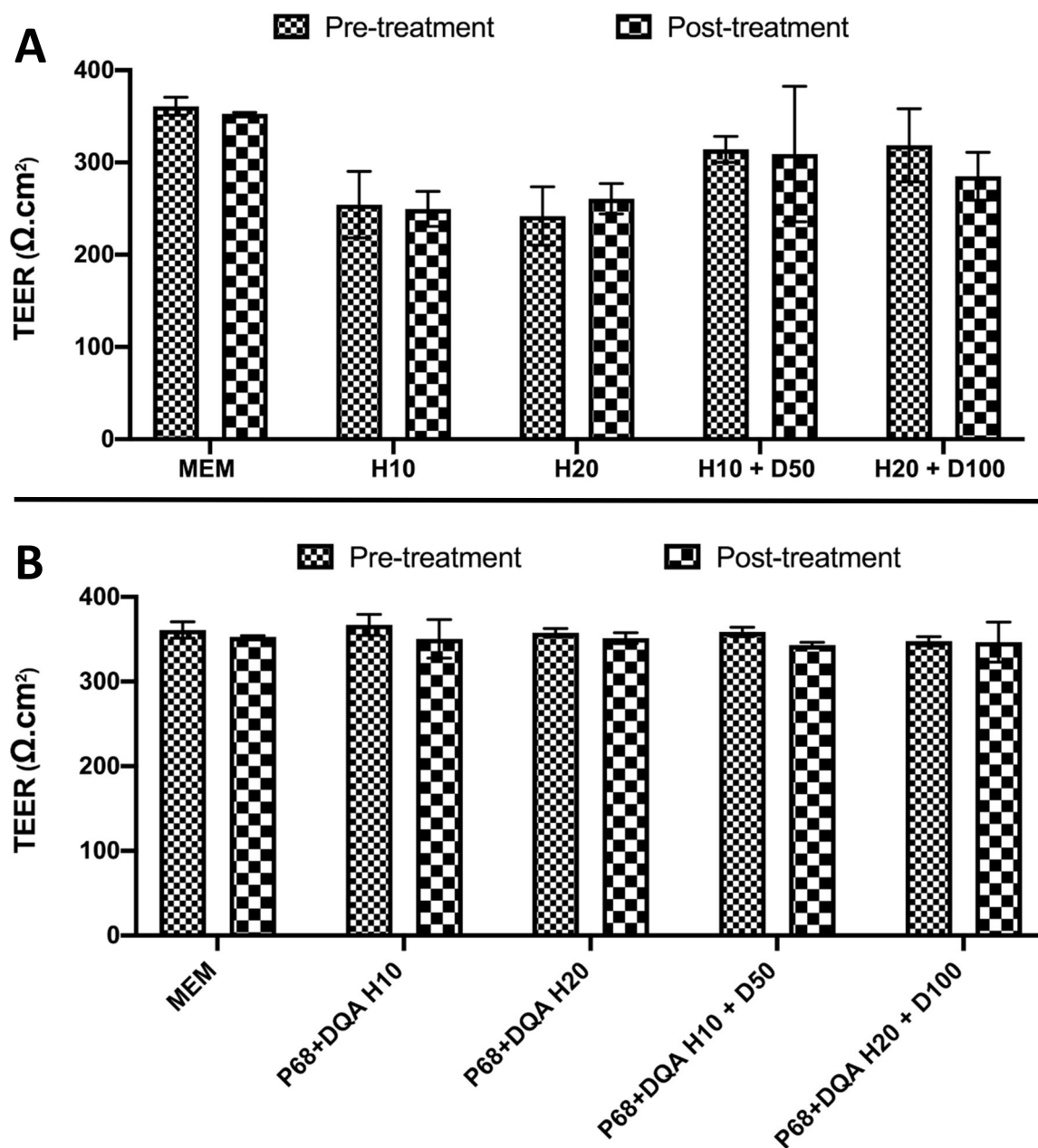
Figure 5. A. Mean TEER of hCMEC/D3 cell monolayers on day 5 post seeding before (pre-treatment) and after (post-treatment) treatment with HT and combined HT and DFO free drug treatments. B. Corresponding TEER results for the P68+DQA nanoformulated HT and HT+DFO treatments.
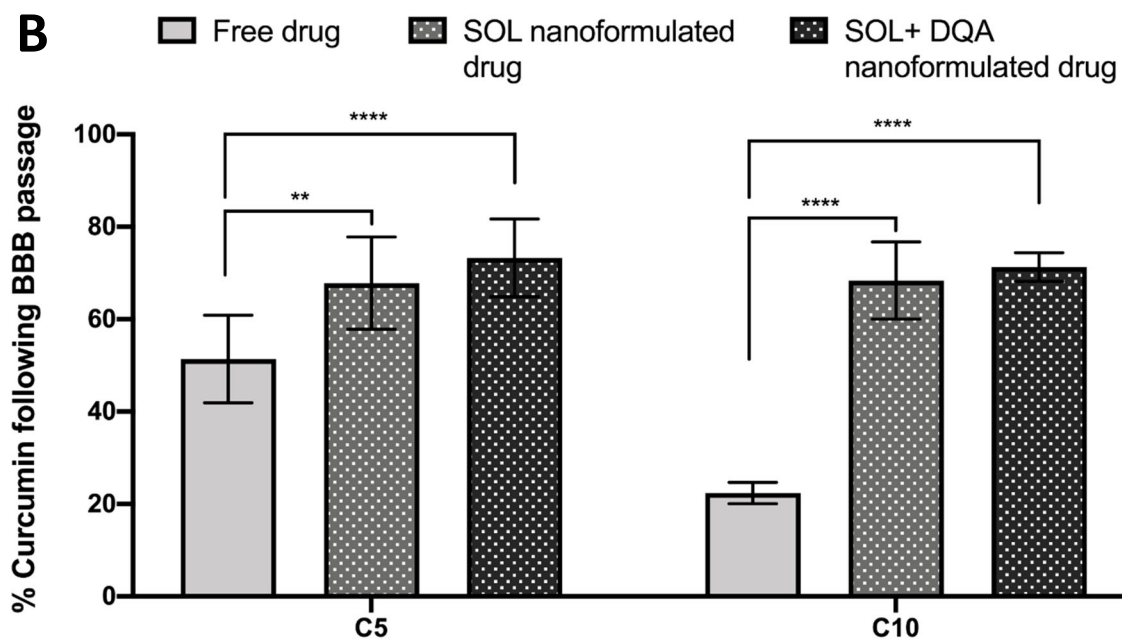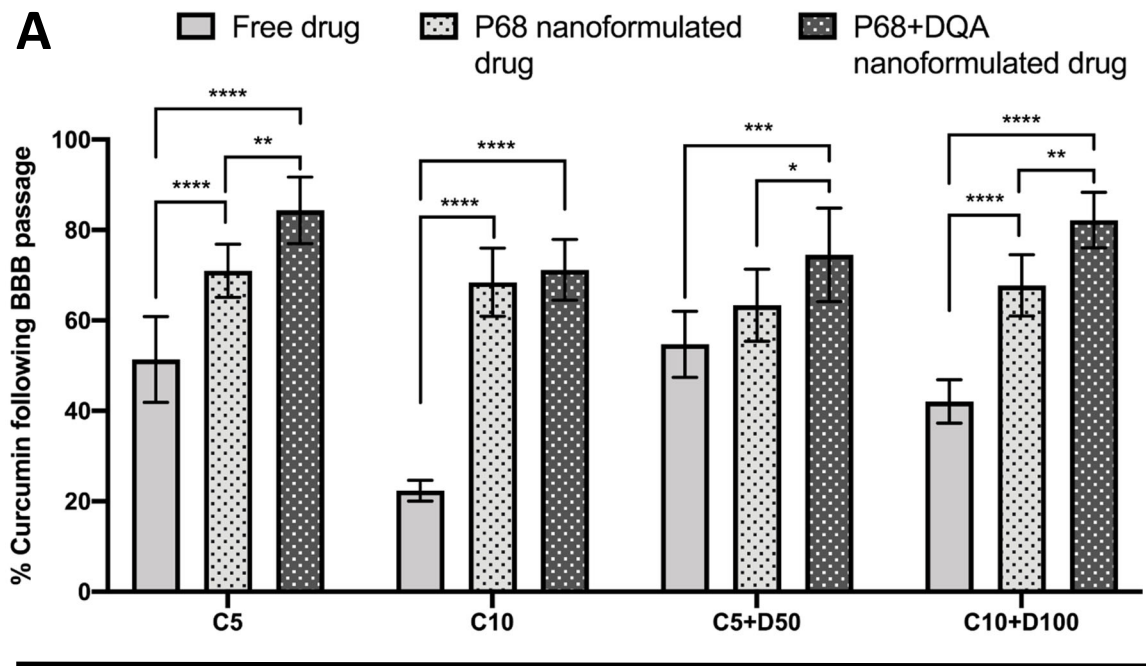
Figure 6. A. Mean percentage of curcumin in the basolateral compartment of the hCMEC/D3 Transwell® system following 60 min treatment with free, P68 or P68+DQA curcumin (5 and 10 µM) and combined curcumin and DFO (5 and 10 µM curcumin + 50 and 100 µM DFO, respectively). B. Mean percentage of curcumin in the basolateral compartment of the hCMEC/D3 Transwell® system following 60 min treatment with free, SOL or SOL+DQA 5 and 10 µM curcumin. Percentage curcumin = ((absorbance of the basolateral compartment sample – control) / (absorbance of the treatment- control)) X 100, where the absorbance was read at 423 nm and the control was MEM. * represents significance values of nanoformulated drug compared to free drug within the same treatment condition (**** p < 0.0001, *** p < 0.001, ** p < 0.01, * p < 0.05).

There was also a significantly higher percentage of curcumin passage across the BBB achieved with the P68+DQA formulation of 5 μM curcumin + 50 μM DFO compared the P68 formulation (p = 0.0482) (figure 6a). Similarly, when comparing the SOL and SOL+DQA formulations to free curcumin, both formulations resulted in higher percentages of curcumin post-BBB passage (p < 0.0001 in all cases, except with SOL 5 μM curcumin where p = 0.0021), with the largest differences also observed at 10 μM curcumin (46.0 and 48.9% for Sol and SOL+DQA, respectively) (figure 6b). However, there were no significant differences between the SOL and SOL+DQA formulations and neither achieved more than 70% curcumin (figure 6b).
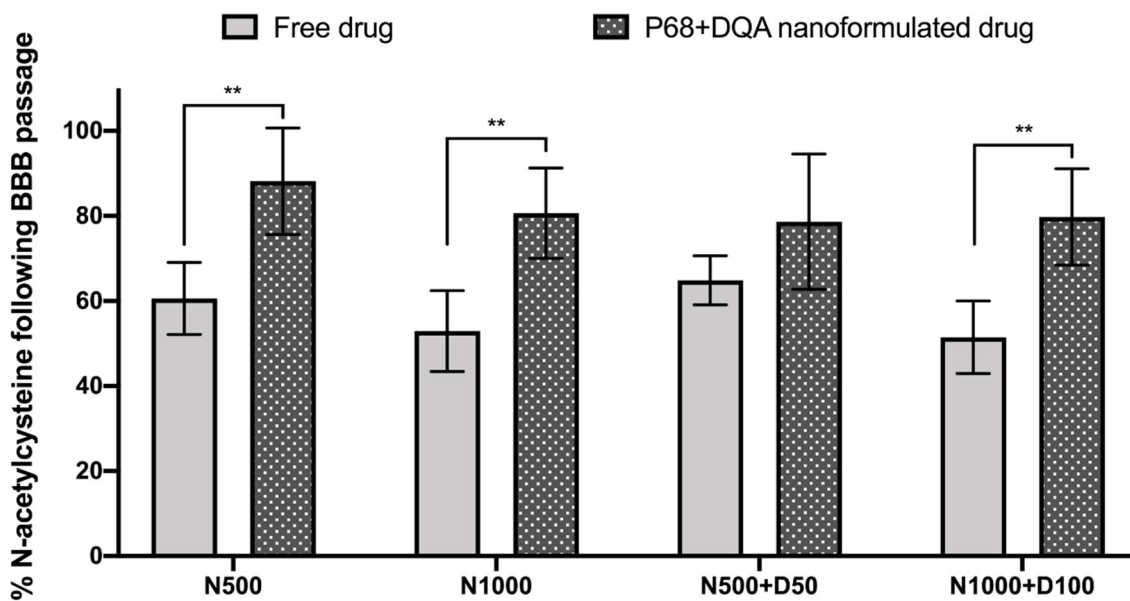
Figure 7. Mean percentage of NAC in the basolateral compartment of the hCMEC/D3 Transwell® system following 60 min treatment with free or P68+DQA NAC (500 and 1000 μM) and combined NAC and DFO (500 and 1000 μM NAC + 50 and 100 μM DFO, respectively). Percentage NAC = ((absorbance of the basolateral compartment sample – control) / (absorbance of the treatment- control)) X 100, where the absorbance was read at 234 nm and the control was MEM. * represents significance values of nanoformulated drug compared to free drug within the same treatment condition (** p < 0.01).

Likewise, when comparing the P68+DQA nanoformulation and free drug treatments of NAC, NAC + DFO and HT and HT + DFO, significant differences in the percentage of both NAC ($F_{(1, 32)}$ = 44.73, p < 0.0001) and HT ($F_{(1, 32)}$ = 406.4, p < 0.0001) were observed following BBB passage (figure 7, 8). The P68+DQA formulations resulted in significantly higher NAC for all conditions except 500 μM NAC + 50 μM DFO, resulting in between 13.8% and 28.3% more NAC compared to the free drug treatments (500 μM NAC – p = 0.0026, 1000 μM NAC – p = 0.0024 and 1000 μM NAC + 100 μM DFO – p = 0.0079) (figure 7). The highest percentage of

NAC following BBB passage (88.2%) was achieved using P68+DQA 500 µM NAC, however all P68+DQA formulations resulted in more than 78% NAC in the basolateral compartment (figure 7). All P68+DQA formulations of HT and HT + DFO also resulted in significantly more HT (between 34.8 – 50.1%) compared to the free drug treatments (p < 0.0001 in all cases), reaching more than 76% HT following passage across the hCMEC/D3 monolayer with the P68+DQA 10 µM HT treatment (figure 8).
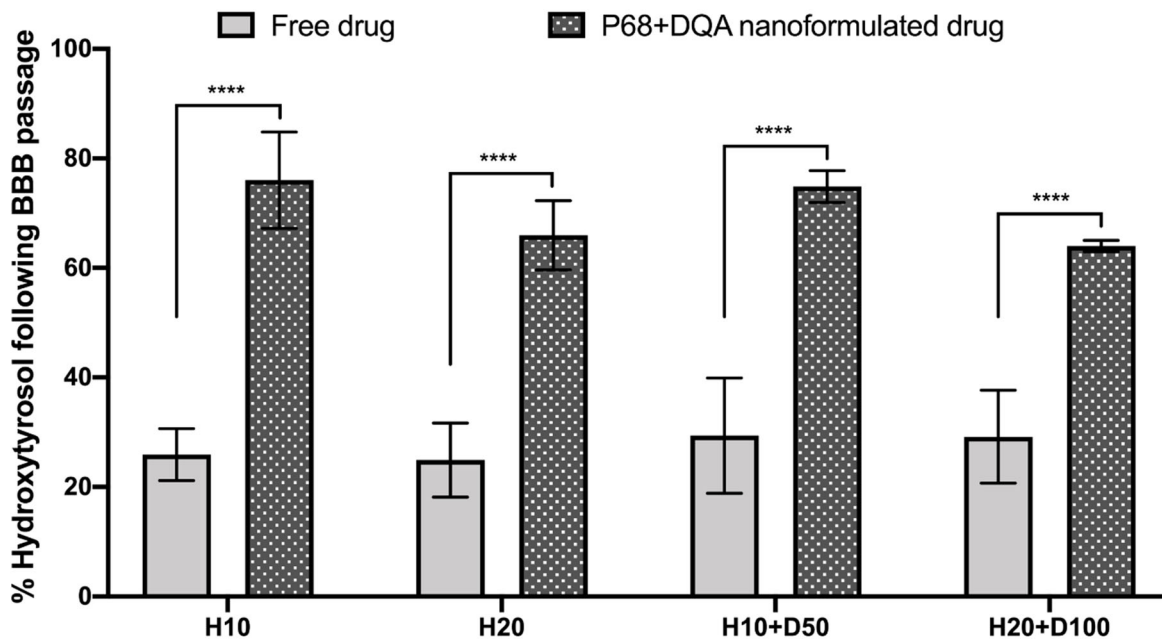
*Figure 8. Mean percentage of HT in the basolateral compartment of the hCMEC/D3 Transwell® system following 60 min treatment with free or P68+DQA HT (10 and 20 µM) and combined HT and DFO (10 and 20 µM HT + 50 and 100 µM DFO, respectively). Percentage HT = ((absorbance of the basolateral compartment sample – control) / (absorbance of the treatment- control)) X 100, where the absorbance was read at 280 nm and the control was MEM. * represents significance values of nanoformulated drug compared to free drug within the same treatment condition (**** p < 0.0001).*

Significant differences in the percentages of DFO passing the BBB monolayer were also observed between the different preparation types, when comparing free, P68 and P68+DQA DFO and curcumin + DFO ($F_{(2, 33)}$ = 126.2, p < 0.0001) and when comparing free and P68+DQA HT + DFO and NAC + DFO conditions ($F_{(1,32)}$ = 234.8, p < 0.0001) (figure 9). In all cases, the P68 and P68+DQA nanoformulated preparations resulted in significantly more DFO (between 29.3 and 53.6%) compared to the free drug treatments (p < 0.0001 in all cases), with the highest increase of DFO observed when using the P68 100 µM DFO treatment (figure 9).
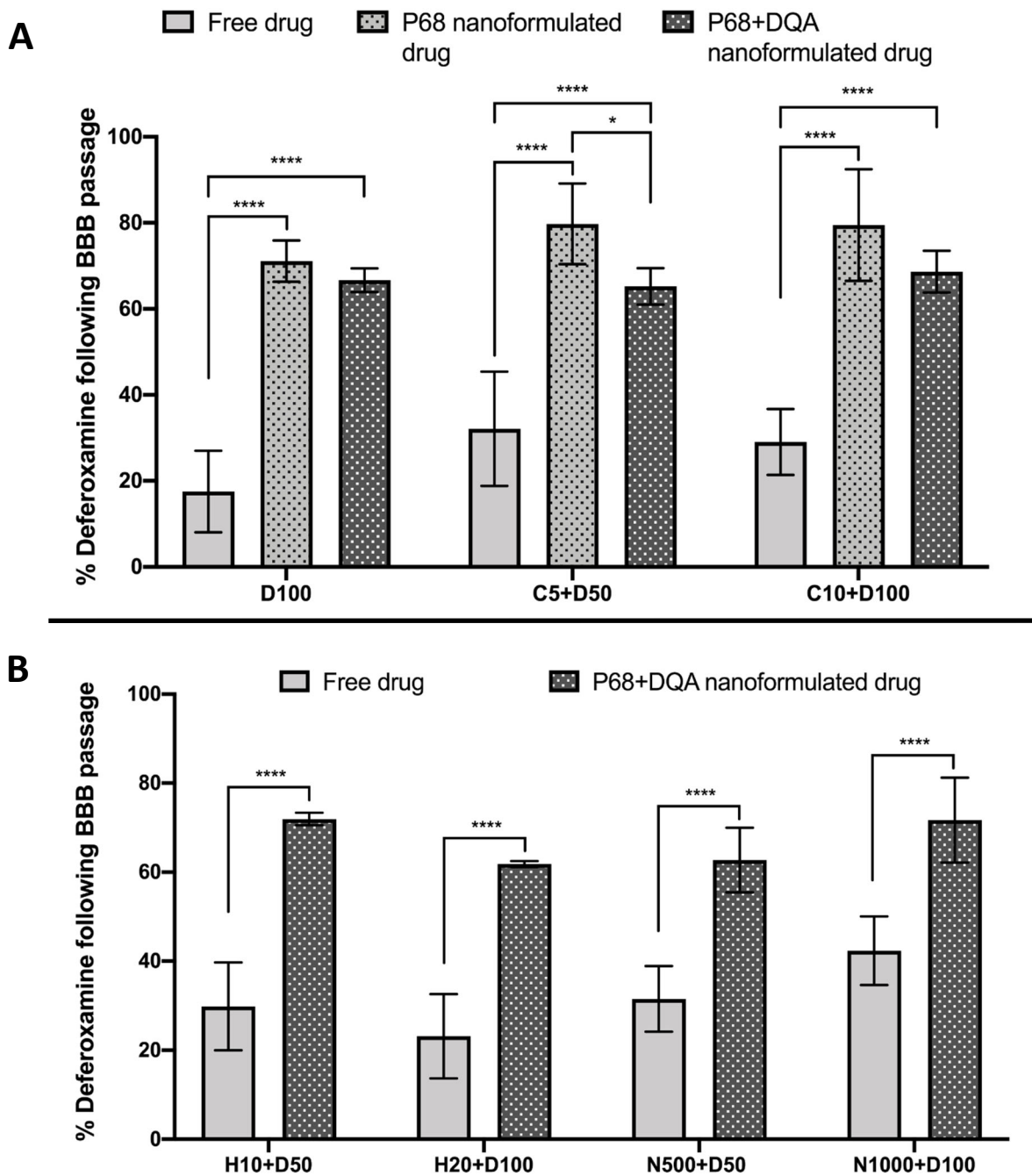
Figure 9. A. Mean percentage of DFO in the basolateral compartment of the hCMEC/D3 Transwell® system following 60 min treatment with free, P68 or P68+DQA DFO (100 µM) and combined curcumin and DFO (5 and 10 µM curcumin + 50 and 100 µM DFO, respectively). B. The corresponding mean percentage of DFO following 60 min treatment with free or P68+DQA combined HT and DFO (10 and 20 µM HT + 50 and 100 µM DFO, respectively) or NAC and DFO (500 and 1000 µM NAC + 50 and 100 µM DFO, respectively). Percentage DFO = ((absorbance of the basolateral compartment sample – control) / (absorbance of the treatment- control)) X 100, where the absorbance was read at 204 nm and the control was MEM. * represents significance values of nanoformulated drug compared to free drug within the same treatment condition (**** p < 0.0001, * p < 0.05).
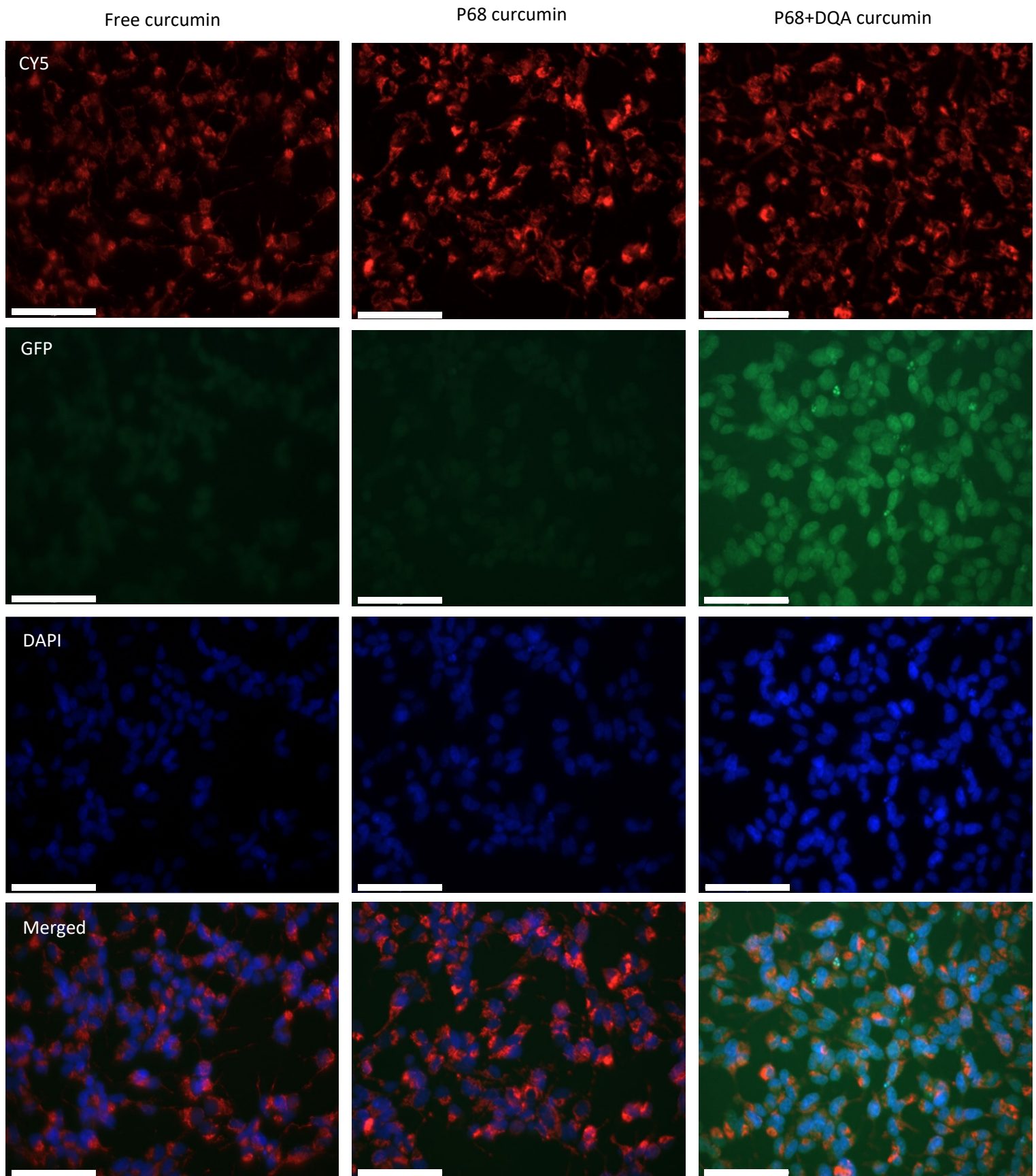
Figure 10. Mitochondrial targeting with P68+DQA curcumin compared to free and P68 curcumin in SH-SY5Y cells following passage across the hCMEC/D3 Transwell® model. Mitotracker™-stained mitochondria are shown in red (Cy5 objective), internalised curcumin is shown in green (GFP objective), stained nuclei are shown in blue (DAPI objective) and orange indicates the overlap of curcumin and mitochondrial fluorescence (merged image). Scale bars = 75 μm.

Due to the ability of curcumin to auto-fluoresce, free and nanoformulated forms of curcumin were used to assess the mitochondrial targeting properties of the P68+DQA nanocarriers. The fluorescent microscopy imaging presented in figure 10 shows high levels of curcumin accumulation in SH-SY5Y cells following treatment with P68+DQA curcumin, indicating high cellular uptake of these nanocarriers following passage across the hCMEC/D3 monolayer. Some curcumin accumulation was also observed with the P68 and free curcumin treatments, although to a lesser extent (figure 10). The merged image for the P68+DQA treatment shows significant overlap of curcumin and cell mitochondria fluorescence (figure 10), indicating co-location of the curcumin released from the P68+DQA nanocarriers and mitochondria. There was no clear overlap between curcumin and mitochondria with either P68 or free curcumin treatments (figure 10).

When assessing the ability of free, P68 and P68+DQA curcumin and curcumin + DFO to protect against rotenone induced cytotoxicity following BBB passage, significant differences were observed ($F_{(16, 62.2)}$ = 71.68, $p < 0.0001$) (figure 11a). 3 h pre-treatment with all free and formulated curcumin and curcumin + DFO conditions significantly protected against the 53.2% reduction in cell viability induced by rotenone ($p \leq 0.0001$ in all cases except with P68+DQA 5 µM curcumin where $p = 0.0021$). Pre-treatment with both the P68 and P68+DQA preparations of 10 µM curcumin + 100 µM DFO resulted significantly higher cell viability (10.4%, $p = 0.0145$ and 16.8%, $p = 0.0002$, respectively) compared to the free drug preparations (figure 11a). The P68+DQA 10 µM curcumin + 100 µM DFO condition was the most protective against rotenone induce reduction in cell viability, maintaining cell viability at 88.2% of control (figure 11a). Significant differences were also observed when comparing the ability of SOL, SOL+DQA and free curcumin to protect SH-SY5Y cells against rotenone in the Transwell® model ($F_{(7, 22.5)}$ = 60.8, $p < 0.0001$) (figure 11b). All SOL, SOL+DQA and free drug pre-treatments were able to significantly protect against the rotenone induced reduction in cell viability (5 µM curcumin – SOL: $p = 0.0017$, SOL+DQA: $p = 0.0003$, 10 µM curcumin – SOL: 0.0001, SOL+DQA: $p < 0.0001$), however there were no significant differences between the nanoformulations and the free drug preparations, with all conditions resulting in between 66.2 and 72.4% cell viability (figure 11b). A significant difference in cell viability was observed between the SOL and SOL+DQA 10 µM curcumin, with the SOL+DQA preparation resulting in 9.7% more cell viability ($p = 0.0089$) (figure 11b).

Figure 11. A. SH-SY5Y MTT assay results for free, P68 and P68+DQA preparations of 5 and 10 μM curcumin, 100 μM DFO or combined curcumin and DF0 (5 or 10 μM curcumin + 50 or 100 μM DFO, respectively) following passage across the hCMEC/D3 – SH-SY5Y co-culture Transwell® system. The hCMEC/D3 cells were grown on the insert and the SH-SY5Y cells were located at the bottom of the basolateral compartment. Treatments were added to the apical compartment of the Transwell® system and incubated for 3 h, the SH-SY5Y cells were then incubated with 100 μM rotenone for 24 h. These results were compared to rotenone treatment alone. MEM represents the control condition where cells were only treated with media (mean ± S.D., n=6). B. Corresponding MTT assay results for free, SOL and SOL+DQA curcumin (5 and 10 μM curcumin) treatments. * represents significance values of control or pre-treatment conditions compared to rotenone treatment alone (**** p < 0.0001, *** p < 0.001, ** p < 0.01). # represents significance values of nanoformulated drug compared to free drug within the same treatment condition (### p < 0.001, # p < 0.05). + Represents a significant difference between the two nanoformulations within the same treatment condition (++ p < 0.01).

Likewise, when comparing free and P68+DQA NAC treatments, significant differences in cell viability were also observed ($F_{(9, 34.74)}$ = 44.8, $p < 0.0001$) (figure 12). All free and P68+DQA NAC pre-treatments were able to protect against rotenone induced cytotoxicity following passage across the BBB model ($p < 0.0001$ in all cases except with free 500 µM NAC and free 500 µM NAC + 50 µM DFO where $p = 0.0036$ and $p = 0.005$, respectively). However, P68+DQA 1000 µM NAC and 1000 µM NAC + 100 µM DFO conditions resulted in significantly higher cell viabilities compared to the corresponding free drug conditions (18.6% $p = 0.0067$ and 13.7% $p = 0.0081$, respectively), in both cases maintaining cell viability a more than 90% of control (figure 12).

Figure 12. SH-SY5Y MTT assay results for free and P68+DQA preparations of 500 and 1000 µM NAC and combined NAC and DF0 (500 or 1000 µM NAC + 50 or 100 µM DFO, respectively) following passage across the hCMEC/D3 – SH-SY5Y co-culture Transwell® system. The hCMEC/D3 cells were grown on the insert and the SH-SY5Y cells were located at the bottom of the basolateral compartment. Treatments were added to the apical compartment of the Transwell® system and incubated for 3 h, the SH-SY5Y cells were then incubated with 100 µM rotenone for 24 h. These results were compared to rotenone treatment alone. MEM represents the control condition where cells were only treated with media (mean ± S.D., n=6). * represents significance values of control or pre-treatment conditions compared to rotenone treatment alone (**** $p < 0.0001$, ** $p < 0.01$). # represents significance values of nanoformulated drug compared to free drug within the same treatment condition (## $p < 0.01$).

Significant differences in cell viability were also observed between the free drug and

P68+DQA HT and HT + DFO conditions ($F_{(9, 22.26)} = 49.87$, $p < 0.0001$) (figure 13). All free

and P68+DQA HT and HT + DFO pre-treatments resulted in significantly higher cell viability

compared to rotenone treatment alone (10 µM HT – free: $p = 0.0003$, P68+DQA: $p = 0.0002$,

20 µM HT – free: $p = 0.0001$, P68+DQA: $p = 0.0023$, 10 µM HT + 50 µM DFO – free: $p =$

0.0004, P68+DQA: $p < 0.0001$ and 20 µM HT + 100 µM DFO – free & P68+DQA: $p < 0.0001$),

however only P68+DQA 20 µM HT and P68+DQA 20 µM HT + 100 µM DFO maintained cell

viability at 80% of control (figure 13). The P68+DQA nanoformulations of both

concentrations of combined HT and DFO, resulted in significantly higher cell viability

compared to the corresponding free drug conditions (10 µM HT + 50 µM DFO: 8.7%, $p =$

0.0125 and 20 µM HT + 100 µM DFO: 12.3%, $p = 0.0006$, respectively) (figure 13).
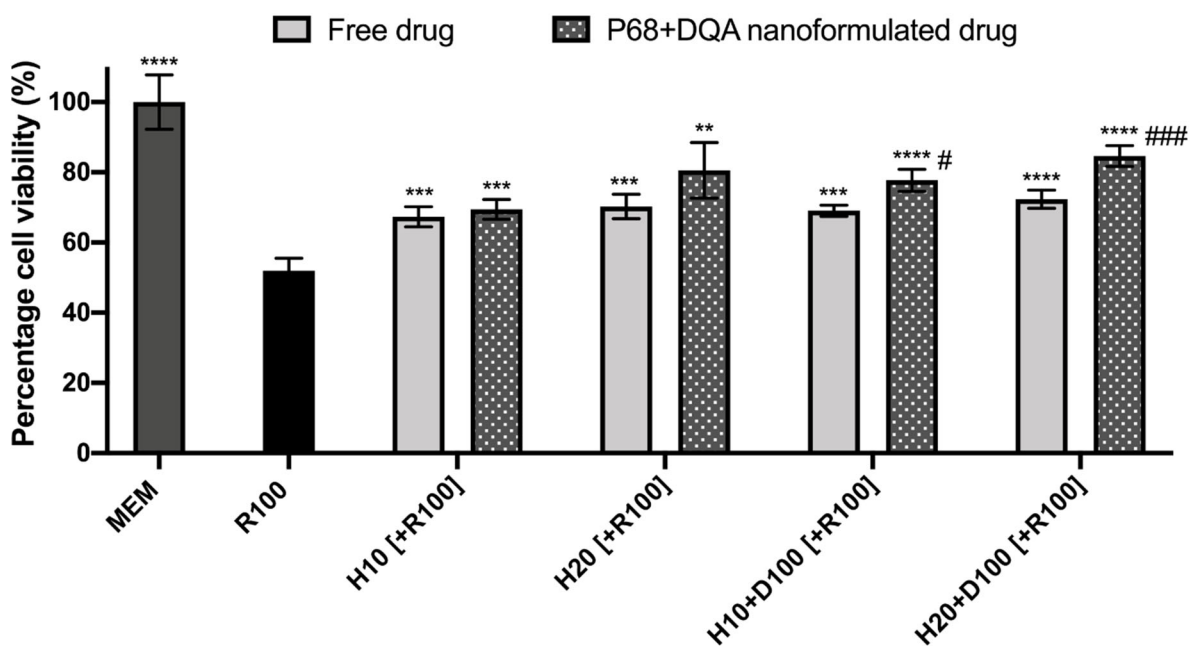
Figure 13. SH-SY5Y MTT assay results for free and P68+DQA preparations of 10 and 20 µM HT and combined HT and DF0 (10 or 20 µM HT + 50 or 100 µM DFO, respectively) following passage across the hCMEC/D3 – SH-SY5Y co-culture Transwell® system. The hCMEC/D3 cells were grown on the insert and the SH-SY5Y cells were located at the bottom of the basolateral compartment. Treatments were added to the apical compartment of the Transwell® system and incubated for 3 h, the SH-SY5Y cells were then incubated with 100 µM rotenone for 24 h. These results were compared to rotenone treatment alone. MEM represents the control condition where cells were only treated with media (mean ± S.D., n=6). * represents significance values of control or pre-treatment conditions compared to rotenone treatment alone (**** $p < 0.0001$, *** $p < 0.001$, ** $p < 0.01$). # represents significance values of nanoformulated drug compared to free drug within the same treatment condition (### $p < 0.001$, # $p < 0.05$).

Mitochondrial hydroxyl levels were also assessed using the Transwell® model to evaluate the ability of the free and nanoformulated treatments to protect against rotenone induced oxidative stress. Significant differences were observed between the different free, P68 and P68+DQA curcumin and curcumin + DFO treatments ($F_{(15, 51.1)}$ = 68.14, $p < 0.0001$) (figure 14a) and when comparing free, SOL and SOL+DQA curcumin conditions ($F_{(6, 23.86)}$ = 54.9, $p < 0.0001$) (figure 14b).

All curcumin and curcumin + DFO free, P68 and P68+DQA conditions, except 5 µM free curcumin, significantly protected against rotenone induced increased hydroxyl levels (free drug: 10 µM curcumin – p = 0.0015, 100 µM DFO – p = 0.0003, 5 µM curcumin + 50 µM DFO and 10 µM curcumin + 100 µM DFO– p = 0.0002 in both cases. P68: 5 µM curcumin – p = 0.00038, 10 µM curcumin – p = 0.0011, 100 µM DFO – p = 0.0014, 5 µM curcumin + 50 µM DFO – p = 0.0002, 10 µM curcumin + 100 µM – p = 0.0005. P68+DQA: $p < 0.0001$ in all cases, apart from 5 µM and 10 µM curcumin where p = 0.0002) (figure 14a). In each case, the P68+DQA preparations were the most protective, resulting in lower percentage hydroxyl levels in all cases compared to the corresponding free drug conditions (between 3.2 and 14.2%) and the corresponding P68 conditions (between 3.3 and 9.1%) (figure 14a), with P68+DQA 10 µM curcumin + 100 µM DFO resulting in the lowest hydroxyl levels, -5.2% relative to control (figure 14a). The differences in hydroxyl were found to be significantly lower when pre-treating with P68+DQA preparations of 5 µM curcumin (p = 0.0069), 10 µM curcumin (p = 0.0140), 5 µM curcumin + 50 µM DFO (p = 0.029) and 10 µM curcumin + 100 µM DFO (p = 0.0005) compared to the corresponding free drug conditions (figure 14a).

Most of these P68+DQA treatments also resulted in significantly lower hydroxyl than when using P68 treatments, except with 5 µM curcumin and 5 µM curcumin + 50 µM DFO where no significant differences were found (10 µM curcumin – p = 0.0003, 10 µM curcumin + 100 µM DFO – p = 0.0077) (figure 14a). Unlike when comparing P68+DQA and free drug conditions, significantly lower hydroxyl was found following pre-treatment with P68+DQA 100 µM DFO compared to the corresponding P68 pre-treatment (p = 0.0199) (figure 14a). There were no significant differences in hydroxyl between any of the P68 and free drug treatments (figure 14a).
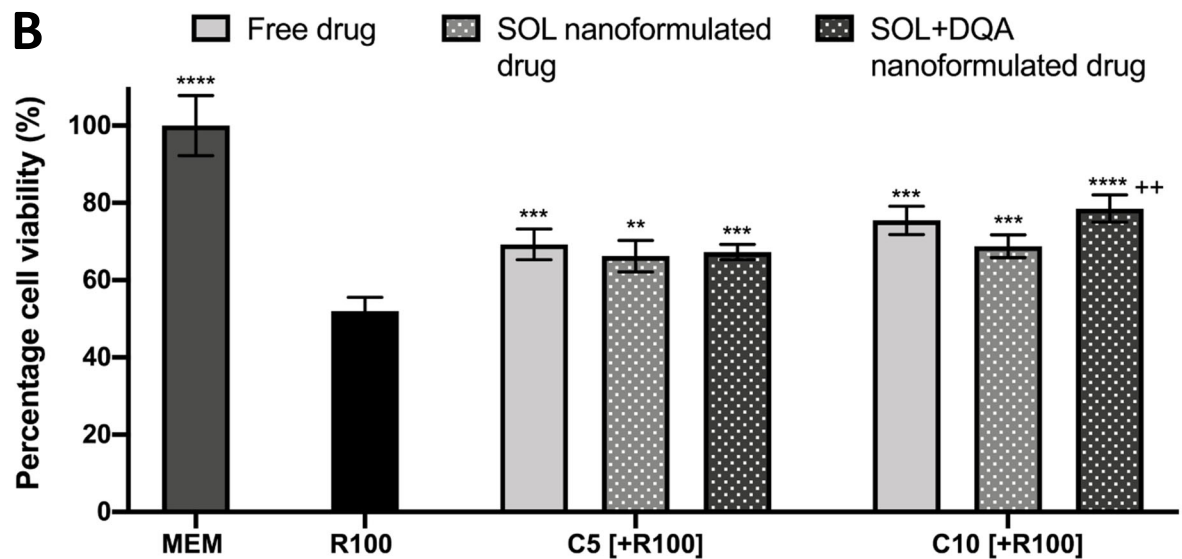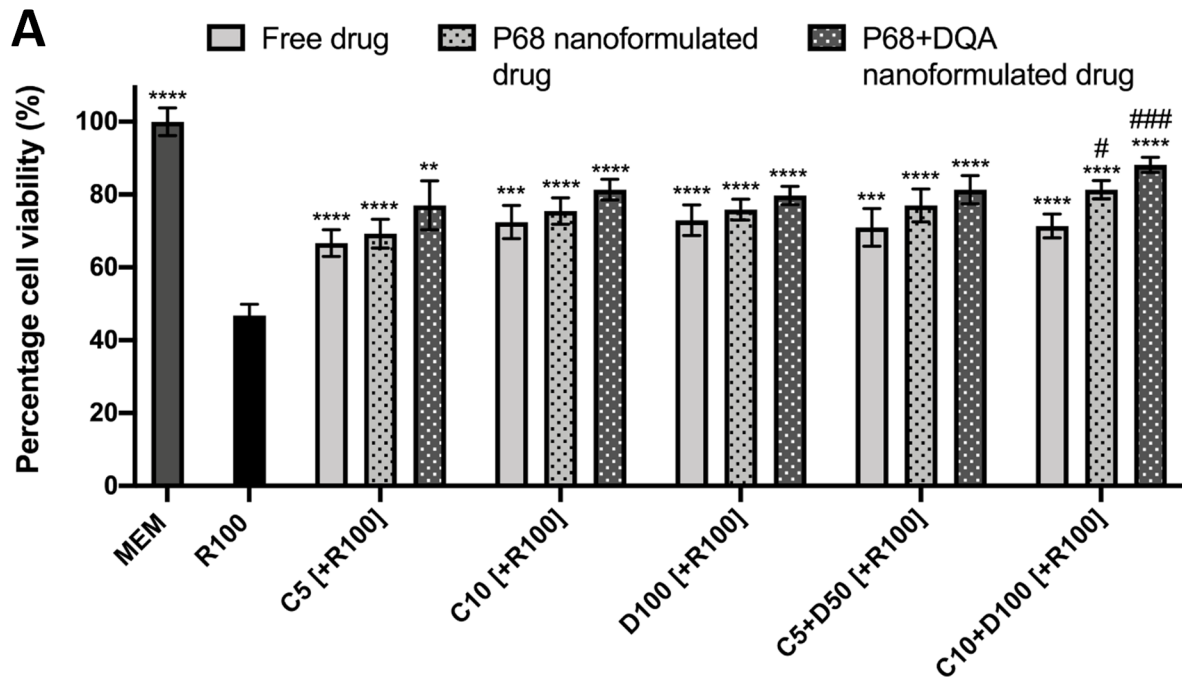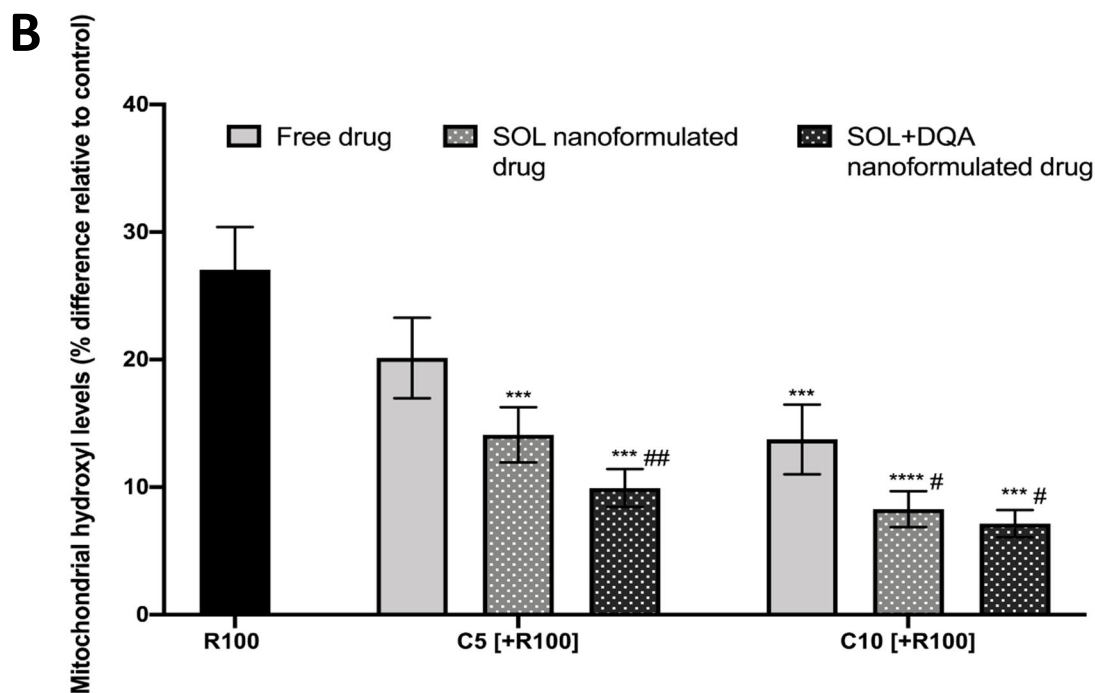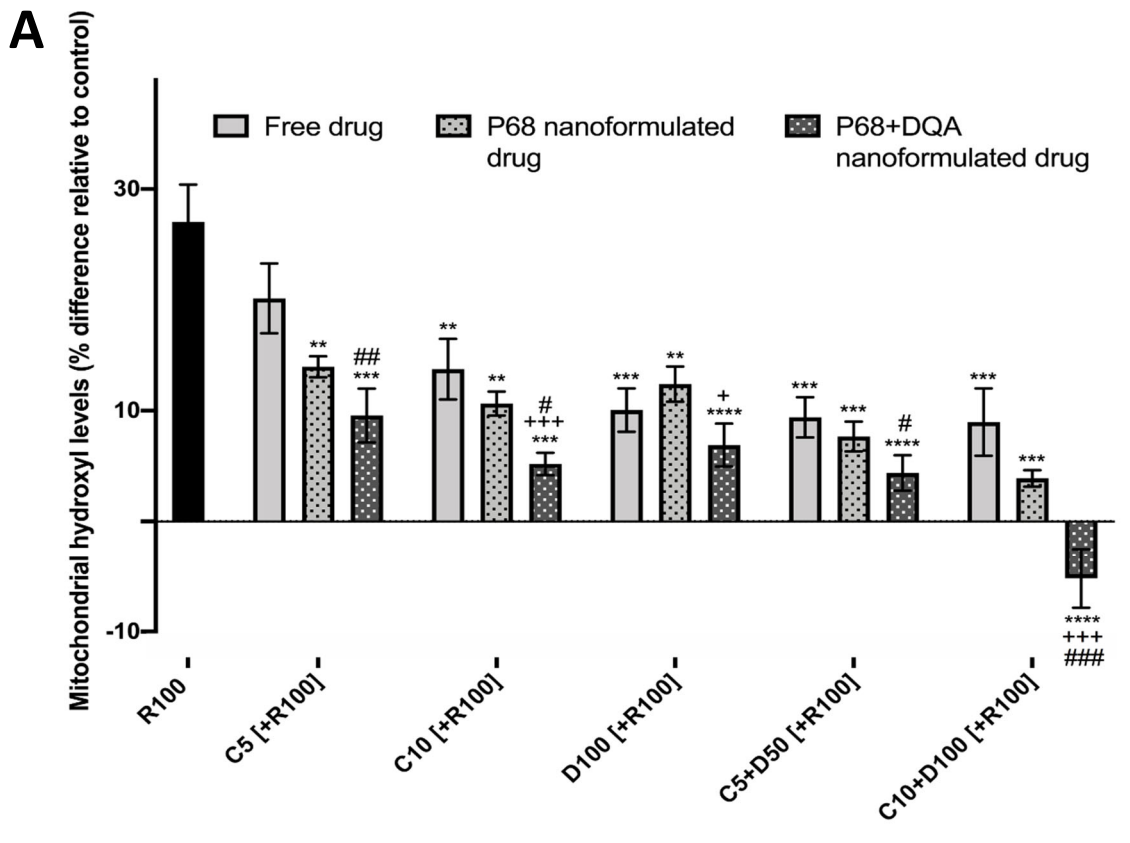
Figure 14. SH-SY5Y mitochondrial hydroxyl assay results for free, P68 and P68+DQA preparations of 5 and 10 µM curcumin, 100 µM DFO or combined curcumin and DF0 (5 or 10 µM curcumin + 50 or 100 µM DFO, respectively) following passage across the hCMEC/D3 – SH-SY5Y co-culture Transwell® system. The hCMEC/D3 cells were grown on the insert and the SH-SY5Y cells were located at the bottom of the basolateral compartment. Treatments were added to the apical compartment of the Transwell® system and incubated for 3 h, the SH-SY5Y cells were then incubated with 100 µM rotenone for 24 h. These results were compared to rotenone treatment alone. Mitochondrial hydroxyl levels are expressed as the percentage of hydroxyl identified in control cells (SH-SY5Y cells treated with MEM media only, for 24 h). (mean ± S.D., n=6). B. Corresponding mitochondrial hydroxyl assay results for free, SOL and SOL+DQA curcumin (5 and 10 µM curcumin) treatments. * represents significance values of control or pre-treatment conditions compared to rotenone treatment alone (**** p < 0.0001, *** p < 0.001, ** p < 0.01). # represents significance values of nanoformulated drug compared to free drug within the same treatment condition (### p < 0.001, ## p < 0.01, # p < 0.05). + Represents a significant difference between the two nanoformulations within the same treatment condition (+++ p < 0.001, + p < 0.05).

172

Similar to the P68+DQA formulations, SOL+DQA curcumin pre-treatments resulted in significantly lower hydroxyl than the free curcumin treatments (5 µM curcumin – p = 0,0027, 10 µM curcumin – p = 0.0191) (figure 14b). No significant differences were observed between the SOL+DQA and SOL treatments, however pre-treatment with SOL 10 µM curcumin resulted in significantly lower mitochondrial hydroxyl than the corresponding free drug condition (p = 0.0441) (figure 14b).
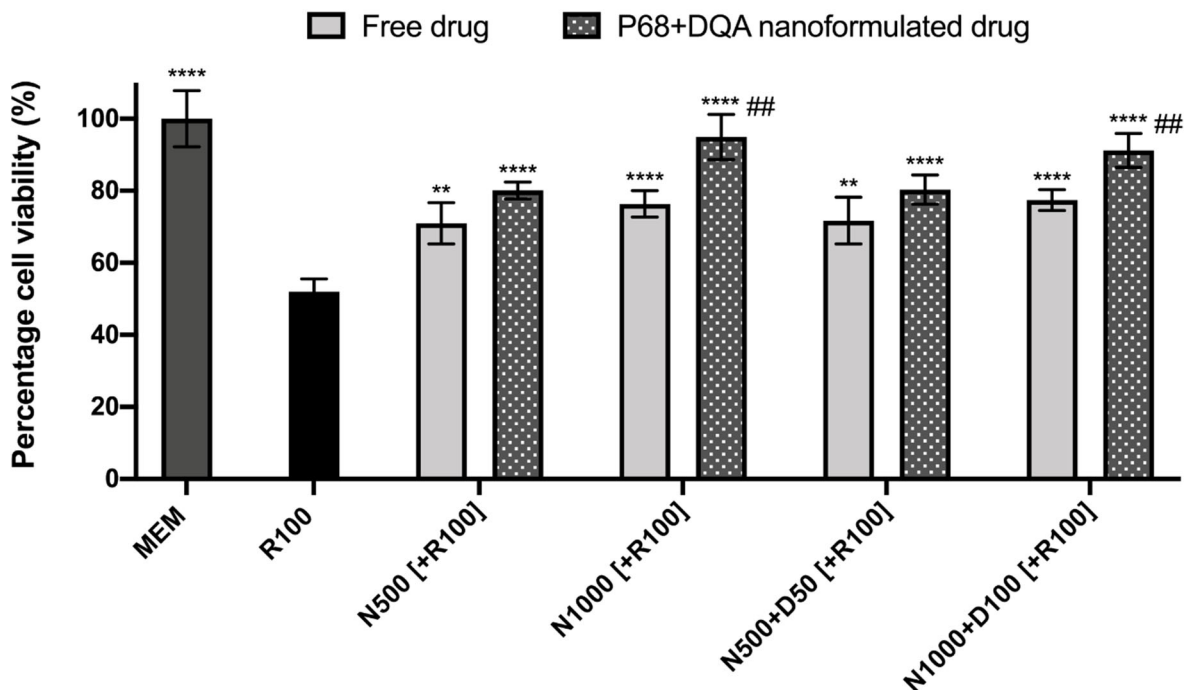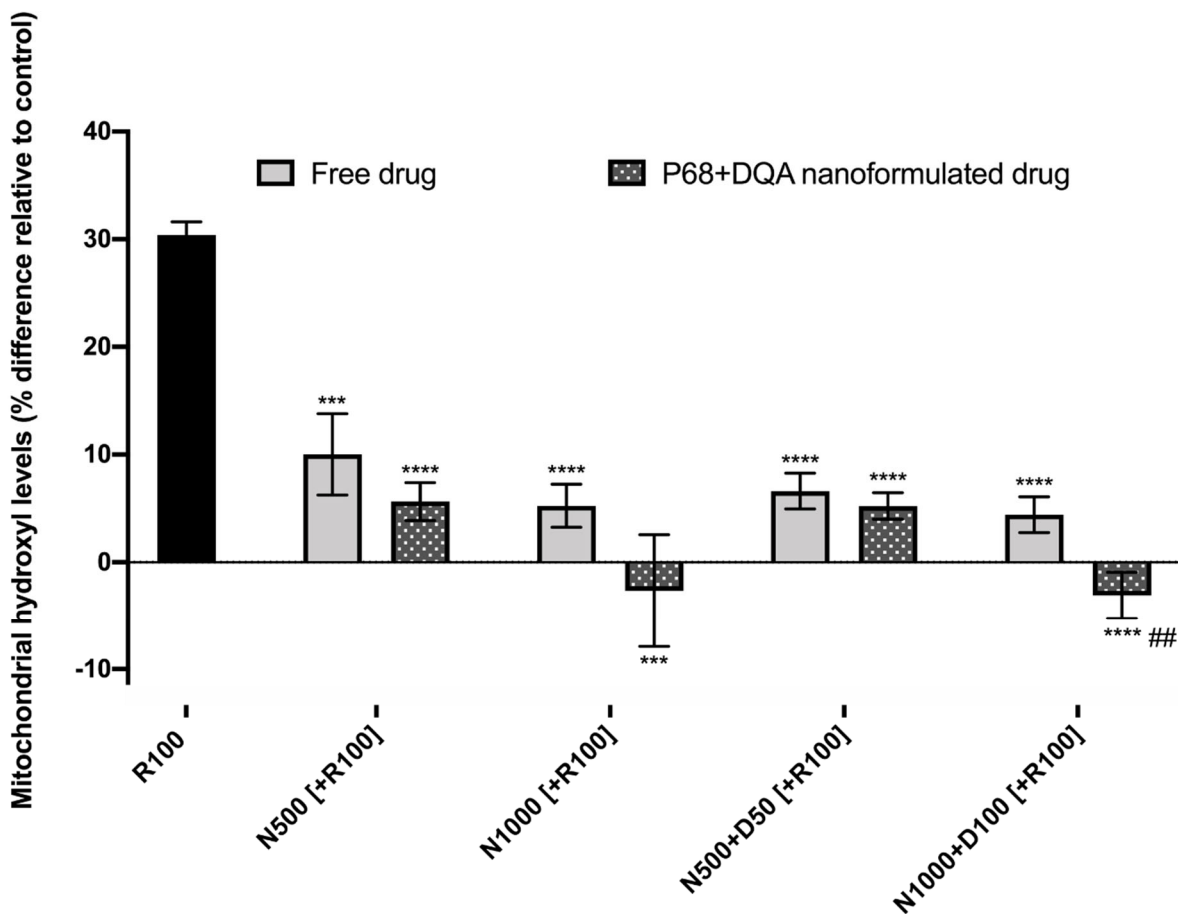

*Figure 15. SH-SY5Y mitochondrial hydroxyl assay results for free and P68+DQA preparations of 500 and 1000 µM NAC and combined NAC and DF0 (500 or 1000 µM NAC + 50 or 100 µM DFO, respectively) following passage across the hCMEC/D3 – SH-SY5Y co-culture Transwell® system. The hCMEC/D3 cells were grown on the insert and the SH-SY5Y cells were located at the bottom of the basolateral compartment. Treatments were added to the apical compartment of the Transwell® system and incubated for 3 h, the SH-SY5Y cells were then incubated with 100 µM rotenone for 24 h. These results were compared to rotenone treatment alone. Mitochondrial hydroxyl levels are expressed as the percentage of hydroxyl identified in control cells (SH-SY5Y cells treated with MEM media only, for 24 h). (mean ± S.D., n=6). * represents significance values of control or pre-treatment conditions compared to rotenone treatment alone (**** p < 0.0001, *** p < 0.001). # represents significance values of nanoformulated drug compared to free drug within the same treatment condition (## p < 0.01).*

Figure 16. SH-SY5Y mitochondrial hydroxyl assay results for free and P68+DQA preparations of 10 and 20 µM HT and combined HT and DF0 (10 or 20 µM HT + 50 or 100 µM DFO, respectively) following passage across the hCMEC/D3 – SH-SY5Y co-culture Transwell® system. The hCMEC/D3 cells were grown on the insert and the SH-SY5Y cells were located at the bottom of the basolateral compartment. Treatments were added to the apical compartment of the Transwell® system and incubated for 3 h, the SH-SY5Y cells were then incubated with 100 µM rotenone for 24 h. These results were compared to rotenone treatment alone. Mitochondrial hydroxyl levels are expressed as the percentage of hydroxyl identified in control cells (SH-SY5Y cells treated with MEM media only, for 24 h). (mean ± S.D., n=6). * represents significance values of control or pre-treatment conditions compared to rotenone treatment alone (**** p < 0.0001, ** p < 0.01). # represents significance values of nanoformulated drug compared to free drug within the same treatment condition (### p < 0.001, # p < 0.05).

Significant differences were also observed when using the mitochondrial hydroxyl assay to assess the ability of free and P68+DQA NAC and NAC + DFO (F(8, 18.79) = 83.49, p < 0.0001) and well as HT and HT + DFO (F(8, 28.41 = 107.9, p < 0.0001) to protect against rotenone induced oxidative stress in the Transwell® model (figure 15, 16). All free and P68+DQA NAC and NAC + DFO conditions significantly protected against the rise in hydroxyl induced by rotenone (p ≤ 0.0001 in all cases, figure 16) as did all the HT and HT + DFO conditions (p < 0.0001 in all cases except 10 µM HT where p = 0.0044). Again, the P68+DQA conditions generally resulted in lower hydroxyl compared to the free drug conditions (figure 15, 16).

However, of the NAC and NAC + DFO treatments, the only significant difference between the P68+DQA and free drug preparations was with 1000 µM NAC + 100 µM DFO (p = 0.0022), where there was a difference of 7.5%, with the percentage of hydroxyl following the P68+DQA treatment reaching -3.1% relative to control levels (figure 15). Whereas, when focusing on the HT and HT + DFO treatments, both 10 µM and 20 µM P68+DQA HT conditions resulted in significantly lower levels of hydroxyl compared to the corresponding free drug conditions (p = 0.0298 and p = 0.0003, respectively) (figure 16). The combination of 10 µM HT and 100 µM DFO in P68+DQA nanoformulations resulted in the lowest percentage mitochondrial hydroxyl levels relative to control (1.3%) compared to all the other HT and HT + DFO treatments (figure 16).

6.3. Discussion

The hCMEC/D3 cell line was used to model the BBB in a Transwell® system as it has been used and described in numerous previous studies (Weksler et al., 2005; Cristante et al., 2013; Weksler et al., 2013; Maggioli et al., 2016; Paradis et al., 2016; Hoyles et al., 2018). The model was utilised to test the potential brain penetrance and resulting efficacy of the free and nanoformulated curcumin, DFO, NAC and HT treatments, described in the previous chapters, at protecting against a rotenone model of PD.

The use of the hCMEC/D3 cell line for modelling the BBB has been criticized in the past due to relatively low TEER values achieved in previous studies, between 30 and 50 $\Omega.cm^2$ (Molino et al., 2014; Helms et al., 2016; Elbakary et al., 2020), suggesting that a Transwell® system using these cells may not be the best model of the human BBB due to the leaky nature of the system. However, there are benefits of using this cell line, particularly because of their human origin they maintain a normal BBB phenotype, expressing many of the receptors and transporters present in the *in vivo* BBB, including the transferrin receptor, insulin receptor and GLUT1 (Carl et al., 2010; Urich et al., 2012; Ohtsuki et al., 2012; Weksler et al., 2013). As there is an overarching emphasis on iron-induced oxidative stress in this work, the presence of the transferrin receptor in this cell line is particularly relevant because endocytosis of the transferrin-transferrin receptor complex is part of the mechanism of iron uptake into the brain (McCarthy & Kosman, 2015). Furthermore, the main limitation of these cells, the low TEER reported in early studies, has been somewhat overcome using

hydrocortisone, the presence of which can increase TEER values to around 300 $\Omega.cm^2$ due to corticosteroids being able to modulate the expression of tight junctional proteins such as occludin and claudin-5 and prevent endothelial barrier breakdown (Förster et al., 2008; Weksler et al., 2013; Molino et al., 2014; Gonzalez-Carter et al., 2019). The results of this study further support this notion, as the hCMEC/D3 cells were grown in the presence of hydrocortisone and the mean TEER values peaked at 320 $\Omega.cm^2$. The mean permeability of the hCMEC/D3 monolayers ($0.91 \pm 0.13 \times 10^{-3}$ cm/min) was also consistent with previous studies which have reported that a permeability of less than 1.2×10^{-3} cm/min to be acceptable in this cell line (Förster et al., 2008; Paolinelli et al., 2013; Eigenmann et al., 2013). Although these cells may be more permeable than other models such as those which use porcine primary cell culture where TEER values in excess of 800 $\Omega.cm^2$ have been reported (Ruben et al., 1991; Cantrill et al., 2012; Patabendige et al., 2013; Kaur et al., 2017; Elbakary et al., 2020), this is not necessarily an issue when using the BBB model in the evaluation of drugs for PD because brain endothelial dysfunction is thought to contribute to many neurodegenerative diseases (Weksler et al.,2013). And as amyloid peptide toxicity has been shown to increase the permeability of the BBB (Tai et al., 2012), the use of a slightly leaky BBB model may actually be more accurate when testing drugs for neurodegeneration.

The different free and nanoformulated curcumin, NAC, and HT treatments, alone and in combination with DFO, were tested on this model to assess whether they are likely to enter the brain *in vivo* and to evaluated whether the protective effects of these treatments against rotenone induced oxidative stress (as outlined in chapters 4 and 5) are retained after BBB passage. Importantly, no significant differences in TEER values were observed following treatment with all free, P68 and P68+DQA curcumin, NAC, HT and combined DFO conditions, suggesting that none of these treatments are likely to cause toxicity to the BBB. 100 µM free DFO and 10 µM Sol+DQA formulated curcumin treatments did however cause a significant reduction in TEER and therefore may not be suitable as treatments for PD. The fact that 100 µM free DFO resulted in some cytotoxicity of the hCMEC/D3 cells but the corresponding nanoformulated treatments did not, suggests that formulation protects against this effect. Furthermore, none of the combination treatments containing 100 µM DFO resulted in any cytotoxicity, including the free drug conditions, suggesting that in this case the presence of the antioxidant in the free drug treatments may act as protective

agents. However, if this is the case, the antioxidant power of the free drug conditions may be being partially used at the site of the BBB, reducing the activity available at the site of neurodegeneration. This highlights the benefit of nanoformulation for these drugs to enable targeted delivery.

In line with previous literature (D'Angelo et al., 2001; Boddaert et al., 2007; Schaffer et al., 2007; Reyes et al., 2016; Katz et al., 2015; Tsai et al., 2011), these results indicate that curcumin, DFO, NAC and HT can all pass across the BBB to some extent. However, in every case the P68+DQA nanoformulation of these drugs increased the percentage of each antioxidant reaching the basolateral compartment of the Transwell® model by up to 49% for curcumin (with 10 µM curcumin), 28% for NAC (with 1000 µM NAC and 1000 µM NAC + 100 µM DFO), and 50% for HT (with 10 µM HT) (figures 7 - 9). This trend was also observed for treatments containing DFO, where the percentage of DFO passing the BBB reached up to 72% with the combined P68+DQA NAC + DFO and HT + DFO treatments (figure 10b). An increase in percentage of each drug passing the BBB model was also observed with the relevant P68, SOL and SOL+DQA treatments, however in every case the corresponding P68+DQA formulations were superior, suggesting that the P68+DQA formulations might be the most suitable for treating PD. Although the highest increase in BBB passage was observed with the HT treatments when using the P68+DQA formulation, this does not necessarily suggest that the HT formulations are better for brain delivery, as both free curcumin and NAC had higher starting penetrance than free HT and, like the HT treatments, all curcumin and NAC containing P68+DQA formulations also resulted in at least 71% of the drug reaching the basolateral compartment.

As previously reported (Weissig et al., 1998; Lyrawati et al., 2011; Zupančič et al., 2014), DQA is a mitochondria targetter; this was also indicated by the mitochondrial localisation assessments presented here which showed for the first time that the P68+DQA formulations resulted in more curcumin released at the mitochondria compared to both the P68 and free curcumin treatments (figure 10). This suggests mitochondrial-specific accumulation of curcumin when using the P68+DQA nanocarriers due to the ability of DQA to specifically target cellular mitochondria. The P68+DQA nanocarriers may therefore be the most beneficial for PD because mitochondria are the main site of oxidative stress (Thomas et al., 2009; Bratic & Nils-Larsson, 2013; Kandola et al., 2015; Costa-mallen et al., 2017) and

mitochondrial dysfunction has been linked to the development and progression of PD (Langston, 1987; Jenner & Olanowm, 1996; Schapira, 2007; Zhou et al., 2008; Camilleri & Vassallo, 2014; Gautier et al., 2014; Moon & Paek, 2015; Barodia et al 2017). This is further supported by the SH-SY5Y cell viability and mitochondrial hydroxyl results which show that the P68+DQA formulations of each treatment consistently resulted in the most protection against rotenone, which is a mitochondrial complex 1 inhibitor (Tanner et al., 2011), following passage across the hCMEC/D3 Transwell® model.

Overall, the cell viability and mitochondrial hydroxyl results were consistent with those reported in chapters 4 and 5, in that all treatments were able to protect against rotenone to some extent, indicating that some level of potency for each treatment is retained once it has passed the BBB and reached the target site. That said, unlike the results reported in the previous chapters and in Mursaleen et al (2020a) where for the most part the formulations were only at least as good as the free drug conditions at protecting against rotenone, when using the Transwell® model the nanoformulated treatments were superior in every case, particularly those formulated with P68+DQA. In line with the mitochondrial localisation assessments this suggests that the P68+DQA formulations were able to mostly stay intact until reaching the mitochondria within the SH-SY5Y cells, as demonstrated by their ability to be the most effective at protecting against rotenone compared to the free drug conditions and other formulations which did not contain DQA. This further highlights the added value of targeted delivery.

There was, however, little change compared to the SH-SY5Y only results presented in the previous chapters in terms of which concentrations of the treatments were the most successful at protecting against rotenone. The highest concentrations of the P68+DQA combinations of curcumin and DFO and HT and DFO were the most effective of the treatments containing curcumin and HT at protecting against rotenone induce cytotoxicity and increased mitochondrial hydroxyl, in both cases maintaining cell viability above 80% and hydroxyl at least in line with control levels (figures 12, 14, 15 and 17). However, there was no significant difference between the 20 µM HT and 20 µM HT + 100 µM DFO pre-treatments, suggesting that there may not be much added value in combining HT and DFO, despite the combination treatments being the most effective overall. Of the treatments containing NAC, P68+DQA 1000 µM NAC was equally as effective as the combination of

1000 µM NAC with 100 µM DFO, in each case maintaining cell viability above 91% and hydroxyl 2.7% below control levels (figure 14 and 16). This further suggests that NAC and HT unlike curcumin does not necessarily benefit from the addition of an iron chelator as they may have similarly potent chelating capabilities (Hjortsrø et al., 1990; Melidou et al., 2005; Do Van et al., 2016; Kitsati et al., 2016; Wongjaikam et al., 2017), as implied in chapter 5.

6.4. Conclusion

In summary, taken together, these results indicate that the P68+DQA nanoformulations were the most successful at enhancing the effects of curcumin, NAC, HT and/or DFO by increasing the brain penetrance and targeted delivery of the associated drugs within the cellular Transwell® system. These results provide further support that this nanocarrier strategy may be an effective approach to fully utilise the therapeutic benefit of these antioxidants for PD. This study has also provided additional data to support future testing of these formulations in *in vivo* models of PD, where a head-to-head comparison of the different antioxidant P68+DQA formulations could be carried out to establish which treatments are able to translate into long-term phenotypic protection.

Chapter 7 - Overview and future directions

7.1. Overview

PD is a progressive neurodegenerative condition which is becoming increasingly prevalent in the global population, with more than 6 million cases reported worldwide in 2016 compared to 2.5 million in 1990 (Dorsey et al., 2018). In the UK alone, it is estimated that there is a 1 in 37 lifetime risk of developing the condition (Parkinson's UK, 2018). Currently available treatments only work to alleviate the symptoms and are not focused on modifying the disease progression. Although many drugs have been investigated as potential disease modifying agents, progress has been limited often due to issues such as brain penetrance and off-target side effects. One area which has generated interest as a potential target for PD is oxidative stress. Oxidative stress is thought the be involved in both the development and progression of PD and has been linked to elevated iron levels in the SN of the mid-brain (Kroemer & Reed, 2000; Schapira, 2007; Simpkins & Dykens, 2008; Kandola et al., 2015; Do Van et al., 2016; Barodia et al 2017; Jiang et al., 2017). It is therefore unsurprising that numerous antioxidants and iron chelators have been investigated as potential therapeutics for PD.

This study focused on three antioxidants (curcumin, NAC, and HT) as well as the iron chelator DFO because all these compounds have previously been shown to be effective against oxidative stress in models of PD, however, clinical advancement for PD has been limited because of their inability to access the brain at therapeutic concentrations (Cotgreave & Moldeus, 1987; Yang et al., 2007; Bavarsad Shahripour et al., 2014; Martin-Bastida et al., 2017; Robles-Almazan et al., 2018). Due to their phenolic nature, curcumin and HT can act as direct free radical scavengers (Santos et al., 2016; Robles-Almazon et al., 2018). Although NAC being a thiol compound has some propensity to directly scavenge free radicals, it exerts most of its antioxidant effects through its ability to act as a precursor to the endogenous antioxidant glutathione, levels of which have been shown to be reduced in PD (Sian et al, 1994; Kandola et al., 2015). They have all also been shown to increase Nrf2 signalling which oxidative stressors, like rotenone, inhibit to limit the activation of genes encoding endogenous antioxidants defence mechanisms (Zrelli et al 2011; Magesh et al., 2012; Zhang et al., 2014; Abrahams et al 2019). All these antioxidants are available as

dietary supplements, with curcumin and HT being considered 'generally recognised as safe (GRAS)' by the FDA (FDA, 2020a, b). Although NAC is often marketed as a dietary supplement (Goldstein et al., 2017), it is also approved as a drug to counteract paracetamol overdose (FDA, 2020c). DFO, on the other hand, is approved for iron overload disorders such as Beta-thalassemia and haemochromatosis due to its potent affinity to chelate iron (Mobarra et al., 2016; FDA, 2020d; Kontoghiorghes & Kontoghiorghes, 2020), which in PD could be used to prevent the excessive build-up of hydroxyl radicals which go on to cause catastrophic oxidative damage to proteins, lipids, and DNA (Gerlach et al., 1994; Halliwell et al., 2001).

Following ingestion, each of these compounds have limited brain penetrance for different reasons. Curcumin is hydrophobic in nature, making it highly insoluble and therefore has very low bioavailability (Abrahams et al., 2019). This has been verified by numerous clinical trials of curcumin being unsuccessful, likely due to poor absorption (Abrahams et al., 2019). For example, Ringman et al (2012) tested curcumin in a trial of Alzheimer's disease and showed no change in tau or amyloid beta levels with a daily dose of 2 or 4g and showed a mean of only 7.32 ng/ml curcumin in plasma following treatment. Numerous studies have attempted to improve the bioavailability of curcumin by chemical modification, but this has often led to reduced efficacy as an antioxidant and increased side effects due to the change in chemical structure (Begum et al 2008; Agrawal et al., 2012). Any curcumin that is absorbed has a high potential for modification through both phase 1 and phase 2 metabolism, where the double bonds are removed through the action of alcohol dehydrogenase during hydrolysis (Siviero et al., 2015) and curcumin is rapidly conjugated mainly to glucuronides and sulphates at the phenol positions, respectively (Nelson et al., 2017). This is likely another major reason for the lack of success free curcumin has had in clinical trials to date.

Unlike curcumin, HT is soluble and is generally well absorbed *via* passive transport in the small bowel and colon (Robles-Almazan et al 2018). However, like curcumin, due to its phenolic nature HT also suffers from intestinal/hepatic first pass and second pass metabolism, ultimately being transformed into glucuronide, methylate, and sulphate by-products (Suárez et al, 2011). In line with this, Miro-Casas et al (2003) showed that following administration of olive oil, only 2% of the HT detected in the plasma and urine was in its free

form, the majority being in the glucuronide form. Other studies have highlighted that although there is widespread distribution of HT following administration, it has a half-life of only 1-2 minutes (D'Angelo et al., 2001; Granados-Principal et al., 2014), which is a major limiting factor for any potential therapeutic.

In contrast, NAC is a thiol compound and is relatively stable (Aldini et al., 2018). As it is synthetic it does not require an extraction process like curcumin and HT which results in poor stability (Zafra-Gómez et al., 2011; Schneider et al., 2015). However, NAC is subject to extensive first pass metabolism in the liver and kidneys where it is hydrolysed by cytosolic acylase 1 (Anders & Dekant, 1994). Studies have shown that NAC can counteract glutathione depletion in the liver and brain in the mouse paraquat model (Ortiz et al., 2016) and that in healthy rats NAC increases glutathione levels by 20% in the skin and 50% in the liver following one dose of 1200 mg/kg NAC but that the lungs and kidneys were unaffected (Arfsten et al., 2007). However, it has been shown that human oral administration of 200 mg NAC is largely undetectable following ingestion, and that the oral formulation appears to be less than 5% bioavailable (Cotgreave & Moldeus, 1987; Bavarsad Shahripour et al., 2014). Due to this and its rapid metabolism, it is therefore improbable that NAC would be able to reach the brain at therapeutic concentrations following oral administration.

DFO is a small molecule hexadentate iron chelator which binds to iron in a 1:1 ratio (Hatcher et al., 2009; Farr & Xiong, 2020) but is metabolised hepatically *via* oxidative deamination (Porter, 2001). Although DFO is already used clinically to treat acute iron poisoning and chronic iron overload disorders (Porter, 2001), it has been associated with many systemic toxicities including toxicity of the cardiovascular and respiratory systems as well as reduced renal and liver function at doses greater than 2.5 g per infusion (Brittenham, 2011; Di Nicola et al., 2015; Bayanzay & Alzoebie, 2016). This, alongside the need to administer DFO as continuous subcutaneous injections due to its short half-life of 20-30 minutes, has resulted in low patient compliance (Brittenham, 2011; Bayanzay & Alzoebie, 2016). The widespread use of DFO to mitigate against iron accumulation in other conditions has therefore been limited by its profile for adverse side effects (Di Nicola et al., 2015; Farr & Xiong, 2020) and its mode of administration (Brittenham, 2011; Bayanzay & Alzoebie, 2016). And although Ward et al (1995) showed that DFO can cross the BBB in rats and decrease iron content in the cerebellum and cerebral cortex, it has been reported that it is only neuroprotective at

high doses due to limited permeation of the BBB (Shachar et al., 2004), and it is these high doses which are associated with the systemic toxicities (Brittenham, 2011; Bayanzay & Alzoebie, 2016).

All these compounds could therefore benefit from either increased stability, increased solubility, targeted delivery to minimise off-target effects, and/or increased membrane permeation. Using nanocarrier delivery systems may be the best approach to achieve this without risking compromising the protective properties of these compounds which often occurs when attempting chemical modification (Begum et al 2008; Agrawal et al., 2012). Using nanocarriers in order to increase stability of compounds, enhance the passage across biological membranes, and to aid targeted delivery has been established for many other health conditions with a small number now being clinically available, such as the FDA approved poly(lactic-co-glycolic acid) liposome nanoformulation which has been used to test curcumin in previous studies (Tsai et al., 2011). However, none so far have been developed specifically for these antioxidants and iron chelators in the treatment of PD. The overarching aim of this research was therefore to develop nanocarriers to enhance the effects of these compounds by increasing BBB penetration and targeting mitochondria, the main site of oxidative stress (Thomas et al., 2009; Bratic & Nils-Larsson, 2013; Kandola et al., 2015; Costa-mallen et al., 2017).

In summary, the results demonstrated the successful formulation of P68 and P68+DQA curcumin and/or DFO nanocarriers with the ideal characteristics to improve stability, pass the BBB, and aid combination therapy without inducing toxicity. SOL and SOL+DQA nanocarriers were also developed and exhibited most of these characteristics, however they reduced the cell viability of SH-SY5Y cells when combined with DFO. All the nanocarriers successfully delivered their associated drugs (curcumin and/or DFO) to protect against oxidative stress induced by an SH-SY5Y rotenone model of PD. However, it was noted and reported in Mursaleen et al (2020a) that the ability of the P68+DQA nanocarriers to target mitochondria appeared to enhance the positive effects of curcumin and DFO to protect against oxidative stress and loss of dopamine induced by rotenone. Due to this, and the inability of the SOL formulations to incorporate DFO without inducing cytotoxicity, only the P68+DQA nanocarriers were utilised for the delivery of NAC and HT, alone or in combination with DFO. Of all the nanoformulations tested, the P68+DQA formulations were the most

successful at enhancing the effects of curcumin, alone and in combination with DFO, by increasing the brain penetrance and targeted delivery of the associated drugs within the cellular Transwell® system. These nanocarriers were also able to significantly enhance the delivery and effectiveness of NAC and HT, alone and in combination with DFO, in the Transwell® model. Taken together, these results support the idea that the P68+DQA nanocarrier strategy may be an effective approach to fully utilise the therapeutic value of these compounds for PD.

Table 1. Comparison of the most effective curcumin, HT, and NAC P68+DQA nanocarriers, alone and in combination with DFO, in their ability to protect against the effects of rotenone in the SH-SY5Y model only. In each case, the values given are the mean difference between the pre-treatment condition and R100 treatment only. R100 = 100 µM rotenone, C10 = 10 µM curcumin, D100 = 100 µM DFO, H20 = 20 µM HT, N1000 = 1000 µM NAC.

P68+DQA Condition	Increase in cell viability (%)	Reduction in non-ferritin iron (ng/mg total protein)	Reduction in TBARS (uM)	Reduction in mitochondrial hydroxyl (%)
C10	27.41	7425	12.05	28.83
C10+D100	38.72	7538	12.25	31.21
H20	39.02	9515	10.08	14.17
H20+D100	33.22	10246	9.36	23.96
N1000	32.34	10783	12.94	15.82
N1000+D100	30.78	10800	12.78	18.54

When focusing on the most effective curcumin, HT, and NAC P68+DQA nanocarriers, it is clear that curcumin, and to some extent HT, benefit from combination with an iron chelator as the effects observed with the antioxidant alone appear to be enhanced with the addition of DFO in the majority of cases (table 1, 2). However, in most cases 1000 µM NAC had equivalent effects to 1000 µM NAC + 100 µM DFO, suggesting that the effects of NAC are not enhanced by DFO (table 1, 2). This is likely because NAC has been shown to act as a potent iron chelator in addition to its antioxidant capabilities (Hjortsrø et al., 1990; Do Van et al., 2016; Wongjaikam et al., 2017). However, Curcumin and HT are also reported to exhibit iron chelator properties (Melidou et al., 2005; Jiao et al., 2006; Kitsati et al., 2016)

and the logarithm of the concentration of free metal ion at equilibrium (pM or pFe(III) for iron specifically), which is used as a measure of metal-ligand affinities, is similar for curcumin (pFe(III) = 16.6), HT (pFe(III) = 16.3) and NAC (pFe(III) = 16.6) (Tosato & Di Marco, 2019; Bernabé-Pineda et al., 2004). The higher the pM the stronger the ligand:iron complex and although these values are not as high as compared to the iron chelators deferiprone and deferoxiamine (pFe(III) = 19.3 and 26.8, respectively), 16.1-16.6 is similar to the pM of many other iron chelators such as nitrilotriacetic acid (Martell & Smith, 1974; Buss et al., 2003; Bernabe-Pineda et al., 2004; Tosato & Di Marco, 2019). pM is dependent on the total metal concentration, the total ligand concentrations and pH, the pFe(III) are caluated at a pH 7.4 and for 10 uM ligand and 1 uM ferrous iron (Bernabé-Pineda et al., 2004; Tosato & Di Marco, 2019), therefore the reason NAC may have exhibited more iron chelator properties in these experiments is likely because the concentration of NAC used was much higher than curcumin and HT, 500 and 1000 μM compared to 5 and 10 μM curcumin and 10 and 20 μM HT. This is supported by the results in this study which showed that curcumin and HT were both also able to protect against the increase in iron induced by rotenone, but that NAC was more protective in each case (table 1).

Table 2. Comparison of the most effective curcumin, HT, and NAC P68+DQA nanocarriers in their ability to pass the BBB and protect against rotenone using the hCMEC/D3 and SH-SY5Y Transwell® model. For cell viability and mitochondrial hydroxyl, the values given are the mean difference between the pre-treatment condition and R100 treatment only. R100 = 100 μM rotenone, C10 = 10 μM curcumin, D100 = 100 μM DFO, H20 = 20 μM HT, N1000 = 1000 μM NAC.

P68+DQA Condition	Percentage of antioxidant passing the BBB (%)	Increase in SH-SY5Y cell viability (%)	Reduction in SH-SY5Y mitochondrial hydroxyl (%)
C10	71.19	34.55	21.85
C10+D100	82.17	41.35	32.24
H20	65.97	28.59	26.62
H20+D100	64.00	32.63	29.04
N1000	80.64	42.97	33.06
N1000+D100	79.75	39.20	33.47

Although each drug was not compared directly in this study, when you look at the results of the most successful concentrations of each drug condition, P68+DQA 1000 μM NAC appears to be the most protective following passage across the BBB model (table 2). This is likely due to more than 80% of NAC within the treatment being able to pass the BBB and reach the SH-SY5Y cells in the lower chamber of the model (table 2). Although comparable results are shown with the combination of curcumin and DFO (table 2), the fact that such a high level of protection can be achieved by NAC without the addition of DFO may be beneficial because with combination therapy there is an increased possibility of side effects due to the separate pharmacokinetic and safety profiles of the drugs (Mursaleen et al., 2020b), as well as the possibility of negative interactions between the compounds. That said, iron chelators have shown promising results in clinical studies of PD (Devos et al., 2014), possibly because excess levels of free iron have also been associated with many of the other hallmarks of the disease including α-syn aggregation (Ostrerova-Golts et al., 2000; Hare & Double, 2016; Brundin & Kordower, 2017), neuroinflammation (Saleppico et al., 1996; Urrutia et al., 2013) and mitochondrial dysfunction (Simpkins et al., 2008; Jiang et al., 2017) and therefore the results of this study may be limited due to its primary focus on antioxidant outcome measures. Thus, before making any decisions about which of these antioxidants, alone or in combination with DFO, would be best for PD therapeutics, these formulations need to be further evaluated in a head-to-head comparison to assess their effects in PD models which incorporate other aspects of PD in addition to oxidative stress.

The results show that rotenone treatment increases non-ferritin bound iron and lipid peroxidation and decreases cell viability. Therefore, given the elevated levels of iron and lipid peroxidation, such rotenone-induced cell death could be explained, not only by iron-induced oxidative stress but by iron-related necrosis and ferroptosis, both of which are linked to excessive levels of iron-induced lipid peroxidation (Dixon et al., 2012; Al-Qenaei et al., 2014; Mahoney-Sanchez et al., 2021). Further to the increase in ferrous iron availability that results following rotenone's inhibition of mitochondrial complex 1 (Mastroberardino et al., 2009; Horowitz et al., 2010; Mena et al., 2011;), inhibition of mitochondrial complex 1 disrupts mitochondrial membrane potential (Jayaraj et al., 2013). Any further evaluations of the nanoformulations should, therefore, include specific assessments of mitochondrial function, necrosis, and ferroptosis. Flow cytometry could be used to evaluate levels of

necrosis (Al-Qenaei et al., 2014) and the NADPH activity assay could be utilised to measure changes in GPx4 activity as an indicator of ferroptosis (Yang et al., 2014). Mitochondrial function studies could be carried out using the Seahorse system as previously described by Little et al (2020) where chemical fluorescent stains and high-content imaging were implemented into the Seahorse metabolic flux assay to assess mitochondrial bioenergetics and properties. This could be complemented by measuring ATP levels and assessing mitochondrial membrane potential using the tetramethylrhodamine methyl ester (TMRM) assay which results in an accumulation of a dye in active mitochondria with intact membrane potentials (Reelfs et al., 2019). As these nanoformulations have been specially targeted to mitochondria with the aim of reducing the mitochondrial labile iron pool and mitochondrial ROS production, it would be beneficial to measure the exact mitochondrial ROS levels using mitoSOX™ (Reelfs et al., 2019) and utilise the mitochondria-specific fluorescent iron sensors developed by Abbate et al (2015) which use mitochondria-homing SS-peptides as carriers of sensitive iron chelators to evaluate mitochondrial labile iron. It may also be useful to undertake such studies in a more sophisticated BBB model, for example by co-culturing the BBB cell line with astrocytes and pericytes on the Transwell® insert in order to more closely mimic the *in vivo* BBB, as recently described by Stone et al (2019).

Overall, this study indicates that the P68+DQA nanoformulations of curcumin, NAC, and HT, alone or in combination with DFO, may be protective against PD, and could therefore potentially be used as treatments for PD. Such formulations may be most suited for newly diagnosed patients who are early on in the disease progression, and for prodromal patients who exhibit signs and symptoms that increase their risk of being diagnosed with PD but do not currently meet the diagnostic criteria (e.g. bradykinesia and at least one other cardinal motor symptom) (Mantry & Morley, 2018). This is because the main mechanism of action of these formulations is to reduce iron-induced oxidative stress and the resultant dopaminergic cell death, which could be protective against both the onset of the disease and the ongoing progression of neurodegeneration exhibited in PD. As all the experiments in this study were carried out in cellular models of PD, it would be essential to do subsequent comparisons in *in vivo* models of PD, not only using a neurotoxin like rotenone but also using an α-syn model. This is because it has been highlighted that a variety of

models are required before moving from preclinical to clinical testing (Brundin & Wyse, 2019), but also because α-syn models may be more representative of the slow progression of the disease compared to neurotoxin models which are usually used to trigger an abrupt insult (Konnova and Swanberg, 2018). Therefore α-syn models could be more useful in assessing the ability of the formulations to protect against the ongoing progression of the disease. Such additional data could also help to establish which treatments are more likely to translate into long-term phenotypic protection as *in vivo* models may provide a more reliable indicator of the clinical effects of these treatments compared to the *in vitro* models used in this study.

7.2. Future directions

The longer-term aim of this work is to develop disease modifying treatments for PD therefore it is important to outline a plan to reach clinical translation. In addition to the data required from animal models of PD, for these formulations to be used in people there is a requirement for long-term stability data, a minimum of 6 months is recommended by the FDA in the US (FDA, 2020e) and 3-6 months by the Medicines and Healthcare products Regulatory Agency (MHRA) in the UK (MHRA, 2020). In this study, formulation dispersions were used for all experiments. The next step would therefore be to assess the suitability of the lyophilized formulations as powder is more suitable for long-term storage and can be used for nasal administration (Tas et al., 2009; Siow et al., 2016). The long-term stability of the lyophilized formulations can be evaluated by assessing size, charge, encapsulation efficiency, drug loading and chemical structure as shown in this study but at different time points to ensure the established characteristics are retained.

In parallel, pharmacokinetic and distribution studies of the lyophilized formulations could be evaluated in rodent models to ensure that the nanoformulations can reach the target site of the SN before being metabolised and without causing excessive off-target effects. The formulations could also be modified to become more targeted to the brain, this could be achieved by adding a coating of the non-ionic surfactant, Tween 80, which has shown brain specificity in previous studies *via* its ability to bind with plasma Apo-E lipoprotein and subsequently bind to low density lipoprotein receptors on brain microvascular endothelial cells (Kreuter, 2001; Yadav et al., 2017). However additional safety and stability tests would

need to be carried out on any modified formulations. Alternatively, the existing lyophilized formulations could be administered intranasally to limit systemic circulation, reducing the propensity for systemic off-target effects (Illum, 2003; Ruigrok & de Lange, 2015; Alexander & Saraf, 2018). This method may also be favourable because it bypasses phase 1 metabolism and the BBB as the nasal cavity is innervated by olfactory and trigeminal nerves and is therefore connected to the olfactory bulb and the pons of the brain stem (Crowe et al., 2018). However, the respiratory region of the nasal cavity, the part which is innervated by trigeminal nerves, is also highly vascularised due to its large surface area so any drugs that reach the respiratory region has a high likelihood of being circulated systemically (Crowe et al., 2018). That said, most of the drug enters the brain *via* the olfactory region following intranasal administration, and when using this mode of administration much lower drug concentrations can be given due to reduced metabolism, therefore any risk of side effects would be vastly decreased and any formulations that end up in circulation could still access the brain *via* the BBB (Crowe et al., 2018).

Once these additional studies are complete, the formulations could then be tested in phase 1 safety trials of healthy volunteers. However, as all these compounds are already approved either as dietary supplements or as a pharmaceutical, the route to clinical translation may be shorter when using the P68+DQA nanoformulation. This is because the P68 and DQA components of the nanocarrier are also already widely used; P68, otherwise known as Poloxamer 188, is used as an inactive ingredient in numerous FDA approved drugs (FDA, 2020f) and DQA is used to treat bacterial vaginosis in the UK due to its bactericidal anti-infective properties (NICE, 2020). Furthermore, the use of lipid nanoparticles to deliver the Pfizer-BioNTech (Oliver et al., 2020) and the SARS-CoV-2 (Keech et al., 2020) COVID-19 vaccinations has made great progress in promoting the use of nanocarrier delivery systems in clinical therapy. Therefore, it is possible that the formulations could be tested directly in phase 2a safety studies of people with PD rather than healthy volunteers, because all the constituent parts of all these formulations are already considered safe for human use and similar nanoformulations are already being used clinically for vaccinations. It would be worthwhile discussing this option with the FDA and MHRA in advance to determine whether phase 1 is required because bypassing this step would shorten the timeline needed for

these formulations to be potentially translated into real world treatments for people with PD.

7.3. Conclusion

Overall, it is clear that this study has achieved its primary aim outlined in chapter one: to develop novel nanoformulations of iron chelators and antioxidants that can pass the BBB and target mitochondria, to reduce oxidative stress and dopaminergic neuronal death in a cellular PD model. These promising results therefore pave the way for additional preclinical testing of these novel formulations so they can be moved forward as potential disease modifying treatments for people with PD.

References

Abbate, V., Reelfs, O., Hider, R. C., & Pourzand, C. (2015). Design of novel fluorescent mitochondria-targeted peptides with iron-selective sensing activity. *Biochemical Journal*, *469*(3), 357-366.

Åberg, C. (2016). Quantitative analysis of nanoparticle transport through in vitro blood-brain barrier models. *Tissue barriers*, *4*(1), e1143545.

Abbott, N. J., Rönnbäck, L., & Hansson, E. (2006). Astrocyte–endothelial interactions at the blood–brain barrier. Nature Reviews Neuroscience, 7(1), 41.9.

Abrahams, S., Haylett, W. L., Johnson, G., Carr, J. A., & Bardien, S. (2019). Antioxidant effects of curcumin in models of neurodegeneration, aging, oxidative and nitrosative stress: A review. *Neuroscience*, *406*, 1-21.

Acorda Theraputics (2017). Acorda Announces Long-Term Safety Data for CVT-301. Retrieved from Accorda Theraputics: http://s1.q4cdn.com/271808180/files/doc_news/2017/FINAL-004E-005-Press-Release-032917.pdf. Accessed April 26, 2018.

Agrawal, S. S., Gullaiya, S., Dubey, V., Singh, V., Kumar, A., Nagar, A., & Tiwari, P. (2012). Neurodegenerative shielding by curcumin and its derivatives on brain lesions induced by 6-OHDA model of Parkinson's disease in albino wistar rats. *Cardiovascular psychiatry and neurology*, *2012*.

Aldini, G., Altomare, A., Baron, G., Vistoli, G., Carini, M., Borsani, L., & Sergio, F. (2018). N-Acetylcysteine as an antioxidant and disulphide breaking agent: the reasons why. *Free radical research*, *52*(7), 751-762.

Alexander, A., & Saraf, S. (2018). Nose-to-brain drug delivery approach: A key to easily accessing the brain for the treatment of Alzheimer's disease. *Neural regeneration research*, *13*(12), 2102.

Al-Qenaei, A., Yiakouvaki, A., Reelfs, O., Santambrogio, P., Levi, S., Hall, N. D., ... & Pourzand, C. (2014). Role of intracellular labile iron, ferritin, and antioxidant defence in resistance of chronically adapted Jurkat T cells to hydrogen peroxide. *Free Radical Biology and Medicine*, *68*, 87-100.

Amic, D., Davidovic-Amic, D., Beslo, D., Rastija, V., Lucic, B., & Trinajstic, N. (2007). SAR and QSAR of the antioxidant activity of flavonoids. *Current medicinal chemistry*, *14*(7), 827-845.

Ammon, H. P., & Wahl, M. A. (1991). Pharmacology of Curcuma longa. *Planta medica*, *57*(01), 1-7.

Andersen, J. K. (2004). Oxidative stress in neurodegeneration: cause or consequence? *Nature medicine*, *10*(7), S18.

Anders, M. W., & Dekant, W. (1994). Aminoacylases. *Advances in Pharmacology*, *27*, 431-431.

Anselmo, A. C., & Mitragotri, S. (2016). Nanoparticles in the clinic. *Bioengineering & translational medicine*, *1*(1), 10-29.

Anon, A. O. A. C. (2012). SMPR 2011.011. Standard method performance requirements for in vitro determination of total antioxidant activity in foods, beverages, food ingredients, and dietary supplements. *J. AOAC Int*, *956*, 1557.

Arakawa, M., & Ito, Y. (2007). N-acetylcysteine and neurodegenerative diseases: basic and clinical pharmacology. *The Cerebellum*, *6*(4), 308-314.

Arvizo, R. R., Miranda, O. R., Moyano, D. F., Walden, C. A., Giri, K., Bhattacharya, R., ... & Mukherjee, P. (2011). Modulating pharmacokinetics, tumor uptake and biodistribution by engineered nanoparticles. *PloS one*, *6*(9), e24374.

Arfsten, D. P., Johnson, E. W., Wilfong, E. R., Jung, A. E., & Bobb, A. J. (2007). Distribution of radio-labeled N-Acetyl-L-Cysteine in Sprague-Dawley rats and its effect on glutathione metabolism following single and repeat dosing by oral gavage. *Cutaneous and ocular toxicology*, *26*(2), 113-134.

Arstall, M. A., Yang, J., Stafford, I., Betts, W. H., & Horowitz, J. D. (1995). N-acetylcysteine in combination with nitroglycerin and streptokinase for the treatment of evolving acute myocardial infarction: safety and biochemical effects. *Circulation*, *92*(10), 2855-2862.

Artus, C., Glacial, F., Ganeshamoorthy, K., Ziegler, N., Godet, M., Guilbert, T., ... & Couraud, P. O. (2014). The Wnt/planar cell polarity signaling pathway contributes to the

integrity of tight junctions in brain endothelial cells. *Journal of Cerebral Blood Flow & Metabolism*, *34*(3), 433-440.

Ak, T., & Gülçin, İ. (2008). Antioxidant and radical scavenging properties of curcumin. *Chemico-biological interactions*, *174*(1), 27-37.

Ayton, S., Lei, P., Duce, J. A., Wong, B. X., Sedjahtera, A., Adlard, P. A., ... & Finkelstein, D. I. (2013). Ceruloplasmin dysfunction and therapeutic potential for Parkinson disease. *Annals of neurology*, *73*(4), 554-559.

Bae, Y., Jung, M. K., Lee, S., Song, S. J., Mun, J. Y., Green, E. S., ... & Choi, J. S. (2018). Dequalinium-based functional nanosomes show increased mitochondria targeting and anticancer effect. *European Journal of Pharmaceutics and Biopharmaceutics*, *124*, 104-115.

Bali, P. K., Zak, O., & Aisen, P. (1991). A new role for the transferrin receptor in the release of iron from transferrin. *Biochemistry*, *30*(2), 324-328.

Balogun, E., Hoque, M., Gong, P., Killeen, E., Green, C. J., Foresti, R., Alam, J., & Motterlini, R. (2003). Curcumin activates the haem oxygenase-1 gene via regulation of Nrf2 and the antioxidant-responsive element. *Biochemical Journal*, *371*(3), 887-895.

Barbusiński, K. (2009). Fenton reaction-controversy concerning the chemistry. *Ecological Chemistry and Engineering. S*, *16*(3), 347-358.

Barodia, S. K., Creed, R. B., & Goldberg, M. S. (2017). Parkin and PINK1 functions in oxidative stress and neurodegeneration. *Brain research bulletin*, *133*, 51-59.

Barua, S., & Mitragotri, S. (2014). Challenges associated with penetration of nanoparticles across cell and tissue barriers: a review of current status and future prospects. *Nano today*, *9*(2), 223-243.

Barzi, F., Woodward, M., Marfisi, R. M., Tavazzi, L., Valagussa, F., & Marchioli, R. (2003). Mediterranean diet and all-causes mortality after myocardial infarction: results from the GISSI-Prevenzione trial. *European journal of clinical nutrition*, *57*(4), 604.

Batrakova, E. V., & Kabanov, A. V. (2008). Pluronic block copolymers: evolution of drug delivery concept from inert nanocarriers to biological response modifiers. *Journal of controlled release*, *130*(2), 98-106.

Bayanzay, K., & Alzoebie, L. (2016). Reducing the iron burden and improving survival in transfusion-dependent thalassemia patients: current perspectives. *Journal of blood medicine*, *7*, 159.

Bavarsad Shahripour, R., Harrigan, M. R., & Alexandrov, A. V. (2014). N-acetylcysteine (NAC) in neurological disorders: mechanisms of action and therapeutic opportunities. *Brain and behavior*, *4*(2), 108-122.

Begum, A. N., Jones, M. R., Lim, G. P., Morihara, T., Kim, P., Heath, D. D., Rock, C.L., Pruitt, M.A., Yang, F., Hudspeth, B. & Hu, S. (2008). Curcumin structure-function, bioavailability, and efficacy in models of neuroinflammation and Alzheimer's disease. *Journal of Pharmacology and Experimental Therapeutics*, *326*(1), 196-208.

Ben-Shachar, D., & Youdim, M. B. H. (1991). Intranigral iron injection induces behavioral and biochemical "parkinsonism" in rats. Journal of neurochemistry, 57(6), 2133-2135.

Bernabé-Pineda, M., Ramírez-Silva, M. T., Romero-Romo, M. A., González-Vergara, E., & Rojas-Hernández, A. (2004). Spectrophotometric and electrochemical determination of the formation constants of the complexes Curcumin–Fe (III)–water and Curcumin–Fe (II)–water. *Spectrochimica Acta Part A: Molecular and Biomolecular Spectroscopy*, *60*(5), 1105-1113.

Betarbet, R., Canet-Aviles, R. M., Sherer, T. B., Mastroberardino, P. G., McLendon, C., Kim, J. H., ... & Greenamyre, J. T. (2006). Intersecting pathways to neurodegeneration in Parkinson's disease: Effects of the pesticide rotenone on DJ-1, α-synuclein, and the ubiquitin–proteasome system. *Neurobiology of disease*, *22*(2), 404-420.

Birch-Machin, M. A. (2000). Mitochondria and skin disease. *Clinical and experimental dermatology*, *25*(2), 141-146.

Birch-Machin, M. A. (2006). The role of mitochondria in ageing and carcinogenesis. *Clinical and experimental dermatology*, *31*(4), 548-552.

Birch-Machin, M. A., & Swalwell, H. (2009). How mitochondria record the effects of UV exposure and oxidative stress using human skin as a model tissue. *Mutagenesis*, *25*(2), 101-107.

Bissonette, G. B., & Roesch, M. R. (2016). Development and function of the midbrain dopamine system: what we know and what we need to. *Genes, Brain and Behavior*, *15*(1), 62-73.

Boddaert, N., Le Quan Sang, K. H., Rötig, A., Leroy-Willig, A., Gallet, S., Brunelle, F., ... & Cabantchik, Z. I. (2007). Selective iron chelation in Friedreich ataxia: biologic and clinical implications. *Blood*, *110*(1), 401-408.

Bou-Abdallah, F., McNally, J., Liu, X. X., & Melman, A. (2011). Oxygen catalyzed mobilization of iron from ferritin by iron (III) chelate ligands. *Chemical communications*, *47*(2), 731-733.

Bou-Abdallah, F., Paliakkara, J. J., Melman, G., & Melman, A. (2018). Reductive mobilization of iron from intact ferritin: mechanisms and physiological implication. *Pharmaceuticals*, *11*(4), 120.

Bourassa, P., Kanakis, C. D., Tarantilis, P., Pollissiou, M. G., & Tajmir-Riahi, H. A. (2010). Resveratrol, genistein, and curcumin bind bovine serum albumin. *The Journal of Physical Chemistry B*, *114*(9), 3348-3354.

Bradbury, M. W. B. (1997). Transport of Iron in the Blood-Brain-Cerebrospinal Fluid System. *Journal of neurochemistry*, *69*(2), 443-454.

Bratic, A., & Larsson, N. G. (2013). The role of mitochondria in aging. *The Journal of clinical investigation*, *123*(3), 951-957.

Bramini, M., Ye, D., Hallerbach, A., Nic Raghnaill, M., Salvati, A., Aberg, C., & Dawson, K. A. (2014). Imaging approach to mechanistic study of nanoparticle interactions with the blood–brain barrier. ACS Nano, 8, 4304-4312.

Bressler, J., Clark, K., & O'Driscoll, C. (2013). Assessing Blood–Brain Barrier Function Using In Vitro Assays. In *Cell-Cell Interactions* (pp. 67-79). Humana Press, Totowa, NJ.

Brittenham, G. M. (2011). Iron-chelating therapy for transfusional iron overload. *New England Journal of Medicine*, *364*(2), 146-156.

Brundin, P., & Wyse, R. K. (2019). The Linked Clinical Trials initiative (LCT) for Parkinson's disease. *European Journal of Neuroscience*, *49*(3), 307-315.

Brundin, P., Dave, K. D., & Kordower, J. H. (2017). Therapeutic approaches to target alpha-synuclein pathology. *Experimental neurology*, *298*, 225-235.

Bulteau, A. L., O'Neill, H. A., Kennedy, M. C., Ikeda-Saito, M., Isaya, G., & Szweda, L. I. (2004). Frataxin acts as an iron chaperone protein to modulate mitochondrial aconitase activity. *Science*, *305*(5681), 242-245

Burdo, J. R., Martin, J., Menzies, S. L., Dolan, K. G., Romano, M. A., Fletcher, R. J., ... & Connor, J. R. (1999). Cellular distribution of iron in the brain of the Belgrade rat. Neuroscience, 93(3), 1189-1196.

Burdo, J. R., Simpson, I. A., Menzies, S., Beard, J., & Connor, J. R. (2004). Regulation of the profile of iron-management proteins in brain microvasculature. *Journal of Cerebral Blood Flow & Metabolism*, *24*(1), 67-74.

Burkhart, A., Skjørringe, T., Johnsen, K. B., Siupka, P., Thomsen, L. B., Nielsen, M. S., ... & Moos, T. (2016). Expression of iron-related proteins at the neurovascular unit supports reduction and reoxidation of iron for transport through the blood-brain barrier. *Molecular neurobiology*, *53*(10), 7237-7253.

Buss, J. L., Torti, F. M., & Torti, S. V. (2003). The role of iron chelation in cancer therapy. *Current medicinal chemistry*, *10*(12), 1021-1034.

Cahill, C. M., Lahiri, D. K., Huang, X., & Rogers, J. T. (2009). Amyloid precursor protein and alpha synuclein translation, implications for iron and inflammation in neurodegenerative diseases. *Biochimica et Biophysica Acta (BBA)-General Subjects*, *1790*(7), 615-628.

Camilleri, A., & Vassallo, N. (2014). The centrality of mitochondria in the pathogenesis and treatment of Parkinson's disease. *CNS neuroscience & therapeutics*, *20*(7), 591-602.

Cantrill, C. A., Skinner, R. A., Rothwell, N. J., & Penny, J. I. (2012). An immortalised astrocyte cell line maintains the in vivo phenotype of a primary porcine in vitro blood–brain barrier model. *Brain research*, *1479*, 17-30.

Carl, S. M., Lindley, D. J., Das, D., Couraud, P. O., Weksler, B. B., Romero, I., ... & Knipp, G. T. (2010). ABC and SLC transporter expression and proton oligopeptide transporter (POT) mediated permeation across the human blood--brain barrier cell line, hCMEC/D3 [corrected]. *Molecular pharmaceutics*, *7*(4), 1057-1068.

Carlsson, A. (2006). The neurochemical circuitry of schizophrenia. *Pharmacopsychiatry, 39*(1), S10-S14.

Catalá, A. (2009). Lipid peroxidation of membrane phospholipids generates hydroxy-alkenals and oxidized phospholipids active in physiological and/or pathological conditions. *Chemistry and physics of lipids*, *157*(1), 1-11.

Cerami, C. (2017). Iron nutriture of the fetus, neonate, infant, and child. *Annals of Nutrition and Metabolism*, *71*(Suppl. 3), 8-14.

Cerrato, C. P., Pirisinu, M., Vlachos, E. N., & Langel, Ü. (2015). Novel cell-penetrating peptide targeting mitochondria. *The FASEB Journal*, *29*(11), 4589-4599.

Chan, D. K. Y., Xu, Y. H., Chan, L. K. M., Braidy, N., & Mellick, G. D. (2017). Mini-review on initiatives to interfere with the propagation and clearance of alpha-synuclein in Parkinson's disease. *Translational neurodegeneration*, *6*(1), 33.

Chakraborti, S., Chakraborty, S., Saha, S., Manna, A., Banerjee, S., Adhikary, A., ... & Chakrabarti, P. (2017). PEG-functionalized zinc oxide nanoparticles induce apoptosis in breast cancer cells through reactive oxygen species-dependent impairment of DNA damage repair enzyme NEIL2. *Free Radical Biology and Medicine*, *103*, 35-47.

Chen, C. M., Yin, M. C., Hsu, C. C., & Liu, T. C. (2007). Antioxidative and anti-inflammatory effects of four cysteine-containing agents in striatum of MPTP-treated mice. *Nutrition*, *23*(7), 589-597.

Chen, H., Lukas, T. J., Du, N., Suyeoka, G., & Neufeld, A. H. (2009). Dysfunction of the retinal pigment epithelium with age: increased iron decreases phagocytosis and lysosomal activity. *Investigative ophthalmology & visual science*, *50*(4), 1895-1902.

Chen, L., Hambright, W. S., Na, R., & Ran, Q. (2015). Ablation of the ferroptosis inhibitor glutathione peroxidase 4 in neurons results in rapid motor neuron degeneration and paralysis. Journal of Biological Chemistry, 290(47), 28097-28106.

Chen, X., Zou, L. Q., Niu, J., Liu, W., Peng, S. F., & Liu, C. M. (2015). The stability, sustained release and cellular antioxidant activity of curcumin nanoliposomes. *Molecules*, *20*(8), 14293-14311.

Chiabrando, D., Vinchi, F., Fiorito, V., Mercurio, S., & Tolosano, E. (2014). Heme in patho-physiology: a matter of scavenging, metabolism and trafficking across cell membranes. *Frontiers in pharmacology*, *5*, 61.

Chiang, S., Kalinowski, D. S., Jansson, P. J., Richardson, D. R., & Huang, M. L. H. (2018). Mitochondrial dysfunction in the neuro-degenerative and cardio-degenerative disease, Friedreich's ataxia. *Neurochemistry international*, *117*, 35-48.

Choi, J. J., Wang, S., Tung, Y. S., Morrison III, B., & Konofagou, E. E. (2010). Molecules of various pharmacologically-relevant sizes can cross the ultrasound-induced blood-brain barrier opening in vivo. *Ultrasound in medicine & biology*, *36*(1), 58-67.

Chu, Y., Morfini, G. A., Langhamer, L. B., He, Y., Brady, S. T., & Kordower, J. H. (2012). Alterations in axonal transport motor proteins in sporadic and experimental Parkinson's disease. *Brain*, *135*(7), 2058-2073.

Chung, C. Y., Koprich, J. B., Siddiqi, H., & Isacson, O. (2009). Dynamic changes in presynaptic and axonal transport proteins combined with striatal neuroinflammation precede dopaminergic neuronal loss in a rat model of AAV α-synucleinopathy. *Journal of Neuroscience*, *29*(11), 3365-3373.

Chung, K. K., Thomas, B., Li, X., Pletnikova, O., Troncoso, J. C., Marsh, L., ... & Dawson, T. M. (2004). S-nitrosylation of parkin regulates ubiquitination and compromises parkin's protective function. *Science*, *304*(5675), 1328-1331.

Ciechanover, Aa, A. L. Schwartz, A. Dautry-Varsat, and H. F. Lodish. "Kinetics of internalization and recycling of transferrin and the transferrin receptor in a human hepatoma cell line. Effect of lysosomotropic agents." *Journal of Biological Chemistry* 258, no. 16 (1983): 9681-9689.

Clark, J., Clore, E. L., Zheng, K., Adame, A., Masliah, E., & Simon, D. K. (2010). Oral N-acetyl-cysteine attenuates loss of dopaminergic terminals in α-synuclein overexpressing mice. *PLoS One*, *5*(8), e12333.

ClinicalTrials.gov. (2018a, March 29). *Study of Parkinson's Early Stage With Deferiprone (SKY)*. Retrieved from NIH U.S. NAtional Library of Medicine: ClinicalTrials.gov: https://clinicaltrials.gov/ct2/show/NCT02728843?term=deferiprone&cond=Parkinson&rank=1

ClinicalTrials.gov. (2018b, March 29). *Conservative Iron Chelation as a Disease-modifying Strategy in Parkinson's Disease (FAIRPARKII)*. Retrieved from NIH U.S. National Library of Medicine: Clinical Trials.gov: https://clinicaltrials.gov/ct2/show/NCT02655315?term=deferiprone&cond=Parkinson&rank=4

ClinicalTrials.gov. (2018c, March 29). *NAC | Parkinson*. Retrieved from NIH U.S. National Library of Medicine: ClinicalTrials.gov: https://clinicaltrials.gov/ct2/results?cond=Parkinson&term=NAC&cntry=&state=&city=&dist=&Search=Search

Committee for Medicinal Products for Human Use (CHMP). (2018). Qualification opinion on dopamine transporter imaging as an enrichment biomarker for Parkinson's disease clinical trials in patients with early Parkinsonian symptoms. Retrieved from European Medicines Agency: https://www.ema.europa.eu/en/documents/regulatory-procedural-guideline/qualification-opinion-dopamine-transporter-imaging-enrichment-biomarker-parkinsons-disease-clinical_en.pdf. Accessed May 4, 2020.

Costa-Mallen, P., Gatenby, C., Friend, S., Maravilla, K. R., Hu, S. C., Cain, K. C., ... & Anzai, Y. (2017). Brain iron concentrations in regions of interest and relation with serum iron levels in Parkinson disease. *Journal of the neurological sciences*, *378*, 38-44.

Costa-Mallen, P., Zabetian, C. P., Agarwal, P., Hu, S. C., Yearout, D., Samii, A., ... & Checkoway, H. (2015). Haptoglobin phenotype modifies serum iron levels and the effect of smoking on Parkinson disease risk. *Parkinsonism & related disorders*, *21*(9), 1087-1092.

Cotgreave, I. A., & Moldéus, P. (1987). Methodologies for the analysis of reduced and oxidized N-acetylcysteine in biological systems. *Biopharmaceutics & drug disposition*, *8*(4), 365-375.

Crichton, R. R., Wilmet, S., Legssyer, R., & Ward, R. J. (2002). Molecular and cellular mechanisms of iron homeostasis and toxicity in mammalian cells. *Journal of inorganic biochemistry*, *91*(1), 9-18.

Crichton, R., & Ward, R. (2013). *Metal-based neurodegeneration: from molecular mechanisms to therapeutic strategies*. John Wiley & Sons.
Da Poian, A. T., BACHA, T., & Luz, M. R. M. P. (2010). Nutrient Utilization in Humans: Metabolic Pathways.

Cristante, E., McArthur, S., Mauro, C., Maggioli, E., Romero, I. A., Wylezinska-Arridge, M., ... & Malaspina, A. (2013). Identification of an essential endogenous regulator of blood–brain barrier integrity, and its pathological and therapeutic implications. *Proceedings of the National Academy of Sciences*, *110*(3), 832-841.

Crowe, T. P., Greenlee, M. H. W., Kanthasamy, A. G., & Hsu, W. H. (2018). Mechanism of intranasal drug delivery directly to the brain. *Life sciences*, *195*, 44-52.

Cruz, L. J., Stammes, M. A., Que, I., van Beek, E. R., Knol-Blankevoort, V. T., Snoeks, T. J., ... & Löwik, C. W. (2016). Effect of PLGA NP size on efficiency to target traumatic brain injury. *Journal of Controlled Release*, *223*, 31-41.

D'Angelo, S., Manna, C., Migliardi, V., Mazzoni, O., Morrica, P., Capasso, G., G., Pontoni, G., Galletti, P. & Zappia, V. (2001). Pharmacokinetics and metabolism of hydroxytyrosol, a natural antioxidant from olive oil. *Drug Metabolism and Disposition*, *29*(11), 1492-1498.

de las Hazas, M. C. L., Godinho-Pereira, J., Macià, A., Almeida, A. F., Ventura, M. R., Motilva, M. J., & Santos, C. N. (2018). Brain uptake of hydroxytyrosol and its main circulating metabolites: Protective potential in neuronal cells. *Journal of Functional Foods*, *46*, 110-117.

Do Van, B., Gouel, F., Jonneaux, A., Timmerman, K., Gele, P., Petrault, M., ... & Devos, D. (2016). Ferroptosis, a newly characterized form of cell death in Parkinson's disease that is regulated by PKC. *Neurobiology of disease*, *94*, 169-178.

Dalle-Donne, I., Giustarini, D., Colombo, R., Rossi, R., & Milzani, A. (2003a). Protein carbonylation in human diseases. *Trends in molecular medicine*, *9*(4), 169-176.

Dalle-Donne, I., Rossi, R., Giustarini, D., Milzani, A., & Colombo, R. (2003b). Protein carbonyl groups as biomarkers of oxidative stress. *Clinica chimica acta*, *329*(1-2), 23-38. D'Angelo, S., Manna, C., Migliardi, V., Mazzoni, O., Morrica, P., Capasso, G., ... & Zappia, V. (2001). Pharmacokinetics and metabolism of hydroxytyrosol, a natural antioxidant from olive oil. *Drug Metabolism and Disposition*, *29*(11), 1492-1498.

Das, D., Luo, X., Singh, A., Gu, Y., Ghosh, S., Mukhopadhyay, C. K., ... & Singh, N. (2010). Paradoxical role of prion protein aggregates in redox-iron induced toxicity. *PLoS One*, *5*(7), e11420.

Davis, B. M., Pahlitzsch, M., Guo, L., Balendra, S., Shah, P., Ravindran, N., ... & Noor, A. (2018). Topical curcumin nanocarriers are neuroprotective in eye disease. *Scientific reports*, *8*(1), 11066.

Decressac, M., Kadkhodaei, B., Mattsson, B., Laguna, A., Perlmann, T., & Björklund, A. (2012). α-synuclein–induced down-regulation of Nurr1 disrupts GDNF signaling in nigral dopamine neurons. *Science translational medicine*, *4*(163), 163ra156-163ra156.

Decressac, M., Ulusoy, A., Mattsson, B., Georgievska, B., Romero-Ramos, M., Kirik, D., & Björklund, A. (2011). GDNF fails to exert neuroprotection in a rat α-synuclein model of Parkinson's disease. *Brain*, *134*(8), 2302-2311.

Dexter, D.T., Statton, S.A., Whitmore, C., Freinbichler, W., Weinberger, P., Tipton, K.F., Della Corte, L., Ward, R.J. and Crichton, R.R., (2011). Clinically available iron chelators induce neuroprotection in the 6-OHDA model of Parkinson's disease after peripheral administration. *Journal of neural transmission*, *118*(2), 223-231.

Dexter, D. T., Wells, F. R., Agid, F., Agid, Y., Lees, A. J., Jenner, P., & Marsden, C. D. (1987). Increased nigral iron content in postmortem parkinsonian brain. *The Lancet*, *330*(8569), 1219-1220.

Dinkova-Kostova, A. T., Massiah, M. A., Bozak, R. E., Hicks, R. J., & Talalay, P. (2001). Potency of Michael reaction acceptors as inducers of enzymes that protect against carcinogenesis depends on their reactivity with sulfhydryl groups. *Proceedings of the National Academy of Sciences*, *98*(6), 3404-3409.

Di Nicola, M., Barteselli, G., Dell'Arti, L., Ratiglia, R., & Viola, F. (2015). Functional and structural abnormalities in deferoxamine retinopathy: a review of the literature. *BioMed research international*, *2015*.

Dixon, S. J., Lemberg, K. M., Lamprecht, M. R., Skouta, R., Zaitsev, E. M., Gleason, C. E., ... & Morrison III, B. (2012). Ferroptosis: an iron-dependent form of nonapoptotic cell death. Cell, 149(5), 1060-1072.

Dlouhy, A. C., & Outten, C. E. (2013). The iron metallome in eukaryotic organisms. In *Metallomics and the Cell* (pp. 241-278). Springer, Dordrecht.

Dorsey, E. R., Elbaz, A., Nichols, E., Abd-Allah, F., Abdelalim, A., Adsuar, J. C., Ansha, M.G., Brayne, C., Choi, J.Y.J., Collado-Mateo, D & Dahodwala, N. (2018). Global, regional, and national burden of Parkinson's disease, 1990–2016: a systematic analysis for the Global Burden of Disease Study 2016. *The Lancet Neurology*, *17*(11), 939-953.

Doughan, A. K., & Dikalov, S. I. (2007). Mitochondrial redox cycling of mitoquinone leads to superoxide production and cellular apoptosis. *Antioxidants & redox signaling*, *9*(11), 1825-1836.

Dove, A., 2008. Breaching the barrier: the blood-brain barrier has confounded the development of many neurological treatments over the years. Now, several companies are claiming they can tackle the problem. Alan Dove reports. *Nature biotechnology*, *26*(11), pp.1213-1216.

Duck, K. A., Neely, E. B., Simpson, I. A., & Connor, J. R. (2017b). A role for sex and a common HFE gene variant in brain iron uptake. Journal of Cerebral Blood Flow & Metabolism, 0271678X17701949.

Duck, K. A., Simpson, I. A., & Connor, J. R. (2017a). Regulatory mechanisms for iron transport across the blood-brain barrier. *Biochemical and biophysical research communications*, *494*(1-2), 70-75.

Duffy, P. E., & Tennyson, V. M. (1965). Phase and electron microscopic observations of Lewy bodies and melanin granules in the substantia nigra and locus caeruleus in Parkinson's disease. *Journal of Neuropathology & Experimental Neurology*, *24*(3), 398-414.

Dutta, R. K., Nenavathu, B. P., Gangishetty, M. K., & Reddy, A. V. R. (2012). Studies on antibacterial activity of ZnO nanoparticles by ROS induced lipid peroxidation. *Colloids and Surfaces B: Biointerfaces*, *94*, 143-150.

Doggui, S.; Sahni, J.K.; Arseneault, M.; Dao, L.; Ramassamy, C. Neuronal uptake and neuroprotective effect of curcumin-loaded PLGA nanoparticles on the human SK-N-SH cell line. J. Alzheimers Dis. 2012, 30, 377–392.

Eigenmann, D. E., Xue, G., Kim, K. S., Moses, A. V., Hamburger, M., & Oufir, M. (2013). Comparative study of four immortalized human brain capillary endothelial cell lines, hCMEC/D3, hBMEC, TY10, and BB19, and optimization of culture conditions, for an in vitro blood–brain barrier model for drug permeability studies. *Fluids and Barriers of the CNS*, *10*(1), 33.

Elbakary, B., & Badhan, R. K. (2020). A dynamic perfusion based blood-brain barrier model for cytotoxicity testing and drug permeation. *Scientific Reports*, *10*(1), 1-12.

Elezaby, R. S., Gad, H. A., Metwally, A. A., Geneidi, A. S., & Awad, G. A. (2017). Self-assembled amphiphilic core-shell nanocarriers in line with the modern strategies for brain delivery. *Journal of Controlled Release*, *261*, 43-61.

Elliott, R. L., & Head, J. F. (2012). Cancer: tumor iron metabolism, mitochondrial dysfunction and tumor immunosuppression;"a tight partnership—was Warburg correct?".

Elston, T., Wang, H., & Oster, G. (1998). Energy transduction in ATP synthase. *Nature*, *391*(6666), 510.

Erikson, K. M., Pinero, D. J., Connor, J. R., & Beard, J. L. (1997). Regional brain iron, ferritin and transferrin concentrations during iron deficiency and iron repletion in developing rats. *The Journal of nutrition*, *127*(10), 2030-2038.

España, R. A., & Jones, S. R. (2013). Presynaptic dopamine modulation by stimulant self-administration. *Frontiers in bioscience (Scholar edition)*, *5*, 261.

Exner, N., Lutz, A. K., Haass, C., & Winklhofer, K. F. (2012). Mitochondrial dysfunction in Parkinson's disease: molecular mechanisms and pathophysiological consequences. *The EMBO journal*, *31*(14), 3038-3062.

Farcich, E. A., & Morgan, E. H. (1992). Uptake of transferrin-bound and nontransferrin-bound iron by reticulocytes from the belgrade laboratory rat: Comparison with wistar rat transferrin and reticulocytes. *American journal of hematology*, *39*(1), 9-14.

Farr, A. C., & Xiong, M. P. (2020). Challenges and Opportunities of Deferoxamine Delivery for Treatment of Alzheimer's Disease, Parkinson's Disease, and Intracerebral Hemorrhage. *Molecular Pharmaceutics, 9*(1456), 1-43.

Fasano, M., Bergamasco, B., & Lopiano, L. (2006). Modifications of the iron–neuromelanin system in Parkinson's disease. *Journal of neurochemistry*, *96*(4), 909-916.

Fato, R., Bergamini, C., Bortolus, M., Maniero, A. L., Leoni, S., Ohnishi, T., & Lenaz, G. (2009). Differential effects of mitochondrial Complex I inhibitors on production of reactive oxygen species. *Biochimica et Biophysica Acta (BBA)-Bioenergetics*, *1787*(5), 384-392.

FDA . (2020a, December 11th). GRAS Notices - Curcumin. Retrieved from U.S. Food and Drug Administration:
https://www.cfsanappsexternal.fda.gov/scripts/fdcc/?set=GRASNotices&sort=GRN_No&order=DESC&startrow=1&type=basic&search=curcumin

FDA. (2020b, December 11th). GRAS Notices. Retrieved from U.S. Food and Drug Administration:
https://www.cfsanappsexternal.fda.gov/scripts/fdcc/?set=GRASNotices&sort=GRN_No&order=DESC&startrow=1&type=basic&search=hydroxytyrosol

FDA. (2020c, December 11th). Drug Approval Package - Acetadote. Retrieved from U.S. Food and Drug Administration:
https://www.accessdata.fda.gov/drugsatfda_docs/nda/2004/21-539_Acetadote.cfm

FDA. (2020d, December 11th). Drug Approval Package - Deferoxamine Mesylate Injection. Retrieved from U.S. Food and Drug Administration:
https://www.accessdata.fda.gov/drugsatfda_docs/nda/2004/076019_s000_DeferoxamineTOC.cfm

FDA. (2020e, December 11th). Guidance for Industry ANDAs: Stability Testing of Drug Substances and Products. Retrieved from U.S Food and Drug Administrator:
https://www.fda.gov/media/87051/download#:~:text=The%20FDA%20stability%20guidance%20recommends,scientific%20review%20of%20the%20DMF

FDA. (2020f, December 11th). Inactive Ingredient Search for Approved Drug Products. Retrieved from U.S. Food and Drug Administration:
https://www.accessdata.fda.gov/scripts/cder/iig/index.cfm?event=browseByLetter.page&Letter=P

Feart, C., Samieri, C., Rondeau, V., Amieva, H., Portet, F., Dartigues, J. F., ... & Barberger-Gateau, P. (2009). Adherence to a Mediterranean diet, cognitive decline, and risk of dementia. *Jama*, *302*(6), 638-648.

Ferreira, L. F., Campbell, K. S., & Reid, M. B. (2011). N-acetylcysteine in handgrip exercise: plasma thiols and adverse reactions. *International journal of sport nutrition and exercise metabolism*, *21*(2), 146-154.

Ferrari, E., Benassi, R., Sacchi, S., Pignedoli, F., Asti, M., & Saladini, M. (2014). Curcumin derivatives as metal-chelating agents with potential multifunctional activity for pharmaceutical applications. *Journal of Inorganic Biochemistry*, *139*, 38-48.

Fineberg, N. A., Haddad, P. M., Carpenter, L., Gannon, B., Sharpe, R., Young, A. H., ... & Sahakian, B. J. (2013). The size, burden and cost of disorders of the brain in the UK. *Journal of Psychopharmacology*, *27*(9), 761-770.

Forno, L. S., & Norville, R. L. (1976). Ultrastructure of Lewy bodies in the stellate ganglion. *Acta neuropathologica*, *34*(3), 183-197.

Förster, C., Burek, M., Romero, I. A., Weksler, B., Couraud, P. O., & Drenckhahn, D. (2008). Differential effects of hydrocortisone and TNFα on tight junction proteins in an in vitro model of the human blood–brain barrier. *The Journal of physiology*, *586*(7), 1937-1949.

Frazier, M. D., Mamo, L. B., Ghio, A. J., & Turi, J. L. (2011). Hepcidin expression in human airway epithelial cells is regulated by interferon-γ. *Respiratory research*, *12*(1), 100.

Friedlich, A. L., Tanzi, R. E., & Rogers, J. T. (2007). The 5'-untranslated region of Parkinson's disease α-synuclein messengerRNA contains a predicted iron responsive element. *Molecular psychiatry*, *12*(3), 222.

Funakohi-Tago, M., Sakata, T., Fujiwara, S., Sakakura, A., Sugai, T., Tago, K., & Tamura, H. (2018). Hydroxytyrosol butyrate inhibits 6-OHDA-induced apoptosis through activation of the Nrf2/HO-1 axis in SH-SY5Y cells. *European journal of pharmacology*, *834*, 246-256.

Gakh, O., Park, S., Liu, G., Macomber, L., Imlay, J.A., Ferreira, G.C. and Isaya, G., 2006. Mitochondrial iron detoxification is a primary function of frataxin that limits oxidative damage and preserves cell longevity. *Human molecular genetics*, *15*(3), pp.467-479.

Galanello, R. (2007). Deferiprone in the treatment of transfusion-dependent thalassemia: a review and perspective. *Therapeutics and clinical risk management*, *3*(5), 795.

Gałązka-Friedman, J., Bauminger, E. R., Friedman, A., Barcikowska, M., Hechel, D., & Nowik, I. (1996). Iron in parkinsonian and control substantia nigra—A Mössbauer spectroscopy study. Movement disorders, 11(1), 8-16.

Gałązka-Friedman, J., Bauminger, E. R., Friedman, A., Koziorowski, D., & Szlachta, K. (2005). Human nigral and liver iron–comparison by Mössbauer spectroscopy, electron microscopy and ELISA. Hyperfine interactions, 165(1-4), 285-288.

Ganz, T. (2013). Systemic iron homeostasis. *Physiological reviews*, *93*(4), 1721-1741.
Ganz, T., & Nemeth, E. (2012). Hepcidin and iron homeostasis. *Biochimica et Biophysica Acta (BBA)-Molecular Cell Research*, *1823*(9), 1434-1443.

Ganz, T., & Nemeth, E. (2015). Iron homeostasis in host defence and inflammation. *Nature Reviews Immunology*, *15*(8), 500.

Ganesan, P.; Narayanasamy, D. Lipid nanoparticles: Different preparation techniques, characterization, hurdles, and strategies for the production of solid lipid nanoparticles and nanostructured lipid carriers for oral drug delivery. Sustain. Chem. Pharm. 2017, 6, 37–56.

Ganguly, U., Ganguly, A., Sen, O., Ganguly, G., Cappai, R., Sahoo, A., & Chakrabarti, S. (2019). Dopamine cytotoxicity on SH-SY5Y cells: Involvement of α-synuclein and relevance in the neurodegeneration of sporadic Parkinson's disease. *Neurotoxicity research*, *35*(4), 898-907.

Gaucher, G., Dufresne, M. H., Sant, V. P., Kang, N., Maysinger, D., & Leroux, J. C. (2005). Block copolymer micelles: preparation, characterization and application in drug delivery. *Journal of controlled release*, *109*(1-3), 169-188.

Grabrucker, A. M., Ruozi, B., Belletti, D., Pederzoli, F., Forni, F., Vandelli, M. A., & Tosi, G. (2016). Nanoparticle transport across the blood brain barrier. *Tissue barriers*, *4*(1), e1153568.

Griffiths, P. D., Dobson, B. R., Jones, G. R., & Clarke, D. T. (1999). Iron in the basal ganglia in Parkinson's disease: An in vitro study using extended X-ray absorption fine structure and cryo-electron microscopy. Brain, 122(4), 667-673.

Garrick, M. D., Gniecko, K., Liu, D. S., Cohan, D. S., & Garrick, L. M. (1993). Transferrin and the transferrin cycle in Belgrade rat reticulocytes. Journal of Biological Chemistry, 268(20), 14867-14874.

Garrido, M., Tereshchenko, Y., Zhevtsova, Z., Taschenberger, G., Bähr, M., & Kügler, S. (2011). Glutathione depletion and overproduction both initiate degeneration of nigral dopaminergic neurons. *Acta neuropathologica*, *121*(4), 475-485.

Gautier, C. A., Corti, O., & Brice, A. (2014). Mitochondrial dysfunctions in Parkinson's disease. *Revue neurologique*, *170*(5), 339-343.

Gerlach, M., Ben-Shachar, D., Riederer, P., & Youdim, M. B. H. (1994). Altered brain metabolism of iron as a cause of neurodegenerative diseases?. Journal of neurochemistry, 63(3), 793-807.

Gerlach, M., Double, K. L., Youdim, M. B. H., & Riederer, P. (2006). Potential sources of increased iron in the substantia nigra of parkinsonian patients. In Parkinson's Disease and Related Disorders (pp. 133-142). Springer, Vienna.

Gimenez, F., Krauze, M. T., Valles, F., Hadaczek, P., Bringas, J., Sharma, N., ... & Bankiewicz, K. S. (2011). Image-guided convection-enhanced delivery of GDNF protein into monkey putamen. *Neuroimage*, *54*, S189-S195.

Glinka, Y., Gassen, M., & Youdim, M. B. H. (1997). Mechanism of 6-hydroxydopamine neurotoxicity. In *Advances in Research on Neurodegeneration* (pp. 55-66). Springer, Vienna.

Gnana-Prakasam, J. P., Martin, P. M., Mysona, B. A., Roon, P., Smith, S. B., & Ganapathy, V. (2008). Hepcidin expression in mouse retina and its regulation via lipopolysaccharide/Toll-like receptor-4 pathway independent of Hfe. *Biochemical Journal*, *411*(1), 79-88.

Godin, B., Chiappini, C., Srinivasan, S., Alexander, J. F., Yokoi, K., Ferrari, M., ... & Liu, X. (2012). Drug Delivery: Discoidal Porous Silicon Particles: Fabrication and Biodistribution in Breast Cancer Bearing Mice (Adv. Funct. Mater. 20/2012). *Advanced Functional Materials*, *22*(20), 4186-4186.

Goldman-Rakic, P. S. (1995). Cellular basis of working memory. *Neuron, 14*, 477-485.

Goldstein, D. S., Jinsmaa, Y., Sullivan, P., & Sharabi, Y. (2017). N-Acetylcysteine Prevents the Increase in Spontaneous Oxidation of Dopamine During Monoamine Oxidase Inhibition in PC12 Cells. *Neurochemical research*, *42*(11), 3289-3295.

Golts, N., Snyder, H., Frasier, M., Theisler, C., Choi, P., & Wolozin, B. (2002). Magnesium inhibits spontaneous and iron-induced aggregation of α-synuclein. *Journal of Biological Chemistry*, *277*(18), 16116-16123.

González-Correa, J. A., Navas, M. D., Lopez-Villodres, J. A., Trujillo, M., Espartero, J. L., & De La Cruz, J. P. (2008). Neuroprotective effect of hydroxytyrosol and hydroxytyrosol acetate in rat brain slices subjected to hypoxia–reoxygenation. *Neuroscience letters*, *446*(2-3), 143-146.

Götz, M. E., Double, K. A. Y., Gerlach, M., Youdim, M. B., & Riederere, P. (2004). The relevance of iron in the pathogenesis of Parkinson's disease. Annals of the New York Academy of Sciences, 1012(1), 193-208.

Govoni, G., Gauthier, S., Billia, F., Iscove, N. N., & Gros, P. (1997). Cell-specific and inducible Nramp1 gene expression in mouse macrophages in vitro and in vivo. *Journal of leukocyte biology*, *62*(2), 277-286.

Goldstein, D. S., Jinsmaa, Y., Sullivan, P., & Sharabi, Y. (2017). N-acetylcysteine prevents the increase in spontaneous oxidation of dopamine during monoamine oxidase inhibition in PC12 cells. *Neurochemical research*, *42*(11), 3289-3295.

Goldstein, D. S., Jinsmaa, Y., Sullivan, P., Holmes, C., Kopin, I. J., & Sharabi, Y. (2016). 3, 4-Dihydroxyphenylethanol (hydroxytyrosol) mitigates the increase in spontaneous oxidation of dopamine during monoamine oxidase inhibition in PC12 cells. *Neurochemical research*, *41*(9), 2173-2178.

Gonzalez-Carter, D., Goode, A. E., Kiryushko, D., Masuda, S., Hu, S., Lopes-Rodrigues, R., ... & Porter, A. E. (2019). Quantification of blood–brain barrier transport and neuronal toxicity of unlabelled multiwalled carbon nanotubes as a function of surface charge. *Nanoscale*, *11*(45), 22054-22069.

Graham, J. M., Paley, M. N., Grünewald, R. A., Hoggard, N., & Griffiths, P. D. (2000). Brain iron deposition in Parkinson's disease imaged using the PRIME magnetic resonance sequence. *Brain*, *123*(12), 2423-2431.

Granados-Principal, S., El-Azem, N., Pamplona, R., Ramirez-Tortosa, C., Pulido-Moran, M., Vera-Ramirez, L., ... & Perez-Lopez, P. (2014). Hydroxytyrosol ameliorates oxidative stress and mitochondrial dysfunction in doxorubicin-induced cardiotoxicity in rats with breast cancer. *Biochemical pharmacology*, *90*(1), 25-33.

Greene, J. C., Whitworth, A. J., Andrews, L. A., Parker, T. J., & Pallanck, L. J. (2005). Genetic and genomic studies of Drosophila parkin mutants implicate oxidative stress and innate immune responses in pathogenesis. *Human molecular genetics*, *14*(6), 799-811.

Griffiths, P. D., Dobson, B. R., Jones, G. R., & Clarke, D. T. (1999). Iron in the basal ganglia in Parkinson's disease: An in vitro study using extended X-ray absorption fine structure and cryo-electron microscopy. *Brain*, *122*(4), 667-673.

Guerzoni, L. P., Nicolas, V., & Angelova, A. (2017). In vitro modulation of TrkB receptor signaling upon sequential delivery of curcumin-DHA loaded carriers towards promoting neuronal survival. *Pharmaceutical research*, *34*(2), 492-505.

Gynther, M., Laine, K., Ropponen, J., Leppänen, J., Mannila, A., Nevalainen, T., ... & Rautio, J. (2008). Large neutral amino acid transporter enables brain drug delivery via prodrugs. *Journal of medicinal chemistry*, *51*(4), 932-936.

Hagl, S., Kocher, A., Schiborr, C., Kolesova, N., Frank, J., & Eckert, G. P. (2015). Curcumin micelles improve mitochondrial function in neuronal PC12 cells and brains of NMRI mice–Impact on bioavailability. *Neurochemistry international*, *89*, 234-242.

Halliwell, B. (2001). Role of free radicals in the neurodegenerative diseases. Drugs & aging, 18(9), 685-716.

Hamdi, A., Roshan, T. M., Kahawita, T. M., Mason, A. B., Sheftel, A. D., & Ponka, P. (2016). Erythroid cell mitochondria receive endosomal iron by a "kiss-and-run" mechanism. *Biochimica Et Biophysica Acta (BBA)-Molecular Cell Research*, *1863*(12), 2859-2867.

Han, J. M., Lee, Y. J., Lee, S. Y., Kim, E. M., Moon, Y., Kim, H. W., & Hwang, O. (2007). Protective effect of sulforaphane against dopaminergic cell death. *Journal of Pharmacology and Experimental Therapeutics*, *321*(1), 249-256.

Hanke, M. L., & Kielian, T. (2011). Toll-like receptors in health and disease in the brain: mechanisms and therapeutic potential. *Clinical Science*, *121*(9), 367-387.

Hare, D. J., Adlard, P. A., Doble, P. A., & Finkelstein, D. I. (2013). Metallobiology of 1-methyl-4-phenyl-1, 2, 3, 6-tetrahydropyridine neurotoxicity. *Metallomics*, *5*(2), 91-109.

Hare, D. J., Lei, P., Ayton, S., Roberts, B. R., Grimm, R., George, J. L., ... & Volitakis, I. (2014). An iron–dopamine index predicts risk of parkinsonian neurodegeneration in the substantia nigra pars compacta. *Chemical Science*, *5*(6), 2160-2169.

Hashimoto, T., Ibi, M., Matsuno, K., Nakashima, S., Tanigawa, T., Yoshikawa, T., & Yabe-Nishimura, C. (2004). An endogenous metabolite of dopamine, 3, 4-dihydroxyphenylethanol, acts as a unique cytoprotective agent against oxidative stress-induced injury. *Free Radical Biology and Medicine*, *36*(5), 555-564.

Hayashida, K., Oyanagi, S., Mizutani, Y., & Yokochi, M. (1993). An early cytoplasmic change before Lewy body maturation: an ultrastructural study of the substantia nigra from an autopsy case of juvenile parkinsonism. *Acta neuropathologica*, *85*(4), 445-448.

Heinz, S., Freyberger, A., Lawrenz, B., Schladt, L., Schmuck, G., & Ellinger-Ziegelbauer, H. (2017). Mechanistic investigations of the mitochondrial complex I inhibitor rotenone in the context of pharmacological and safety evaluation. *Scientific reports*, *7*(1), 1-13.

Helms, H. C., Abbott, N. J., Burek, M., Cecchelli, R., Couraud, P. O., Deli, M. A., ... & Stebbins, M. J. (2016). In vitro models of the blood–brain barrier: an overview of commonly used brain endothelial cell culture models and guidelines for their use. *Journal of Cerebral Blood Flow & Metabolism*, *36*(5), 862-890.

Hidalgo, C. and Núñez, M.T., 2007. Calcium, iron and neuronal function. *IUBMB life*, *59*(4-5), pp.280-285.

Hill, J. M., & Switzer Iii, R. C. (1984). The regional distribution and cellular localization of iron in the rat brain. *Neuroscience*, *11*(3), 595-603.

Hochstrasser, H., Bauer, P., Walter, U., Behnke, S., Spiegel, J., Csoti, I., ... & Riess, O. (2004). Ceruloplasmin gene variations and substantia nigra hyperechogenicity in Parkinson disease. *Neurology*, *63*(10), 1912-1917.

Hong, W., Shi, H., Qiao, M., Zhang, Z., Yang, W., Dong, L., ... & Kang, L. (2017). pH-sensitive micelles for the intracellular co-delivery of curcumin and Pluronic L61 unimers for synergistic reversal effect of multidrug resistance. *Scientific Reports*, *7*, 42465.

Hörmann, K., & Zimmer, A. (2016). Drug delivery and drug targeting with parenteral lipid nanoemulsions—a review. *Journal of Controlled Release*, *223*, 85-98.

Horowitz, M. P., & Greenamyre, J. T. (2010). Mitochondrial iron metabolism and its role in neurodegeneration. *Journal of Alzheimer's disease*, *20*(s2), S551-S568.

Hu, B., Ting, Y., Zeng, X., & Huang, Q. (2013). Bioactive peptides/chitosan nanoparticles enhance cellular antioxidant activity of (−)-epigallocatechin-3-gallate. *Journal of agricultural and food chemistry*, *61*(4), 875-881.

Hu, X., Yang, F. F., Quan, L. H., Liu, C. Y., Liu, X. M., Ehrhardt, C., & Liao, Y. H. (2014). Pulmonary delivered polymeric micelles–pharmacokinetic evaluation and biodistribution studies. *European Journal of Pharmaceutics and Biopharmaceutics*, *88*(3), 1064-1075.

Hung, H. I., Schwartz, J. M., Maldonado, E. N., Lemasters, J. J., & Nieminen, A. L. (2013). Mitoferrin-2-dependent mitochondrial iron uptake sensitizes human head and neck squamous carcinoma cells to photodynamic therapy. *Journal of Biological Chemistry*, *288*(1), 677-686.

Hunot, S., & Hirsch, E. C. (2003). Neuroinflammatory processes in Parkinson's disease. *Annals of neurology*, *53*(S3).

Hunter, R. L., Liu, M., Choi, D. Y., Cass, W. A., & Bing, G. (2008). Inflammation and age-related iron accumulation in F344 rats. *Current aging science*, *1*(2), 112-121.

Huang, X., Li, L., Liu, T., Hao, N., Liu, H., Chen, D., & Tang, F. (2011). The shape effect of mesoporous silica nanoparticles on biodistribution, clearance, and biocompatibility in vivo. *ACS nano*, *5*(7), 5390-5399.

Hassan, M. A. M., & Tolba, O. A. (2016). Iron chelation monotherapy in transfusion-dependent beta-thalassemia major patients: a comparative study of deferasirox and deferoxamine. *Electronic physician*, *8*(5), 2425.

Hjortsrø, E., Fomsgaard, J. S., & Fogh-Andersen, N. (1990). Does N-acetylcysteine increase the excretion of trace metals (calcium, magnesium, iron, zinc and copper) when given orally?. *European journal of clinical pharmacology*, *39*(1), 29-31.

Hoyles, L., Snelling, T., Umlai, U. K., Nicholson, J. K., Carding, S. R., Glen, R. C., & McArthur, S. (2018). Microbiome–host systems interactions: protective effects of propionate upon the blood–brain barrier. *Microbiome*, *6*(1), 55.

Iadecola, C. (2004). Neurovascular regulation in the normal brain and in Alzheimer's disease. Nature Reviews Neuroscience, 5(5), 347.

Illum, L. (2003). Nasal drug delivery—possibilities, problems and solutions. *Journal of controlled release*, *87*(1-3), 187-198.

Jankovic J. Parkinson's disease: clinical features and diagnosis. *J Neurol Neurosurg Psychiatry.* 2008;79(4):368–376.

Jáuregui-Lobera, I. (2014). Iron deficiency and cognitive functions. *Neuropsychiatric disease and treatment*, *10*, 2087.

Jauslin, M. L., Meier, T., Smith, R. A., & Murphy, P. M. (2003). Mitochondria-targeted antioxidants protect Friedreich Ataxia fibroblasts from endogenous oxidative stress more effectively than untargeted antioxidants. *The FASEB journal*, *17*(13), 1-10.

Jayaraj, Richard L., Kuppusamy Tamilselvam, Thamilarasan Manivasagam, and Namasivayam Elangovan. "Neuroprotective effect of CNB-001, a novel pyrazole derivative of curcumin on biochemical and apoptotic markers against rotenone-induced SK-N-SH cellular model of Parkinson's disease." *Journal of Molecular Neuroscience* 51, no. 3 (2013): 863-870.

Jenner, P., & Olanow, C. W. (1996). Oxidative stress and the pathogenesis of Parkinson's disease. *Neurology*, *47*(6 Suppl 3), 161S-170S.

Jiang, H., Wang, J., Rogers, J., & Xie, J. (2017). Brain iron metabolism dysfunction in Parkinson's disease. Molecular neurobiology, 54(4), 3078-3101.

Jiang, T. F., Zhang, Y. J., Zhou, H. Y., Wang, H. M., Tian, L. P., Liu, J., ... & Chen, S. D. (2013). Curcumin ameliorates the neurodegenerative pathology in A53T α-synuclein cell model of Parkinson's disease through the downregulation of mTOR/p70S6K signaling and the recovery of macroautophagy. *Journal of Neuroimmune Pharmacology*, *8*(1), 356-369.

Jiao, Y., Wilkinson IV, J., Pietsch, E. C., Buss, J. L., Wang, W., Planalp, R., ... & Torti, S. V. (2006). Iron chelation in the biological activity of curcumin. *Free Radical Biology and Medicine*, *40*(7), 1152-1160.

Juillerat-Jeanneret, L. (2008). The targeted delivery of cancer drugs across the blood–brain barrier: chemical modifications of drugs or drug-nanoparticles?. *Drug discovery today*, *13*(23-24), 1099-1106.

Kandola, K., Bowman, A., & Birch-Machin, M. A. (2015). Oxidative stress–a key emerging impact factor in health, ageing, lifestyle and aesthetics. *International journal of cosmetic science*, *37*(S2), 1-8.

Kataoka, K., Harada, A., & Nagasaki, Y. (2012). Block copolymer micelles for drug delivery: design, characterization and biological significance. *Advanced drug delivery reviews*, *64*, 37-48.

Katz, M., Won, S. J., Park, Y., Orr, A., Jones, D. P., Swanson, R. A., & Glass, G. A. (2015). Cerebrospinal fluid concentrations of N-acetylcysteine after oral administration in Parkinson's disease. *Parkinsonism & related disorders*, *21*(5), 500-503.

Kaur, M., & Badhan, R. K. (2017). Phytochemical mediated-modulation of the expression and transporter function of breast cancer resistance protein at the blood-brain barrier: An in-vitro study. *Brain research*, *1654*, 9-23.

Kaushal, V., & Schlichter, L. C. (2008). Mechanisms of microglia-mediated neurotoxicity in a new model of the stroke penumbra. *Journal of Neuroscience*, *28*(9), 2221-2230.

Kawamura, E., Yamada, Y., Yasuzaki, Y., Hyodo, M., & Harashima, H. (2013). Intracellular observation of nanocarriers modified with a mitochondrial targeting signal peptide. *Journal of bioscience and bioengineering*, *116*(5), 634-637.

Keech, C., Albert, G., Cho, I., Robertson, A., Reed, P., Neal, S., ... & Glenn, G. M. (2020). Phase 1–2 trial of a SARS-CoV-2 recombinant spike protein nanoparticle vaccine. *New England Journal of Medicine*, *383*(24), 2320-2332.

Khalatbary, A. R. (2013). Olive oil phenols and neuroprotection. *Nutritional neuroscience*, *16*(6), 243-249.

Khalil, S., Holy, M., Grado, S., Fleming, R., Kurita, R., Nakamura, Y., & Goldfarb, A. (2017). A specialized pathway for erythroid iron delivery through lysosomal trafficking of transferrin receptor 2. *Blood advances*, *1*(15), 1181-1194.

Kitsati, N., Mantzaris, M. D., & Galaris, D. (2016). Hydroxytyrosol inhibits hydrogen peroxide-induced apoptotic signaling via labile iron chelation. *Redox biology*, *10*, 233-242.

Knutson, M. D. (2017). Iron transport proteins: Gateways of cellular and systemic iron homeostasis. *Journal of Biological Chemistry*, *292*(31), 12735-12743.

Knutson, M., Menzies, S., Connor, J., & Wessling-Resnick, M. (2004). Developmental, regional, and cellular expression of SFT/UbcH5A and DMT1 mRNA in brain. *Journal of neuroscience research*, *76*(5), 633-641.

Konnova, E. A., & Swanberg, M. (2018). Animal models of Parkinson's disease. *Exon Publications*, 83-106.

Kontoghiorghes, G. J., & Kontoghiorghe, C. N. (2020). Iron and Chelation in Biochemistry and Medicine: New Approaches to Controlling Iron Metabolism and Treating Related Diseases. *Cells*, *9*(6), 1456.

Koziorowski, D., Friedman, A., Arosio, P., Santambrogio, P., & Dziewulska, D. (2007). ELISA reveals a difference in the structure of substantia nigra ferritin in Parkinson's disease and incidental Lewy body compared to control. Parkinsonism & related disorders, 13(4), 214-218.

Kreuter, J. (2001). Nanoparticulate systems for brain delivery of drugs. *Advanced drug delivery reviews*, *47*(1), 65-81.

Krige, D., Carroll, M. T., Cooper, J. M., Marsden, C. D., Schapira, A. H., & Royal Kings Queens Parkinson Disease Research Group). (1992). Platelet mitochondria function in Parkinson's disease. *Annals of neurology*, *32*(6), 782-788.

Kroemer, G., & Reed, J. C. (2000). Mitochondrial control of cell death. *Nature medicine*, *6*(5), 513.

Kumar, T. A., David, G. F., Sankaranarayanan, A., Puri, V., & Sundram, K. R. (1982). Pharmacokinetics of progesterone after its administration to ovariectomized rhesus monkeys by injection, infusion, or nasal spraying. *Proceedings of the National Academy of Sciences*, *79*(13), 4185-4189.

Kumar, S. S. D., Mahesh, A., Mahadevan, S., & Mandal, A. B. (2014). Synthesis and characterization of curcumin loaded polymer/lipid based nanoparticles and evaluation of their antitumor effects on MCF-7 cells. *Biochimica et Biophysica Acta (BBA)-General Subjects*, *1840*(6), 1913-1922.

Kwok, J. B. (2010). Role of epigenetics in Alzheimer's and Parkinson's disease. *Epigenomics*, *2*(5), 671-682.

Kwon, G. S., & Okano, T. (1996). Polymeric micelles as new drug carriers. *Advanced drug delivery reviews*, *21*(2), 107-116.

Lamberts, J. T., Hildebrandt, E. N., & Brundin, P. (2015). Spreading of α-synuclein in the face of axonal transport deficits in Parkinson's disease: a speculative synthesis. *Neurobiology of disease*, *77*, 276-283.

Langston, W. (1987). MPTP: insights into the etiology of Parkinson's disease. *European neurology*, *26*(Suppl. 1), 2-10.

Laschinski, G., Kittner, B., & Bräutigam, M. (1986). Direct inhibition of tyrosine hydroxylase from PC-12 cells by catechol derivatives. *Naunyn-Schmiedeberg's archives of pharmacology*, *332*(4), 346-350.

LaVoie, M. J., Ostaszewski, B. L., Weihofen, A., Schlossmacher, M. G., & Selkoe, D. J. (2005). Dopamine covalently modifies and functionally inactivates parkin. *Nature medicine*, *11*(11), 1214.

Lee, H. J., Khoshaghideh, F., Patel, S., & Lee, S. J. (2004). Clearance of α-synuclein oligomeric intermediates via the lysosomal degradation pathway. *Journal of Neuroscience*, *24*(8), 1888-1896.

Lee, J. M., & Johnson, J. A. (2004). An important role of Nrf2-ARE pathway in the cellular defense mechanism. *BMB Reports*, *37*(2), 139-143.

Lees, A. J., Hardy, J., & Revesz T. (2009) Parkinson's disease. *Lancet 373,* 2055–2066.

Levi, S., & Finazzi, D. (2014). Neurodegeneration with brain iron accumulation: update on pathogenic mechanisms. *Frontiers in pharmacology*, *5*, 99.

Levi, S., & Rovida, E. (2009). The role of iron in mitochondrial function. *Biochimica et Biophysica Acta (BBA)-General Subjects*, *1790*(7), 629-636.

Levi, S., Santambrogio, P., Cozzi, A., Rovida, E., Corsi, B., Tamborini, E., ... & Arosio, P. (1994). The role of the L-chain in ferritin iron incorporation: studies of homo and heteropolymers.

Lewis, D. A., & Gonza ´lez-Burgos, G. (2008). Neuroplasticityof neocortical circuits in schizophrenia.

Lee, M. H., Shin, G. H., & Park, H. J. (2018). Solid lipid nanoparticles loaded thermoresponsive pluronic–xanthan gum hydrogel as a transdermal delivery system. *Journal of Applied Polymer Science*, *135*(11), 46004.

Li, N., Ragheb, K., Lawler, G., Sturgis, J., Rajwa, B., Melendez, J. A., & Robinson, J. P. (2003). Mitochondrial complex I inhibitor rotenone induces apoptosis through enhancing mitochondrial reactive oxygen species production. *Journal of Biological Chemistry*, *278*(10), 8516-8525.

Little, A. C., Kovalenko, I., Goo, L. E., Hong, H. S., Kerk, S. A., Yates, J. A., ... & Lyssiotis, C. A. (2020). High-content fluorescence imaging with the metabolic flux assay reveals insights into mitochondrial properties and functions. *Communications biology*, *3*(1), 1-10.

Liu, Z., Li, T., Yang, D., & Smith, W. W. (2013). Curcumin protects against rotenone-induced neurotoxicity in cell and drosophila models of Parkinson's disease. Advances in Parkinson'S Disease, 2(01), 18.

Liu, Z., Shen, H. C., Lian, T. H., Mao, L., Tang, S. X., Sun, L., ... & Zuo, L. J. (2017). Iron deposition in substantia nigra: abnormal iron metabolism, neuroinflammatory mechanism and clinical relevance. Scientific reports, 7(1), 14973.

Liu, J. S., Wang, J. H., Zhou, J., Tang, X. H., Xu, L., Shen, T., ... & Hong, Z. (2014). Enhanced brain delivery of lamotrigine with Pluronic® P123-based nanocarrier. *International journal of nanomedicine*, *9*, 3923.

Liu, Z., Purro, M., Qiao, J., & Xiong, M. P. (2017). Multifunctional polymeric micelles for combining chelation and detection of iron in living cells. *Advanced healthcare materials*, *6*(17), 1700162.

Liu, L., Mao, K., Wang, W., Pan, H., Wang, F., Yang, M., & Liu, H. (2016). Kolliphor® HS 15 micelles for the delivery of coenzyme Q10: preparation, characterization, and stability. *AAPS PharmSciTech*, *17*(3), 757-766.

Luo, Y., Eggler, A. L., Liu, D., Liu, G., Mesecar, A. D., & van Breemen, R. B. (2007). Sites of alkylation of human Keap1 by natural chemoprevention agents. *Journal of the American Society for Mass Spectrometry*, *18*(12), 2226-2232.

Lockman, P. R., Koziara, J. M., Mumper, R. J., & Allen, D. D. (2004). Nanoparticle surface charges alter blood–brain barrier integrity and permeability. *Journal of drug targeting*, *12*(9-10), 635-641.

Lombardo, L., Grasso, F., Lanciano, F., Loria, S., & Monetti, E. (2018). Broad-spectrum health protection of extra virgin olive oil compounds. In *Studies in natural products chemistry* (Vol. 57, pp. 41-77). Elsevier.

Lopez, A., Munoz, A., Guerra, M. J., & Labandeira-Garcia, J. L. (2001). Mechanisms of the effects of exogenous levodopa on the dopamine-denervated striatum. *Neuroscience*, *103*(3), 639-651.

Lyrawati, D., Trounson, A., Cram, D. (2011). Expression of GFP in the mitochondrial compartment using DQAsome-mediated delivery of an artificial mini-mitochondrial genome. Pharm. Res., 28 (11), 2848–62.

Ma, Z.; Haddadi, A.; Molavi, O.; Lavasanifar, A.; Lai, R.; Samuel, J. Micelles of poly(ethyleneoxide)-b-poly(epsilon-caprolactone) as vehicles for the solubilization, stabilization, and controlled delivery of curcumin. J. Biomed. Mater. Res. A 2008, 86, 300–310.

Magesh, S., Chen, Y., & Hu, L. (2012). Small molecule modulators of Keap1-Nrf2-ARE pathway as potential preventive and therapeutic agents. *Medicinal research reviews*, *32*(4), 687-726.

Mahoney-Sánchez, L., Bouchaoui, H., Ayton, S., Devos, D., Duce, J. A., & Devedjian, J. C. (2021). Ferroptosis and its potential role in the physiopathology of Parkinson's Disease. *Progress in neurobiology*, *196*, 101890.

Mantri, S., & Morley, J. F. (2018). Prodromal and early Parkinson's disease diagnosis. *PRACTICAL NEUROLOGY, 28-51*.

Martell, A. E., & Smith, R. M. (1974). *Critical stability constants* (Vol. 1, p. 135). New York: Plenum press.

Martin, W. R. W., Wieler, M., & Gee, M. (2008). Midbrain iron content in early Parkinson disease A potential biomarker of disease status. Neurology, 70(16 Part 2), 1411-1417.

Martin-Bastida, A., Ward, R. J., Newbould, R., Piccini, P., Sharp, D., Kabba, C., ... & Crichton, R. R. (2017). Brain iron chelation by deferiprone in a phase 2 randomised double-blinded placebo controlled clinical trial in Parkinson's disease. Scientific reports, 7(1), 1398.

Martin, W. R. W., Wieler, M., & Gee, M. (2008). Midbrain iron content in early Parkinson disease A potential biomarker of disease status. *Neurology*, *70*(16 Part 2), 1411-1417.

Martin-Bastida, A., Ward, R. J., Newbould, R., Piccini, P., Sharp, D., Kabba, C., ... & Crichton, R. R. (2017). Brain iron chelation by deferiprone in a phase 2 randomised double-blinded placebo controlled clinical trial in Parkinson's disease. *Scientific reports*, *7*(1), 1398.

Masserini, M., 2013. Nanoparticles for brain drug delivery. ISRN biochemistry, 2013.

Mastroberardino, P. G., Hoffman, E. K., Horowitz, M. P., Betarbet, R., Taylor, G., Cheng, D., ... & Greenamyre, J. T. (2009). A novel transferrin/TfR2-mediated mitochondrial iron transport system is disrupted in Parkinson's disease. *Neurobiology of disease*, *34*(3), 417-431.

Matak, P., Matak, A., Moustafa, S., Aryal, D. K., Benner, E. J., Wetsel, W., & Andrews, N. C. (2016). Disrupted iron homeostasis causes dopaminergic neurodegeneration in mice. *Proceedings of the National Academy of Sciences*, *113*(13), 3428-3435.

Mathur, S., Mursaleen, L., Stamford, J., DeWitte, S., Robledo, I., & Isaacs, T. (2017). Challenges of Improving Patient-Centred Care in Parkinson's Disease. *Journal of Parkinson's disease*, *7*(1), 163-174.

Matsuda, N., Sato, S., Shiba, K., Okatsu, K., Saisho, K., Gautier, C. A., ... & Kimura, M. (2010). PINK1 stabilized by mitochondrial depolarization recruits Parkin to damaged mitochondria and activates latent Parkin for mitophagy. *The Journal of cell biology*, *189*(2), 211-221.

Maggioli, E., McArthur, S., Mauro, C., Kieswich, J., Kusters, D. H. M., Reutelingsperger, C. P. M., ... & Solito, E. (2016). Estrogen protects the blood–brain barrier from inflammation-induced disruption and increased lymphocyte trafficking. *Brain, behavior, and immunity*, *51*, 212-222.

Martínez, M. A., Rodríguez, J. L., Lopez-Torres, B., Martínez, M., Martínez-Larrañaga, M. R., Maximiliano, J. E., ... & Ares, I. (2020). Use of human neuroblastoma SH-SY5Y cells to evaluate glyphosate-induced effects on oxidative stress, neuronal development and cell death signaling pathways. *Environment International*, *135*, 105414.

Melidou, M., Riganakos, K., & Galaris, D. (2005). Protection against nuclear DNA damage offered by flavonoids in cells exposed to hydrogen peroxide: the role of iron chelation. *Free Radical Biology and Medicine*, *39*(12), 1591-1600.
Mena, N. P., Bulteau, A. L., Salazar, J., Hirsch, E. C., & Núñez, M. T. (2011). Effect of mitochondrial complex I inhibition on Fe–S cluster protein activity. *Biochemical and biophysical research communications*, *409*(2), 241-246.

MHRA. (2020, December 11th). Medicines & Healthcare products Regulatory Agency. Common Issues: Pharmaceutical. Retrieved from GOV.UK: https://www.gov.uk/government/publications/common-issues-identified-during-clinical-trial-applications/common-issues-pharmaceutical

Miro-Casas, E., Covas, M. I., Farre, M., Fito, M., Ortuño, J., Weinbrenner, T., Roset, P. & de la Torre, R. (2003). Hydroxytyrosol disposition in humans. *Clinical chemistry*, *49*(6), 945-952.

Monti, D. A., Zabrecky, G., Kremens, D., Liang, T. W., Wintering, N. A., Bazzan, A. J., ... & Newberg, A. B. (2019). N-Acetyl Cysteine Is Associated With Dopaminergic Improvement in Parkinson's Disease. *Clinical Pharmacology & Therapeutics*, *106*(4), 884-890.

Mouhape, C., Costa, G., Ferreira, M., Abin-Carriquiry, J. A., Dajas, F., & Prunell, G. (2019). Nicotine-induced neuroprotection in rotenone in vivo and in vitro models of Parkinson's disease: Evidences for the involvement of the labile iron pool level as the underlying mechanism. *Neurotoxicity research*, *35*(1), 71-82.

McCarthy, R. C., & Kosman, D. J. (2012). Mechanistic analysis of iron accumulation by endothelial cells of the BBB. *Biometals*, *25*(4), 665-675.

McCarthy, R. C., & Kosman, D. J. (2013). Ferroportin and exocytoplasmic ferroxidase activity are required for brain microvascular endothelial cell iron efflux. Journal of Biological Chemistry, 288(24), 17932-17940.

McCarthy, R. C., & Kosman, D. J. (2014). Glial cell ceruloplasmin and hepcidin differentially regulate iron efflux from brain microvascular endothelial cells. PLoS One, 9(2), e89003.

McCarthy, R. C., & Kosman, D. J. (2015). Iron transport across the blood–brain barrier: development, neurovascular regulation and cerebral amyloid angiopathy. *Cellular and molecular life sciences*, *72*(4), 709-727.

Melis, J. P., van Steeg, H., & Luijten, M. (2013). Oxidative DNA damage and nucleotide excision repair. *Antioxidants & redox signaling*, *18*(18), 2409-2419.

Meyer-Lindenberg, A. (2010). From maps to mechanisms through neuroimaging of schizophrenia. *Nature, 468*(11), 194-202.

Middleton, F. A., & Strick, P. L. (2000). basal ganglia output and cognition: Evidence from anatomical, behavioural and clinical studies. *Brain and Cognition, 42*, 183-200.

Misaka, E., & Tappel, A. L. (1971). Inhibition studies of cathepsins A, B, C and D from rat liver lysosomes. Comparative Biochemistry and Physiology Part B: Comparative Biochemistry, 38(4), 651-662.

Mobarra, N., Shanaki, M., Ehteram, H., Nasiri, H., Sahmani, M., Saeidi, M., ... & Azad, M. (2016). A review on iron chelators in treatment of iron overload syndromes. *International journal of hematology-oncology and stem cell research*, *10*(4), 239.

Mogi, M., Harada, M., Kondo, T., Riederer, P., Inagaki, H., Minami, M., & Nagatsu, T. (1994a). Interleukin-1β, interleukin-6, epidermal growth factor and transforming growth factor-α are elevated in the brain from parkinsonian patients. *Neuroscience letters*, *180*(2), 147-150.

Mogi, M., Harada, M., Narabayashi, H., Inagaki, H., Minami, M., & Nagatsu, T. (1996). Interleukin (IL)-1β, IL-2, IL-4, IL-6 and transforming growth factor-α levels are elevated in ventricular cerebrospinal fluid in juvenile parkinsonism and Parkinson's disease. *Neuroscience letters*, *211*(1), 13-16.

Mogi, M., Harada, M., Riederer, P., Narabayashi, H., Fujita, K., & Nagatsu, T. (1994b). Tumor necrosis factor-α (TNF-α) increases both in the brain and in the cerebrospinal fluid from parkinsonian patients. *Neuroscience letters*, *165*(1-2), 208-210.

Mohanty, C., & Sahoo, S. K. (2010). The in vitro stability and in vivo pharmacokinetics of curcumin prepared as an aqueous nanoparticulate formulation. Biomaterials, 31(25), 6597-6611.

Molino, Y., Jabès, F., Lacassagne, E., Gaudin, N., & Khrestchatisky, M. (2014). Setting-up an in vitro model of rat blood-brain barrier (BBB): a focus on BBB impermeability and receptor-mediated transport. *Journal of visualized experiments: JoVE*, (88).

Monteiro, H. P., & Winterbourn, C. C. (1989). 6-Hydroxydopamine releases iron from ferritin and promotes ferritin-dependent lipid peroxidation. *Biochemical pharmacology*, *38*(23), 4177-4182.

Monti, D. A., Zabrecky, G., Kremens, D., Liang, T. W., Wintering, N. A., Cai, J., ... & Intenzo, C. M. (2016). N-acetyl cysteine may support dopamine neurons in Parkinson's disease: Preliminary clinical and cell line data. *PloS one*, *11*(6), e0157602.

Moon, H. E., & Paek, S. H. (2015). Mitochondrial dysfunction in Parkinson's disease. *Experimental neurobiology*, *24*(2), 103-116.

Moore, T. J., Glenmullen, J., & Mattison, D. R. (2014). Reports of pathological gambling, hypersexuality, and compulsive shopping associated with dopamine receptor agonist drugs. *JAMA internal medicine*, *174*(12), 1930-1933.

Moos, T., & Morgan, E. H. (2004). The significance of the mutated divalent metal transporter (DMT1) on iron transport into the Belgrade rat brain. Journal of neurochemistry, 88(1), 233-245.

Mursaleen, L., Somavarapu, S., & Zariwala, M. G. (2020a). Deferoxamine and Curcumin Loaded Nanocarriers Protect Against Rotenone-Induced Neurotoxicity. *Journal of Parkinson's Disease*, *10*(1), 99-111.

Mursaleen, L., Noble, B., Chan, S. H. Y., Somavarapu, S., & Zariwala, M. G. (2020b). N-Acetylcysteine nanocarriers protect against oxidative stress in a cellular model of Parkinson's disease. *Antioxidants*, *9*(7), 600.

Mursaleen, L. R., & Stamford, J. A. (2016). Drugs of abuse and Parkinson's disease. *Progress in Neuro-Psychopharmacology and Biological Psychiatry*, *64*, 209-217.

Mursaleen, L. R., Stamford, J. A., Butterfield, T., Edwards, G., Kustow, P., Kustow, P. A., ... & Dudgeon, M. G. (2017). Descriptive symptom terminology used by Parkinson's patients and caregivers. *Journal of Parkinsonism and Restless Legs Syndrome*, *7*, 71-78.

Nakamura, Y., & Miyoshi, N. (2010). Electrophiles in foods: the current status of isothiocyanates and their chemical biology. *Bioscience, biotechnology, and biochemistry*, *74*(2), 242-255.

Narendra, D., Tanaka, A., Suen, D. F., & Youle, R. J. (2008). Parkin is recruited selectively to impaired mitochondria and promotes their autophagy. *The Journal of cell biology*, *183*(5), 795-803.

National Center for Biotechnology Information (2020). PubChem Compound Summary for CID 2973, Deferoxamine. Retrieved December 31, 2020 from https://pubchem.ncbi.nlm.nih.gov/compound/Deferoxamine.

Nelson, K. M., Dahlin, J. L., Bisson, J., Graham, J., Pauli, G. F., & Walters, M. A. (2017). The essential medicinal chemistry of curcumin: miniperspective. *Journal of medicinal chemistry*, *60*(5), 1620-1637.

Nguyen, T., Nioi, P., & Pickett, C. B. (2009). The Nrf2-antioxidant response element signaling pathway and its activation by oxidative stress. *Journal of Biological Chemistry*, *284*(20), 13291-13295.

NICE. (2020, December 11th). DEQUALINIUM CHLORIDE. Retrieved from National Institute for Health and Care Excellence : https://bnf.nice.org.uk/drug/dequalinium-chloride.html

Nutl, J. G., & Fellman, J. H. (1984). Pharmacokinetics of levodopa. *Clinical neuropharmacology*, *7*(1), 35-50.

Oakley, A. E., Collingwood, J. F., Dobson, J., Love, G., Perrott, H. R., Edwardson, J. A., ... & Morris, C. M. (2007). Individual dopaminergic neurons show raised iron levels in Parkinson disease. *Neurology*, *68*(21), 1820-1825.

Ohkuma, S., Moriyama, Y., & Takano, T. (1982). Identification and characterization of a proton pump on lysosomes by fluorescein-isothiocyanate-dextran fluorescence. *Proceedings of the National Academy of Sciences*, *79*(9), 2758-2762.

Ohtsuki, S., Ikeda, C., Uchida, Y., Sakamoto, Y., Miller, F., Glacial, F., ... & Tachikawa, M. (2013). Quantitative targeted absolute proteomic analysis of transporters, receptors and junction proteins for validation of human cerebral microvascular endothelial cell line hCMEC/D3 as a human blood–brain barrier model. *Molecular pharmaceutics*, *10*(1), 289-296.

Oide, T., Yoshida, K., Kaneko, K., Ohta, M., & Arima, K. (2006). Iron overload and antioxidative role of perivascular astrocytes in aceruloplasminemia. Neuropathology and applied neurobiology, 32(2), 170-176.

Oliver, S. E., Gargano, J. W., Marin, M., Wallace, M., Curran, K. G., Chamberland, M., ... & Dooling, K. (2020). The Advisory Committee on Immunization Practices' Interim

Recommendation for Use of Pfizer-BioNTech COVID-19 Vaccine—United States, December 2020. *Morbidity and Mortality Weekly Report*, *69*(50), 1922.

Ong, W. Y., & Farooqui, A. A. (2005). Iron, neuroinflammation, and Alzheimer's disease. *Journal of Alzheimer's Disease*, *8*(2), 183-200.

Ortiz, M. S., Forti, K. M., Martinez, E. B. S., Muñoz, L. G., Husain, K., & Muñiz, W. H. (2016). Effects of antioxidant N-acetylcysteine against paraquat-induced oxidative stress in vital tissues of mice. *International journal of sciences, basic and applied research*, *26*(1), 26.

Ostrerova-Golts, N., Petrucelli, L., Hardy, J., Lee, J. M., Farer, M., & Wolozin, B. (2000). The A53T α-synuclein mutation increases iron-dependent aggregation and toxicity. *Journal of Neuroscience*, *20*(16), 6048-6054.

Palmer, G., Horgan, D. J., Tisdale, H., Singer, T. P., & Beinert, H. (1968). Studies on the respiratory chain-linked reduced nicotinamide adenine dinucleotide dehydrogenase: XIV. Location of the sites of inhibition of rotenone, barbiturates, and piericidin by means of electron paramagnetic resonance spectroscopy. *Journal of Biological Chemistry*, *243*(4), 844-847.

Pantopoulos, K., Porwal, S. K., Tartakoff, A., & Devireddy, L. (2012). Mechanisms of mammalian iron homeostasis. *Biochemistry*, *51*(29), 5705-5724.

Paolinelli, R., Corada, M., Ferrarini, L., Devraj, K., Artus, C., Czupalla, C. J., ... & Couraud, P. O. (2013). Wnt activation of immortalized brain endothelial cells as a tool for generating a standardized model of the blood brain barrier in vitro. *PloS one*, *8*(8), e70233.

Paparidis, G., Akrivou, M., Tsachouridou, V., Shegani, A., Vizirianakis, I. S., Pirmettis, I., ... & Papagiannopoulou, D. (2018). Synthesis and evaluation of 99mTc/Re-tricarbonyl complexes of the triphenylphosphonium cation for mitochondrial targeting. *Nuclear medicine and biology*, *57*, 34-41.

Paradis, A., Leblanc, D., & Dumais, N. (2016). Optimization of an in vitro human blood–brain barrier model: application to blood monocyte transmigration assays. *MethodsX*, *3*, 25-34.

Paradkar, P. N., & Roth, J. A. (2006). Post-translational and transcriptional regulation of DMT1 during P19 embryonic carcinoma cell differentiation by retinoic acid. *Biochemical Journal*, *394*(1), 173-183.

Paradkar, P. N., Zumbrennen, K. B., Paw, B. H., Ward, D. M., & Kaplan, J. (2009). Regulation of mitochondrial iron import through differential turnover of mitoferrin 1 and mitoferrin 2. *Molecular and cellular biology*, *29*(4), 1007-1016.

Pardridge, W. M. (2007). Blood–brain barrier delivery. *Drug discovery today*, *12*(1-2), 54-61.

Park, S. W., Kim, S. H., Park, K. H., Kim, S. D., Kim, J. Y., Baek, S. Y., ... & Kang, C. D. (2004). Preventive effect of antioxidants in MPTP-induced mouse model of Parkinson's disease. *Neuroscience letters*, *363*(3), 243-246.

Parkinson Québec. (2015). Levodopa and protein: medication absorption concerns. Retrieved from Parkinson Québec: http://parkinsonquebec.ca/wp-content/uploads/2015/09/levedopa.pdf. Accessed April 26, 2018.

Parkinson Study Group. (2004). Levodopa and the progression of Parkinson's disease. *New England Journal of Medicine*, *351*(24), 2498-2508.

Parkinson's UK. (2018, March 29). *The incidence and prevalence of Parkinson's in the UK report*. Retrieved from Parkinson's UK: https://www.parkinsons.org.uk/professionals/resources/incidence-and-prevalence-parkinsons-uk-report

Pasban-Aliabadi, H., Esmaeili-Mahani, S., Sheibani, V., Abbasnejad, M., Mehdizadeh, A., & Yaghoobi, M. M. (2013). Inhibition of 6-hydroxydopamine-induced PC12 cell apoptosis by olive (Olea europaea L.) leaf extract is performed by its main component oleuropein. *Rejuvenation research*, *16*(2), 134-142.

Patabendige, A., Skinner, R. A., & Abbott, N. J. (2013). Establishment of a simplified in vitro porcine blood–brain barrier model with high transendothelial electrical resistance. *Brain research*, *1521*, 1-15.

Perluigi, M., Coccia, R., & Butterfield, D. A. (2012). 4-Hydroxy-2-nonenal, a reactive product of lipid peroxidation, and neurodegenerative diseases: a toxic combination illuminated by redox proteomics studies. *Antioxidants & redox signaling*, *17*(11), 1590-1609.

Perry, T. L., Yong, V. W., Clavier, R. M., Jones, K., Wright, J. M., Foulks, J. G., & Wall, R. A. (1985). Partial protection from the dopaminergic neurotoxin N-methyl-4-phenyl-1, 2, 3, 6-tetrahydropyridine by four different antioxidants in the mouse. *Neuroscience letters*, *60*(2), 109-114.

Petri, S., Körner, S., & Kiaei, M. (2012). Nrf2/ARE signaling pathway: key mediator in oxidative stress and potential therapeutic target in ALS. *Neurology research international*, *2012*.

Pezzella, A., d'Ischia, M., Napolitano, A., Misuraca, G., & Prota, G. (1997). Iron-mediated generation of the neurotoxin 6-hydroxydopamine quinone by reaction of fatty acid hydroperoxides with dopamine: a possible contributory mechanism for neuronal degeneration in Parkinson's disease. *Journal of medicinal chemistry*, *40*(14), 2211-2216.

Pichler, I., Fabiola Del Greco, M., Gögele, M., Lill, C. M., Bertram, L., Do, C. B., ... & Keller, M. F. (2013). Serum iron levels and the risk of Parkinson disease: a mendelian randomization study. *PLoS medicine*, *10*(6), e1001462.

Pietrangelo, A. (2015). Pathogens, metabolic adaptation, and human diseases—an iron-thrifty genetic model. *Gastroenterology*, *149*(4), 834-838.

Pino, J., da Luz, M. H., Antunes, H. K., Giampá, S. Q., Martins, V. R., & Lee, K. S. (2017). Iron-Restricted Diet Affects Brain Ferritin Levels, Dopamine Metabolism and Cellular Prion Protein in a Region-Specific Manner. *Frontiers in molecular neuroscience*, *10*, 145.

Porter, J. B. (2001, January). Deferoxamine pharmacokinetics. In *Seminars in hematology* (Vol. 38, pp. 63-68). WB Saunders.

Porter, J., Viprakasit, V., & Kattamis, A. (2014). Iron overload and chelation. In *Guidelines for the Management of Transfusion Dependent Thalassaemia (TDT)[Internet]. 3rd edition*. Thalassaemia International Federation.

Pucci, C., De Pasquale, D., Marino, A., Martinelli, C., Lauciello, S., & Ciofani, G. (2020). Hybrid magnetic nanovectors promote selective glioblastoma cell death through a combined effect of lysosomal membrane permeabilization and chemotherapy. *ACS Applied Materials & Interfaces*.

Priyadarsini, K. I. (2013). Chemical and structural features influencing the biological activity of curcumin. *Current pharmaceutical design*, *19*(11), 2093-2100.

Priyadarsini, K. I. (2014). The chemistry of curcumin: from extraction to therapeutic agent. *Molecules*, *19*(12), 20091-20112.

Qosa, H., Mohamed, L. A., Al Rihani, S. B., Batarseh, Y. S., Duong, Q. V., Keller, J. N., & Kaddoumi, A. (2016). High-throughput screening for identification of blood-brain barrier integrity enhancers: A drug repurposing opportunity to rectify vascular amyloid toxicity. *Journal of Alzheimer's Disease*, *53*(4), 1499-1516.

Rahimmi, A., Khosrobakhsh, F., Izadpanah, E., Moloudi, M. R., & Hassanzadeh, K. (2015). N-acetylcysteine prevents rotenone-induced Parkinson's disease in rat: An investigation into the interaction of parkin and Drp1 proteins. *Brain research bulletin*, *113*, 34-40.

Rasmussen, K. M. (2001). Is there a causal relationship between iron deficiency or iron-deficiency anemia and weight at birth, length of gestation and perinatal mortality?. *The Journal of nutrition*, *131*(2), 590S-603S.

Rakotoarisoa, M., & Angelova, A. (2018). Amphiphilic nanocarrier systems for curcumin delivery in neurodegenerative disorders. *Medicines*, *5*(4), 126.

Reelfs, O., Abbate, V., Cilibrizzi, A., Pook, M. A., Hider, R. C., & Pourzand, C. (2019). The role of mitochondrial labile iron in Friedreich's ataxia skin fibroblasts sensitivity to ultraviolet A. *Metallomics*, *11*(3), 656-665.

Reelfs, O., Abbate, V., Hider, R. C., & Pourzand, C. (2016). A powerful mitochondria-targeted iron chelator affords high photoprotection against solar ultraviolet a radiation. *Journal of Investigative Dermatology*, *136*(8), 1692-1700.

Reif, D. W. (1992). Ferritin as a source of iron for oxidative damage. *Free Radical Biology and Medicine*, *12*(5), 417-427.

Reyes, R. C., Cittolin-Santos, G. F., Kim, J. E., Won, S. J., Brennan-Minnella, A. M., Katz, M., ... & Swanson, R. A. (2016). Neuronal glutathione content and antioxidant capacity can be normalized in situ by N-acetyl cysteine concentrations attained in human cerebrospinal fluid. *Neurotherapeutics*, *13*(1), 217-225.

Richardson, D. R., Lane, D. J., Becker, E. M., Huang, M. L. H., Whitnall, M., Rahmanto, Y. S., ... & Ponka, P. (2010). Mitochondrial iron trafficking and the integration of iron metabolism between the mitochondrion and cytosol. *Proceedings of the National Academy of Sciences*, *107*(24), 10775-10782.

Ringman, J. M., Frautschy, S. A., Teng, E., Begum, A. N., Bardens, J., Beigi, M., Gylys, K.H., Badmaev, V., Heath, D.D., Apostolova, L.G. & Porter, V. (2012). Oral curcumin for Alzheimer's disease: tolerability and efficacy in a 24-week randomized, double blind, placebo-controlled study. *Alzheimer's research & therapy*, *4*(5), 43.

Ristagno, G., Fumagalli, F., Porretta-Serapiglia, C., Orrù, A., Cassina, C., Pesaresi, M., ... & Cervo, L. (2012). Hydroxytyrosol attenuates peripheral neuropathy in streptozotocin-induced diabetes in rats. *Journal of agricultural and food chemistry*, *60*(23), 5859-5865.

Robles-Almazan, M., Pulido-Moran, M., Moreno-Fernandez, J., Ramirez-Tortosa, C., Rodriguez-Garcia, C., Quiles, J. L., & Ramirez-Tortosa, M. (2018). Hydroxytyrosol: Bioavailability, toxicity, and clinical applications. *Food Research International*, *105*, 654-667.

Rossi, M., Ruottinen, H., Soimakallio, S., Elovaara, I., & Dastidar, P. (2013). Clinical MRI for iron detection in Parkinson's disease. *Clinical imaging*, *37*(4), 631-636.

Rothaug, M., Zunke, F., Mazzulli, J. R., Schweizer, M., Altmeppen, H., Lüllmann-Rauch, R., ... & Saftig, P. (2014). LIMP-2 expression is critical for β-glucocerebrosidase activity and α-synuclein clearance. *Proceedings of the National Academy of Sciences*, *111*(43), 15573-15578.

Rouault, T. A. (2013). Iron metabolism in the CNS: implications for neurodegenerative diseases. *Nature Reviews Neuroscience*, *14*(8), 551.

Rouault, T. A., & Cooperman, S. (2006, September). Brain iron metabolism. In *Seminars in pediatric neurology* (Vol. 13, No. 3, pp. 142-148). Elsevier.

Rubin, L. L., Hall, D. E., Porter, S., Barbu, K., Cannon, C., Horner, H. C., ... & Morales, J. (1991). A cell culture model of the blood-brain barrier. *The Journal of cell biology*, *115*(6), 1725-1735.

Ruigrok, M. J., & de Lange, E. C. (2015). Emerging insights for translational pharmacokinetic and pharmacokinetic-pharmacodynamic studies: towards prediction of nose-to-brain transport in humans. *The AAPS journal*, *17*(3), 493-505.

Russo, S. J., & Nestler, E. J. (2013). The brain reward circuitry in mood disorders. *Nature Reviews Neuroscience*, *14*(9), 609.

Saha, A. R., Hill, J., Utton, M. A., Asuni, A. A., Ackerley, S., Grierson, A. J., ... & Hanger, D. P. (2004). Parkinson's disease α-synuclein mutations exhibit defective axonal transport in cultured neurons. *J Cell Sci*, *117*(7), 1017-1024.

Salem, M., Rohani, S., & Gillies, E. R. (2014). Curcumin, a promising anti-cancer therapeutic: a review of its chemical properties, bioactivity and approaches to cancer cell delivery. *RSC advances*, *4*(21), 10815-10829.

Saleppico, S., Mazzolla, R., Boelaert, J. R., Puliti, M., Barluzzi, R., Bistoni, F., & Blasi, E. (1996). Iron regulates microglial cell-mediated secretory and effector functions. *Cellular immunology*, *170*(2), 251-259.

Saleppico, S., Mazzolla, R., Boelaert, J. R., Puliti, M., Barluzzi, R., Bistoni, F., & Blasi, E. (1996). Iron regulates microglial cell-mediated secretory and effector functions. *Cellular immunology*, *170*(2), 251-259.

Samuni, Y., Goldstein, S., Dean, O. M., & Berk, M. (2013). The chemistry and biological activities of N-acetylcysteine. *Biochimica et Biophysica Acta (BBA)-General Subjects*, *1830*(8), 4117-4129.

Sandoval-Acuña, C., Ferreira, J., & Speisky, H. (2014). Polyphenols and mitochondria: an update on their increasingly emerging ROS-scavenging independent actions. *Archives of Biochemistry and Biophysics*, *559*, 75-90.

Santos, E. L., Maia, B. H. L. N. S., Ferriani, A. P., & Teixeira, S. D. (2017). *Flavonoids: Classification, biosynthesis and chemical ecology* (Vol. 6, p. 482). InTech.

Saraiva, C., Praça, C., Ferreira, R., Santos, T., Ferreira, L., & Bernardino, L. (2016). Nanoparticle-mediated brain drug delivery: overcoming blood–brain barrier to treat neurodegenerative diseases. *Journal of Controlled Release*, *235*, 34-47.

Sarbishegi, M., Gorgich, E. A. C., Khajavi, O., Komeili, G., & Salimi, S. (2018). The neuroprotective effects of hydro-alcoholic extract of olive (Olea europaea L.) leaf on rotenone-induced Parkinson's disease in rat. *Metabolic brain disease*, *33*(1), 79-88.

Savica, R., Grossardt, B. R., Carlin, J. M., Icen, M., Bower, J. H., Ahlskog, J. E., ... & Rocca, W. A. (2009). Anemia or low hemoglobin levels preceding Parkinson disease A case-control study. *Neurology*, *73*(17), 1381-1387.

Savjani, K. T., Gajjar, A. K., & Savjani, J. K. (2012). Drug solubility: importance and enhancement techniques. *International Scholarly Research Notices*, *2012*.

Saxena, V., & Hussain, M. D. (2013). Formulation and in vitro evaluation of 17-allyamino-17-demethoxygeldanamycin (17-AAG) loaded polymeric mixed micelles for glioblastoma multiforme. *Colloids and Surfaces B: Biointerfaces*, *112*, 350-355.

Schaffer, S., Podstawa, M., Visioli, F., Bogani, P., Müller, W. E., & Eckert, G. P. (2007). Hydroxytyrosol-rich olive mill wastewater extract protects brain cells in vitro and ex vivo. *Journal of agricultural and food chemistry*, *55*(13), 5043-5049.

Schapira, A. H. V. "Complex I: inhibitors, inhibition and neurodegeneration." *Experimental neurology* 224, no. 2 (2010): 331-335.

Schapira, A. H. V. "Mitochondrial dysfunction in Parkinson's disease." (2007): 1261.

Schneider, C., Gordon, O. N., Edwards, R. L., & Luis, P. B. (2015). Degradation of curcumin: from mechanism to biological implications. *Journal of agricultural and food chemistry*, *63*(35), 7606-7614.

Schrade, A., Sade, H., Couraud, P. O., Romero, I. A., Weksler, B. B., & Niewoehner, J. (2012). Expression and localization of claudins-3 and-12 in transformed human brain endothelium. *Fluids and barriers of the CNS*, *9*(1), 1-5.

Seo, S. W., Han, H. K., Chun, M. K., & Choi, H. K. (2012). Preparation and pharmacokinetic evaluation of curcumin solid dispersion using Solutol® HS15 as a carrier. *International journal of pharmaceutics*, *424*(1-2), 18-25.

Shaikh, J., Ankola, D. D., Beniwal, V., Singh, D., & Kumar, M. R. (2009). Nanoparticle encapsulation improves oral bioavailability of curcumin by at least 9-fold when compared to curcumin administered with piperine as absorption enhancer. *European Journal of Pharmaceutical Sciences*, *37*(3-4), 223-230.

Sharma, A., Kaur, P., Kumar, V., & Gill, K. D. (2007). Attenuation of 1-methyl-4-phenyl-1, 2, 3, 6-tetrahydropyridine induced nigrostriatal toxicity in mice by N-acetyl cysteine. *Cellular and molecular biology (Noisy-le-Grand, France)*, *53*(1), 48-55.

Shachar, D. B., Kahana, N., Kampel, V., Warshawsky, A., & Youdim, M. B. (2004). Neuroprotection by a novel brain permeable iron chelator, VK-28, against 6-hydroxydopamine lesion in rats. *Neuropharmacology*, *46*(2), 254-263.

Shaw, G. C., Cope, J. J., Li, L., Corson, K., Hersey, C., Ackermann, G. E., ... & Paw, B. H. (2006). Mitoferrin is essential for erythroid iron assimilation. *Nature*, *440*(7080), 96-100.

Sheftel, A. D., Zhang, A. S., Brown, C., Shirihai, O. S., & Ponka, P. (2007). Direct interorga-nellar transfer of iron from endosome to mitochondrion. *Blood, The Journal of the American Society of Hematology*, *110*(1), 125-132.

Shi, M., Zhang, J., Li, X., Pan, S., Li, J., Yang, C., ... & Zhao, X. (2018). Mitochondria-targeted delivery of doxorubicin to enhance antitumor activity with HER-2 peptide-mediated multifunctional pH-sensitive DQAsomes. *International journal of nanomedicine*, *13*, 4209.

Shvartsman, M., Kikkeri, R., Shanzer, A., & Cabantchik, Z. I. (2007). Non-transferrin-bound iron reaches mitochondria by a chelator-inaccessible mechanism: biological and clinical implications. *American Journal of Physiology-Cell Physiology*, *293*(4), C1383-C1394.

Sian, J., Dexter, D.T., Lees, A.J., Daniel, S., Agid, Y., Javoy-Agid, F., Jenner, P. and Marsden, C.D., 1994. Alterations in glutathione levels in Parkinson's disease and other neurodegenerative disorders affecting basal ganglia. *Annals of neurology*, *36*(3), pp.348-355.

Sian-Hülsmann, J., Mandel, S., Youdim, M. B., & Riederer, P. (2011). The relevance of iron in the pathogenesis of Parkinson's disease. *Journal of neurochemistry*, *118*(6), 939-957.

Siddappa, A. J. M., Rao, R. B., Wobken, J. D., Leibold, E. A., Connor, J. R., & Georgieff, M. K. (2002). Developmental changes in the expression of iron regulatory proteins and iron transport proteins in the perinatal rat brain. *Journal of neuroscience research*, *68*(6), 761-775.

Simmons, D. A., Casale, M., Alcon, B., Pham, N. H. A., Narayan, N., & Lynch, G. (2007). Ferritin accumulation in dystrophic microglia is an early event in the development of Huntington's disease. Glia, 55(10), 1074-1084.

Simpkins, J. W., & Dykens, J. A. (2008). Mitochondrial mechanisms of estrogen neuroprotection. *Brain research reviews*, *57*(2), 421-430.

Siow, C. R. S., Wan Sia Heng, P., & Chan, L. W. (2016). Application of freeze-drying in the development of oral drug delivery systems. *Expert Opinion on Drug Delivery*, *13*(11), 1595-1608.

Sipe, D. M., & Murphy, R. F. (1991). Binding to cellular receptors results in increased iron release from transferrin at mildly acidic pH. *Journal of Biological Chemistry*, *266*(13), 8002-8007.

Siviero, A., Gallo, E., Maggini, V., Gori, L., Mugelli, A., Firenzuoli, F., & Vannacci, A. (2015). Curcumin, a golden spice with a low bioavailability. *Journal of Herbal Medicine*, *5*(2), 57-70.

Slattery, J., Kumar, N., Delhey, L., Berk, M., Dean, O., Spielholz, C., & Frye, R. (2015). Clinical trials of N-acetylcysteine in psychiatry and neurology: a systematic review. *Neuroscience & Biobehavioral Reviews*, *55*, 294-321.

Smith, J. A., Das, A., Ray, S. K., & Banik, N. L. (2012). Role of pro-inflammatory cytokines released from microglia in neurodegenerative diseases. *Brain research bulletin*, *87*(1), 10-20.

Song, Z.; Feng, R.; Sun, M.; Guo, C.; Gao, Y.; Li, L.; Zhai, G. Curcumin-loaded PLGA-PEG-PLGA triblock copolymeric micelles: Preparation, pharmacokinetics and distribution in vivo. J. Colloid Interface Sci. 2011, 354, 116–123.

Soto-Otero, R., Méndez-Álvarez, E., Hermida-Ameijeiras, Á., Muñoz-Patiño, A. M., & Labandeira-Garcia, J. L. (2000). Autoxidation and neurotoxicity of 6-hydroxydopamine in the presence of some antioxidants: potential implication in relation to the pathogenesis of Parkinson's disease. *Journal of neurochemistry*, *74*(4), 1605-1612.

Sripetchwandee, J., Pipatpiboon, N., Chattipakorn, N. and Chattipakorn, S. (2014). Combined therapy of iron chelator and antioxidant completely restores brain dysfunction induced by iron toxicity. PLoS One, 9(1), p.e85115.

Stone, N. L., England, T. J., & O'Sullivan, S. E. (2019). A novel transwell blood brain barrier model using primary human cells. *Frontiers in cellular neuroscience*, *13*, 230.

Suárez, M., Valls, R. M., Romero, M. P., Macia, A., Fernández, S., Giralt, M., Sola, R. & Motilva, M. J. (2011). Bioavailability of phenols from a phenol-enriched olive oil. *British journal of nutrition*, *106*(11), 1691-1701.

Sun, M., Yang, D., Wang, C., Bi, H., Zhou, Y., Wang, X., ... & Yang, P. (2019). AgBiS 2-TPP nanocomposite for mitochondrial targeting photodynamic therapy, photothermal therapy and bio-imaging under 808 nm NIR laser irradiation. *Biomaterials science*, *7*(11), 4769-4781.

Tai, L. M., Holloway, K. A., Male, D. K., Loughlin, A. J., & Romero, I. A. (2010). Amyloid-β-induced occludin down-regulation and increased permeability in human brain endothelial cells is mediated by MAPK activation. *Journal of cellular and molecular medicine*, *14*(5), 1101-1112.

Tanner, C. M., Kamel, F., Ross, G. W., Hoppin, J. A., Goldman, S. M., Korell, M., ... & Langston, J. W. (2011). Rotenone, paraquat, and Parkinson's disease. *Environmental health perspectives*, *119*(6), 866-872.

Tas, C., Ozkan, C. K., Savaser, A., Ozkan, Y., Tasdemir, U., & Altunay, H. (2009). Nasal administration of metoclopramide from different dosage forms: in vitro, ex vivo, and in vivo evaluation. *Drug delivery*, *16*(3), 167-175.

Thanvi, B. R., & Lo, T. C. N. (2004). Long term motor complications of levodopa: clinical features, mechanisms, and management strategies. *Postgraduate medical journal*, *80*(946), 452-458.

Thomas, C., Mackey, M.M., Diaz, A.A. and Cox, D.P., 2009. Hydroxyl radical is produced via the Fenton reaction in submitochondrial particles under oxidative stress: implications for diseases associated with iron accumulation. *Redox Report*, *14*(3), pp.102-108.

Toba, S., Jin, M., Yamada, M., Kumamoto, K., Matsumoto, S., Yasunaga, T., ... & Fushiki, S. (2017). Alpha-synuclein facilitates to form short unconventional microtubules that have a unique function in the axonal transport. *Scientific reports*, *7*(1), 16386.

Tosato, M., & Di Marco, V. (2019). Metal chelation therapy and Parkinson's disease: A critical review on the thermodynamics of complex formation between relevant metal ions and promising or established drugs. *Biomolecules*, *9*(7), 269.

Trichopoulou, A. (2004). Traditional Mediterranean diet and longevity in the elderly: a review. *Public health nutrition*, *7*(7), 943-947.

Trichopoulou, A., Costacou, T., Bamia, C., & Trichopoulos, D. (2003). Adherence to a Mediterranean diet and survival in a Greek population. *New England Journal of Medicine*, *348*(26), 2599-2608.

Trinh, J., & Farrer, M. (2013). Advances in the genetics of Parkinson disease. *Nature Reviews Neurology*, *9*(8), 445.

Tsai, Y. M., Chien, C. F., Lin, L. C., & Tsai, T. H. (2011). Curcumin and its nano-formulation: the kinetics of tissue distribution and blood–brain barrier penetration. *International journal of pharmaceutics*, *416*(1), 331-338.

Tu, Z. S., Wang, Q., Sun, D. D., Dai, F., & Zhou, B. (2017). Design, synthesis, and evaluation of curcumin derivatives as Nrf2 activators and cytoprotectors against oxidative death. *European Journal of Medicinal Chemistry*, *134*, 72-85.

Tutar, Y., Özgür, A., & Tutar, L. 2013. Role of protein aggregation in neurodegenerative diseases. *InTech Publ.* 55-76.

Tse, H. N., Raiteri, L., Wong, K. Y., Yee, K. S., Ng, L. Y., Wai, K. Y., ... & Chan, M. H. (2013). High-dose N-acetylcysteine in stable COPD: the 1-year, double-blind, randomized, placebo-controlled HIACE study. *Chest*, *144*(1), 106-118.

Uchiyama, A., Kim, J. S., Kon, K., Jaeschke, H., Ikejima, K., Watanabe, S., & Lemasters, J. J. (2008). Translocation of iron from lysosomes into mitochondria is a key event during oxidative stress-induced hepatocellular injury. *Hepatology*, *48*(5), 1644-1654.

Ulla, M., Bonny, J. M., Ouchchane, L., Rieu, I., Claise, B., & Durif, F. (2013). Is R2* a new MRI biomarker for the progression of Parkinson's disease? A longitudinal follow-up. *PLoS One*, *8*(3), e57904.

Unger, E. L., Bianco, L. E., Jones, B. C., Allen, R. P., & Earley, C. J. (2014). Low brain iron effects and reversibility on striatal dopamine dynamics. *Experimental neurology*, *261*, 462-468.

Urich, E., Lazic, S. E., Molnos, J., Wells, I., & Freskgård, P. O. (2012). Transcriptional profiling of human brain endothelial cells reveals key properties crucial for predictive in vitro blood-brain barrier models. *PloS one*, *7*(5), e38149.

Urrutia, P., Aguirre, P., Esparza, A., Tapia, V., Mena, N. P., Arredondo, M., ... & Núñez, M. T. (2013). Inflammation alters the expression of DMT1, FPN1 and hepcidin, and it causes iron accumulation in central nervous system cells. *Journal of neurochemistry*, *126*(4), 541-549.

Usenovic, M., Tresse, E., Mazzulli, J. R., Taylor, J. P., & Krainc, D. (2012). Deficiency of ATP13A2 leads to lysosomal dysfunction, α-synuclein accumulation, and neurotoxicity. *Journal of Neuroscience*, *32*(12), 4240-4246.

Van der Merwe, C., Van Dyk, H. C., Engelbrecht, L., van der Westhuizen, F. H., Kinnear, C., Loos, B., & Bardien, S. (2017). Curcumin rescues a PINK1 knock down SH-SY5Y cellular model of Parkinson's disease from mitochondrial dysfunction and cell death. Molecular neurobiology, 54(4), 2752-2762.

Wallis, L. I., Paley, M. N., Graham, J. M., Grünewald, R. A., Wignall, E. L., Joy, H. M., & Griffiths, P. D. (2008). MRI assessment of basal ganglia iron deposition in Parkinson's disease. Journal of Magnetic Resonance Imaging, 28(5), 1061-1067.

Wang, L. L., He, D. D., Wang, S. X., Dai, Y. H., Ju, J. M., & Zhao, C. L. (2018). Preparation and evaluation of curcumin-loaded self-assembled micelles. *Drug development and industrial pharmacy*, *44*(4), 563-569.

Wang, X. X., Li, Y. B., Yao, H. J., Ju, R. J., Zhang, Y., Li, R. J., ... & Lu, W. L. (2011). The use of mitochondrial targeting resveratrol liposomes modified with a dequalinium polyethylene glycol-distearoylphosphatidyl ethanolamine conjugate to induce apoptosis in resistant lung cancer cells. *Biomaterials*, *32*(24), 5673-5687.

Ward, R.J., Dexter, D., Florence, A., Aouad, F., Hider, R., Jenner, P. and Crichton, R.R. (1995). Brain iron in the ferrocene-loaded rat: its chelation and influence on dopamine metabolism. *Biochemical pharmacology*, *49*(12), 1821-1826.

Watanabe, I., Vachal, E., & Tomita, T. (1977). Dense core vesicles around the Lewy body in incidental Parkinson's disease: an electron microscopic study. *Acta neuropathologica*, *39*(2), 173-175.

Wayne Martin, W. R., Ye, F. Q., & Allen, P. S. (1998). Increasing striatal iron content associated with normal aging. Movement Disorders, 13(2), 281-286.

Weiss, M. J., & Chen, L. B. (1984). Rhodamine 123: a lipophilic, cationic mitochondrial-specific vital dye. *Kodak Lab. Chem. Bull*, *55*, 1-4.

Weiss, M. J., Wong, J. R., Ha, C. S., Bleday, R., Salem, R. R., Steele, G. D., & Chen, L. B. (1987). Dequalinium, a topical antimicrobial agent, displays anticarcinoma activity based on selective mitochondrial accumulation. *Proceedings of the National Academy of Sciences*, *84*(15), 5444-5448.

Weissig, V. (2015). DQAsomes as the prototype of mitochondria-targeted pharmaceutical nanocarriers: Preparation, characterization, and use. In *Mitochondrial medicine* (pp. 1-11). Humana Press, New York, NY.

Weissig, V., Lasch, J., Erdos, G., Meyer, H. W., Rowe, T. C., Hughes, J. (1998). DQAsomes: a novel potential drug and gene delivery system made from Dequalinium. Pharm. Res. 1998, 15 (2), 334–7.

Welzel, L., Twele, F., Schidlitzki, A., Töllner, K., Klein, P., & Löscher, W. (2019). Network pharmacology for antiepileptogenesis: Tolerability and neuroprotective effects of novel multitargeted combination treatments in nonepileptic vs. post-status epilepticus mice. *Epilepsy research*, *151*, 48-66.

Whone, A., Luz, M., Boca, M., Woolley, M., Mooney, L., Dharia, S., ... & Gill, S. S. (2019). Randomized trial of intermittent intraputamenal glial cell line-derived neurotrophic factor in Parkinson's disease. *Brain*, *142*(3), 512-525.

Wiley, D. T., Webster, P., Gale, A., & Davis, M. E. (2013). Transcytosis and brain uptake of transferrin-containing nanoparticles by tuning avidity to transferrin receptor. *Proceedings of the National Academy of Sciences*, *110*(21), 8662-8667.

Werner, C. J., Heyny-von Haussen, R., Mall, G., & Wolf, S. (2008). Proteome analysis of human substantia nigra in Parkinson's disease. *Proteome science*, *6*(1), 8. Wrighting, D. M., & Andrews, N. C. (2006). Interleukin-6 induces hepcidin expression through STAT3. *Blood*, *108*(9), 3204-3209.

Wu, K. C., Liou, H. H., Kao, Y. H., Lee, C. Y., & Lin, C. J. (2017). The critical role of Nramp1 in degrading α-synuclein oligomers in microglia under iron overload condition. *Neurobiology of disease*, *104*, 61-72.

Wu, Y., Li, X., Xie, W., Jankovic, J., Le, W., & Pan, T. (2010). Neuroprotection of deferoxamine on rotenone-induced injury via accumulation of HIF-1α and induction of autophagy in SH-SY5Y cells. *Neurochemistry international*, *57*(3), 198-205.

Wu, Y. T., Lin, L. C., & Tsai, T. H. (2009). Measurement of free hydroxytyrosol in microdialysates from blood and brain of anesthetized rats by liquid chromatography with fluorescence detection. *Journal of Chromatography A*, *1216*(16), 3501-3507.

Wypijewska, A., Galazka-Friedman, J., Bauminger, E. R., Wszolek, Z. K., Schweitzer, K. J., Dickson, D. W., ... & Friedman, A. (2010). Iron and reactive oxygen species activity in parkinsonian substantia nigra. *Parkinsonism & related disorders*, *16*(5), 329-333.

Wolfe, K. L., & Liu, R. H. (2007). Cellular antioxidant activity (CAA) assay for assessing antioxidants, foods, and dietary supplements. *Journal of agricultural and food chemistry*, *55*(22), 8896-8907.

Weksler, B. B., Subileau, E. A., Perriere, N., Charneau, P., Holloway, K., Leveque, M., ... & Male, D. K. (2005). Blood-brain barrier-specific properties of a human adult brain endothelial cell line. *The FASEB journal*, *19*(13), 1872-1874.

Weksler, B., Romero, I. A., & Couraud, P. O. (2013). The hCMEC/D3 cell line as a model of the human blood brain barrier. *Fluids and Barriers of the CNS*, *10*(1), 16.

Wolff, N. A., Garrick, M. D., Zhao, L., Garrick, L. M., Ghio, A. J., & Thévenod, F. (2018). A role for divalent metal transporter (DMT1) in mitochondrial uptake of iron and manganese. *Scientific reports*, *8*(1), 1-12.

Wolff, N. A., Ghio, A. J., Garrick, L. M., Garrick, M. D., Zhao, L., Fenton, R. A., & Thévenod, F. (2014). Evidence for mitochondrial localization of divalent metal transporter 1 (DMT1). *The FASEB Journal*, *28*(5), 2134-2145.

Wongjaikam, S., Kumfu, S., Khamseekaew, J., Chattipakorn, S. C., & Chattipakorn, N. (2017). Restoring the impaired cardiac calcium homeostasis and cardiac function in iron overload rats by the combined deferiprone and N-acetyl cysteine. *Scientific reports*, *7*, 44460.

Xie, L. X., Wu, H. L., Fang, Y., Kang, C., Xiang, S. X., Zhu, L., ... & Yu, R. Q. (2015). Simultaneous determination of tyrosine and levodopa in human plasma using enzyme-induced excitation-emission-kinetic third-order calibration method. *Chemometrics and Intelligent Laboratory Systems*, *148*, 9-19.

Xicoy, H., Wieringa, B., & Martens, G. J. (2017). The SH-SY5Y cell line in Parkinson's disease research: a systematic review. *Molecular neurodegeneration*, *12*(1), 1-11.

Yadav, M., Parle, M., Sharma, N., Dhingra, S., Raina, N., & Jindal, D. K. (2017). Brain targeted oral delivery of doxycycline hydrochloride encapsulated Tween 80 coated

chitosan nanoparticles against ketamine induced psychosis: behavioral, biochemical, neurochemical and histological alterations in mice. *Drug delivery*, *24*(1), 1429-1440.

Yamada, Y., & Harashima, H. (2013). Enhancement in selective mitochondrial association by direct modification of a mitochondrial targeting signal peptide on a liposomal based nanocarrier. *Mitochondrion*, *13*(5), 526-532.

Yamamuro, A., Yoshioka, Y., Ogita, K., & Maeda, S. (2006). Involvement of endoplasmic reticulum stress on the cell death induced by 6-hydroxydopamine in human neuroblastoma SH-SY5Y cells. *Neurochemical research*, *31*(5), 657-664.

Yang, K. Y., Lin, L. C., Tseng, T. Y., Wang, S. C., & Tsai, T. H. (2007). Oral bioavailability of curcumin in rat and the herbal analysis from Curcuma longa by LC–MS/MS. Journal of chromatography B, 853(1-2), 183-189.

Yang, W. M., Jung, K. J., Lee, M. O., Lee, Y. S., Lee, Y. H., Nakagawa, S., ... & Kim, D. W. (2011). Transient expression of iron transport proteins in the capillary of the developing rat brain. *Cellular and molecular neurobiology*, *31*(1), 93-99.

Yang, W. S., SriRamaratnam, R., Welsch, M. E., Shimada, K., Skouta, R., Viswanathan, V. S., ... & Stockwell, B. R. (2014). Regulation of ferroptotic cancer cell death by GPX4. *Cell*, *156*(1-2), 317-331.

Yoshino, H., Nakagawa-Hattori, Y., Kondo, T., & Mizuno, Y. (1992). Mitochondrial complex I and II activities of lymphocytes and platelets in Parkinson's disease. *Journal of neural transmission-Parkinson's disease and dementia section*, *4*(1), 27-34.

Youdim, M. B., Stephenson, G., & Shachar, D. B. (2004). Ironing iron out in Parkinson's disease and other neurodegenerative diseases with iron chelators: a lesson from 6-hydroxydopamine and iron chelators, desferal and VK-28. Annals of the New York Academy of Sciences, 1012(1), 306-325.

Youdim, M. B. H., & Green, A. R. (1978). Iron deficiency and neurotransmitter synthesis and function. Proceedings of the Nutrition Society, 37(02), 173-179.

Youdim, M. B., Stephenson, G., & Shachar, D. B. (2004). Ironing iron out in Parkinson's disease and other neurodegenerative diseases with iron chelators: a lesson from 6-hydroxydopamine and iron chelators, desferal and VK-28. Annals of the New York Academy of Sciences, 1012(1), 306-325.

Youdim, M. B. H., & Green, A. R. (1978). Iron deficiency and neurotransmitter synthesis and function. *Proceedings of the Nutrition Society*, *37*(02), 173-179.

Youle, R. J., & Van Der Bliek, A. M. (2012). Mitochondrial fission, fusion, and stress. *Science*, *337*(6098), 1062-1065.

Yu, G., Deng, A., Tang, W., Ma, J., Yuan, C., & Ma, J. (2016). Hydroxytyrosol induces phase II detoxifying enzyme expression and effectively protects dopaminergic cells against dopamine-and 6-hydroxydopamine induced cytotoxicity. *Neurochemistry international*, *96*, 113-120.

Yu, X., Du, T., Song, N., He, Q., Shen, Y., Jiang, H., & Xie, J. (2013). Decreased iron levels in the temporal cortex in postmortem human brains with Parkinson disease. *Neurology*, *80*(5), 492-495.

Yu, H.; Li, J.; Shi, K.; Huang, Q. Structure of modified epsilon-polylysine micelles and their application in improving cellular antioxidant activity of curcuminoids. Food Funct. 2011, 2, 373–380.

Yu, G., Deng, A., Tang, W., Ma, J., Yuan, C., & Ma, J. (2016). Hydroxytyrosol induces phase II detoxifying enzyme expression and effectively protects dopaminergic cells against dopamine-and 6-hydroxydopamine induced cytotoxicity. *Neurochemistry international*, *96*, 113-120.

Yusof, H. I., Owusu-Apenten, R., & Nigam, P. S. (2018). Determination of iron (III) reducing antioxidant capacity for manuka honey and comparison with ABTS and other methods.

Zafra-Gómez, A., Luzón-Toro, B., Capel-Cuevas, S., & Morales, J. C. (2011). Stability of hydroxytyrosol in aqueous solutions at different concentration, temperature and with different ionic content: a study using UPLC-MS. *Food and Nutrition Sciences*, *2011*.

Zariwala, M. G., Somavarapu, S., Farnaud, S., & Renshaw, D. (2013). Comparison study of oral iron preparations using a human intestinal model. *Scientia pharmaceutica*, *81*(4), 1123.

Zhang, L., Zhu, Z., Liu, J., Zhu, Z., & Hu, Z. (2014). Protective effect of N-acetylcysteine (NAC) on renal ischemia/reperfusion injury through Nrf2 signaling pathway. *Journal of Receptors and Signal Transduction*, *34*(5), 396-400.

Zhang, P., Hu, L., Yin, Q., Zhang, Z., Feng, L., & Li, Y. (2012). Transferrin-conjugated polyphosphoester hybrid micelle loading paclitaxel for brain-targeting delivery: synthesis, preparation and in vivo evaluation. *Journal of controlled release*, *159*(3), 429-434.

Zecca, L., Youdim, M. B., Riederer, P., Connor, J. R., & Crichton, R. R. (2004). Iron, brain ageing and neurodegenerative disorders. *Nature Reviews Neuroscience*, *5*(11), 863.

Zhang, G., Zhang, Z., Liu, L., Yang, J., Huang, J., Xiong, N., & Wang, T. (2014). Impulsive and compulsive behaviors in Parkinson's disease. Frontiers in aging neuroscience, 6, 318.

Zhang, W., Yan, Z. F., Gao, J. H., Sun, L., Huang, X. Y., Liu, Z., ... & Hu, Y. (2014). Role and mechanism of microglial activation in iron-induced selective and progressive dopaminergic neurodegeneration. *Molecular neurobiology*, *49*(3), 1153-1165.

Zhao, L., Du, J., Duan, Y., Zhang, H., Yang, C., Cao, F., & Zhai, G. (2012). Curcumin loaded mixed micelles composed of Pluronic P123 and F68: preparation, optimization and in vitro characterization. *Colloids and Surfaces B: Biointerfaces*, *97*, 101-108.

Zhou, C., Huang, Y., & Przedborski, S. (2008). Oxidative stress in Parkinson's disease. *Annals of the New York Academy of Sciences*, *1147*(1), 93-104.

Zhou, Y., Peng, Z., Seven, E. S., & Leblanc, R. M. (2018). Crossing the blood-brain barrier with nanoparticles. *Journal of controlled release*, *270*, 290-303.

Zhu, Y., Fotinos, A., Mao, L.L., Atassi, N., Zhou, E.W., Ahmad, S., Guan, Y., Berry, J.D., Cudkowicz, M.E. and Wang, X. (2015). Neuroprotective agents target molecular mechanisms of disease in ALS. *Drug discovery today*, *20*(1), 65-75.

Zrelli, H., Matsuoka, M., Kitazaki, S., Araki, M., Kusunoki, M., Zarrouk, M., & Miyazaki, H. (2011). Hydroxytyrosol induces proliferation and cytoprotection against oxidative injury in vascular endothelial cells: role of Nrf2 activation and HO-1 induction. *Journal of agricultural and food chemistry*, *59*(9), 4473-4482.

Zucca, F. A., Basso, E., Cupaioli, F. A., Ferrari, E., Sulzer, D., Casella, L., & Zecca, L. (2014). Neuromelanin of the human substantia nigra: an update. *Neurotoxicity research*, *25*(1), 13-23.

Zucca, F. A., Segura-Aguilar, J., Ferrari, E., Muñoz, P., Paris, I., Sulzer, D., ... & Zecca, L. (2017). Interactions of iron, dopamine and neuromelanin pathways in brain aging and Parkinson's disease. *Progress in neurobiology*, *155*, 96-119.

Zupančič, S., Kocbek, P., Zariwala, M. G., Renshaw, D., Gul, M. O., Elsaid, Z., ... & Somavarapu, S. (2014). Design and development of novel mitochondrial targeted nanocarriers, DQAsomes for curcumin inhalation. *Molecular pharmaceutics*, *11*(7), 2334-2345.